

AD-A248 205



①

SD
DTIC
ELECTE
APR 01 1992
D



MODULAR SIMULATION OF
HEI FRAGMENTS AND BLAST PRESSURE

THESIS

Gordon Galloway
Captain

AFTT/GOR/ENS/92M-11

This document has been approved
for public release and sale; its
distribution is unlimited.

92-08132



DEPARTMENT OF THE AIR FORCE
AIR UNIVERSITY
AIR FORCE INSTITUTE OF TECHNOLOGY

Wright-Patterson Air Force Base, Ohio

92 3 31 079

AFIT/GOR/ENS/92M-11

1

DTIC
ELECTE
APR 01 1992
S D

MODULAR SIMULATION OF
HEI FRAGMENTS AND BLAST PRESSURE

THESIS

Gordon Galloway
Captain

AFIT/GOR/ENS/92M-11

Accession For	
NTIS CRA&I	<input checked="" type="checkbox"/>
DTIC TAB	<input type="checkbox"/>
Unannounced	<input type="checkbox"/>
Justification	
By	
Distribution /	
Availability Codes	
Dist	Avail and/or Special
A-1	

QUALITY
CONTROLLED
3

Approved for public release; distribution unlimited

AFIT/GOR/ENS/92M-11

MODULAR SIMULATION OF
HEI FRAGMENTS AND BLAST PRESSURE

THESIS

Presented to the Faculty of the School of Engineering
of the Air Force Institute of Technology

Air University

In Partial Fulfillment of the
Requirements for the Degree of
Masters of Operations Research

Gordon Galloway, B.A.

Captain

March, 1992

Approved for public release; distribution unlimited


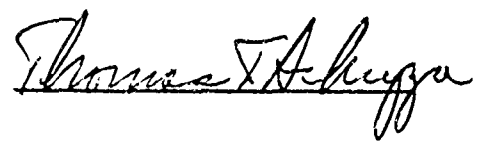
THESIS APPROVAL

STUDENT: Gordon L. Galloway

CLASS: GOR/92M

THESIS TITLE: Modular Simulation of HEI Fragmentation and Blast Pressure

DEFENSE DATE: 11 March 1992

COMMITTEE:	NAME/DEPARTMENT	SIGNATURE
Advisor	Kenneth W. Bauer, MAJ	
Reader	Thomas F. Schuppe, COL	

Acknowledgments

I would like to thank Mr. Bill Rieder & family for their support and help with many of the 3-D equations.

I would also like to thank Ms. Kathy Pike for the many late nights editing and reworking figures.

Also, a special thanks to MAJ Kenneth W. Bauer and COL Thomas F. Schuppe for their patience and support.

Gordon Galloway

Table of Contents

	Page
Acknowledgments	ii
Table of Contents	iii
List of Figures	viii
List of Tables	xii
Abstract	xiv
I. The Problem	1
1.1 Background	3
1.1.1 Current Programs	3
1.1.2 Cost of Empirical Study	5
1.1.3 HEI Explosion	5
1.1.4 Blast Pressure	6
1.1.5 Fire Suppressant Tests	7
1.2 Purpose	8
1.2.1 HEI Simulation	8
1.3 Problem Specifics	9
1.3.1 Testing	10
1.3.2 Blast Pressure	10
1.3.3 Inputs	11
1.3.4 Outputs	11
1.3.5 Fragmentation Pattern	12
1.3.6 Target Surroundings	12

	Page
II. Literature Review	14
2.1 Overview	14
2.2 HEIVAM	15
2.2.1 HEIVAM Focus	16
2.2.2 Vulnerability Analysis	16
2.2.3 Relevant Use	20
2.2.4 Input Requirements	21
2.2.5 Projectile Characteristics	22
2.2.6 Component Association Table	33
2.2.7 Fault Tree	35
2.2.8 Damage Modes	37
2.2.9 TS Damage Model	46
2.3 COVART	46
2.3.1 COVART vs HEIVAM	48
2.3.2 Repair Time	50
2.4 HEI Fragmentation	51
2.4.1 Background Information	51
2.4.2 Test Arena	54
2.4.3 Jones Study	57
2.4.4 Reeves Study	75
2.4.5 Gilbert Study	81
2.4.6 Avery Study	87
2.5 HEI Blast Pressure	90
2.5.1 Jones Study	93
2.5.2 Weeding Study	99
2.5.3 Avery Study	103
2.5.4 Inconsistent Pressure Measurements	107

	Page
2.6 Related Material	107
2.6.1 Target Overlay Grid	107
2.6.2 Ballistic Limit	108
2.6.3 Fire Suppression	109
III. Analysis and Test Recommendations	111
3.0.4 Statistical Proof	112
3.0.5 Test Recommendations	119
3.1 Simulating the Dependence	121
3.1.1 Standard Fragmentation	121
3.1.2 Dependent Fragmentation	122
3.1.3 Comparison of Results	123
IV. Methodology	125
4.1 Simulation Overview	125
4.1.1 Simulation Modules	126
4.1.2 Simulation Output	126
4.1.3 Provisions for Future Enhancements	127
4.2 User Inputs	128
4.2.1 Output File Name	130
4.2.2 Projectile Type	130
4.2.3 Obliquity Angle	131
4.2.4 Angle of Rotation	132
4.2.5 Projectile Velocity	132
4.2.6 Fuse Delay	133
4.2.7 Object Surface	133
4.3 Static Fragmentation	134
4.4 Attack Scenario	137

	Page
4.4.1 Dynamic Shift	138
4.4.2 Burst Point and Projectile Direction	138
4.5 Object Construction	141
4.5.1 Limitation on Object Definition	142
4.5.2 Object Analysis	143
4.6 Target Impact	146
4.7 Peak Blast Pressure on the Target	147
4.8 Blast Pressure Decay on the Target	150
4.9 Outputs	150
V. Recommendations & Conclusions	156
5.1 HEI Process Descriptions	156
5.2 HEI Simulation	157
5.3 Data and Testing Recommendations	158
5.4 Future Study	159
Appendix A. Data from Jones Study	160
Appendix B. Data from Reeves Study	191
Appendix C. Simulation Code	198
C.1 MAIN	198
C.2 INTLC	199
C.3 STATE	201
C.4 EVENT	202
C.5 RECOBJ	204
C.6 DYNCSHFT	208
C.7 OBJECT	209
C.8 OBJHIT	210

	Page
C.9 ELINE	211
C.10 ROWSWAP	212
C.11 INTERSCT	213
C.12 ATTCK	216
C.13 EPLANE	218
C.14 VECTLGTH	220
C.15 UPPER	221
C.16 DET	222
C.17 FRAGHIT	223
C.18 BLASTUP	226
C.19 BLASTIME	231
C.20 TSTFRAGS	232
C.21 REGFRAGS	234
Bibliography	236

List of Figures

Figure	Page
1. Typical Aircraft Dry Bay Configuration	2
2. The HEI Threat to Dry Bays	4
3. Interrelationship of HEIVAM Input Systems	17
4. Typical HEI Projectile Fragmentation Zones	23
5. FMU 128/B Fuse	24
6. M785 Fuse	25
7. Two HEI Projectiles with Firing Shell	26
8. Effect of Velocity on HEI Fragment Trajectories	29
9. Fragmentation Data Geometry for Three Zones	30
10. Geometry of Dynamic Shift	32
11. Sample Portion of Component Association Table	34
12. Breakdown of Group	36
13. Burst Point Regions Where Damage Models are Used	38
14. Typical Single $P_{K H}$ Step Function	42
15. Typical Lethal Radii Damage Function	45
16. 20-mm HEI Fuel Tank Back Wall Rupture	47
17. Vector Diagram for Apparent Yaw	49
18. Fragment Zone Analogy to the Earth	53
19. Schematic of 8-foot Radius Open Fragmentation Test Arena	55
20. Schematic of Modified 20-mm Thin-Walled HEI Projectiles	58
21. Cumulative Fragment Hits per Zone - Standard 20-mm HEI	64
22. Fragment Velocities by Zone - Standard 20-mm HEI	65
23. Cumulative Fragment Hits per Zone - Min Weight 20-mm HEI	67
24. Fragment Velocities by Zone - Min Weight 20-mm HEI	68

Figure	Page
25. Cumulative Fragment Hits per Zone - Max Explosive 20-mm HEI . .	70
26. Fragment Velocities by Zone - Max Explosive 20-mm HEI	71
27. Cumulative Fragment Hits per Zone - By Projectile Type	72
28. Standard 20-mm HEI Weight Distributions	76
29. Minimum Weight 20-mm HEI Weight Distributions	77
30. Maximum Explosive 20-mm HEI Weight Distributions	78
31. Flash X-Ray of the 30-mm Projectile Case Break-up	83
32. Fragment Weight Frequency Distribution for Test #1	84
33. Fragment Initial Velocity Data for Test #3	88
34. Typical Model of 23-mm HEI and Static Fragmentation	91
35. 23-mm HEI Pressure Breakdown	94
36. Schematic of 20-mm Airblast Measurement Arena	96
37. Pressure vs Time Plot for a Standard 20-mm HEI	100
38. Average Maximum Side-On Peak Pressure Versus Striking Velocity for Several Target Plates at 45 Degrees Obliquity	102
39. Overpressure From Confined Detonation is the Result of Two Pressure Components	105
40. Blast Pressure Angle of Incidence	106
41. Flash X-Ray of the 30-mm Projectile Case Break-up	115
42. Test Results of the Radial Position	123
43. Test Results of the Velocity	124
44. Example of the SCENARIO.DAT Data File	129
45. Fragment Characterization File	132
46. Obliquity Angle and Rotation Angle	133
47. Component Placement	135
48. Object Limitation - Part A	144
49. Object Limitation - Part B	144
50. Determining if an Object is Hit	147

Figure	Page
51. Weight Histogram	151
52. Velocity Histogram	152
53. Radial Position Histogram	153
54. Simulated Target Impacted by Fragments	153
55. Surface Plot of the Blast Pressure Through Distance and Time . . .	155
56. Pressure vs Time Plot for a Standard 20-mm HEI at P1=1.5 Feet . .	173
57. Pressure vs Time Plot for a Standard 20-mm HEI at P2=1.5 Feet . .	174
58. Pressure vs Time Plot for a Standard 20-mm HEI at P3=4.0 Feet . .	175
59. Pressure vs Time Plot for a Standard 20-mm HEI at P5=4.0 Feet . .	176
60. Pressure vs Time Plot for a Standard 20-mm HEI at P4=4.5 Feet . .	177
61. Pressure vs Time Plot for a Standard 20-mm HEI at P6=4.5 Feet . .	178
62. Pressure vs Time Plot for a Minimum Weight 20-mm HEI at P1=1.5 Feet	179
63. Pressure vs Time Plot for a Minimum Weight 20-mm HEI at P2=1.5 Feet	180
64. Pressure vs Time Plot for a Minimum Weight 20-mm HEI at P3=4.0 Feet	181
65. Pressure vs Time Plot for a Minimum Weight 20-mm HEI at P5=4.0 Feet	182
66. Pressure vs Time Plot for a Minimum Weight 20-mm HEI at P4=4.5 Feet	183
67. Pressure vs Time Plot for a Minimum Weight 20-mm HEI at P6=4.5 Feet	184
68. Pressure vs Time Plot for a Maximum Explosive 20-mm HEI at P1=1.5 Feet	185
69. Pressure vs Time Plot for a Maximum Explosive 20-mm HEI at P2=1.5 Feet	186
70. Pressure vs Time Plot for a Maximum Explosive 20-mm HEI at P3=4.0 Feet	187

Figure	Page
71. Pressure vs Time Plot for a Maximum Explosive 20-mm HEI at P5=4.0 Feet	188
72. Pressure vs Time Plot for a Maximum Explosive 20-mm HEI at P4=4.5 Feet	189
73. Pressure vs Time Plot for a Maximum Explosive 20-mm HEI at P6=4.5 Feet	190

List of Tables

Table	Page
1. Summary of 20-mm HEI Projectiles Tested	59
2. Standard 20-mm HEI Data and Statistics - Shot #1	60
3. Standard 20-mm HEI Data and Statistics - Shot #2	61
3. Standard 20-mm HEI Data and Statistics - Shot #2 (con't)	62
4. 2 Round Average for Standard 20-mm HEI	63
5. 3 Round Average for Minimum Weight 20-mm HEI	66
6. 3 Round Average for Maximum Explosion 20-mm HEI	69
7. Fragmentation Data Summary for the Soviet 23-mm HEI-T Projectile Used in the NR/NS-23 Aircraft Guns	79
7. Fragmentation Data Summary for the Soviet 23-mm HEI-T Projectile Used in the NR/NS-23 Aircraft Guns	80
8. Summary of Fragment Spatial Dispersion by Weight Range and as a Function of Polar Zone	86
9. Fragmentation Data for Projectiles A, B, and C	89
10. HEI Fragment Distribution and Static Firing Data	92
11. Summary of 20-mm Projectile Airblast Data	97
12. 20-mm Airblast Summary	98
13. Peak Pressure for HEI Against 0.5-inch Aluminum Target Plates at 45 Degree Obliquity	103
14. 20-mm Airblast Summary	118
15. One Ton Detonation of TNT	148
16. Minimum Weight 20-mm HEI Data and Statistics - Shot #1	161
16. Minimum Weight 20-mm HEI Data and Statistics - Shot #1 (con't)	162
17. Minimum Weight 20-mm HEI Data and Statistics - Shot #2	163
17. Minimum Weight 20-mm HEI Data and Statistics - Shot #2 (con't)	164

Table	Page
18. Minimum Weight 20-mm HEI Data and Statistics - Shot #3	165
18. Minimum Weight 20-mm HEI Data and Statistics - Shot #3 (con't)	166
19. Maximum Explosive 20-mm HEI Data and Statistics - Shot #1 . . .	167
19. Maximum Explosive 20-mm HEI Data and Statistics - Shot #1 (con't)	168
20. Maximum Explosive 20-mm HEI Data and Statistics - Shot #2 . . .	169
20. Maximum Explosive 20-mm HEI Data and Statistics - Shot #2 (con't)	170
21. Maximum Explosive 20-mm HEI Data and Statistics - Shot #3 . . .	171
21. Maximum Explosive 20-mm HEI Data and Statistics - Shot #3 (con't)	172
22. Fragmentation Data Summary for the Soviet 23-mm HEI-T Projectile Used in the NR/NS-23 Aircraft Guns	192
23. Fragmentation Data Summary for the Soviet 23-mm HEI-T Projectile Used in the NR/NS-23 Aircraft Guns (con't)	193
24. Fragmentation Data Summary for the Soviet 23-mm HEI Projectile Used in the AM-23 and GSh Aircraft Guns	194
25. Fragmentation Data Summary for the Soviet 23-mm HEI Projectile Used in the AM-23 and GSh Aircraft Guns (con't)	195
26. Fragmentation Data Summary for the Soviet 23-mm HEI-T Projectile Used in the ZU-23 and ZSU-23-4 Weapon Systems	196
27. Fragmentation Data Summary for the Soviet 23-mm HEI-T Projectile Used in the ZU-23 and ZSU-23-4 Weapon Systems (con't)	197

AFIT/GOR/ENS/92M-11

Abstract

This thesis takes a critical look at the fragmentation and blast pressures created by a 23-mm High Explosive Incendiary (HEI) projectile. The current body of knowledge describing the processes is reviewed. Discrepancies and gaps in this knowledge are highlighted and examined. Several hypotheses are suggested along with evidence suggesting their truth.

These hypotheses were tested in the simulation developed as part of this thesis effort. The projectile characteristic fragment patterns from the simulation were compared to those reported in the literature. Preliminary results indicate the need for additional data and live HEI testing.

A modular simulation of the HEI fragmentation and blast pressure was developed which allows the user to implement any dry bay and component configuration. A specific attack scenario must also be provided by the user. The attack scenario specifies the projectile to dry bay obliquity angle and rotation, along with velocity and fuse detonation delay.

The modular implementation allows additional HEI projectiles to be included by adding a single data module. The HEI data module specifies the static detonation dispersion data for a specific HEI type. This implementation therefore allows various projectiles to be tested in unlimited configurations of the dry bay.

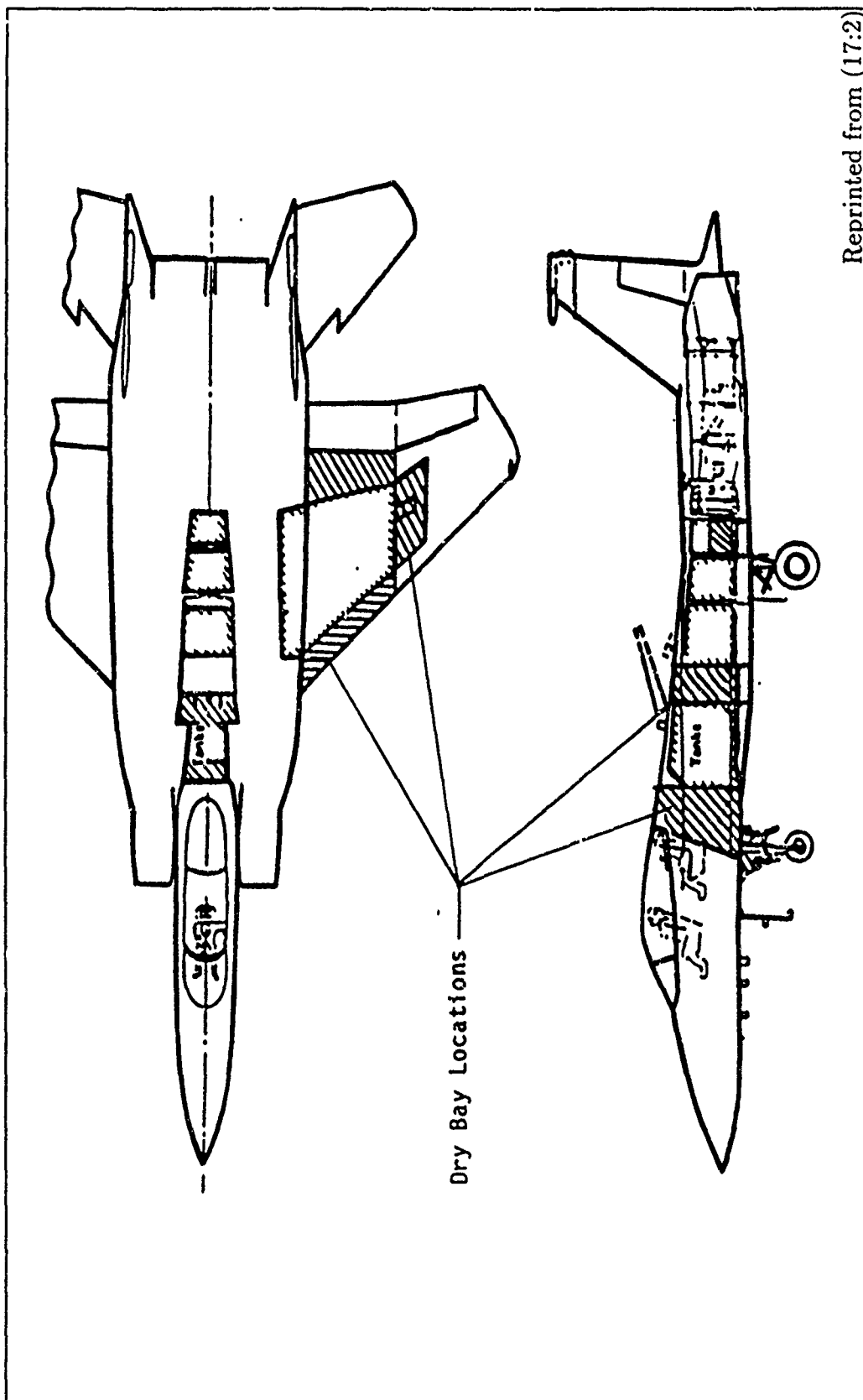
MODULAR SIMULATION OF HEI FRAGMENTS AND BLAST PRESSURE

I. The Problem

Dry bay fires and explosions are major causes of aircraft losses both in combat and peacetime operations. Dry bays are compartments or internal volumes that frequently contain bleed-air, fuel, hydraulic, or coolant lines; electrical and other cables; and containers. They may be located in the leading edges of wings or in the fuselage (Figure 1. Combat damage or equipment can release fluids from adjacent areas or from the lines into the dry bays. An ignition source could ignite the vapors. (17:1)

There are several ongoing programs to assess aircraft survivability. One such program is the Joint Live Fire (JLF) program, chartered in 1984. Its primary objective in 1986 was to "...gather empirical data on the vulnerability of the US front line fixed and rotary wing aircraft to foreign weapons and the lethality of US weapons against foreign targets (27)." This program and similar programs gather empirical information to assess and improve US aircraft survivability. Some of these tests simulate surface-to-air and air-to-air weapon threats against US aircraft. One such threat is the High Explosive Incendiary (HEI) projectile.

Several scenarios are empirically simulated for HEI. One scenario is the quick damp fuel ingestion caused by HEI penetration of a common wall between the fuel cell and the aircraft engine. Another is the vulnerability of hydraulic lines used to control the aircraft against HEI (27). There are also test scenarios designed to test the ability of a defensive subsystem to mitigate or defeat the HEI threat. One such subsystem test is being done by Wright Laboratories, WL/FIVS. That office is



Reprinted from (17:2)

Figure 1. Typical Aircraft Dry Bay Configuration

conducting performance tests on the ability of various fire suppressant subsystems to extinguish dry bay fuel fires caused by HEI (17).

The protection of aircraft dry bays represents one of the most critical applications of halon fire extinguishing agents and is fundamental to aircraft survivability. Currently, Halon 1301 is used because of its cleanliness, dispersal characteristics, and effectiveness against a wide variety of fire threats. It is likely that no one agent will replace all of the uses of Halon 1301 on an aircraft, and several different agents may have to be employed. (17:3)

A replacement for halon is sought because recent "...calculations and limited experimental data indicate that halon, like chlorofluorocarbons (CFCs), deplete stratospheric ozone (17:1)."

The problem investigated in this thesis is the 23mm HEI threat to the dry bay. Figure 2 shows one possible breakdown of this problem. Only the 'HEI Fragmentation and Blast Pressure'

sub-problem is addressed by this thesis. In a separate research effort, Crawford is addressing the 'Fuel Cell Explosion' sub-problem (8). These two sub-problems culminate in simulations which will be combined in a follow-on thesis to form a 'basis' simulation. The sub-problems illustrated outside the central box will most likely be addressed in subsequent theses and integrated into the basis simulation. In this way, a full computer implementation of the problem will be developed. Subsequently, this full scale simulation will be iteratively used and improved along with a reduced empirical study of the HEI fuel fire threat to dry bays.

1.1 Background

1.1.1 Current Programs Virtually all of the work to assess and improve aircraft survivability is empirical. There are two computer programs which run attack scenarios against aircraft. These programs are used to predict damage and the cost to

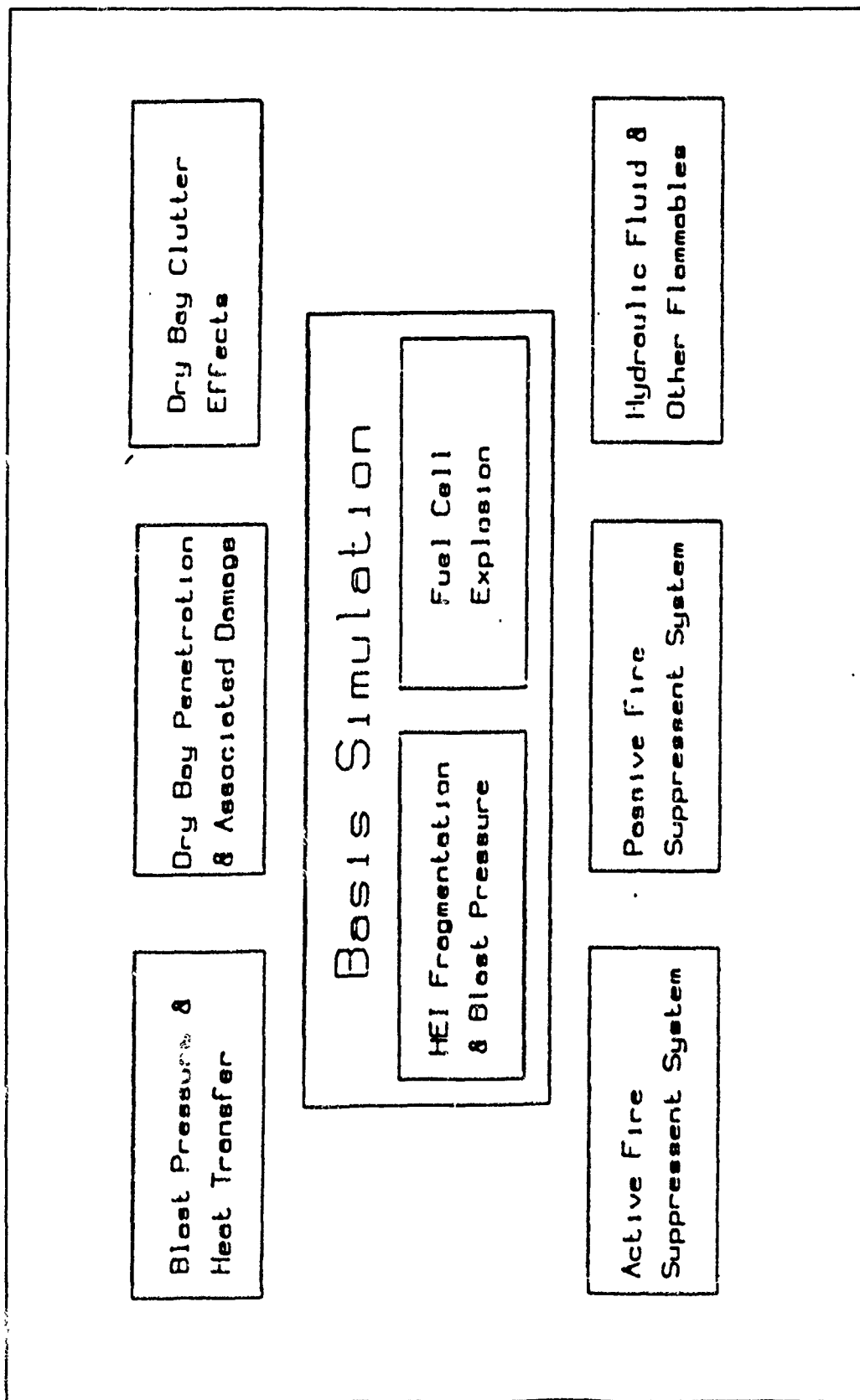


Figure 2. The HEI Threat to Dry Bays

repair that damage. The two computer programs, COVART (21) and HEIVAM (6), assess an aircraft's vulnerability to API [non-explosive projectile] and HEI projectiles respectively. The use of these computer programs in the study of HEI fuel fires in the dry bay was considered and rejected because of their complexity, and large input requirements. Also, the programs do not model the actual HEI processes. Instead, they predict damage based on statistical probabilities.

1.1.2 Cost of Empirical Study The cost of empirical tests is very high. Entire aircraft are shot, exploded, and repaired so they can be shot and exploded again. This of course means that the aircraft must already exist, and that many man hours are spent setting up the tests. If the tests were not empirically based, or could be done prior to aircraft development, the cost of changes indicated by the tests would be relatively small. But, because the aircraft already exist, empirical studies revealing excessive vulnerability may require modifications to be made. Modifications to already constructed aircraft are very expensive. Thus, the high cost of post production empirical testing is incurred from both the tests themselves and any aircraft modifications.

Because of the high cost of empirical testing, any improvement or reduction of the number of tests conducted can save considerable costs. However, any improvement or reduction of empirical test can not be done at a cost to aircraft survivability. Sufficient tests must be done to assess the vulnerability of the aircraft and reduce it if possible. Likewise, any testing that can be conducted prior to the aircraft's production can save the considerable time and expense usually associated with modifications and retrofit.

1.1.3 HEI Explosion An HEI projectile explodes. Because of this it poses a potential fire threat and the fragments expand the area of damage. This is in addition to the physical damage caused by the penetration of the projectile. The explosion is triggered by the fuse which is triggered by the impact of the projectile

nose against the aircraft surface. Fuse triggering is referred to as ' t_0 ,' or 'initiation.' The explosion is initiated by the fuse and therefore occurs a finite amount of time after detonation. The explosion may be delayed or occur 'super-quick' based upon the fuse type. As the projectile penetrates into the aircraft the fuse ignites the explosive charge stored within the HEI body. Upon explosion the outer shell of the HEI fragments. These fragments spread in radial patterns which widen the damage area. The incendiary characteristic of the HEI enables it to ignite fuel or other flammable fluids exposed by the projectile or its fragments.

Fragments radiate out from the explosion point in relatively uniform patterns around the axis of the HEI projectile. As the fragments radiate out they expand the area of damage beyond that of a non-exploding projectile. They also enhance the HEI's ability to cause a fire. Both the fragments heated by the explosion, and the incendiary particles within the explosive are capable of igniting fuel or other flammables. The radial pattern of the fragments is based upon the velocity of the HEI projectile, and the normal fragmentation patterns from a static detonation (6, 28, 16). Section 2.4 describes the fragmentation characteristics.

1.1.4 Blast Pressure In addition to the fragments, the HEI explosion generates a pressure wave. This pressure wave increases the stress on the aircraft and increases the chance of fire. The stress alone can cause structural damage (6). All blast and/or pressure waves caused by explosions have similar characteristics. The specific results of any wave are dependant not only on the exploding material and/or object, but also the surroundings. The surroundings can alleviate the pressure or concentrate it (22). The wave can also be contained or redirected (7). Although pressure waves have been studied in various forms, little empirical data is available on HEI blast pressures. Section 2.5 describes the current understanding of HEI blast pressures.

1.1.5 Fire Suppressant Tests In empirical tests, the explosion of an HEI is intended to ignite the fuel substitute so that various fire suppressant systems can be tested. The fire can be ignited by the HEI explosion, hot fragments splitting from the exploding HEI, sparks from pierced metal or electronics, or high pressures combined with a spark or hot fragment. To protect against fuel fires or explosions caused by the HEI threat, Halon 1301, nitrogen, and foam have been used or considered (DTIC AD-BO30-104). A fuel cell fire usually results in the loss of the aircraft.

Engineering a better fire suppression system to put down or guard against the HEI threat requires complete understanding of the processes leading up to the fire. The first major process is the HEI explosion and its resultant fragments and blast pressure. Other major processes include interaction of fragments with miscellaneous components in the dry bay; blast pressure movement and dissipation conditioned on the characteristics of the dry bay; dynamic interaction between hot fragments, blast pressure, and the fuel tank. Each of these can be subdivided into sub-processes and events.

WL/FIVS is conducting empirical tests now. Their test setup is a facsimile of an uncluttered dry bay. This facsimile is a 3 by 3 by 8 feet rectangular structure. The HEI projectile shot at this structure would travel a short 3 foot from striker plate to target plate if it did not explode. A fuel cell is placed on the back side of this structure as the target plate. The confines of this structure are assumed by WL/FIVS not to reflect any blast pressures prior to the explosion of the fuel cell (4).

The empirical model is uncluttered by the usual components and subsystems although provisions have been made to accommodate these in later tests. Without this clutter blast pressure effects, hydraulic fluids, and sparks from electronics are ignored (4). Currently, the empirical model consists of a striker plate representing the aircraft surface, and a fuel cell located 18 inches behind the striker plate. The projectile used is a 23mm HEI shot at a muzzle velocity of 3200 feet per second. The mock fuel cell is filled 6 inches deep with a flammable fuel substitute (4).

1.2 Purpose

The purpose of this thesis is to simulate the fragments and blast pressure generated by the explosion of an HEI. In preparation for this, all subject matter pertaining to the propagation of HEI fragments and blast pressures is reviewed.

The review of HEI blast pressures is augmented with material not specific to HEIs when such material specific to HEIs cannot be found. However, the depth of these non-HEI reviews will be limited to the fundamental concepts of wave shape, propagation, and intensity. Therefore, because no HEI specific, in-depth information is available, no material is presented on the thermodynamic nature of the blast pressure nor the aerodynamic nature of fragments.

1.2.1 HEI Simulation The simulation is a modular implementation in SLAM II. All modules are written in FORTRAN thus allowing for easy enhancement and up-grade. Only the characteristics and options associated with the 23mm HEI are simulated. Both the fragmentation characteristics and the blast pressure characteristics are modeled.

1.2.1.1 Setting the Scenario. The simulation model is data driven. As such, all of the salient characteristics of a particular HEI threat, and any performance options are easily set and changed without recompilation of the program code.

Although the simulation can be used as a stand alone system with which to study fragmentation characteristics, it is not intended to stand alone. It is intended that future enhancements will integrate other simulation models including the fuel cell explosion model as shown in Figure 2. The integrated models will simulate the entire HEI threat to the dry bay including all events and processes.

1.2.1.2 The Beginning and the End. Because of the intended integration of this simulation model, only the time interval between the initial projectile impact and the last fragment impacts or passes the target component is simulated.

The target component for this thesis, is defined as a flat surface some specified distance from the impact or entry point of the projectile. Other target component characteristics must be defined by the integrating model discussed above.

1.2.1.3 The Dry Bay. A final limitation of the model developed is its supposed surroundings. Although the surroundings of a real dry bay or some other area within an aircraft have boundaries with miscellaneous obstructions within those boundaries, this model will not. The model will assume an open area where only the impact point and the target component exist. These assumed surroundings match those used in the current empirical tests conducted by WL/FIVS for fuel fire suppressant systems (4).

The simulation model developed does have the capability to include other components. But these components only act as barriers within the dry bay. There is no defined interaction between these other components and the fragments or blast pressure. Therefore, when a fragment impacts one of these other components, the fragment is stopped and has no chance of penetrating the component.

1.3 Problem Specifics

The main thrust of this thesis is to model the propagation of fragments and blast pressure through an open [no walls], free of clutter, dry bay to the target component. Only the fragments and blast pressure are simulated. Damage estimates and subsequent explosions other than the HEI are not simulated. For instance, the explosion of an attacking HEI, the generated fragments, and the blast pressure, are simulated from the point where the HEI first strikes the aircraft, to the point at which all fragments and the blast pressures reach or pass the target component. On the other hand, the explosion of the fuel cell and any associated fire are not simulated.

The simulation model developed for this thesis has the ability to be joined with simulation modules such as the fuel explosion mentioned above. Other models may simulate component fires, explosions, etc This modular characteristic allows flexible use of the simulated HEI explosion. Follow on embellishments may further allow various obstructions to be placed between the aircraft skin and the target component.

1.3.1 Testing In order to fully understand and simulate the fragments, the dependencies listed below need to be tested. Unfortunately the data necessary for these tests is disassociated and incomplete. Therefore, Chapter 3 presents empirical indications of these dependencies derived from the literature, and simulates the HEI as though these dependencies had been proven. The results of simulations with and without these dependencies are then compared. Chapter 3 also outlines the data and tests needed to conclusively prove or disprove these dependencies.

- The dependence between a fragment's size/weight and its velocity when statically detonated.
- The dependence between a fragment's position within the projectile casing prior to explosion and its direction of flight when statically detonated.
- The dependence between a fragment's size/weight and its position within the casing prior to explosion.
- The dependence between the blast pressure and the fragment directions.

1.3.2 Blast Pressure There is little information specific to HEI blast pressures. There is some available on 30mm HEI rounds which was recorded only in the test notes from the Gilbert study which were never published (15). Other sources provide similarly limited data on HEI blast pressures. All of this data and other general information about blast pressures will be combined to form a hypothesized pressure wave for the simulation (31, 7, 22, 23, 6).

1.3.3 Inputs Inputs to the simulation are through data statements. The inputs control the selection of subroutines and the characteristic to be simulated. The inputs include at a minimum, information for target placement, the target's forward velocity, the obliquity (attack) angle and rotation, the projectile type, projectile velocity, and fuse delay. The target placement information describes the relative displacement of a bounded plane from the entry point of the HEI into the dry bay. This target can be any size or shape. It can also be placed at any angle within the dry bay.

1.3.3.1 Attack Profile. An exploding HEI has different effects in different situations. The effects in a given situation depend not only on the HEI itself but also the target. The target itself may be moving. Therefore the relative velocity and orientation of the HEI to the target aircraft is very important. This relationship affects the HEI penetration capability and fuse functioning. The fragment pattern and residual velocity are affected in a similar manner. Even the blast pressure is affected.

1.3.3.2 Fuse Control. The explosion timing is controlled by the fuse type used. All fuses are triggered by the HEI nose impacting the aircraft surface.

A super-quick fuse causes the HEI to explode in about 300 microseconds (16). For a projectile traveling at 2800 feet per second this fusing action allows the HEI to travel about 10 inches as calculated below. An HEI with a delayed fuse penetrates the aircraft much further before exploding (6). The length of delay depends directly on the fuse type.

$$2800ft/sec * .000300sec = 0.84ft = 10.3inches$$

1.3.4 Outputs Output from the simulation include time indexed data on the fragments and the blast pressure. This data includes the following information for

each fragment striking the target. Histograms describing the radial position of fragments striking the target, their velocity, and their weight are also output. In addition, the pressure placed upon the target, indexed through time is output.

- Time of impact.
- Location of impact.
- Impact obliquity angle
- Impact velocity
- fragment weight

1.3.5 Fragmentation Pattern The fragmentation pattern generated on the target is a radial pattern based on the relationship between projectile center line and target surface. Therefore, if a projectile enters the dry bay at an angle [anything other than a 0° obliquity angle], the fragment impact pattern generated on a target plate that is parallel to the aircraft surface, will be elliptical (28).

1.3.6 Target Surroundings Although not included in the simulation model developed, the effects of target surroundings are mentioned here for completeness. After the initial impact and penetration of the HEI, other components in the dry bay and the dry bay structure itself affect the fragments and blast pressure. The components can be general clutter, fuel lines, hydraulic lines, etc These can stop fragments before they reach the target component or cause undesired side effects.

The physical boundaries of the dry bay can magnify or redirect the blast pressure. The pressure wave, in effect, bounces off the walls and any components in its path (22, 23, 7). The interaction and resultant effect is nearly impossible to specify. Other systems within the dry bay may actively or passively mitigate the effects of the blast wave (29).

Although these components and systems are not included in the simulation model developed here the design will provide for their later inclusion. Therefore, these options and salient characteristics must also be driven by data statements.

II. Literature Review

In depth vulnerability analysis of material targets to impact by Soviet 23mm High Explosive (HE) projectiles requires detailed data on the fuzing and terminal ballistic characteristics of the projectiles. The probability that a target will be defeated as a result of impact by a 23mm HE projectile is, in most cases, a function of: (1) the trajectory and point of impact of the projectile on the target, (2) fuze functioning characteristics, and (3) the effectiveness of the damage mechanisms (fragments, blast and fireball) associated with a detonating projectile in killing critical components. As an example, in the case of "soft" targets, such as aircraft, HE projectiles with delay action fuzes can perforate a lightweight outer barrier and detonate close to critical components. The vulnerability of the critical components may vary as the distance between a critical component and the HE projectile detonation varies. The existing data base on the effectiveness of Soviet 23mm HE projectiles is limited in many cases to ad hoc test results. (28:9)

2.1 Overview

In this literature review four general topics are covered. The first two topics discuss the computer programs HEIVAM and COVART respectively. The second two topics discuss the HEI projectile detonation characteristics of fragmentation and blast pressure respectively. The basic function of both the HEIVAM and COVART computer programs is the same. Therefore, a full description of their logic is presented in the HEIVAM section and only the difference discussed in the COVART section. The purpose of both these programs is different from the purpose of this thesis. These differences are also pointed out in the first two sections. To facilitate reading, the program developed for this thesis is referred to as *TS*.

Section 3 and 4 introduce the culmination of data and analysis used to describe HEI explosions and their effect. In some cases, there are inconsistencies between sources in the literature. These inconsistencies are highlighted and discussed in this chapter. Selected inconsistencies pertinent to the simulation developed for this

thesis, will be further discussed, analyzed, and experimented with in Chapter 3. The data necessary for the experimentation is introduced here along with the source literature.

There is also one source that inaccurately describes the trigonometric relationship of the projectile fragments to a target plate. Proof of the inaccuracies and the correct relationship is

presented.

The last section highlights supporting literature not directly used in this study. The literature sources reviewed in this section provided the author with invaluable insight and background information. These sources may lead the reader to particular HEI topics of interest.

2.2 HEIVAM

HEIVAM stands for High Explosive Incendiary Vulnerability Assessment Model. The key words to focus on are *vulnerability assessment*. As quoted from the User Manual:

The program predicts damage to aircraft targets when attacked by small (20- to 40-mm) high explosive projectiles (with either contact or delayed fuzes) by determining damage at a component level and using fault tree methodology to combine the component damage values into an overall prediction of damage to the target.

(6:Vol 1, DD FORM 1473).

Much of the text describing this program is quoted directly from the User and System Manuals. An accompanying commentary provides insight into the similarities and differences between the HEIVAM and TS programs. The purpose of presenting both the descriptive quotation directly from HEIVAM manuals and the commentary is two fold. One, the reader is provided a great deal of information and insight

into the fundamental processes occurring within the explosion of an HEI. Two, the reader is shown how these two programs are similar in basic approach and content, but differ greatly in purpose and detail.

2.2.1 HEIVAM Focus The main focus of HEIVAM is to *predict* damage. This damage prediction is done on a massive scale as the entire aircraft is assessed. The *vulnerability* or exposure of each component aboard the aircraft is assessed for a given attack situation. The component vulnerability is then translated into a damage prediction based upon probability data input by the user. A fault tree describing the interrelationship of all aircraft components, is used to combine the individual component damage probabilities into an aircraft damage prediction.

HEIVAM uses probabilities to predict damage instead of modeling the actual damage causing processes. In contrast, TS partially models the HEI damage causing processes. This is the primary distinction between HEIVAM and TS. In addition, the purpose of HEIVAM is to output a damage prediction for the aircraft. The TS program outputs a description of the processes occurring throughout the time leading up to a damage event. In the simplest terms, HEIVAM looks at the expected aircraft damage from a particular HEI threat; TS looks at the processes and events initiating a particular type of damage to a particular component.

2.2.2 Vulnerability Analysis In the following excerpt from the HEIVAM User Manual, the complexity of this program is more fully appreciated. Several programs must be run prior to starting the vulnerability assessment. These programs include FASTGEN (10), SHOTGEN (18), PGEN (26), BPLOC (no documentation of this program has been developed), and CONVERT (9). Figure 3 graphically shows the relationship between all these programs. In turn, each of these programs has its own input requirements. Understanding the full impact each program has upon HEIVAM is important to the understanding of HEIVAM output.

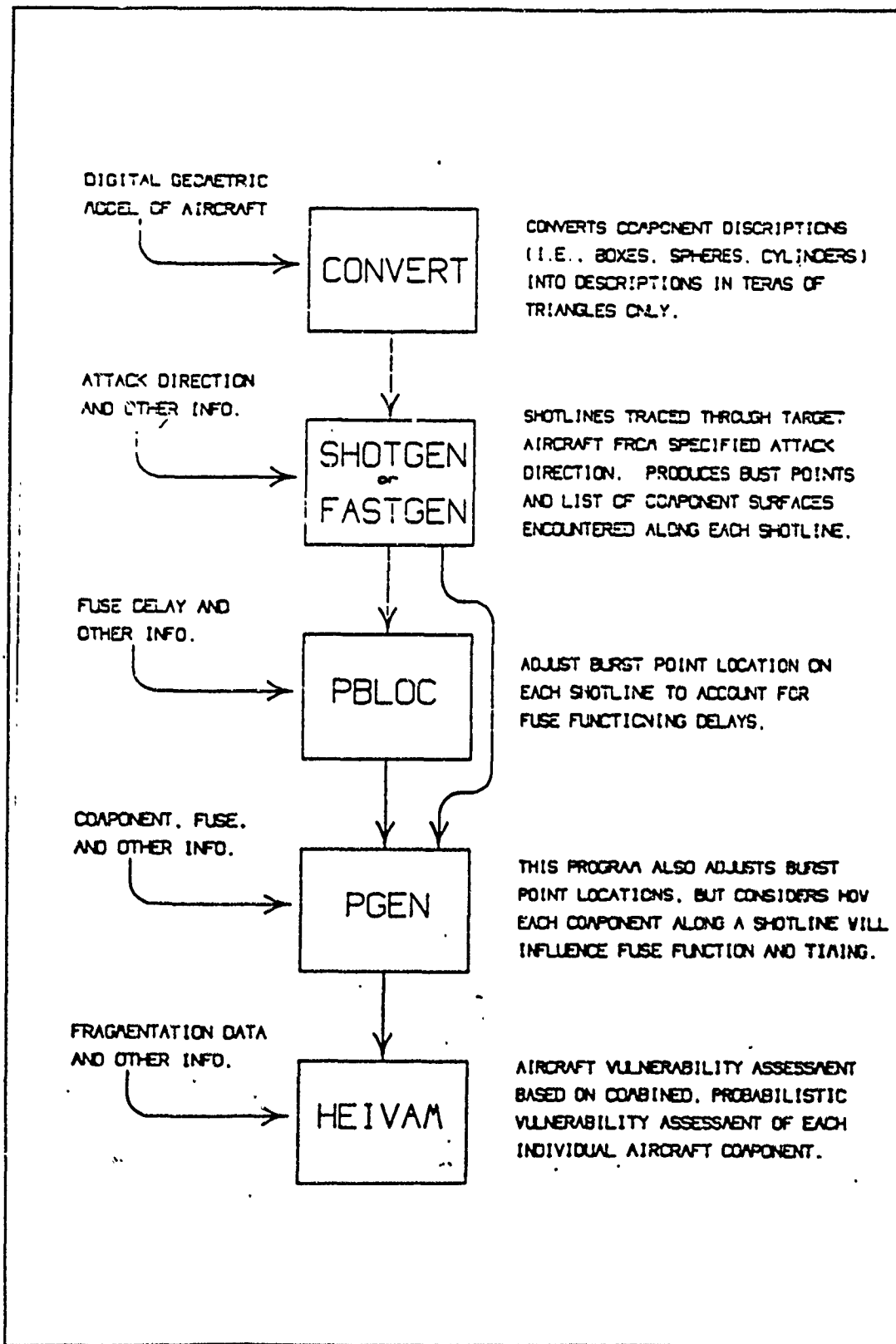


Figure 3. Interrelationship of HEIVAM Input Systems

Before reading the following excerpt, a few definitions are in order.

attack aspect This is simply the angle and direction at which the HEI projectile approaches and subsequently encounters or strikes the target aircraft (6:Vol I, pp.2)

burst point The point in space where the HEI projectile explodes is described in 3-dimensional relation to the target aircraft. This point can be either internal or external to the aircraft (6:Vol I, pp.2).

grid size A grid is most easily visualized as graph paper. It is usually used in conjunction with a specific 2-dimensional view or picture of the target aircraft. The grid size is usually scaled so that the length/width of one square is equal to a specified size on the scaled view of the target. This specified size is often two, four, six, or eight inches (6:Vol I, pp.12).

high density rays The spray of fragments from an exploding HEI are characterized as rays. A *high density* of rays is descriptive of the normal fuse functioning of an HEI projectile. This is also referred to as a *high order detonation* (6:Vol I, pp.6,19-20).

low density rays The spray of fragments from an exploding HEI are characterized as rays. A *low density* of rays is descriptive of a non-normal detonation of an HEI projectile. This most often occurs when the projectile strikes the target aircraft at a very high obliquity angle. This is also referred to as a *low order detonation* (6:Vol I, pp.7,19-20).

obliquity angle An angle, usually measured in degrees, describing the relationship between a projectile (or fragment) flight line and a reference line which is normal (perpendicular) to the target impact surface.

high density component Usually associated with a very small, relative to the grid size, compact component (6:Vol I, pp.6).

low density component Usually associated with a component which is relatively large compared to the grid size (6:Vol I, pp.7).

radius addition A distance which is added to all sides of a component's defining limits (length, width, and depth; front, back, top, bottom, and sides). This enlargement of the component is used to account for the possibility of a fragment or projectile grazing the component. Fragments and projectiles are modeled in HEIVAM as lines which have no width or diameter. Thus, if this line strikes the enlarged (via radius addition) component, then a projectile or fragment with real volume would have struck the component. The distance added via radius addition is dependent on projectile or fragment radius (6:Vol I, pp.9; Vol II, pp.320).

A vulnerability analysis is a study of the interaction between a munition (or weapon) and the target attacked. In the context used in HEIVAM, a vulnerability analysis is performed to determine the effects on an aircraft target system produced as a result of an attack by ...[an HEI]. To begin, an analyst must first have a digital geometric model of the desired target aircraft, a knowledge of the intended function of the aircraft, and a knowledge of the operation of the various systems used in the aircraft. ...[The digital geometric model] must be converted to descriptions containing only triangles. Therefore, a computer program called CONVERT is used to pre-process a BCD [binary coded decimal] file.

... This output file is then input to either the FASTGEN or SHOTGEN computer programs, both of which trace shot lines through the target from user-specified attack directions, and produce an output file containing burst point location coordinates and descriptions of the component surfaces encountered along each individual shot line. Execution of either program requires that decisions be made as to the grid size and radius addition to be used, and the attack aspects that are to be considered. These programs create a grid, large enough to cover the limits of the target, in a plane normal [perpendicular] to a line representing the attack direction, and pass one shot line through each grid cell. ... The shot line file is then input to the PBLOC computer program maintained by AFATL/SAV to create an adjusted burst point coordinate file. These adjusted burst point coordinates reflect detonations at varying distances

beyond the first surface encountered dependent upon fuse functioning characteristics (contact of delayed). This file is coupled with the shot line file and input to a modified version of the PGEN program. Input data to be provided by the user for the PGEN program include a list of critical component code numbers, the average expected radius addition for a fragment, the number of great circle divisions to be used when creating high-[density] and low-density rays, and codes indicating whether a specified critical component is a high-[density] or low-density component, a centroid component, or is to be ignored. ... Now that a burst point library has been obtained, preparations can be made for execution of HEIVAM. (6:Vol I, pp.11-12)

2.2.3 Relevant Use Because of its complexity, HEIVAM is not often used for studies involving subsets of the damage prediction model. At one time, HEIVAM use was considered for the study of fuel fire retardant/extinguisher. One of the major difficulties of this would have been piecing together information, processes, and output required from subsets of the various input programs referenced above and the HEIVAM program itself. The only way to properly do this without piecing together and writing new code, would be to run the entire system (of programs) with all the associated inputs. Even after doing so, the answers would be only partially illuminated.

HEIVAM would predict whether the fuel cell ignited based on the allowable HEIVAM defensive systems, and then output a damage assessment for the aircraft based upon this. The purpose of the fuel fire study is to test and evaluate prospective fuel fire retardant/extinguisher systems. HEIVAM defensive systems only allow the implementation of three inch thicknesses of flexible or rigid void filler foams, or no void filler at all (6:Vol I, pp.38). No Halon 1301, Nitrogen systems, nor any other such systems can be tested in HEIVAM. In addition HEIVAM always assumes an optimal combination of fuel and air for combustion. This may or may not be desired in each fire suppressant test.

2.2.4 *Input Requirements* HEIVAM input requirements include (6:Vol I, pp.12-13):

1. physical data describing the HEI projectile which includes its weight, fragmentation characteristics, etc
2. target geometric model and technical data to create an association table and fault trees.
3. individual component damage function data to calculate a damage value given a fragment's weight and velocity.

Item 1 information is important to the TS program also. Because different types of HEI projectiles have different explosive characteristics, the type of HEI or its characteristics must be identified. Section 2.4.3 describes these differences and why they occur in greater detail. The current TS program requires only fragmentation data. But, depending on the needs of the analyst, this input requirement may expand to include other projectile information.

In HEIVAM the data in item 1 is used along with projectile (or fragment) velocity, obliquity angle, mass, and component penetration and/or damage tables, to determine whether or not a component is penetrated and/or damaged. Similar information is also used to update the subsequent projectile (or fragment) velocity, and mass. This data is very detailed. Reference to Sections 2.4 and 2.5 provide insight to this detail for projectile fragmentation and blast pressure characterization respectively.

The information in item 2 is not required by the TS program. A description of a component's¹ relative position is required. This position is usually set straight back and parallel to the projectile impact point. The component's front surface position and limits are required for the TS program. Projectile or fragment interaction

¹Because there is only one component of interest in the TS program, it is usually referred to as the *target*

with the component is determined by a separate module of the simulation not yet integrated with the TS program; reference Chapter 4.

HEIVAM relies on item 2 information heavily. Along with item 3 information, probabilistic damage values are accumulated to arrive at an overall, aircraft damage prediction. Item 3 data includes component descriptive information such as material make-up and thickness. TS does not contain any component damage data.

2.2.5 Projectile Characteristics As described in Section 2.2.2 the PGEN program is used to provide HEIVAM with a complete listing of what components will be struck by imaginary *rays* emanating from each individual HEI burst point generated from the FASTGEN or SHOTGEN output. Multiple shot lines are generated by FASTGEN and SHOTGEN: one for every grid square as described in Section 2.2.2. These shot lines are therefore only a grid square distance apart. A typical grid distance is 2, 4, or 8 inches. Since there are a large number shot lines, each with an associated burst point, any component is likely to be listed several times for multiple rays generated from each, of several, burst points. HEIVAM overlays this burst point and ray information with the specified HEI characteristics.

Weapon characteristic input to HEIVAM describe the physical aspects of a weapon as well as the manner in which it performs. Projectiles can vary in fuse type and physical characteristics. HEIVAM predicts whether a projectile will function normally, function partially, or ricochet (no functioning). Fragmentation data (i.e., the number, location, and velocity of fragments produced when the projectile detonates) for a projectile are a required input to HEIVAM. When an HEI projectile detonates, the casing is fragmented and these fragments emanate radially from the projectile. These fragments are assumed to radiate from a finite center of detonation and are considered to be distributed within identifiable conical shaped zones. Figure [4] presents a three-dimensional illustration of two fragmentation zones. For purposes of illustration, only two zones are shown, but actually 15 to 30 zones are typically considered. (6:Vol I, pp.17)

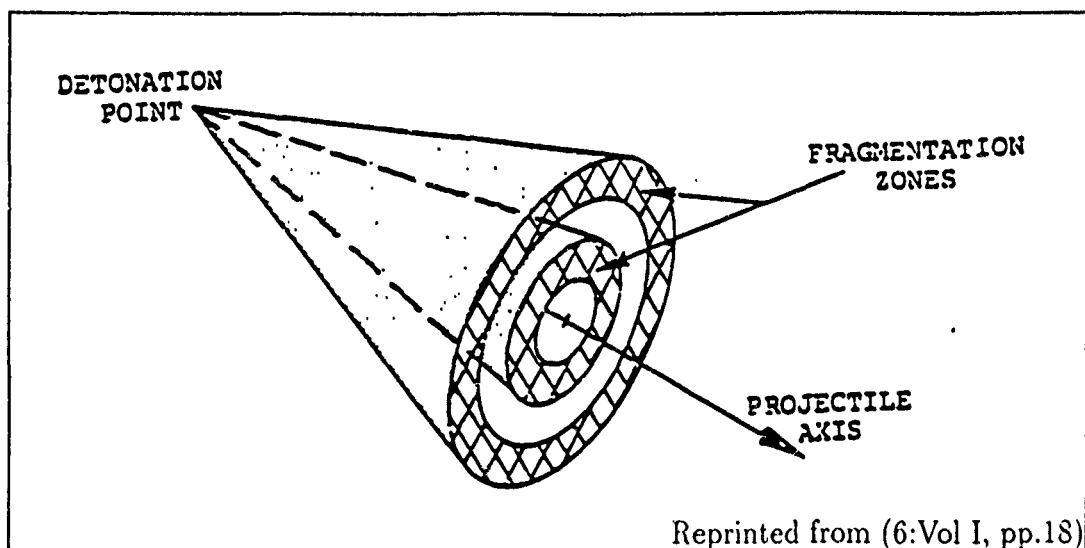


Figure 4. Typical HEI Projectile Fragmentation Zones

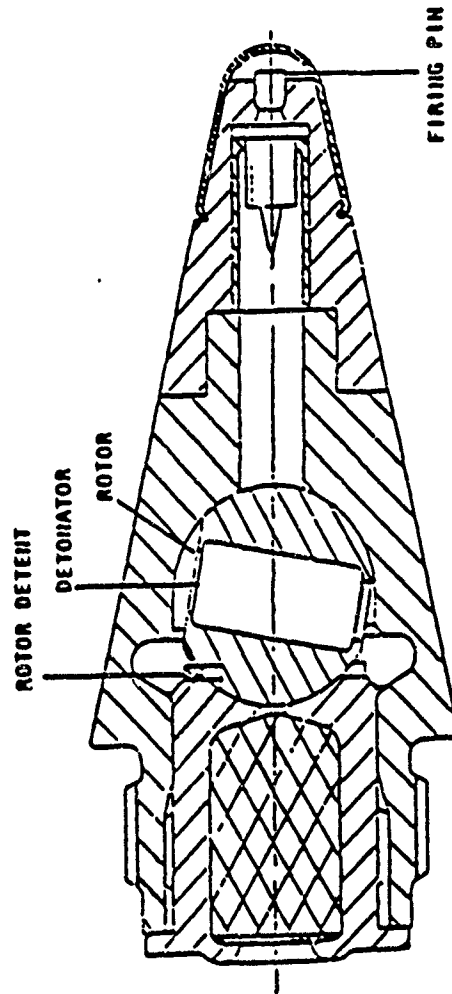
2.2.5.1 *Fuse Characteristics.* Fuse type selection allowed by HEIVAM amounts to a simple selection of *fuse class*: contact or delayed fuse. In actuality, there are many fuse types that fall into each of these classes. Some of these include the contact fuzes MG-25, A-23, and M505A3; and the delayed fuzes B-23, B-23A, FMU 128/B (28, 30). There are other fuzes that have several detonation modes such as the M758 which can detonate from impact, projectile deceleration, or rotational deceleration (30:11).

Differences between fuse type also effect their functioning. The FMU 128/B and M758 fuzes are shown in Figures 5 and 6 respectively. Two complete HEI projectiles assembled with their shells are shown in Figure 7.

Differences in the shape and angle of the fuse greatly affect the functioning. If a projectile strikes the target at a high obliquity angle, a partial, low order functioning will take place instead of the normal, high order functioning. Even greater obliquity angles result in the ricochet of the projectile off the target. The obliquity angles at which partial functioning and ricochet occur depend, in part, on the fuse type.

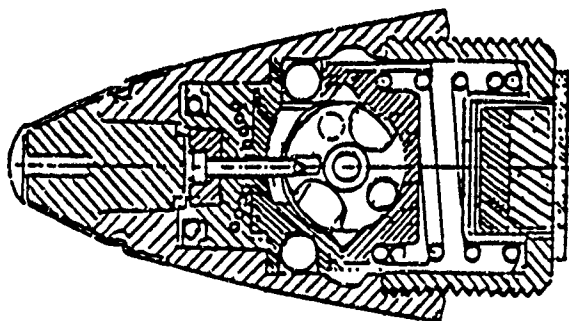
HEIVAM allows some flexibility here through input parameters to its subroutine FUNCTN (6:Vol II, pp.435). In this subroutine finite angles are initialized for

- CASE HARDENED FIRING GUIDE
- MUST SHEAR FIRING PIN FLANGE
- DELAY FUNCTION DUE TO FIRING TRAVEL
- DELAY TIME IMPACT DEPENDENT

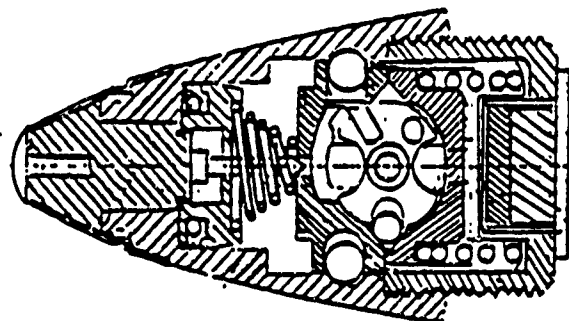


Reprinted from (29:12)

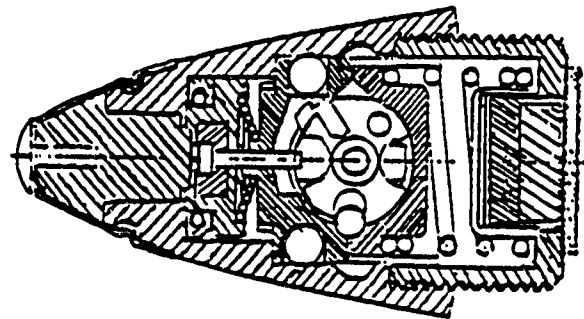
Figure 5. FMU 128/B Fuse



**PRELAUNCH SAFE
CONDITION**



**ARMED CONDITION
ROTOR ALIGNED**



SELF DESTRUCT

Reprinted from (29:13)

Figure 6. M785 Fuse

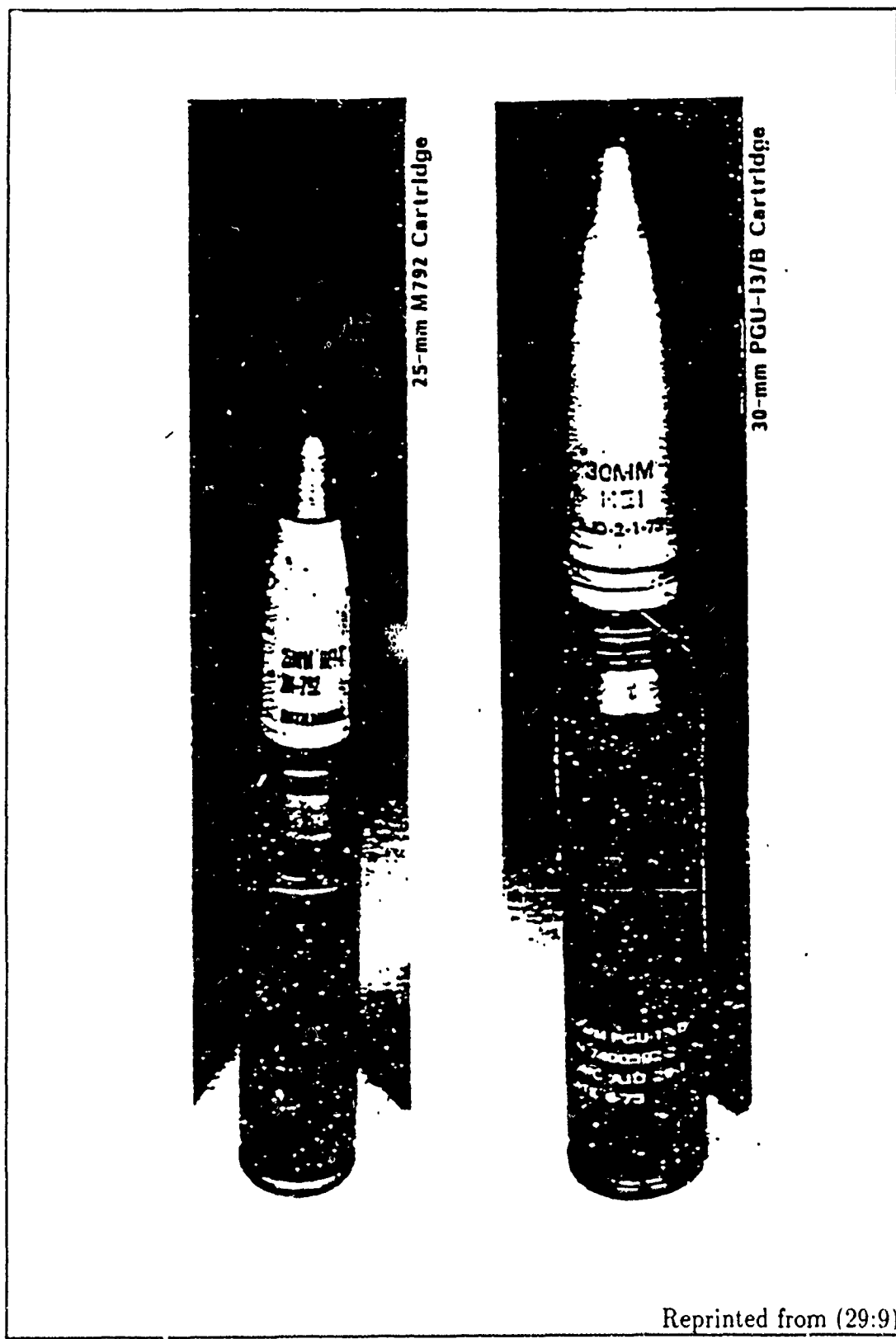


Figure 7. Two HEI projectiles with firing shell

the specified projectile type. No mention of the fuse type is made. As described by Schmeling in 1983:

Those properties considered to have an effect on fuse functioning include projectile diameter, weight, fuse type and nose half angle.

...with increasing obliquity angles, the initial component of force acting on the [firing] pin decreases to zero at some point depending upon the nose half angle. Subsequent penetration may produce new forces on the pin to initiate a high order reaction; otherwise, the projectile may break up, destroying the fuse integrity, and result in a low order reaction. (30:10- 11)

Much of this information is used along with ballistic limit data and equations to determine how the projectile will interact with the target. HEIVAM includes some calculations to determine this, but several recent studies provide better insight and estimation of the ballistic limit and projectile/target interaction. A more detailed discussion of this subject can be found in References (5, 30, 32).

2.2.5.2 Fragment Velocity Vectors. The fragments produced by an exploding HEI do emanate radially from the projectile, but, as cited above, in HEIVAM they are "...assumed to radiate from a finite center of detonation" This *assumption* does not reflect the actual distribution of fragments, though the effect is very similar. A more detailed discussion of the fragment distribution is found in the following two chapters.

Fragment distribution data can be input into HEIVAM as static or dynamic detonation. These two detonation modes are illustrated in Figure 8A and 8B respectively. The dynamic detonation mode accounts for the forward velocity of the projectile. The static detonation mode characterizes a stationary projectile. The information required by HEIVAM includes 1) weight intervals, 2) mean fragment weight for each zone, 3) number of fragments for each zone, and 4) an average

fragment initial velocity for each zone. (6:Vol I, pp.20) The zone boundaries are implicitly defined by these same information inputs.

Zones are defined relative to the longitudinal (direction of flight) axis of the projectile. Just as the earth is divided into 180 latitudinal degrees from North Pole to the South Pole, so is the HEI projectile. In both cases the latitudinal degrees are measured relative to the longitudinal axis. The only difference between the HEI projectile and the Earth is the 0° demarkation. The Earth's latitude starts from the equator at 0°, and increases steadily toward 90° as the distance toward either Pole is traveled. A projectile's latitude starts with 0° at the fuse end, and increases steadily toward 180° at the tracer or trailing end. A zone is therefore designated by two latitudinal markers. These zones are usually, but not always, stepped off in equal, contiguous intervals from 0°- 180°.

If only static fragment information is entered, HEIVAM will *shift* the fragments forward to account for the projectiles forward velocity. This is called a *dynamic shift*. Figures 9 A and B demonstrate the fragment zones and their velocities before and after HEIVAM's dynamic shift. Notice how the zones overlap in Figure 9 B. This is due to the HEIVAM *assumption* that all fragments in a zone display the same characteristic *shift* as the average fragment in that zone. The calculations for this *shift* are simple trigonometric or vector calculations as shown below. Figure 10 visually depicts the layout and relationships.

Trigonometry:

The projectile's forward velocity = PV

Each zone boundary is characterized by:

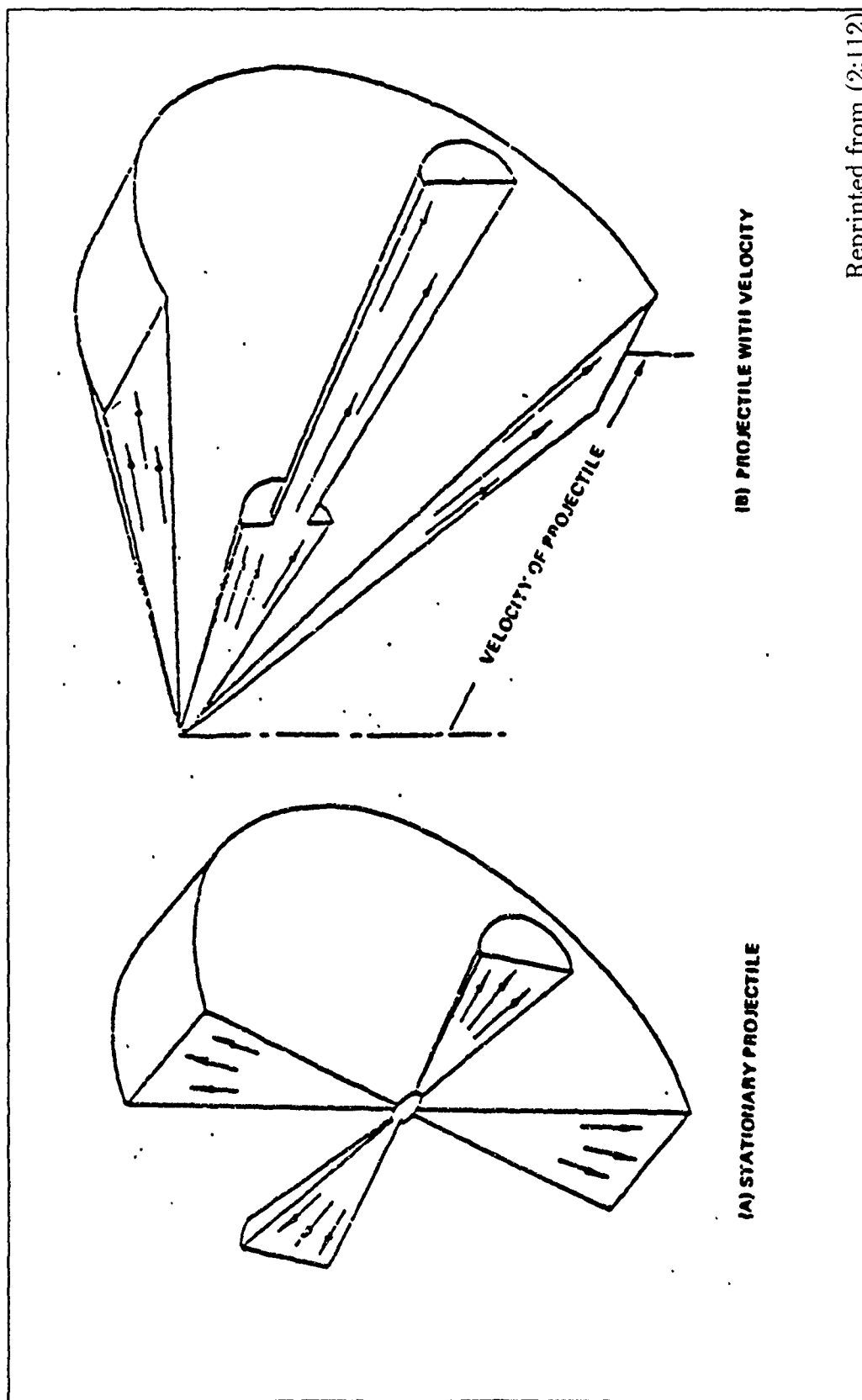
a latitudinal angle = ϕ

a velocity = V_s

After the *dynamic shift* the new zone boundaries are:

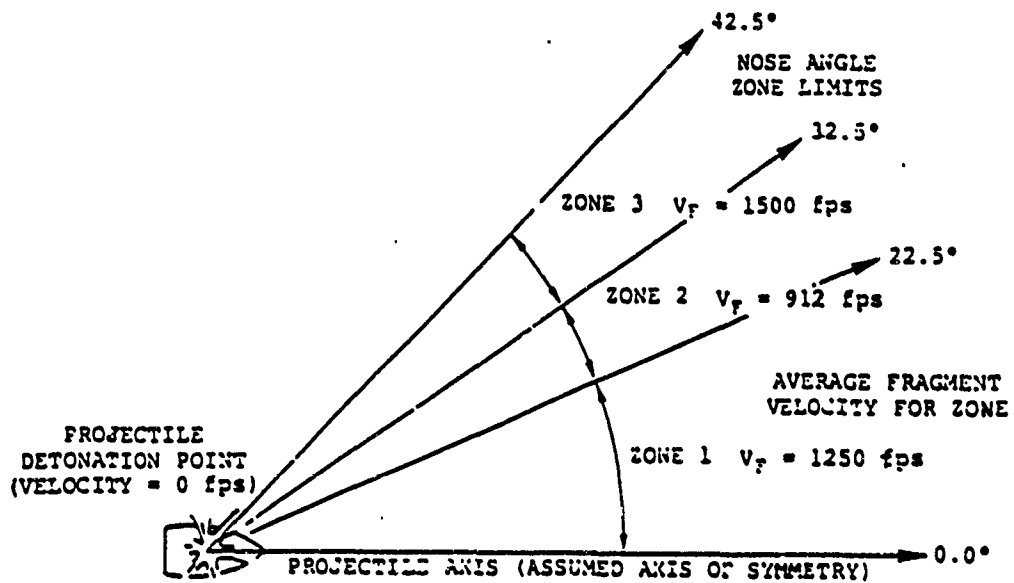
new latitudinal angle = θ

new velocity = V_d

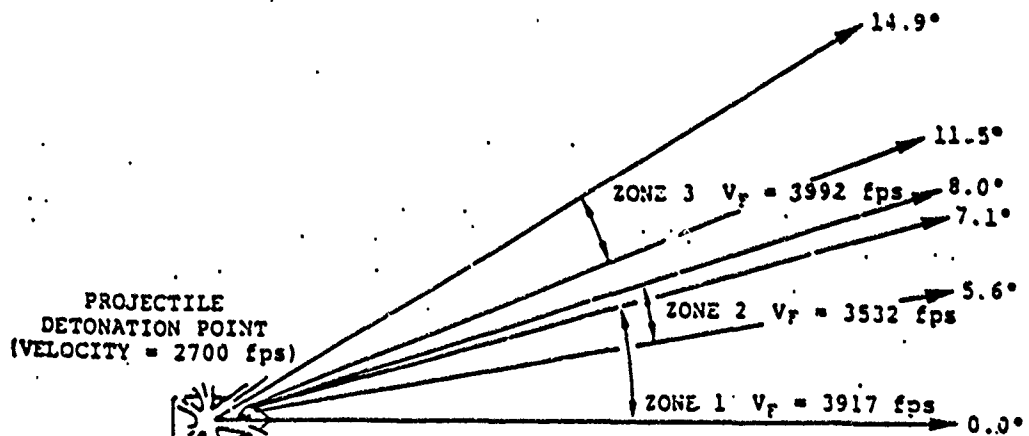


Reprinted from (2:112)

Figure 8. Effect of Velocity on HEI Fragment Trajectories



a. Static Fragmentation Geometry



b. Dynamic Fragmentation Geometry

Reprinted from (6:Vol I, pp.22)

Figure 9. Fragmentation Data Geometry for Three Zones

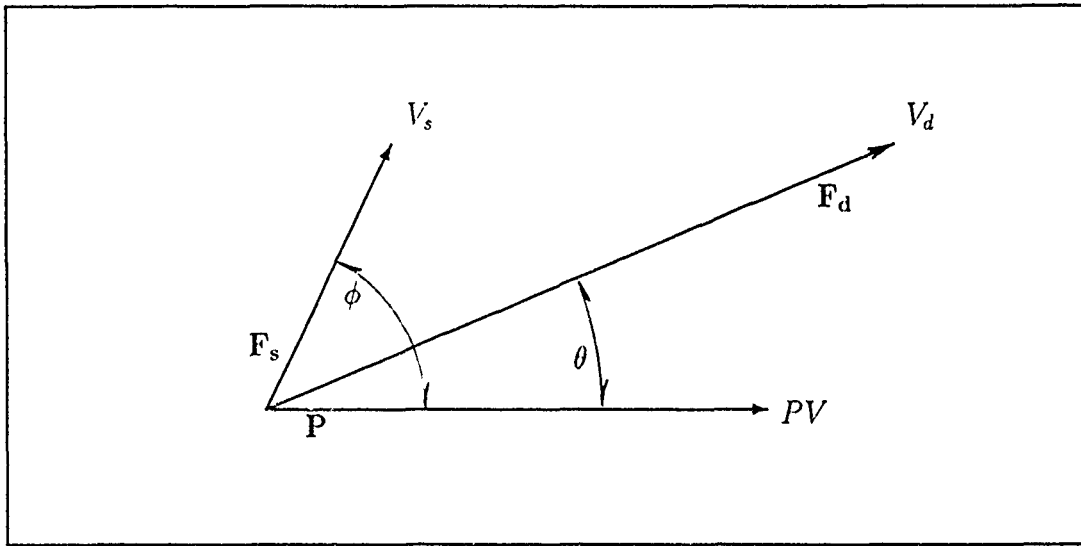


Figure 10. Geometry of Dynamic Shift

$$\theta = \arctan \left[\frac{V_s \cdot \sin \phi}{V_s \cdot \cos \phi + PV} \right] \quad (1)$$

$$\begin{aligned} V_d &= \left[(V_s \cdot \sin \phi)^2 + (V_s \cdot \cos \phi + PV)^2 \right]^{1/2} \\ &= \left[(V_s^2 \cdot \sin^2 \phi) + (V_s^2 \cdot \cos^2 \phi + 2 \cdot V_s \cdot \cos \phi \cdot PV + PV^2) \right]^{1/2} \\ &= \left[V_s^2 (\sin^2 \phi + \cos^2 \phi) + 2 \cdot V_s \cdot \cos \phi \cdot PV + PV^2 \right]^{1/2} \\ &= \left[V_s^2 + 2 \cdot V_s \cdot PV \cdot \cos \phi + PV^2 \right]^{1/2} \end{aligned} \quad (2)$$

Vector Addition:

Vectors convey both direction and magnitude. Therefore, no trigonometric functions are needed.

Let P = the projectile vector.

Let F_s = the static fragment vector.

Let F_d = the dynamic fragment vector.

$$F_d = P + F_s = F_s + P$$

Using Equations 1 and 2 the 22.5° boundary defining both zone 1 and zone 2 is dynamically shifted into two unequal boundaries by HEIVAM. These two distinct boundaries are illustrated in Figure 9.

ZONE 1

$$\begin{aligned}\theta &= \arctan \left[\frac{1250 \cdot \sin(22.5^\circ)}{1250 \cdot \cos(22.5^\circ) + 2700} \right] \\ &= 7.0738\end{aligned}\tag{3}$$

$$\begin{aligned}V_d &= \left[1250^2 + 1250 \cdot 2700 \cdot \cos(22.5^\circ) + 2700^2 \right]^{1/2} \\ &= 3884.4159\end{aligned}\tag{4}$$

ZONE 2

$$\begin{aligned}\theta &= \arctan \left[\frac{912 \cdot \sin(22.5^\circ)}{912 \cdot \cos(22.5^\circ) + 2700} \right] \\ &= 5.6265\end{aligned}\tag{5}$$

$$\begin{aligned}V_d &= \left[912^2 + 2 \cdot 912 \cdot 2700 \cdot \cos(22.5^\circ) + 2700^2 \right]^{1/2} \\ &= 3559.7283\end{aligned}\tag{6}$$

These new velocities given in equations 4 and 6 do not match zone 1 nor zone 2 average velocities, after dynamic shift, as shown in Figure 9B. Because HEIVAM computes the average velocity for the zone, it must compute both boundary velocity vectors for a zone, and average them. This average of the zone boundary velocities becomes the new average velocity for the zone. For zone 2 this velocity is the average result from equations 6 and 7 as demonstrated in equation 8 below.

$$\begin{aligned}V_d &= \left[912^2 + 2 \cdot 912 \cdot 2700 \cdot \cos(32.5^\circ) + 2700^2 \right]^{1/2} \\ &= 3503.6093\end{aligned}\tag{7}$$

$$3531.6688 = \frac{3559.7283 + 3503.6093}{2}\tag{8}$$

2.2.5.3 *TS vs HEIVAM.* The TS program does not address the issue of fuse functioning. This type of processing can be incorporated in the modular structure of TS at a later date if required. But for now, the program assumes that all fuzes function normally. In addition, TS does not calculate ballistic limits. Currently, this is not a factor since no obstructions except the fuel tank itself are incorporated into the empirical testing of fuel fires by WL/FIVST, Wright Patterson AFB, Ohio.

Fragmentation processing is very critical in the TS program. Therefore this processing is much more detailed than the HEIVAM processing. As will be discussed in Chapter 4, each fragment is generated, tracked, and adjusted virtually independent of all other fragments. There are no problems associated with *zone* over-lapping, nor average zone velocity assumptions.

2.2.6 *Component Association Table* Each component that is intersected by a ray as described in Section 2.2.5 requires a damage assessment. If the component is large, and therefore has more than one intersecting ray, the damage assessment increases the expected damage on a usually decreasing marginal basis. If the component is small, the PGEN program will assure at least one intersecting ray.

After the damage assessment of each component intersected is accomplished, HEIVAM uses component association tables to determine the aircraft's vulnerability to the HEI threat. A component association table such as the one shown in Figure 11, itemizes the following information for each component. In part, it indicates and controls the threat or damage mode that a component is susceptible to (6:Vol I, pp.23-27).

NAME Component number.

MATERIAL Component construction material.

DEN Relative density percentage or equivalent material thickness.

ANG Specification to adjust single fragment damage values for multiple fragment hits. The Options are: high density component; low density component; centroid component; or non- critical component.

LU Identifies both the components group and the criticality (non-criticality) to the group.

DM, LX & KILL Damage Mode vulnerability. A component can be listed several times for different damage mode vulnerabilities.

2.2.7 Fault Tree A fault tree describes the functional interrelationship between components. It also controls how individual component damage values are combined to predict the overall aircraft target vulnerability. Figure 12 shows 4 possible excerpts

from a fault tree. Each block represents a component (C), system (S), or group (G).² The progression from Figure 12A through Figure 12D shows the step by step breakdown of a group into its systems, subsystems, then components. The lines indicate the relationships.

The fault trees, input by the user, specify how components higher or lower on the tree, are secondarily affected by the primary component damage. Each of these components, in turn, are related to the next level up or down the association tree. In this way, complete destruction of one component may cause a failure to many other components based upon the line linkages. Ultimately, these links end at the aircraft level. (6:Vol I, pp.48-53)

²There can be many more subdivision levels than the four shown here.

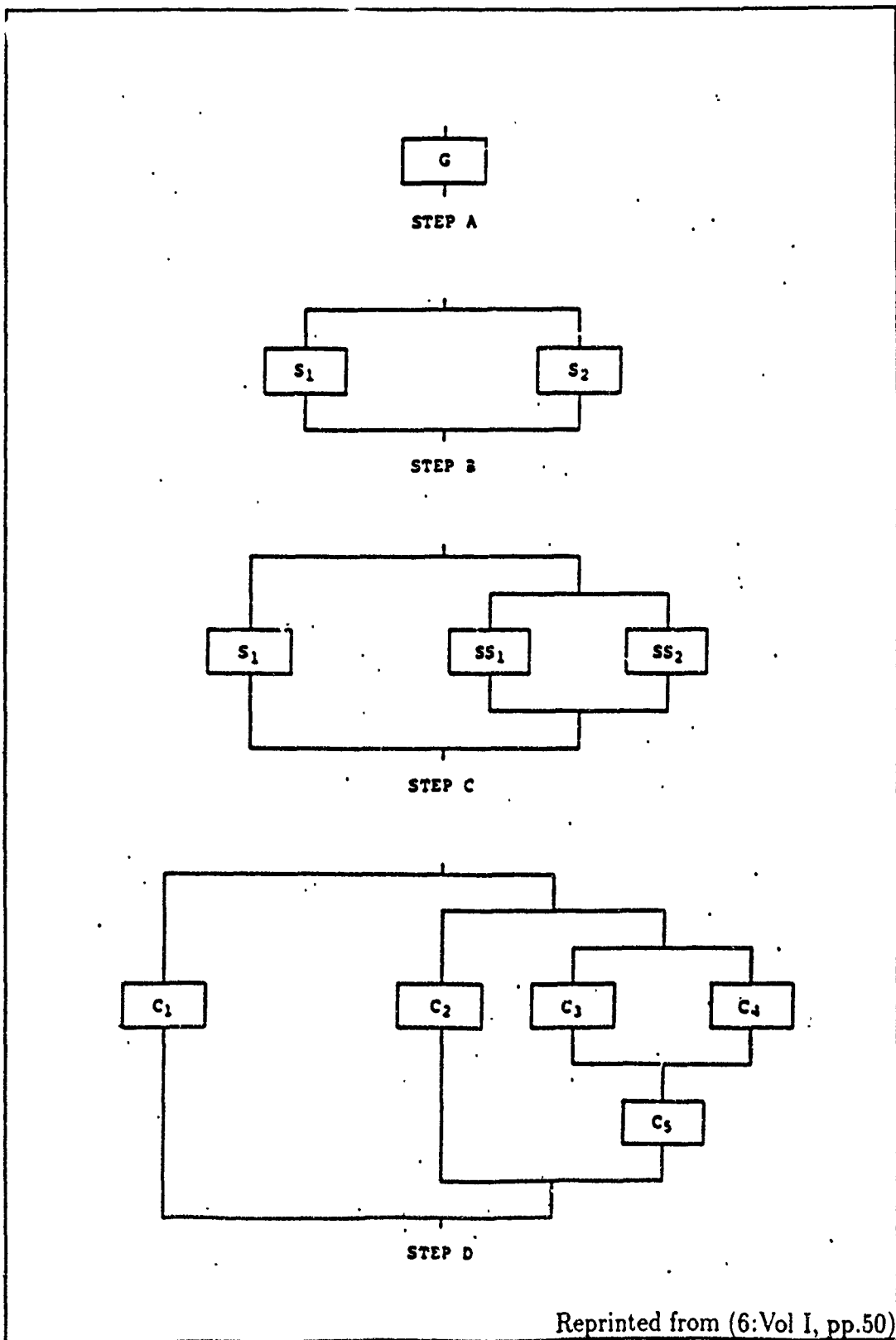


Figure 12. Breakdown of Group

2.2.8 Damage Modes HEIVAM has 5 different damage modes which can individually or combinatorially be applied against any component. The damage modes are listed below. Figure 13 shows the relative regions where the blast, fragmentation, and lethal radii damage modes apply and overlap.

- Blast Pressure
- Conventional Fragmentation
- Fuel Fire
- Lethal Radii
- Hydraulic Ram

2.2.8.1 Blast Pressure.

Pure blast damage is sustained by a component due to disturbances created in the medium surrounding the component when no fragment impacts are possible. In general, a component will sustain a maximum kill if located within a minimum range from the burst point [$R_B(\text{MAX})$], and will sustain no damage if it is located beyond a maximum range from the burst point [$R_B(0.0)$]. These ranges are generally referred to as the maximum damage and the minimum damage range. Between the two ranges, the component will sustain damage at less than the maximum level. (6:Vol I, pp.28)

The effects of blast pressure are very similar to those described for the lethal radii damage mode described below. However, blast pressures surround the HEI upon detonation. HEIVAM assumes these pressures to be more or less "spherical" in nature. This has not been shown to be true as will be discussed in Section 2.5. The HEIVAM model does not consider the surroundings that may change the effect of blast pressures upon the component. This, in effect, assumes an open air explosion. A further discussion of this assumption is contained in Section 2.2.8.4.

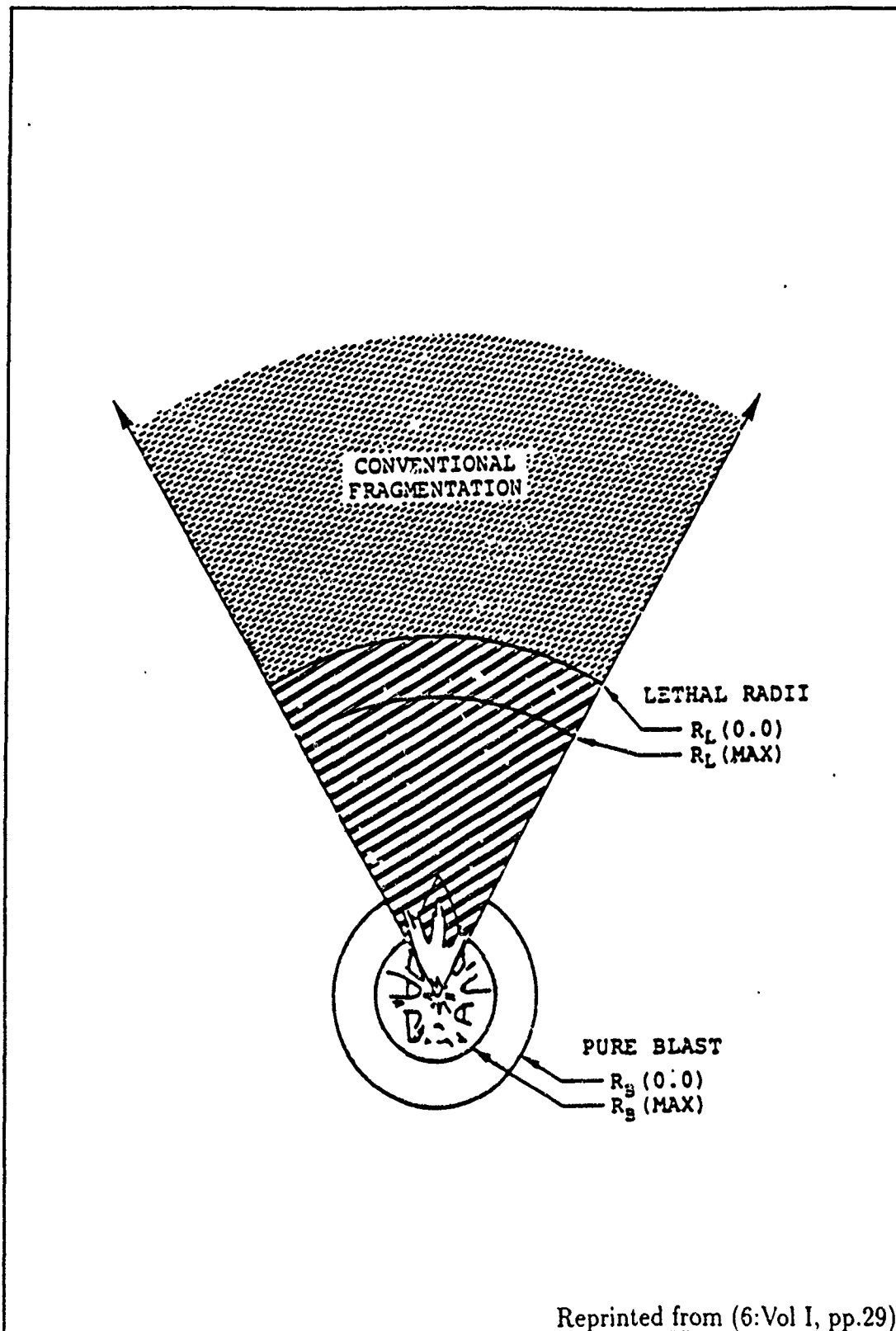


Figure 13. Burst Point Regions Where Damage Models are Used

2.2.8.2 *Conventional Fragmentation.* The distribution of fragments is often measured in fragments per steradian. Therefore, the reader needs to understand what a *steradian* is. As an analogy, the population density of persons within a specific community is measured in persons per square mile: i.e., 2000people/mi². Just as a square mile (mi²) is a measurement of area, so is a steradian. But, whereas square miles measure a squared linear distance, steradians measure a unitless surface area of a sphere. Of course the surface area of a sphere, measured in square miles, changes as the radius of the sphere changes. The equation of this relationship between the sphere surface area (A), and radius (r) is:

$$A = 4\pi \cdot r^2 \quad (9)$$

The unit of measure for the radius (r) might be miles, inches, meters, etc The units of measure is therefore important in the equation above, but it can sometimes be a bother to track. When the units are not particularly important, the *steradian* can be used as the unit of measure. Although the steradian is a unit of measure itself, it has no physical dimensionality such as an inch or a mile. The equation relating the sphere surface area (A), and steradians (S) (similar to equation 9 above) is:

$$A = 4\pi \cdot S \quad (10)$$

There are, therefore, 4π *steradians* (of surface area) for a sphere of any size. This constancy of measurement make an ideal unit of measure for fragments generating outward in a spherical pattern. No matter how far the fragments travel from the center of the sphere, their number does not increase or decrease. The density of particles, measured in fragments per square inch (or other linear measuring unit), diminishes in proportion to the square of the distance traveled. The density of particles, measured in fragments per steradian, does not diminish. This density measure

remains constant regardless of the fragment distance traveled. With this in mind, the following quotation can be understood.

The conventional fragmentation model used by HEIVAM addresses the spray of metallic fragments created as a result of the breakup of the case of a detonating HEI projectile. ... Tests are generally performed on generic components such as fuel pumps, radios, fuel lines, etc. to determine combinations of fragment weights and velocities that will cause the component to fail. These weight and velocity combinations are used to produce a damage function for the component that relates the probability of kill given a hit ($P_{K|H}$) for the component to the mass and velocity of a single striking fragment.

... For rays falling within the fragmentation zones, the probability of kill given a hit, abbreviated as $P_{K|H}$, for the component may be determined given a striking fragments weight and

velocity using a damage function for the component. Since the computed $P_{K|H}$ for the component at this point reflects only the kill for a single fragment traveling along a single ray-line path, it must be adjusted to account for the total number of fragments expected to impact the component. In the PGEN program, the user specifies the number of times the surface area of a sphere is to be divided. A ray is then defined to originate at the center of the sphere that passes through the center of each spherical surface area segment. There is a solid angle associated with each of these segments that is also associated with the ray. When weapon fragmentation data are read from input by the HEIVAM program, fragment spatial densities (in fragments per steradian) are calculated and stored for each zone.

Therefore, knowing the zone within which a ray lies then allows look-up of the fragment spatial density (i.e., the number of fragments per steradian) associated with that zone. This is assumed to be the density of the fragments throughout the solid angle associated with the ray. The total number of fragments associated with the ray under consideration expected to impact the component may then be calculated. Then, given a single fragment $P_{K|H}$ and an expected number of fragment hits N , the component probability of kill P_k is calculated using the expressions:

$$P_K = 1.0 - (1.0 - P_{K|H})^N \text{ for } N > 1$$

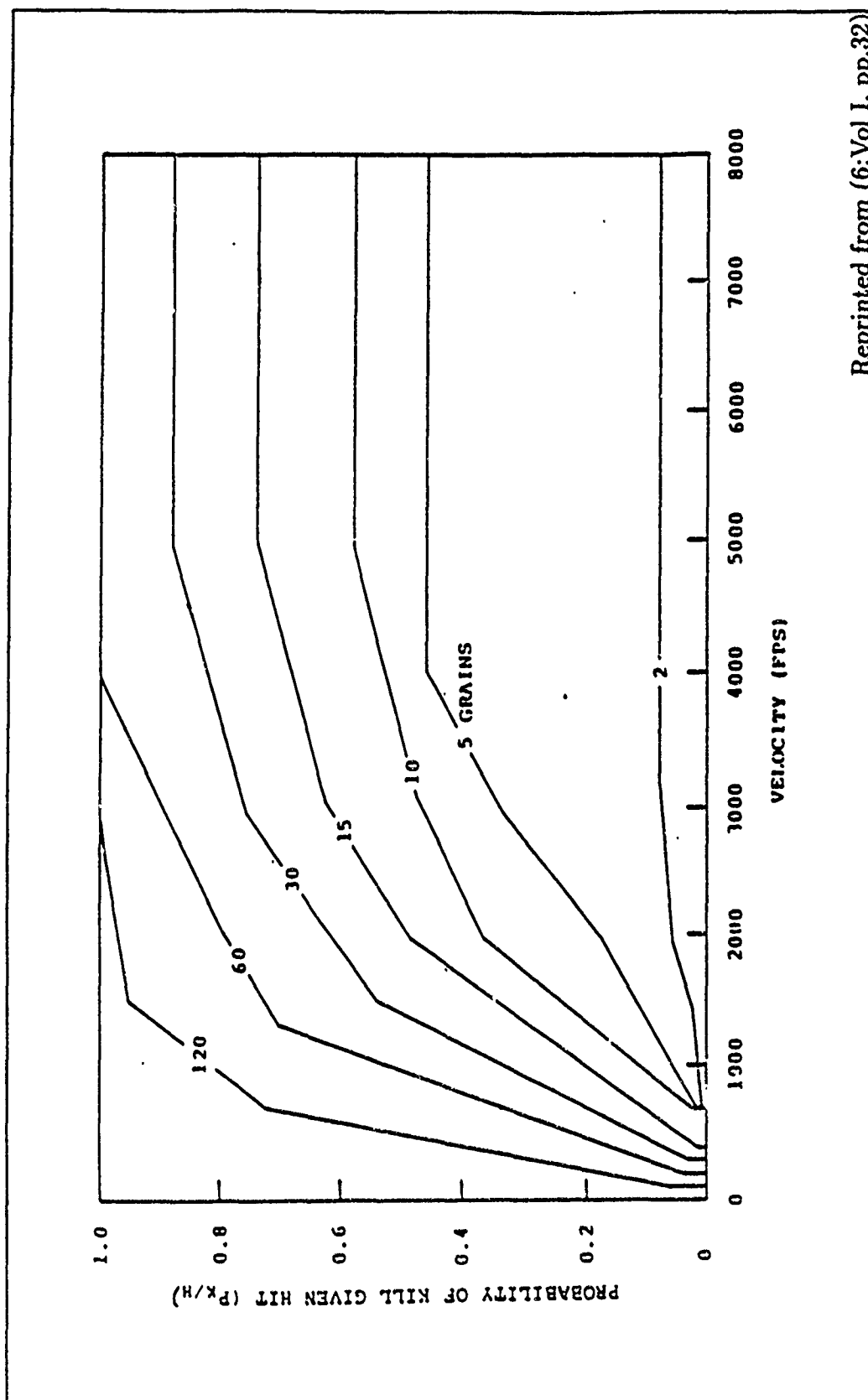
$$\text{and: } P_K = N(P_{K|H}) \text{ for } N \leq 1$$

(6:Vol I, pp.30-32)

For clarity purposes, it should be noted that the first equation above encompasses the second. Therefore the second equation can be eliminated if the condition of the first, $N > 1$, is changed to $N > 0$. It should also be noted that the $P_{K|H}$ and subsequently the P_K , are dependent upon the fragment mass (or weight). Each fragment therefore requires a separate calculation.

Figure 14 shows a typical step function defining the $P_{K|H}$ used by HEIVAM. This type of function does not account for the many other parameters that may have substantially more importance in determining expected damage. Other such parameters include the relative timing of multiple fragment hits, the striking obliquity angle, the temperature of both the fragment and the components, the components structural weak spots, etc But, if these other conditions were active during the tests used to develop the damage function, then these other parameters can basically be ignored. The user of HEIVAM must be aware of the operating conditions assumed by the model and adjust these through the function inputs as required.

The HEIVAM quotation above stresses that the spatial distribution input by the user is *assumed* to be constant throughout the "solid angle [area] associated with the ray." Given a small grid size in relation to the distance between the component and the detonation point, this assumption is virtually true. If the grid size is not small, or the distance between component and detonation point is great, the assumption becomes suspect. To make this clear, imagine viewing a large crowd from 1000 feet above street level. Pick a relatively small area of that crowd that appears to have a uniform density of people. Now view the same small area from 10 feet above street level. The density of people may no longer appear uniform. This same effect is



Reprinted from (6:Vol I, pp.32)

Figure 14. Typical Single $P_{K/H}$ Step Function

true for fragment density when the grid size is large, and/or the detonation- component distance is large. This is especially true when the spatial distributions input by the user are for static detonations. In this case, HEIVAM performs a *dynamic shift*. Section 2.2.5 discussed the problem of separating and overlapping zones created by HEIVAM's dynamic shift routine.

2.2.8.3 Fuel Fire. The purpose of the HEIVAM fuel fire model is to predict the vulnerability of a target aircraft to small HEI projectiles impacting on or around the aircraft fuel tanks. This model has several restrictions. Two are particularly important. One, the model assumes an optimal fuel/air mixture exists which will maximize the probability of a fuel fire. Two, the only fuel fire protection allowed by the model is a 3 inch thickness of either flexible or foam void filler. As in the other damage models, a table look up of the $P_{K|H}$ is performed to arrive at a damage expectancy.

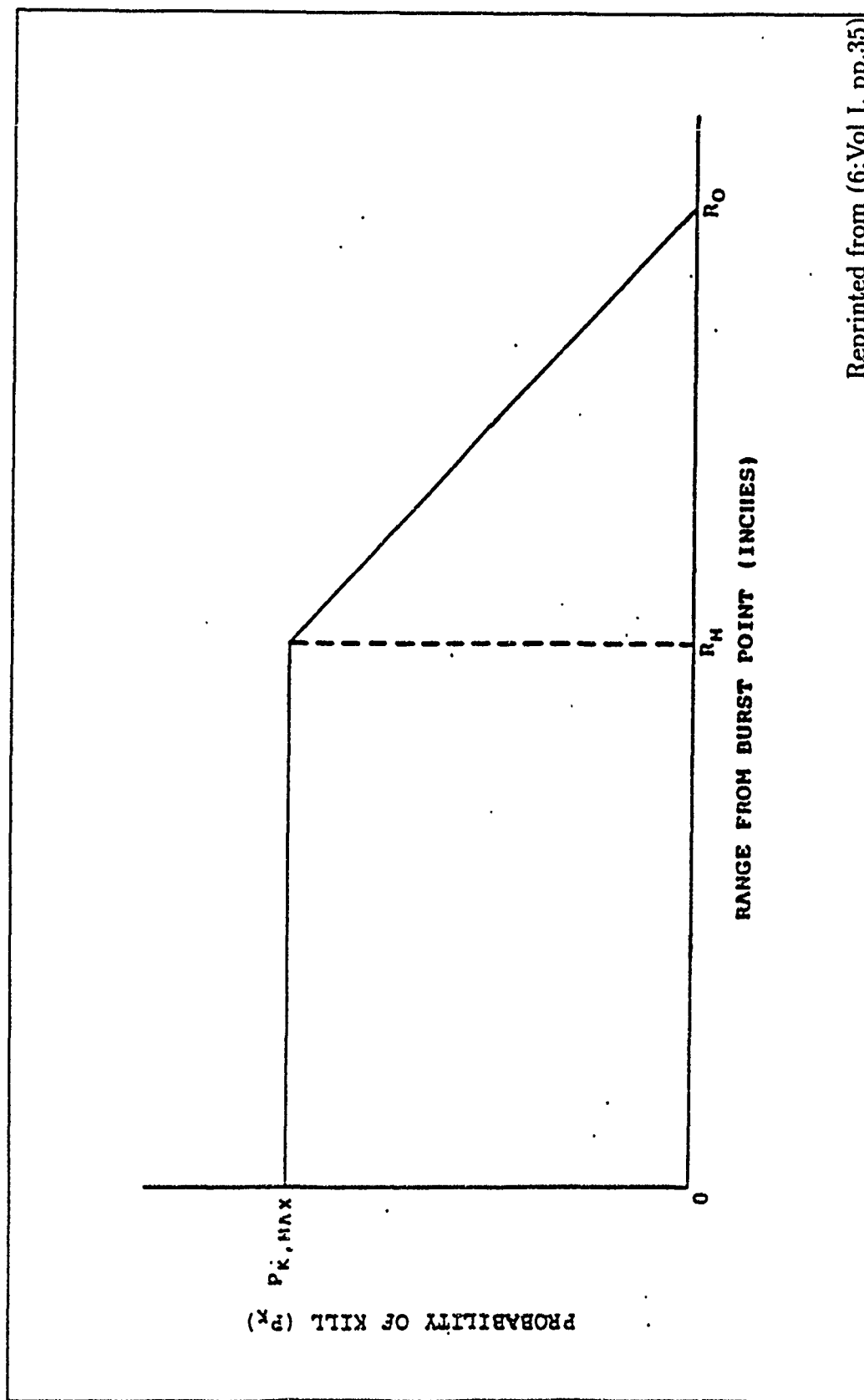
2.2.8.4 Lethal Radii

The lethal radii model used in HEIVAM is designed to treat damage effects in the near field (i.e., in the region within about 12 to 15 inches from the burst [detonation]) where the effects of many small fragments, impacting nearly simultaneously with the arriving blast wave, tend to accumulate. It has been observed that damage in this region is generally more severe than if fragmentation and blast effects were determined separately and then combined. An accurate analytical lethal radii model is not presently available for incorporation into HEIVAM. Therefore, lethal radii effects are considered simply through use of a damage function as illustrated in [Figure 15]. HEIVAM determines the range to the component from the burst point and compares it to the ranges (R_m and R_o) input for the damage function. If the range is less than the range for which maximum damage is sustained (R_m), the associated component $P_{K|H}$ value is assigned the maximum $P_{K|H}$ value associated with the curve (PK_{max}). If the range is beyond the range for which no damage is sustained (R_o), the component damage value is defined as zero. If the range is between R_m and R_o , a linear interpolation is performed to determine the damage value. (6:Vol I, pp.35)

Because of the interaction of blast pressures with their surroundings, HEIVAM makes a couple of simplifying assumptions. First, the surroundings are assumed to be non-existent and therefore unable to reflect, amplify, and redirect pressures. This assumption also underestimates the increased pressure duration caused by surroundings that confine the blast pressure. Second, the surroundings can likewise diminish the blast pressure. If a sufficiently large and stable barrier is positioned between the blast and the component, the pressure exerted on the component can be diminished or eliminated. HEIVAM accomplishes this as described below. It should be noted that HEIVAM does not account for the size of the barrier. The size is critical since a blast wave is capable of going around objects. In fact, these objects, as stated before, can increase or decrease the pressure on the target component depending on their size and position within the dry bay. The limitations of this damage model are, in part, recognized and documented in the User Manual. The implication is 'user beware.'

An additional parameter input for use by the lethal radii model is an equivalent critical thickness of aluminum that may exist between the burst point and the component without having a degrading effect on damage predicted by the lethal radii damage function. If an accumulated equivalent thickness of aluminum greater than this specified amount is encountered, the intervening material will have a degrading effect. The range to the component is adjusted by multiplying it by the ratio of the accumulated thickness encountered to the specified critical thickness. This action is performed prior to entering the lethal radii curve to determine the component P_{KIH} . The increased range has the effect of degrading the predicted damage value to account for the encountered intervening equivalent thickness of aluminum.

One weakness of the lethal radii model is evident in the fact that, however obtained, a lethal radii component curve is truly applicable for only one set of conditions (such as a unique set of fragmentation nose angle zones with a unique set of fragment weight and number distributions related to a single weapon velocity). . . . This and other weaknesses are recognized but, as previously stated, an accurate analytical model to correctly treat the lethal radii phenomena is not presently available (6:Vol I, pp.35-37)



Reprinted from (6:Vol I, pp.35)

Figure 15. Typical Lethal Radii Damage Function

2.2.8.5 *Hydraulic Ram.*

The hydraulic ram damage model used by HEIVAM addresses fuel tank rupture by an HEI projectile resulting in engine failure from rapid fuel ingestion. Fuel ingestion is the result of a quantity of raw fuel from a ruptured fuel tank being deposited directly into an engine air inlet duct (with or without an accompanying fire). (6:Vol I, pp.44)

The probability of hydraulic ram damage is either 1 or 0 depending on whether or not the back wall of the fuel cell is expected to rupture. This, in turn, depends on the projectile's obliquity angle penetration into the liquid fuel [as apposed to the vapors] of the fuel cell, and the distance from entry point to back wall. Given the thickness of the fuel cell material, a relationship such as that shown in Figure 16 is used to categorically decide whether the cell ruptures or not.

2.2.9 TS Damage Model The TS program does not, in its current form, account for any damage and therefore does not use anything analogous to the damage models of HEIVAM. Other on-going research and thesis efforts are currently studying and developing damage models. One such effort, being accomplished by Crawford, will result in a simulation of a fuel cell fire (8). Follow-on work will integrate the fuel fire simulation with the TS program to form a complete simulation of the HEI threat to a fuel cell. Similar follow-on work can also expand the utility of the TS program.

2.3 *COVART*

COVART stands for Computation Of Vulnerable Areas and Repair Times.

The COVART system is very similar to the HEIVAM system described in Section 2.2. in fact, HEIVAM was developed in 1981 by modifying COVART I. Because of this, the descriptive detail of Section 2.2 will not be repeated in this section.

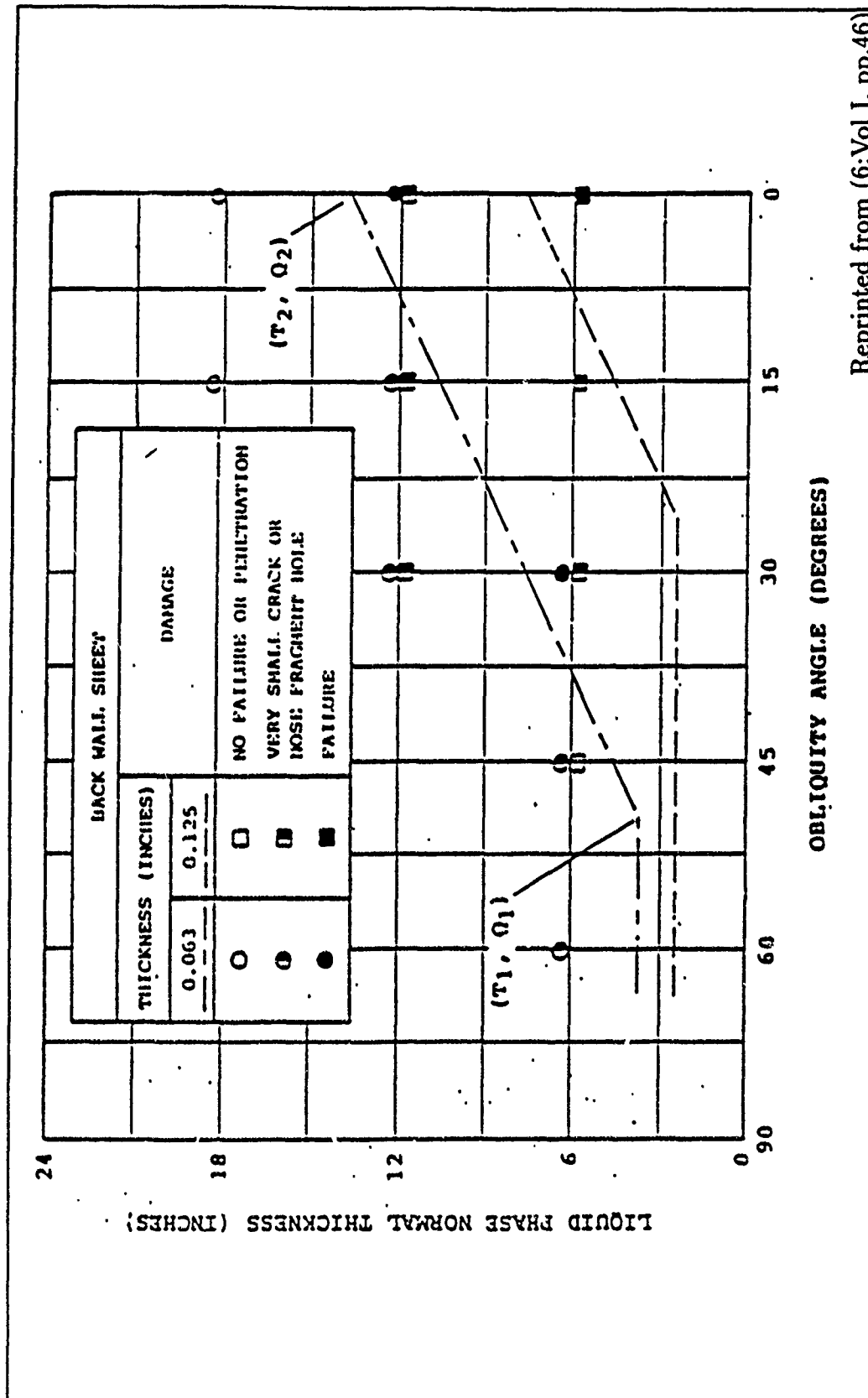


Figure 16. 20-mm HEI Fuel Tank Back Wall Rupture

2.3.1 *COVART vs HEIVAM* COVART processing is very similar to the HEIVAM processing in form, purpose, and function. As such, the COVART system is also similar to the TS system in basic approach and content, but differs greatly in purpose and detail.

Whenever a critical component is struck by the penetrator, the probability that the component is defeated is computed using input conditional probability of kill data. These data express the component kill probabilities as functions of threat impact (weight and speed). The component defeat probabilities are then combined, according to the various target damage definitions, in order to produce the target defeat probabilities for the given threat. (21:1-1,2)

2.3.1.1 *Threat Characteristics.* The primary difference between HEIVAM and COVART is the threat mechanism. In HEIVAM, the threat is a high explosive incendiary projectile. In COVART, the threat is a single kinetic energy penetrator or armor piercing incendiary (API). The COVART threat is often referred to as a *penetrator* rather than a projectile. The API penetrator is non-exploding. As suggested by its name, its function is to penetrate or pierce a target's armor and initiate further damage through incendiary functioning. In general, the thicker the armor that is pierced, the better the incendiary function. Further, the better the incendiary function, the greater the chance of igniting or exploding a target's fuel or other flammable material.

2.3.1.2 *Attack Characteristics.* Penetration equations are more important to COVART than to HEIVAM. They therefore are updated, and studied more in the COVART system. Yet, on the surface, the same fundamental actions are modeled in both systems with one exception. They both model ricochet angle and speed, projectile slow-down in fluids, and incendiary function for their respective threats. But, COVART additionally models the *yaw* of its penetrating projectile.

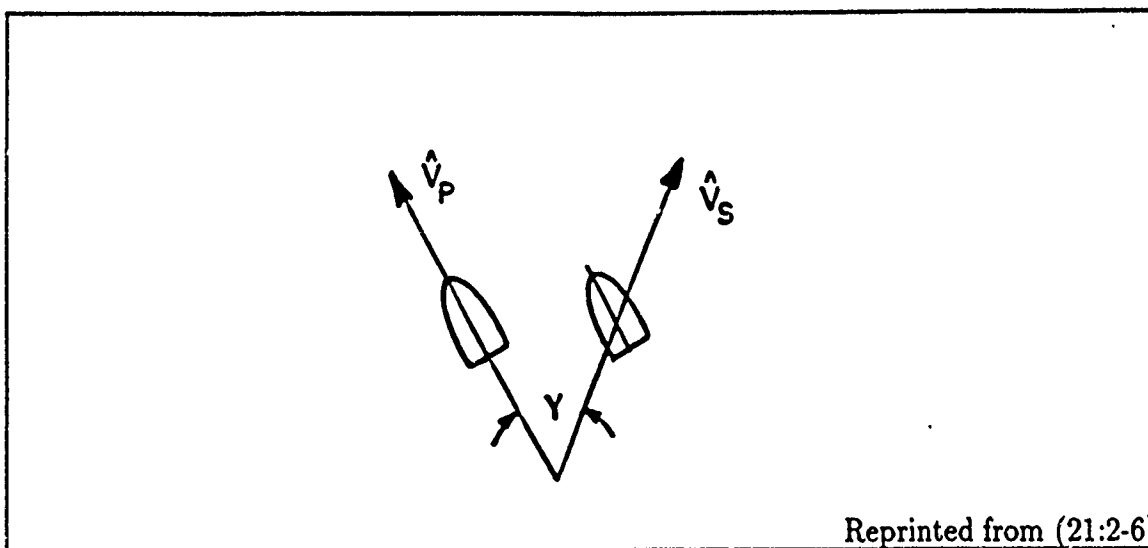


Figure 17. Vector Diagram for Apparent Yaw

The yaw, in COVART, describes the alignment of a projectile's longitudinal axis with the *effective* attack direction. The effective attack direction is the combination of the projectile velocity vector and the target velocity vector. One type of yaw which COVART does not address is the oscillation of a projectile's longitudinal axis around its velocity vector only. This type of yaw is usually thought to be small or non-existent due to the self aligning rotation (due to rifling) of the projectile.

If the penetrator is unyawed along its trajectory in the inertial reference system, it will appear yawed to an observer on the target as a consequence of the target forward speed. The COVART II program includes this yaw in its treatment of penetration equations, as prescribed in the Penetration Equation Handbook (19). [The] Magnitude of this yaw angle, Y , is the magnitude of the angle between the trajectory vector V_p [the effective attack direction], and the shotline vector, V_s [the projectile longitudinal axis]. To illustrate this, consider the vector diagram of Figure [17]. A penetrator moving unyawed in the direction indicated by the vector, V_p , appears to an observer on the target to be approaching along the direction indicated by the vector, V_s . (21:2-5,6)

The yaw is used in the determination of damage probabilities. In general, the more yaw there is, the more presented area a projectile exposes to the target. The

HEIVAM system does not account for yaw. This can be critical to an HEI explosion since a slight change in the projectiles exposure toward a target changes the area from which impacting fragments will originate. Because different zones around an exploding HEI projectile have different fragment densities and weight distributions, the yaw can change the probability of damage to every surrounding component. Reference Section 2.2.8.2.

2.3.1.3 System Inputs. Just as in HEIVAM, COVART requires several input files that are generated from various other systems including FASTGEN (10), SHOTGEN (18), PGEN (26), and GIFT (3). Each of these systems in turn, has its own input requirements. Therefore, understanding COVART output requires an understanding of the impact each of these input systems has upon COVART. However, these systems and there impact are not reviewed here since they perform the same basic function for COVART as they do for HEIVAM.

2.3.2 Repair Time COVART also offers the prediction of repair time if the target is expected to survive to be repaired. This prediction of repair time was one of the overriding motivations for the creation of COVART.

For years aircraft vulnerability and survivability analyses have been concerned almost exclusively with attrition and prevent mission damage categories. In recent years, numerous studies have been made to evaluate damage to aircraft hit by hostile ground fire in Southeast Asia. Damage nomenclature has ranged from "continued to fly" to "shot down and lost". The studies reveal that damaged and recovered aircraft can impose a burden upon the maintenance system when a large volume of minor or major repairs is required. These repairs could be a significant factor in logistic, tactical, and strategic planning. Further consideration of this repair problem demonstrates the need for a new kill category in aircraft vulnerability, sometimes referred to as a "soft" or "mission available" kill. The damage criterion developed for this type of kill is based on repair time. An objective of the COVART program is to provide a method for associating meaningful repair times with specific threat types that are likely to hit deployed aircraft. (21:1-2)

2.4 HEI Fragmentation

This section reviews the current literature describing HEI fragmentation. The first two sub-sections describe the general testing environment used to characterize HEI fragmentation. The remaining sub-sections describe the results reported in the literature. These reports characterize fragmentation via static fragmentation and/or dynamic fragmentation. Both the static and the dynamic characterizations are presented in terms of fragment velocity distributions, and fragment weight distributions.

2.4.1 Background Information The following paragraphs introduce the basic concepts, and terminology needed by the reader. These concepts and terms are explained here so the material presented in later sections can be outlined without confusion.

2.4.1.1 Static vs Dynamic Detonation. The difference between static and dynamic detonations is simply the absence or presence of forward velocity; a static projectile detonation has no forward velocity, and a dynamic projectile detonation has forward velocity. Static detonations thereby eliminate the confounding effects of an active projectile. Confounding effects include forward, *dynamic shift*, of fragments, possible rifling or rotational shift, projectile yaw, etc

Static detonation tests are conducted by replacing the normal fuse with a detonator such as the M48, or the NND 211 detonator. Any additional space within the fuse cavity is usually filled with Composition C-4 or a similar explosive material.

2.4.1.2 Rifling. Rifling is the rotational spin placed on a projectile as it is fired from a gun. The gun has a screw-like groove on the inside length of the barrel which causes the projectile to spin as it travels through it. This longitudinal spin keeps the projectile from tumbling end over end. It also arms the explosive in most HEI projectiles. The spinning action causes the firing pin to align with the explosive charge thus arming it.

Rifling effects are virtually ignored in the literature and are ignored here also. But, in the absence of contrary information, the author believes that rifling may change a fragment's obliquity angle, velocity, and thus its ability to penetrate a target. The reason for this belief is based on the additional velocity placed on the fragments by this rotation. The rotational velocity ranges between 50,000 and 150,000 revolutions per minute. This could add an additional velocity of 1250 feet per second to the fragment. This velocity has a direction normal to the projectile axis and would therefore increase the obliquity angle of the fragment. Future studies may be necessary and warranted to determine the effects of rifling.

2.4.1.3 Zones. Fragment weight and velocity distributions are typically reported for each of several zones. These zones, as pictured in Figure 18, are best visualized as flat, circular slices of a hollow Earth. The projectile, placed at the center of this hollow Earth, is aligned with the Earth's longitudinal axis. The fuse (or front) end of the projectile points toward the North, and the trace (or tail) therefore extends toward the South. Just as the Earth's latitude separates it into circular bands, the *zones* separate the imaginary sphere of exploding fragments into circular bands.

The only difference between the Earth's latitude and the zones is where the 0° marker is placed. The 0° Earth latitude is placed at the equator and increases 90° toward each pole for a total of 180°. The zones 0° latitude is placed at our imaginary sphere's North Pole and increases 180° toward the imaginary South Pole.

The zone size varies from study to study, but is usually between 5° and 15°. Once decided upon, the zone size is usually held constant. Although, there are exceptions such as in HEIVAM inputs.

2.4.1.4 Explosive Charge. The 23-mm HEI has the explosive capability of roughly 13 grams of Composition C-4 explosive. The actual explosive filler is composed of RDX, aluminum and a binder, and weighs between 11 and 14 grams.

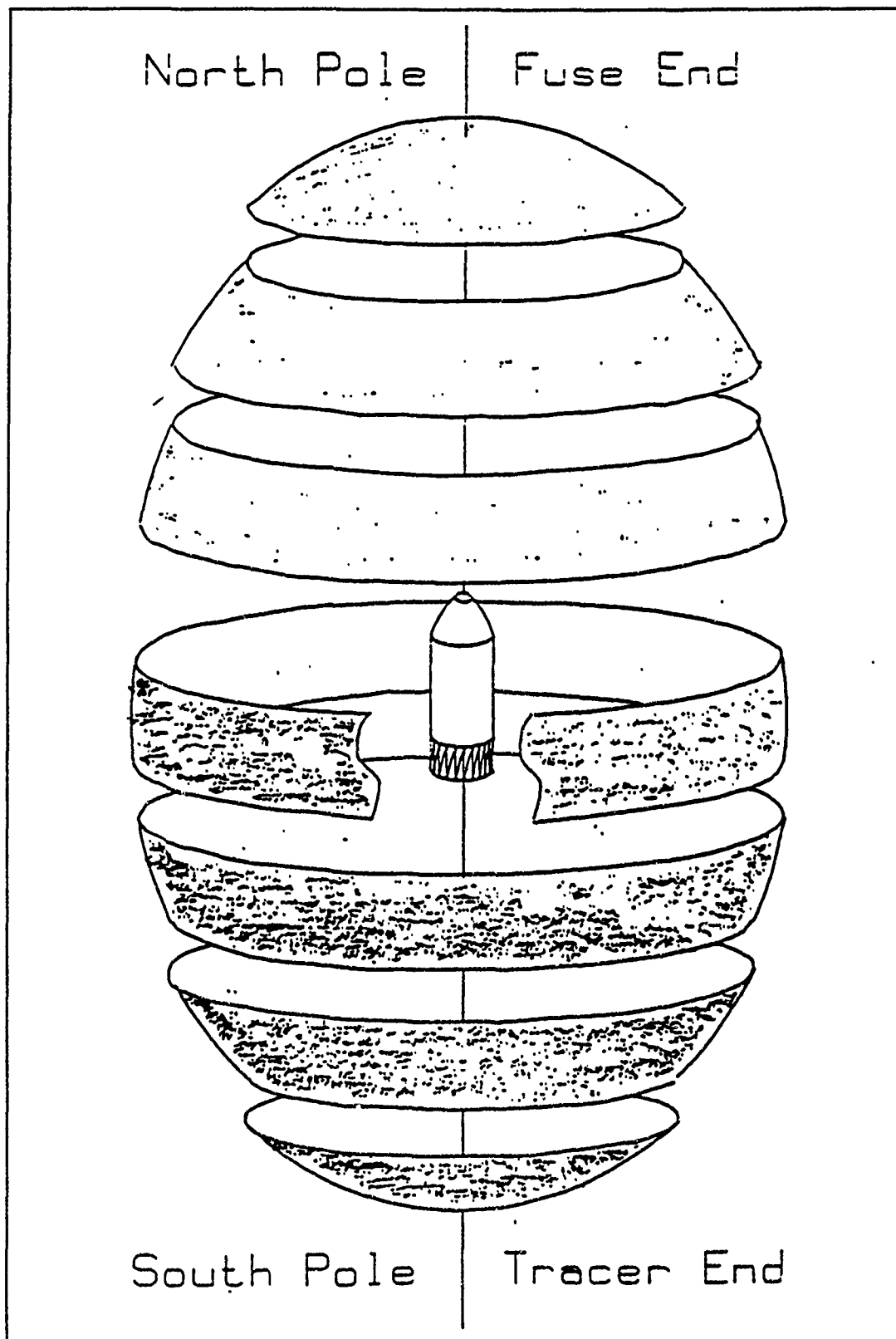


Figure 18. Fragment Zone Analogy to the Earth

The RDX acts as the explosive and the aluminum acts as the incendiary material. Aluminum burns relatively slowly and thus prolongs the potential fire threat beyond the time of explosion (2, 1).

2.4.2 Test Arena The test projectile is placed in the center of a circle or partial circle of bundles which represents the outer limit of the imaginary sphere described in Section 2.4.1.3. This setup is called the open fragmentation test arena. The bundles on the perimeter of this arena act as velocity sensors and/or fragment traps as shown in Figure 19. The open fragmentation test arena must assure that the fragments from which data is gathered have flight paths directly from the test projectile to the bundles along the perimeter. No data is gathered from fragments that skip off the ground or ricochet off of other objects.

2.4.2.1 Arena Size. The distance between the projectile and the bundles must be uniform and measured exactly. These distances are used to determine both the fragment spatial density (fragments per steradian), and the individual fragment velocities. The method used to determine the spatial density is virtually the same in each study. Fragment velocities on the other hand, are determined with similar equipment but different methods and different results. The inconsistency between velocity measurement methods and results is due to timing

precision requirements. Because the velocity statistics vary from study to study the method used will be stated along with the data and result for each study introduced below.

2.4.2.2 Projectile Placement. The axis of the projectile lies in the same plane as the arena's circle of bundles. Further, the projectile axis bisects the ring of bundles so that the distance from the projectile to the top and bottom of each bundle is the same. In this way, the projectile fuse points toward the 0° latitude on

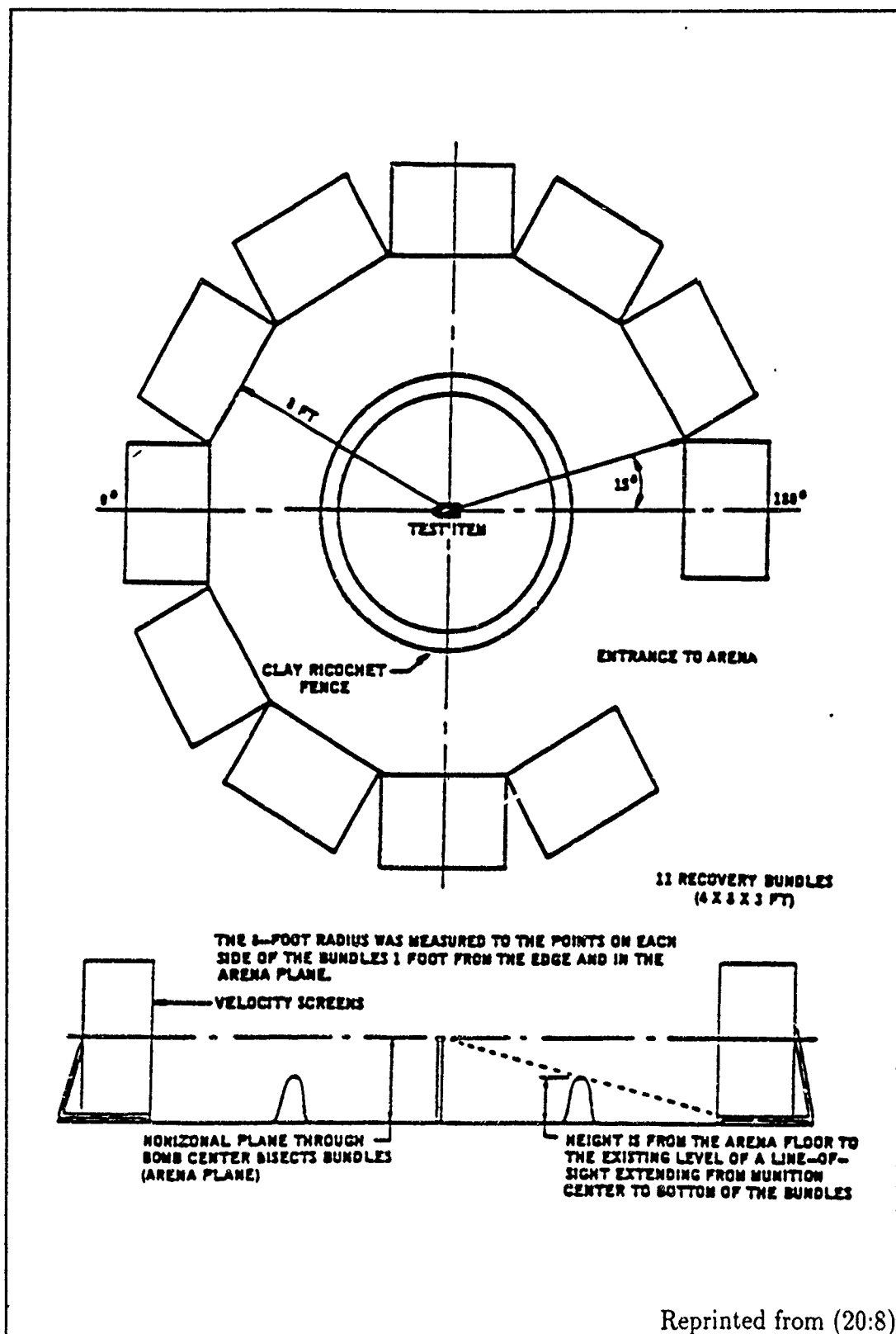


Figure 19. Schematic of 8-foot Radius Open Fragmentation Test Arena

one bundle in the arena circle. The projectile tracer points toward the 180° latitude of the opposite bundle in the arena circle.

2.4.2.3 Zone Statistics. The zones are established at appropriate angular distances around the arena circle. The proportion of each zone represented on the ring of bundles differs from zone to zone. For example, let the arena radius=8 foot and let the surrounding bundle heights=8 foot. With this arena any zone starting at 0° and spanning up to 26° would be completely represented by the bundles as demonstrated by Equation 11. Remember that the bundle height is bisected; $1/2 \cdot 8\text{ft} = 4\text{ft}$.

$$8(\text{ft radius}) \cdot \tan(26.56^\circ) = 4(\text{ft}) \quad (11)$$

On the other hand, a zone bounded by 80° and 100° has roughly 31.8% of the zone represented. The area represented by the bundles is roughly calculated in Equation 12. The equation accounts for the bundles on both sides of the circular arena. Equation 13 calculated the entire zone area.

The expressions in brackets, [*expression*], evaluate θ from 80° to 100°; i.e., the expression evaluated at 80° is subtracted from the expression evaluated at 100°. The ratio of these areas is calculated in Equation 14 is a ratio of proportionality.

$$[\sin(\theta - 90^\circ)]_{80^\circ}^{100^\circ} \cdot 8(\text{ft radius}) \cdot 8(\text{ft height}) \cdot 2 = 44.45(\text{ft})^2 \quad (12)$$

$$2 \cdot \pi \cdot 8^2(\text{ft})^2 \cdot [-\cos(\theta)]_{80^\circ}^{100^\circ} = 139.65(\text{ft})^2 \quad (13)$$

$$\frac{44.45(\text{ft})^2}{139.65(\text{ft})^2} = 31.8\% \quad (14)$$

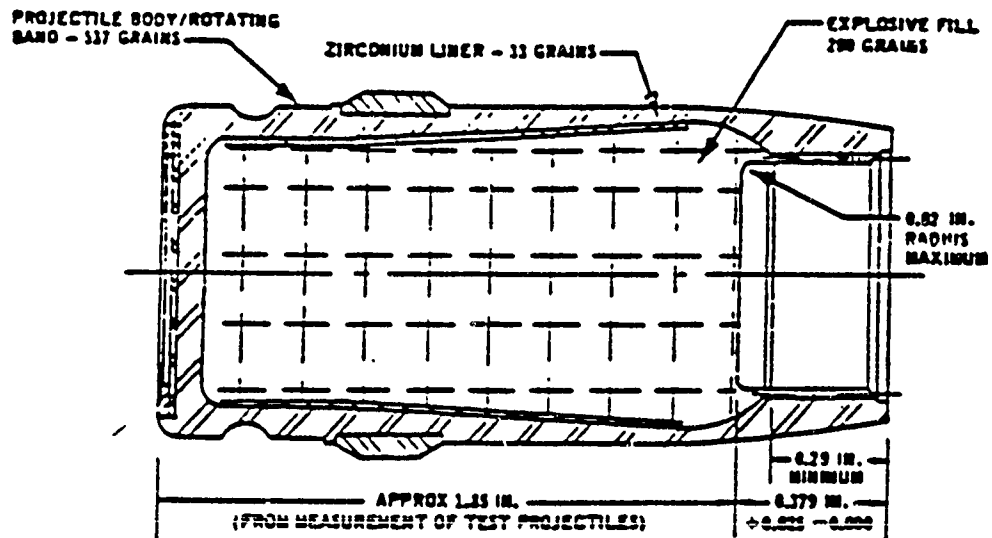
The number of fragments gathered for any zone can be multiplied by the proportion to arrive at the total number of fragments for that zone. Further, the total number of fragments in a zone, divided by the zone's total area yields spatial density of fragments in that zone. The spatial density of fragments is calculated for each zone individually.

Because the surface area of a sphere increases as the radius increases, the spatial density is not unitless. But it can be made unitless by measuring the zone in steradians instead of a squared linear measuring unit. Reference Section 2.2.8.2 for a complete description of steradians.

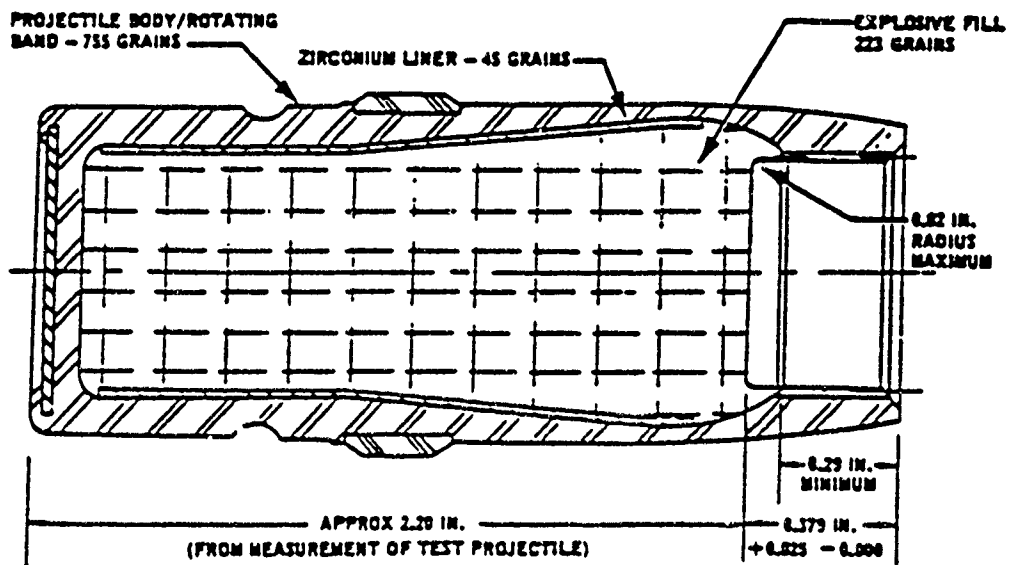
2.4.3 Jones Study This study, conducted by Steven R. Jones and completed in 1976 (20), examines the differences between a standard and two modified 20-mm HEI projectiles. Table 1 provides the weight of the various sub-components of each projectile. Figure 20 shows the casing for the two modified 20-mm HEI projectiles. Both modified projectiles have thin walls compared to the standard 20-mm HEI. Note the difference in overall length, and the slight differences in wall shape and thicknesses at various points within the modified projectiles. The casing material is what is fragmented by the explosion. Because of the projectile casing differences, a significant difference in the number, distribution, and size/weight of the fragments is also expected.

2.4.3.1 Static Detonation - Fragment Velocity. Data and statistics from the standard 20-mm HEI testing are shown in Tables 2-4. In addition, Figures 21 and 22 show summary graphs of the number of fragments per zone and fragment velocity per zone respectively. The shaded area of the fragment velocities represents one standard deviation on either side of the mean.

These tables and graphs are shown here to provide insight into both the fragment patterns, and the data that is typically collected in studies of this type.



A. Minimum Weight HEI



B. Maximum Explosive HEI

Reprinted from (20:3)

Figure 20. Schematic of Modified 20-mm Thin-Walled HEI Projectiles

Projectile body type	Type S std M56A4	Type A, min wt	Type B, max HE
Design component weight (gr)			
Projectile body	1,020	537	755
Explosive fill ^a	170	200	223
Zirconium liner		33	45
Total	1,190	770	1,023
M505A3 fuze type	Standard	Modified	Modified
Approximate fuze weight (gr) ^b	332	400	400
^a Explosive type for all projectiles: 64/34/1, RDX/aluminum/graphite ^b Total weight as modified for static detonation			

Reprinted from (20:2)

Table 1. Summary of 20-mm HEI Projectiles Tested

Data and statistics from the minimum weight 20-mm HEI and the maximum explosive 20-mm HEI testing are shown in Appendix A. The minimum weight 20-mm HEI summary table and graphs are shown in Table 5 and Figures 23-24. Likewise, the maximum explosive 20-mm HEI summary table and graphs are shown in Table 6 and Figures 25-26 respectively.

The reader is warned not to put too much emphasis on the number of fragment hits per zone since the entire zone is not accounted for (reference Section 2.4.2.3). Also, the velocities cited are developed by knowing 1) the time of explosion via the explosion flash, 2) the time of arena bundle penetration via a drop in voltage passed across the surface of these bundles, and 3) the radius of the test arena, which is 8 feet. The velocity measure is therefore the mean velocity over the 8 foot distance and not the instantaneous velocity at the explosion point or the bundle impact point.

Figure 27 shows a composite graph of the number of fragments per zone for all three projectile types. In this figure it appears that the distribution of fragment among the 36 zones varies due to projectile type. This is further supported by the fragment weight distributions presented next.

POLAR ZONE	DEGREES	AVERAGE VELOCITY (FT/SEC)				VBAR	VMAX	VMIN	# OF HITS	SD
1	0-5	1822				1822	1822	1822	1	0.0
2	5-10	1822				1822	1822	1822	1	0.0
3	10-15	0							0	
4	15-20	699				699	699	699	1	0.0
5	20-25	1821				1821	1821	1821	1	0.0
6	25-30	668	516	497		560	668	497	3	93.7
7	30-35	682				682	682	682	1	0.0
8	35-40	0							0	
9	40-45	1030				1030	1030	1030	1	0.0
10	45-50	0							0	
11	50-55	2028	538	536	539	830	2023	530	5	667.5
12	55-60	1179	1155			1157	1179	1155	2	17.1
13	60-65	2553	1752			2153	2553	1752	2	556.7
14	65-70	2093	1825	1789	1729	1849	2093	1729	5	141.3
15	70-75	2878	2808	2637	2486	2702	2878	2486	4	176.0
16	75-80	0							0	
17	80-85	3175				3175	3175	3175	1	0.0
18	85-90	3575	2657			3116	3575	2657	2	649.2
19	90-95	2922	2105	1944		2324	2922	1944	3	524.4
20	95-100	3349	3282	2924	2878	2619	3349	1824	9	554.2
		2171	2152	2147	1824					
21	100-105	2041	2032			2036	2041	2032	2	6.5
22	105-110	2045	1877			1961	2045	1877	2	119.1
:		:				:	:	:	:	:
36	175-180									

Re-created from (20:28-29)

Table 2. Standard 20-mm HEI Data and Statistics - Shot #1

POLAR ZONE	DEGREES	AVERAGE VELOCITY (FT/SEC)	VBAR	VMAX	VMIN	# OF HITS	SD
1	0-5	0				0	
2	5-10	0				0	
3	10-15	0				0	
4	15-20	0				0	
5	20-25	647	647	647	647	1	0.0
6	25-30	510	510	510	510	1	0.0
7	30-35	0				0	
8	35-40	551	551	551	551	1	0.0
9	40-45	551	551	551	551	1	0.0
10	45-50	1078	888	1078	698	2	268.7
11	50-55	661	660	681	659	2	1.2
12	55-60	2165	2165	2165	2165	1	0.0
13	60-65	2103	2183	2183	2183	1	0.0
14	65-70	1777	1599	1777	1200	6	208.3
		1200					
15	70-75	2568	2464	2568	2361	2	146.4
16	75-80	0				0	
17	80-85	3048	2880	3048	2711	2	238.6
18	85-90	0				0	

Re-created from (20:30-31)

Table 3. Standard 20-mm HEI Data and Statistics - Shot #2

POLAR ZONE	DEGREES	AVERAGE VELOCITY (FT/SEC)						VBAR	VMAX	VMIN	# OF HITS	SD
19	90-95	2961	2584	2562	2555			2666	2961	2555	4	197.1
20	95-100	2993	2878	2651	2614	2582		2322	2993	1840	13	393.6
		2462	2167	2151	2022	1977						
		1962	1881	1840								
21	100-105	2932	2022	1901	1822			2160	2932	1822	4	514.9
22	105-110	1938						1938	1938	1938	1	0.0
23	110-115	0									0	
24	115-120	0									0	
25	120-125	0									0	
26	125-130	0									0	
27	130-135	1880	1849					1864	1880	1849	2	21.8
28	135-140	0									0	
29	140-145	1154						1154	1154	1154	1	0.0
30	145-150	0									0	
31	150-155	0									0	
32	155-160	0									0	
33	160-165	0									0	
34	165-170	0									0	
35	170-175	0									0	
36	175-180	2345	2138					2242	2345	2138	2	146.7

Re-created from (20:30-31)

Table 3. Standard 20-mm HEI Data and Statistics - Shot #2 (con't)

POLAR ZONE	DEGREES	VBAR	VMAX	VMIN	# OF HITS	SD
1	0-5	1822	1822	1822	1	0.0
2	5-10	1822	1822	1822	1	0.0
3	10-15				0	
4	15-20	699	699	699	1	0.0
5	20-25	1234	1821	647	2	829.8
6	25-30	547	668	497	4	80.6
7	30-35	682	682	682	1	0.0
8	35-40	551	551	551	1	0.0
9	40-45	790	1030	551	2	339.1
10	45-50	888	1078	698	2	268.7
11	50-55	784	2028	530	7	551.6
12	55-60	1499	2165	1155	3	576.1
13	60-65	2136	2553	1752	3	401.7
14	65-70	1712	2093	1200	11	216.1
15	70-75	2623	2678	2361	6	194.9
16	75-80				0	
17	80-85	2978	3175	2711	3	239.8
18	85-90	3116	3575	2657	2	649.2
19	90-95	2519	2961	1944	72	380.1
20	95-100	2443	3349	1824	22	447.4
21	100-105	2124	2932	1822	6	404.7
22	105-110	1953	2045	1877	3	85.3
23	110-115				0	
24	115-120				0	
25	120-125				0	
26	125-130				0	
27	130-135	1864	1880	1849	2	21.8
28	135-140				0	
29	140-145	1154	1154	1154	1	0.0
30	145-150				0	
31	150-155				0	
32	155-160				0	
33	160-165				0	
34	165-170				0	
35	170-175				0	
36	175-180	2242	2345	2138	2	146.7

Re-created from (20:32)

Table 4. 2 Round Average for Standard 20-mm HEI

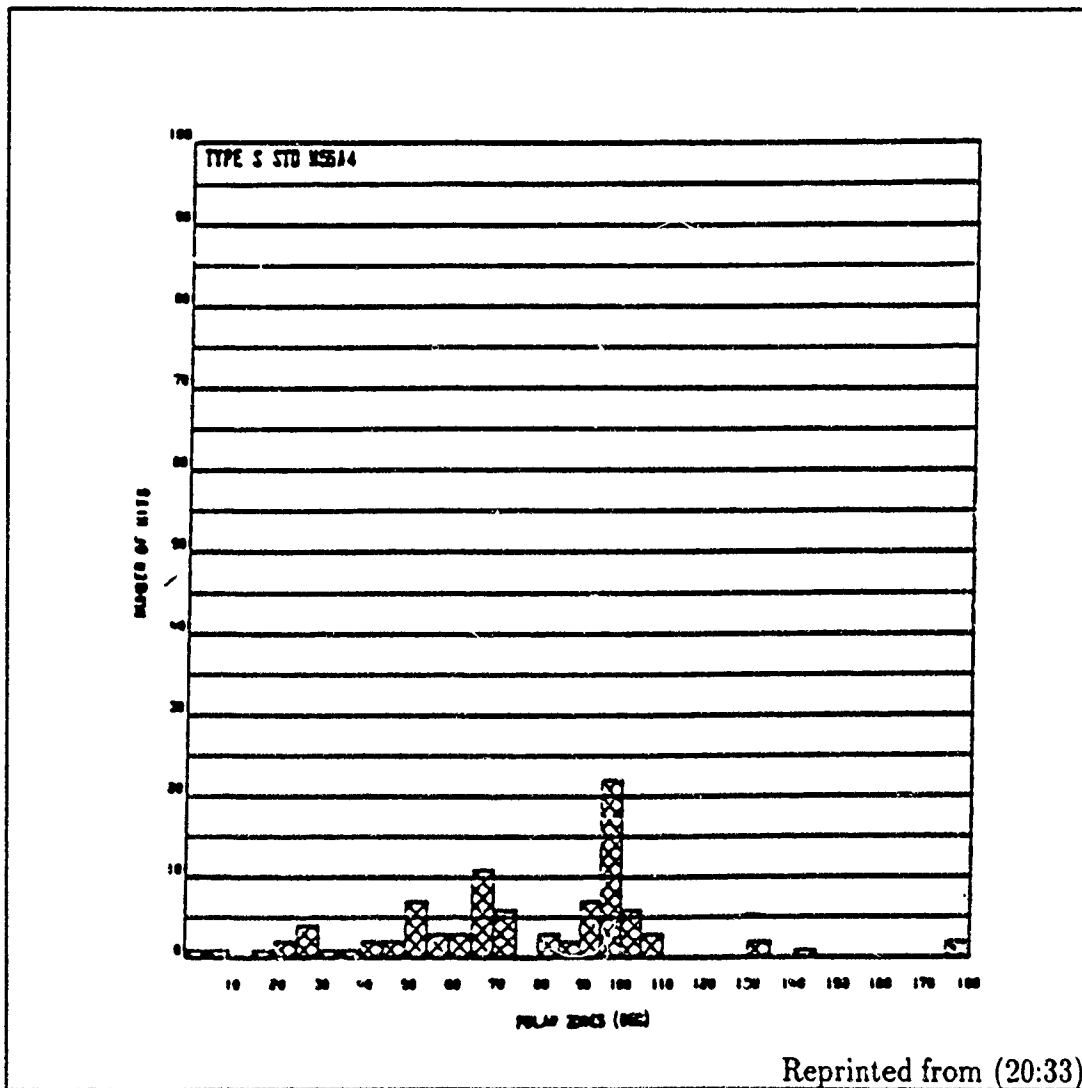


Figure 21. Cumulative Fragment Hits per Zone - Standard 20-mm HEI

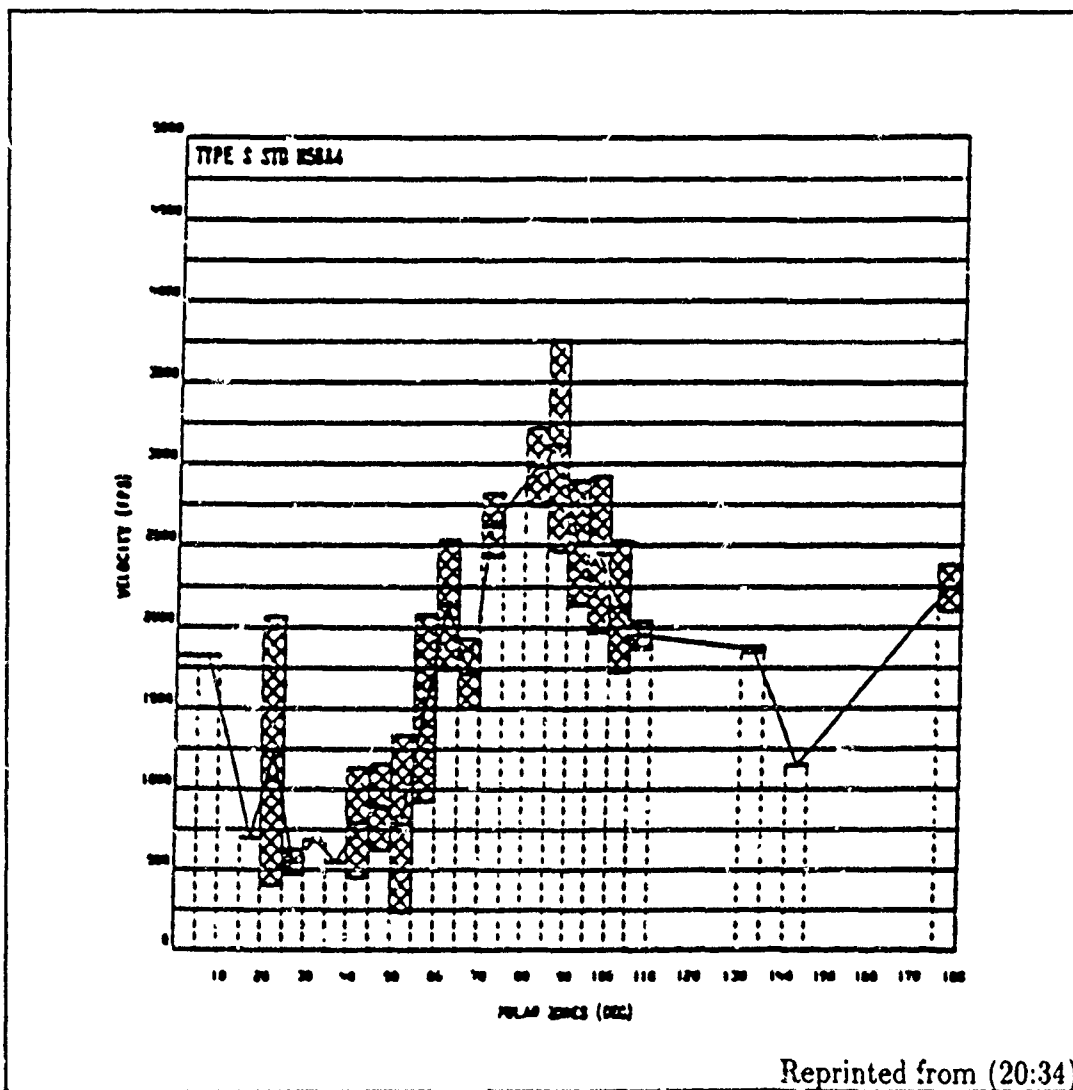


Figure 22. Fragment Velocities by Zone - Standard 20-mm HEI

POLAR ZONE	DEGREES	VBAR	VMAX	VMIN	# OF HITS	SD
1	0-5				0	
2	5-10				0	
3	10-15				0	
4	15-20				0	
5	20-25				0	
6	25-30				0	
7	30-35				0	
8	35-40	1401	3013	593	3	1395.1
9	40-45	1437	2467	791	9	654.9
10	45-50	2236	2444	2028	2	294.0
11	50-55	1857	3155	778	13	789.1
12	55-60	1860	3318	1017	14	678.3
13	60-65	1576	1645	1508	2	96.9
14	65-70	1759	1759	1759	1	0.0
15	70-75	1325	1782	870	2	645.2
16	75-80	1591	1591	1591	1	0.0
17	80-85				0	
18	85-90	1384	1384	1384	1	0.0
19	90-95	4076	5286	2873	19	676.3
20	95-100	3888	5286	3053	50	537.4
21	100-105	3772	4756	3000	29	473.3
22	105-110	2686	3448	2087	8	466.1
23	110-115	2696	2980	2376	8	231.8
24	115-120	2510	3387	1951	6	532.6
25	120-125				0	
26	125-130				0	
27	130-135				0	
28	135-140				0	
29	140-145	1637	1654	1621	2	23.2
30	145-150				0	
31	150-155	1694	1694	1694	1	0.0
32	155-160	2013	2147	1881	2	188.0
33	160-165	2006	2009	2004	2	3.2
34	165-170				0	
35	170-175	2475	2944	1896	10	330.0
36	175-180	2985	3586	2530	10	319.2

Re-created from (20:41)

Table 5. 3 Round Average for Minimum Weight 20-mm HEJ

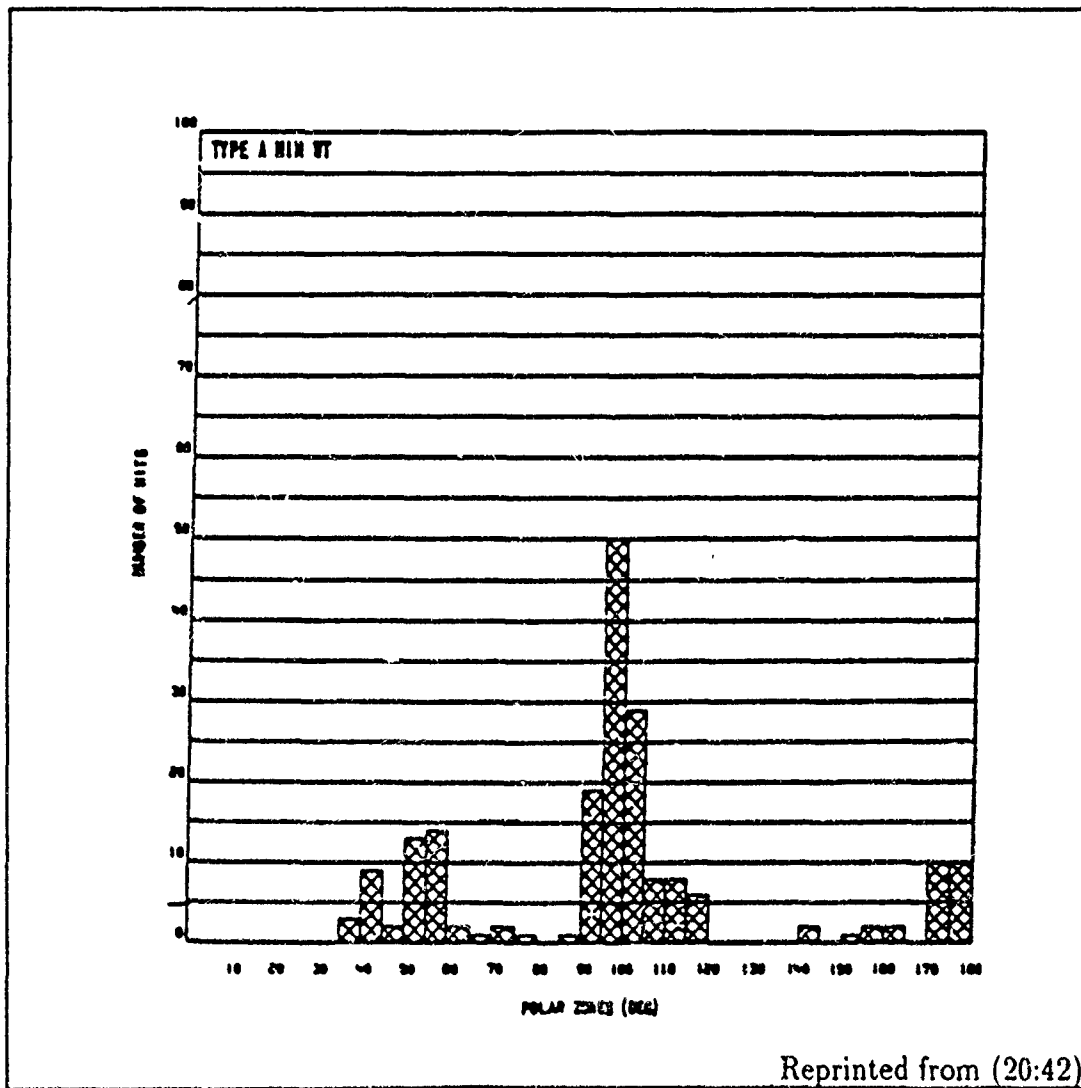


Figure 23. Cumulative Fragment Hits per Zone - Min Weight 20-mm HEI

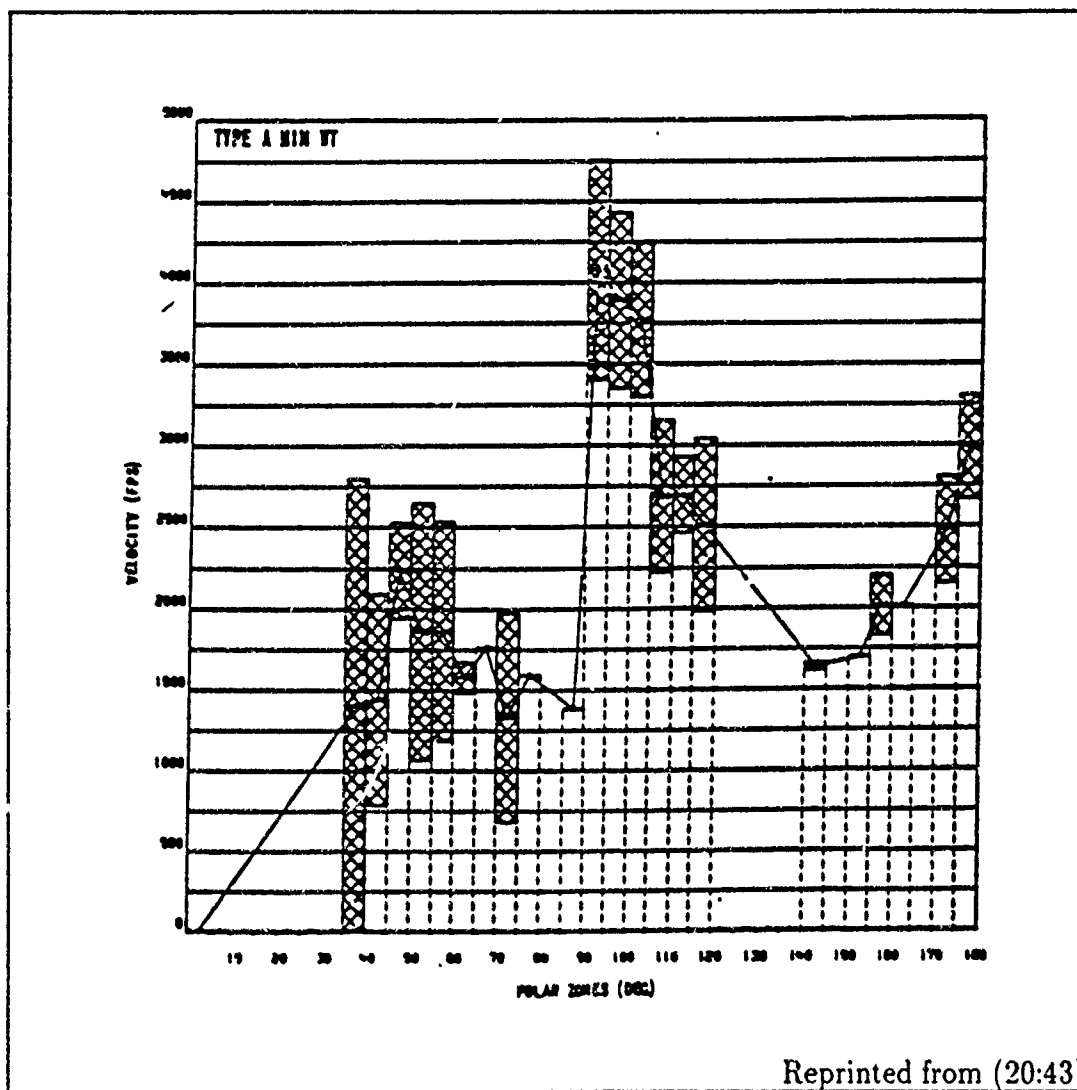


Figure 24. Fragment Velocities by Zone - Min Weight 20-mm HEI

POLAR ZONE	DEGREES	VBAR	VMAX	VMIN	# OF HITS	SD
1	0-5				0	
2	5-10				0	
3	10-15	638	638	638	1	0.0
4	15-20	640	640	640	1	0.0
5	20-25	640	640	640	1	0.0
6	25-30				0	
7	30-35				0	
8	35-40	864	864	863	2	0.9
9	40-45	1904	2432	1435	6	405.2
10	45-50	1598	2055	757	5	506.3
11	50-55	1645	2001	1285	5	261.0
12	55-60	1935	3172	1463	10	623.7
13	60-65	2029	3211	1621	6	628.1
14	65-70	2051	3349	1392	3	1123.8
15	70-75	1398	1605	1192	2	291.7
16	75-80	1392	1392	1392	1	0.0
17	80-85	3894	4301	3488	2	574.7
18	85-90	3156	3571	2742	2	566.6
19	90-95	3276	4114	2416	34	464.7
20	95-100	2675	3727	952	33	548.3
21	100-105	3264	4096	2289	31	566.4
22	105-110	2058	2287	1735	6	205.7
23	110-115				0	
24	115-120				0	
25	120-125				0	
26	125-130				0	
27	130-135				0	
28	135-140				0	
29	140-145				0	
30	145-150	1857	1857	1857	1	0.0
31	150-155	1835	1938	1734	2	143.9
32	155-160	2066	2299	1835	2	328.1
33	160-165	2014	2049	1980	2	48.6
34	165-170	2271	2271	2271	1	0.0
35	170-175	2586	2771	2437	3	169.8
36	175-180	2737	2961	2597	8	132.7

Re-created from (20:50)

Table 6. 3 Round Average for Maximum Explosion 20-mm HEI

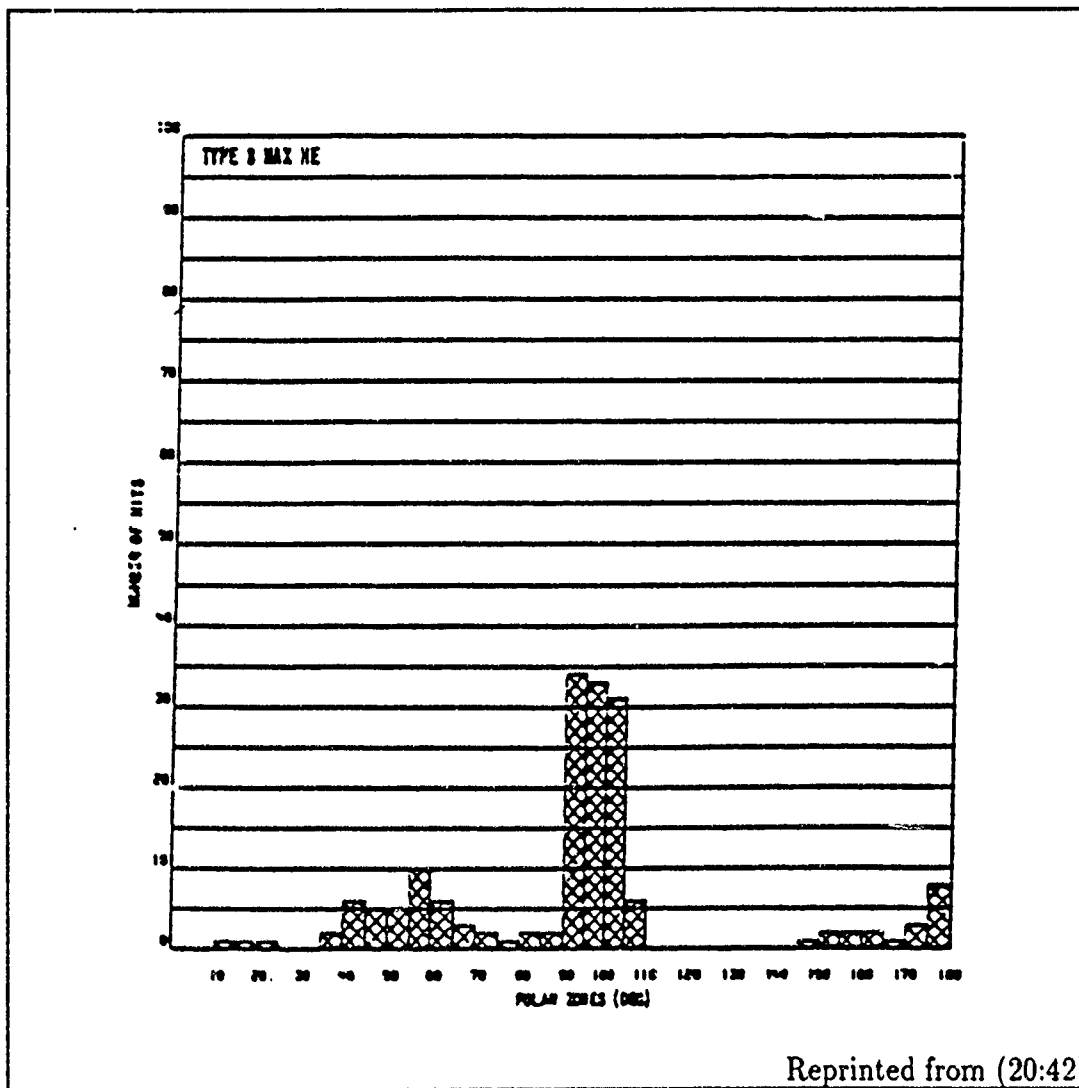


Figure 25. Cumulative Fragment Hits per Zone - Max Explosive 20-mm HEI

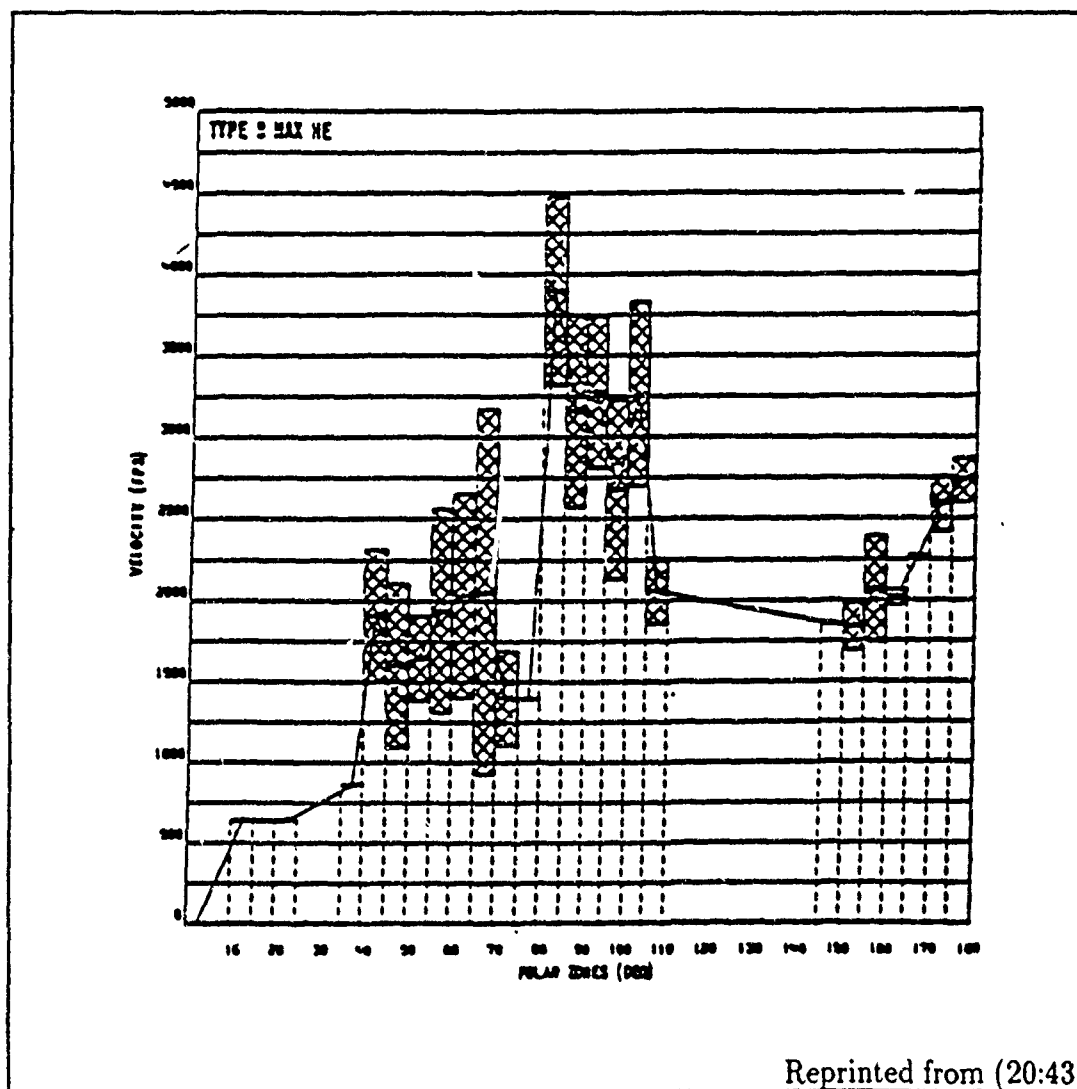
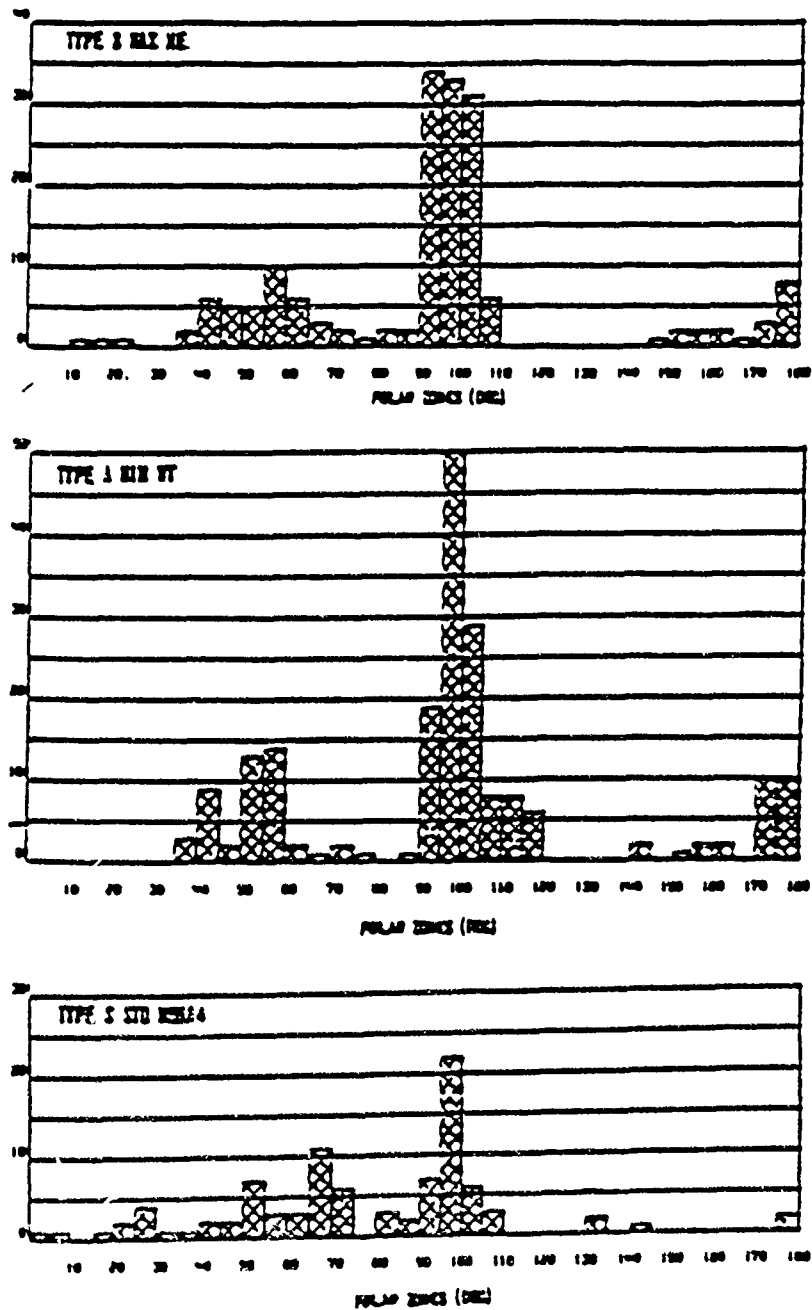


Figure 26. Fragment Velocities by Zone - Max Explosive 20-mm HEI



Developed from (20)

Figure 27. Cumulative Fragment Hits per Zone - By Projectile Type

2.4.3.2 *Static Detonation – Fragment Weight.* Weight Distributions for each of these projectiles are shown in Figures 28–30. The results shown are from an identical testing arena but they are evidently not from the same projectiles as the velocity results shown above. Therefore a fragment's velocity can not be combined with its weight to calculate kinetic energy, or initial velocity. The initial velocity of an average fragment for each zone is calculated using the average velocity and average weight (converted to mass) for each zone and four other parameters. These other parameters are: the air density which is set to .07648; the fragment drag coefficient which is set to .64000; the fragment area/mass constant which is set to 1.36934; and the fragment area/mass exponent which is set to .33333. With the exception of air density, each of these parameters actually differs from fragment to fragment. However, the Jones study, like most studies, holds these parameters constant for all fragments.

Lillard E. Gilbert has done fragment velocity analysis. His work develops, tests, and demonstrates fragment velocity decay. He also shows two ways to calculate the decay coefficient k shown below where V_0 is the calculated initial velocity, and V_1 is the velocity at some distance X from the explosion point. Using the equations, a fragment's initial velocity can be calculated and subsequently, the velocity at any distance X from the explosion point. (14, 13, 11, 12)

$$V_0 = V_1 \cdot \exp^{k \cdot X} \quad (15)$$

$$V_0 \cdot \exp^{-k \cdot X} = V_1 \quad (16)$$

But, as stated earlier, individual fragment velocities in the Jones study are not associated with their respective weights. Thus, this study only calculates a hypothetical initial velocity for the average fragment within each zone. The study's calculated, hypothetical results are not presented here.

Figure ??-30A shows the minimum, maximum, and mean fragment weight for each zone. Figure 28-30B shows the total weight of all fragments gathered for each zone. And Figure 28-30C shows the number of fragments gathered in each zone. The reader is again warned not to place too much significance on the actual number of fragments gathered since the entire zone area is *not* represented. Instead, note the relative weight and number of fragments between zones.

Figures C in each of the Figures 28-30 again show that the different projectile casings appear to have different fragment distributions between zones. Also, in each of the Figures 28-30A, the variability of fragment weights is larger at the end-zones and relatively stable in the mid-zones.

More specifically, Figure 28 shows that the number of fragments per zone for the standard 20-mm HEI, tends to increase from zone 5 through zone 20. But, the fragment weights tend to decrease through that range. The tail, tracer, fragments in zones 35 and 36 are somewhat separated, and larger than those in the mid-zones.

Figure 29 indicates that a large percentage of the fragments from the minimum weight 20-mm HEI are contained within a small percentage of the zones. Additionally, the only large fragments zones are in the tracer end: zones 35 and 36.

An altogether different fragmentation is shown in Figure 30 for the maximum explosive 20-mm HEI. The larger explosive payload of this projectile is contained in a much longer body cavity as portrayed in Figure 20A. Again, because of its thin walls, a large percentage of the fragments are contained within a small percentage of the zones. And, with one exception, the fragment weights are small. In fact, the fragments from this maximum explosive HEI (which has thin walls) are even smaller than the fragments from the minimum weight (thin walled) HEI. Even the tracer end fragments in zones 35 and 36 are significantly smaller. This is most likely the result of the larger explosive force of the projectile.

In each of the projectiles statically tested, the original fuse was replaced by a detonator and C-4 composite. The C-4 composite is itself an explosive. Thus, the zones on the fuse end of the projectile may contain non-representative fragments.

2.4.4 Reeves Study This study of the 23-mm HEI was completed in 1976 by Harry J. Reeves. The 23-mm projectiles included in the study were the "... High Explosive Incendiary-Tracer (HEI-T) with either a Point Detonating Superquick (PDSQ) A-23 or Point Detonating-Delay (PD-Delay) B-23 fuze for use in the NR/NS-23 Aircraft Gun, (2) the High Explosive Incendiary (HEI) with a PD-Delay B-23A fuze for the AM-23 and GSh Aircraft Guns, and (3) the HEI-T with a Point Detonating Self Destroying-Delay (PDSD-Delay) MG-25 fuze for use in the ZU-23 and ZSU-23-4 Weapon Systems (28:9)."

2.4.4.1 Static Detonation - Fragment Velocity. The static tests were conducted in an arena very similar to the previously described arena. However, the method used to capture initial velocity data was based on the "... distance fragments, in each polar zone, traveled in a 45.9 microsecond time interval, i.e., between 47.2 and 93.1 microseconds after detonation (28:12)." Multiple flash X-rays were used to estimate the fragment velocities for 12, 15° zones. Only the average velocity in each zone was calculated. The results for the 23-mm HEI-T shot from the NR/NS-23 Aircraft Gun are shown in Tables 7. These results are reported for 5° zones with two exceptions. The results for the other test projectiles are included in Appendix B.

The average fragment velocity for each 15° zone provides little information since the distribution of the velocity within each zone is unreported. Further, the results that are reported are reported for 5° zones except for the first and last zones which are 2.5° zones.

2.4.4.2 Static Detonation - Fragment Weight. The average and total fragment weight for each of the 5° zones is also reported in Table 7. A finer breakdown

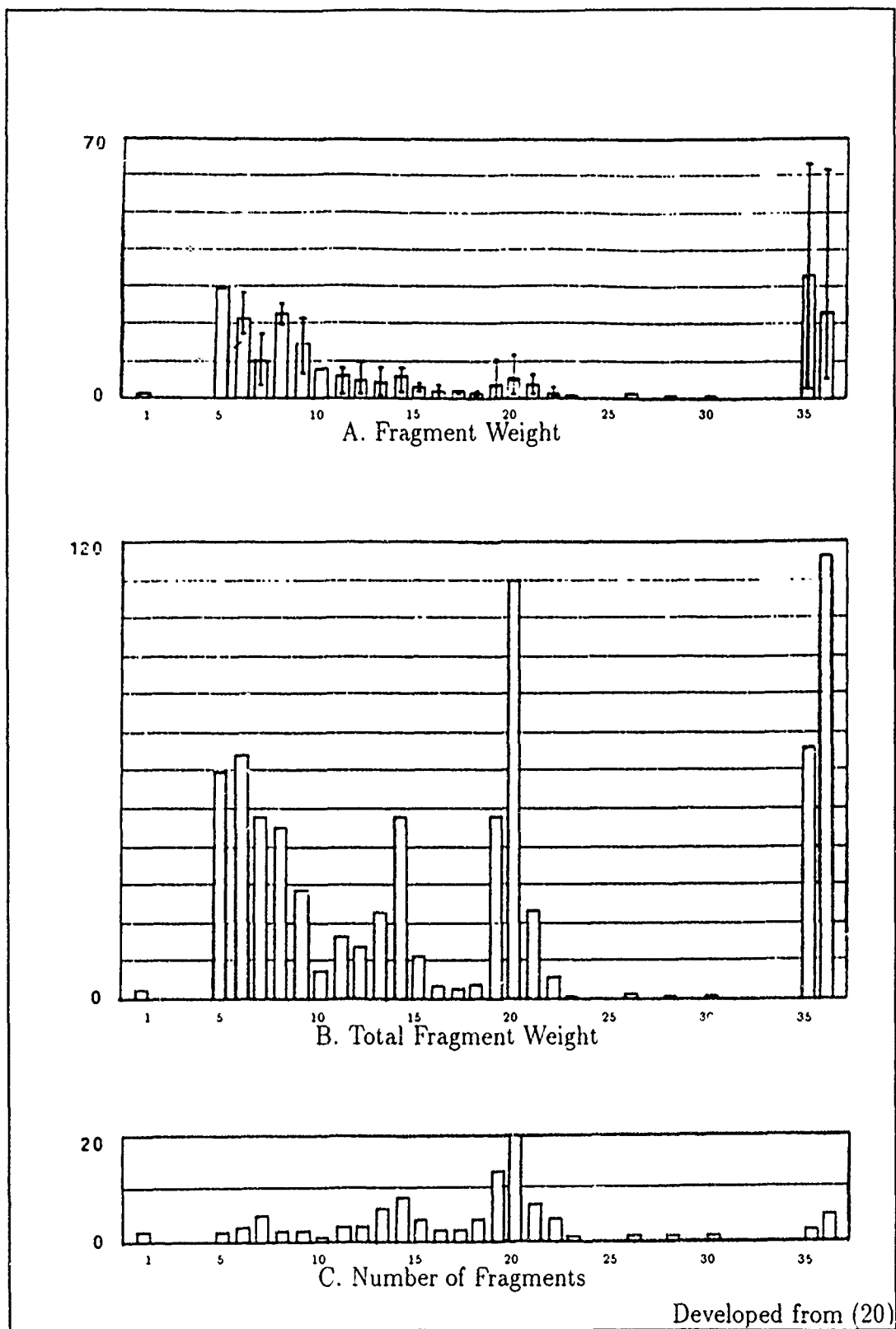


Figure 28. Standard 20-mm HEI Weight Distributions

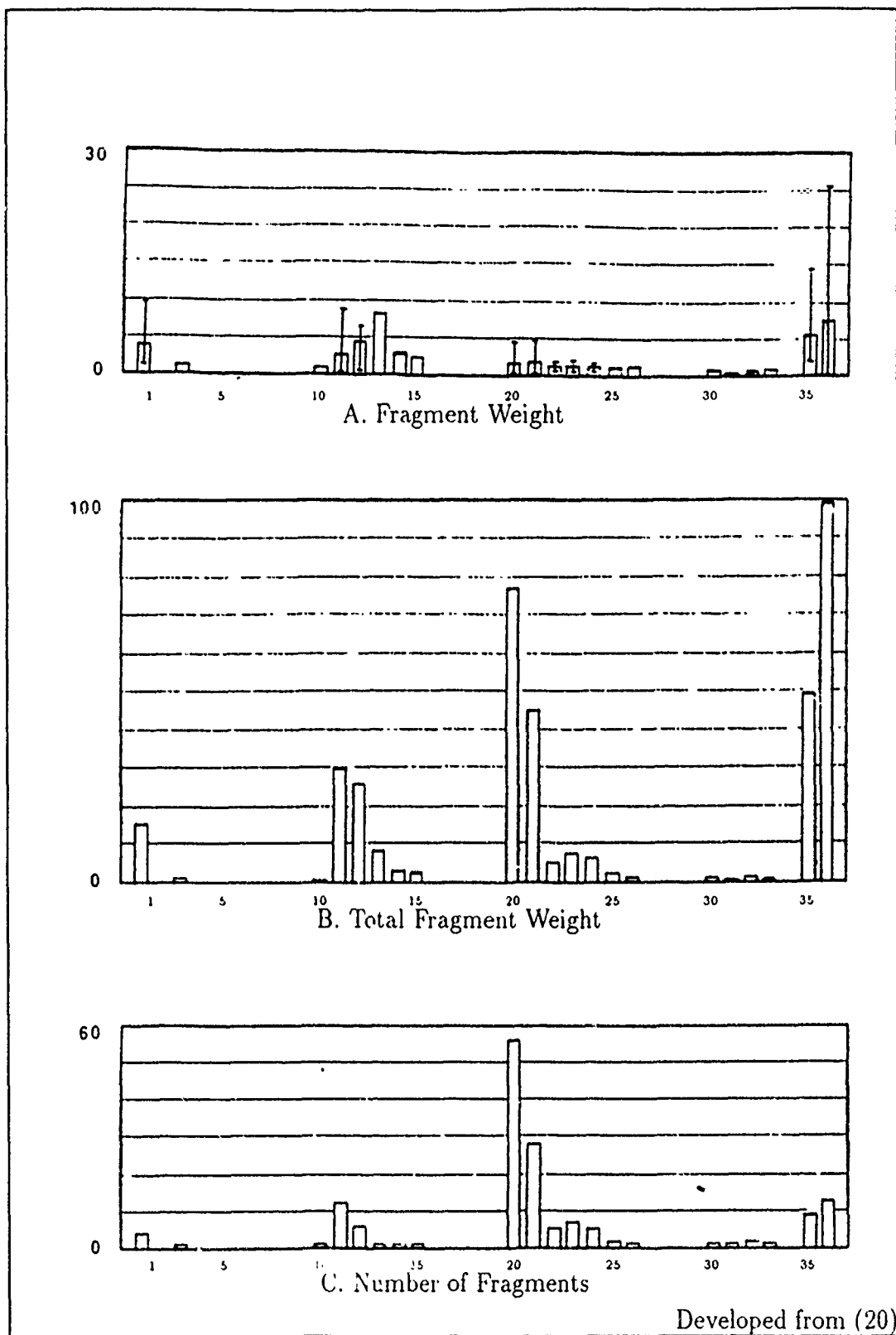


Figure 29. Minimum Weight 20-mm HEI Weight Distributions

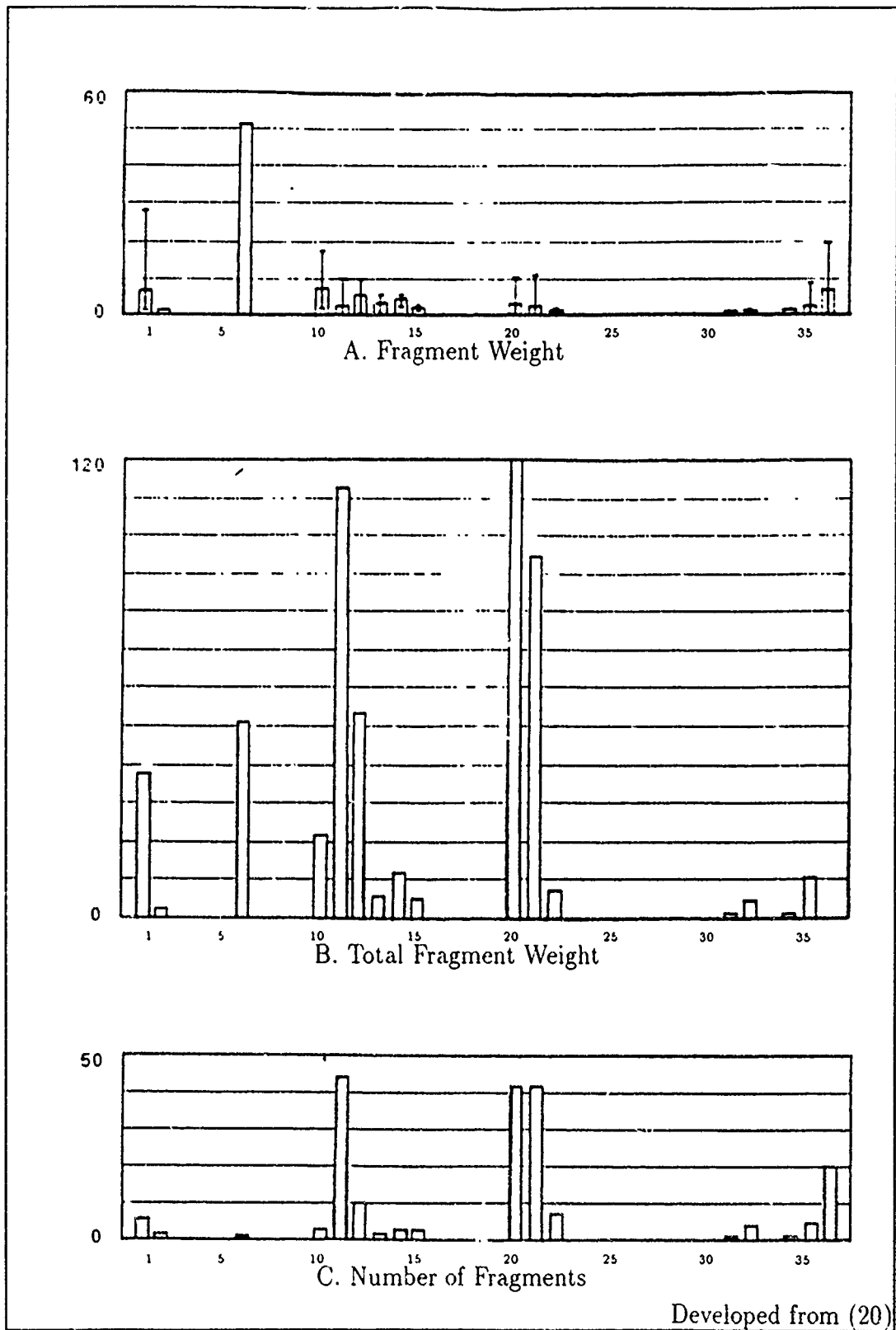


Figure 30. Maximum Explosive 20-mm HEI Weight Distributions

POLAR ZONE (DEG)	AVERAGE OF HEAVIEST FRAGMENTS (GRAMS)	AVERAGE FRAGMENT WEIGHT	TOTAL FRAGMENT WEIGHT	TOTAL NUMBER OF FRAGMENTS	FRAGMENTS PER STERADIAN	INITIAL ^A VELOCITY (M/SEC)
0.0-2.5	0.0	0.0	0.0	0.0	0.0	0.
2.5-7.5	0.0	0.0	0.0	0.0	0.0	0.
7.5-12.5	0.194	0.013	0.013	1.0	10.0	816.
12.5-17.5	0.137	0.009	0.009	1.0	7.0	816.
17.5-22.5	0.0	0.0	0.0	0.0	0.0	0.
22.5-27.5	0.0	0.0	0.0	0.0	0.0	0.
27.5-32.5	0.0	0.0	0.0	0.0	0.0	0.
32.5-37.5	0.0	0.0	0.0	0.0	0.0	0.
37.5-42.5	0.0	0.0	0.0	0.0	0.0	0.
42.5-47.5	0.0	0.0	0.0	0.0	0.0	0.
47.5-52.5	0.0	0.0	0.0	0.0	0.0	0.
52.5-57.5	0.0	0.0	0.0	0.0	0.0	0.
57.5-62.5	0.0	0.0	0.0	0.0	0.0	0.
62.5-67.5	0.0	0.0	0.0	0.0	0.0	0.
67.5-72.5	0.058	0.002	0.014	6.94	13.5	1223.
72.5-77.5	0.067	0.004	0.028	6.98	13.2	1223.
77.5-82.5	0.243	0.010	0.070	7.00	13.0	1223.
82.5-87.5	1.172	0.025	1.053	42.12	77.1	1223.
87.5-92.5	4.831	0.036	2.962	82.29	150.1	1178.
92.5-97.5	6.527	0.012	0.674	36.15	102.8	1178.
97.5-102.5	0.475	0.020	0.280	14.01	26.0	1178.
102.5-107.5	0.431	0.019	0.199	10.46	19.8	1133.
107.5-112.5	0.0	0.0	0.0	0.0	0.0	0.
112.5-117.5	0.0	0.0	0.0	0.0	0.0	0.
117.5-122.5	0.0	0.0	0.0	0.0	0.0	0.
122.5-127.5	0.119	0.008	0.027	3.39	7.5	905.
127.5-132.5	1.106	0.043	0.289	6.73	16.0	905.

Re-created from (28:17-18)

Table 7. Fragmentation Data Summary for the Soviet 23-mm HEI-T Projectile Used in the NR/NS-23 Aircraft Guns

POLAR ZONE (DEG)	AVERAGE OF HEAVIEST FRAGMENTS (GRAMS)	AVERAGE FRAGMENT WEIGHT	TOTAL FRAGMENT WEIGHT	TOTAL NUMBER OF FRAGMENTS	FRAGMENTS PER STERADIAN	INITIAL VELOCITY (M/SEC)
127.5-132.5	1.106	0.043	0.289	6.73	16.0	905.
132.5-137.5	0.0	0.0	0.0	0.0	0.0	0.
137.5-142.5	8.729	0.566	1.115	1.97	5.6	726.
142.5-147.5	4.004	0.115	0.544	4.73	15.0	726.
147.5-152.5	4.698	0.304	0.359	1.18	4.3	680.
152.5-157.5	0.691	0.035	0.057	1.64	7.1	680.
157.5-162.5	0.0	0.0	0.0	0.0	0.0	0.
162.5-167.5	0.0	0.0	0.0	0.0	0.0	0.
167.5-172.5	0.036	0.002	0.002	1.00	13.5	69.
172.5-177.5	2.601	0.042	0.231	5.50	115.1	69.
177.5-180.0	2.789	0.044	0.110	2.5	418.0	69.

AVERAGE OF 2 ROUNDS TESTED AT AAI

c SCALE FACTOR EQUALS 1.005

K EQUALS 668 GRAINS PER CUBIC INCH

A No flash X-ray for this projectile, initial velocity results obtained from Table IV.

b those fragments were observed from the flash X-ray to have an initial velocity of 69 m/sec. Other fragments in the 137.5° - 142.5° polar zone had the initial velocity presented in the above table.

c The scale factor indicates a 99.5% as fired metal weight recovery. However, the actual percent recovery (79.5%) was increased by 20% to account for fragments purposely not recovered. This increase was based on the results of 20-mm projectile fragmentation tests conducted at APG, reference APG-MT-4609.

Re-created from (28:17-18)

Table 7. Fragmentation Data Summary for the Soviet 23-mm HEI-T Projectile Used in the NR/NS-23 Aircraft Guns

of the fragment weights is reported in the appendixes to the Reeves Study. One of these weight tables is reprinted in Appendix B for the readers enlightenment only. It appears that little information about or insight into the weight distributions can be gathered from them although some general weight characteristics can be gleaned.

2.4.4.3 Dynamic Detonation. The Reeves Study also conducted dynamic test shots but these were for the sole purpose of determining ballistic limits. No fragmentation data was reported.

2.4.5 Gilbert Study Lillard E. Gilbert conducted a series of studies culminating in his 1985 study of the Soviet 30-mm HEI. This study focuses on the Dynamic fragmentation of the HEI and the fragment velocities. The test set-up is again similar to the test arena described earlier with one major difference. The projectiles are dynamic, i.e., they are in motion. Gilbert's test shots used a standard operating velocity of 2720 feet per second. Therefore, the test set-up includes a gun to shoot the projectile just as it would be in a live-fire situation.

2.4.5.1 Projectile Rotation.

Traditionally, gun¹ fired projectiles are rotated at 50,000 to 150,000 revolutions per minute about their longitudinal axis. The radial rotation is used to stabilize the projectile in the attitude of least drag and optimize its ballistic trajectory. No reference to the effect of radial rotational velocity was found in the literature reviewed. (14:2)

Just what effect projectile rotation may or may not have on its fragmentation is unknown. Gilbert's study adds nothing to answer this question and, as in Gilbert's study, a literature search has proved fruitless.

2.4.5.2 Dynamic Detonation - Fragment Velocity. It is assumed common knowledge that "Exploding projectiles are known to disperse fragments over

a spherical area. The shape and magnitude of the area where the fragments hit is usually determined by the shape of the projectile and to some extent the fuzing techniques used (14:7)." This is the reason for a circular or spherical test arena. Gilbert further states that "It is known that the projectile fragment initial velocity and frequency per unit area are relatively constant about the axes of symmetry. The 30mm projectile is symmetric about its longitudinal axis and the fragment frequency and initial velocity are relatively constant for $0^\circ \leq \phi \leq 360^\circ$, for any given values of X and ψ_c (14:8)." ψ_c is used by Gilbert to designate a specific zone 'c' of size ψ . ψ is measured in degrees, i.e., if $\psi = 15^\circ$ there would be 12 of these zones.

The results of these dynamic tests "... show that the fragments are not uniform in size, or spatial distribution as a function of $\psi[c]$... (14:11)." This is one of the confounding factors of dynamic tests. Static test results also show a disparity of fragment size and weight. Dynamic tests cause what would have been the static zones of fragmentation to overlap one another in the dynamic zones.

Figure 31 shows a picture of the dynamic fragmentation of a 30-mm HEI projectile. This picture is taken 420 microseconds (0.000420 seconds) after the projectile impacted the fuse trigger plate. The picture's exposure time was 0.020 microseconds (0.000000020 seconds). Traveling at roughly 4,000 feet per second the fragments would travel less than 0.001 inch in the exposure time. The picture is therefore very clear.

Figure 32 graphs the number of fragments in different weight intervals for all fragments collected. The bar graph suggests an exponential distribution of fragment weights. But, because the weights are not differentiated by zone, the distribution is not useful in predicting or simulating fragment damage.

Table 8 does provide some insight into the zone weight distributions. Each row of the table represents a given zone area and the columns represent progressively larger weight ranges. Within each cell are numbers representing the spatial density of fragments given in fragments per steradian. The results for each of the three test

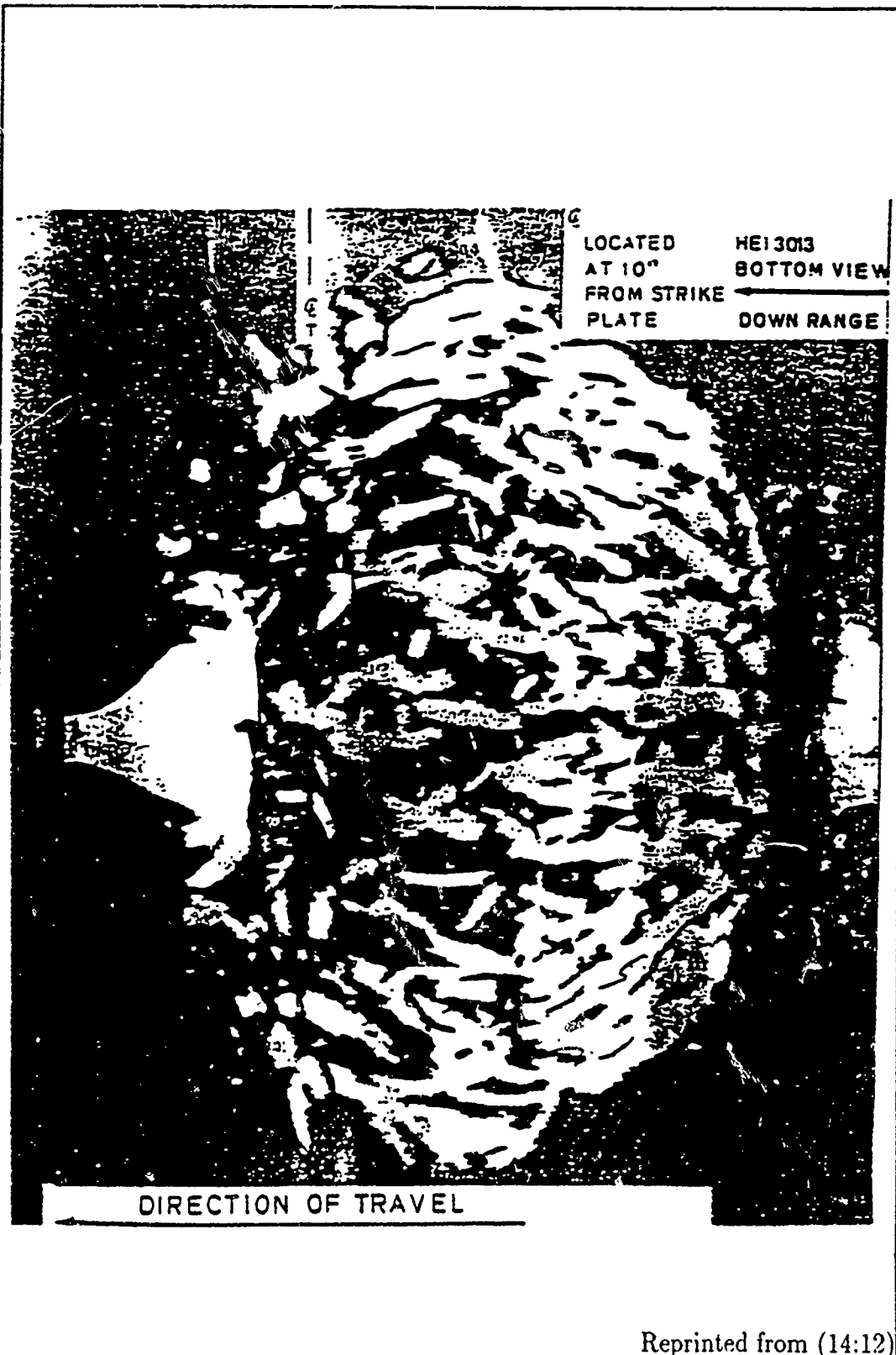


Figure 31. Flash X-Ray of the 30-mm Projectile Case Break-up

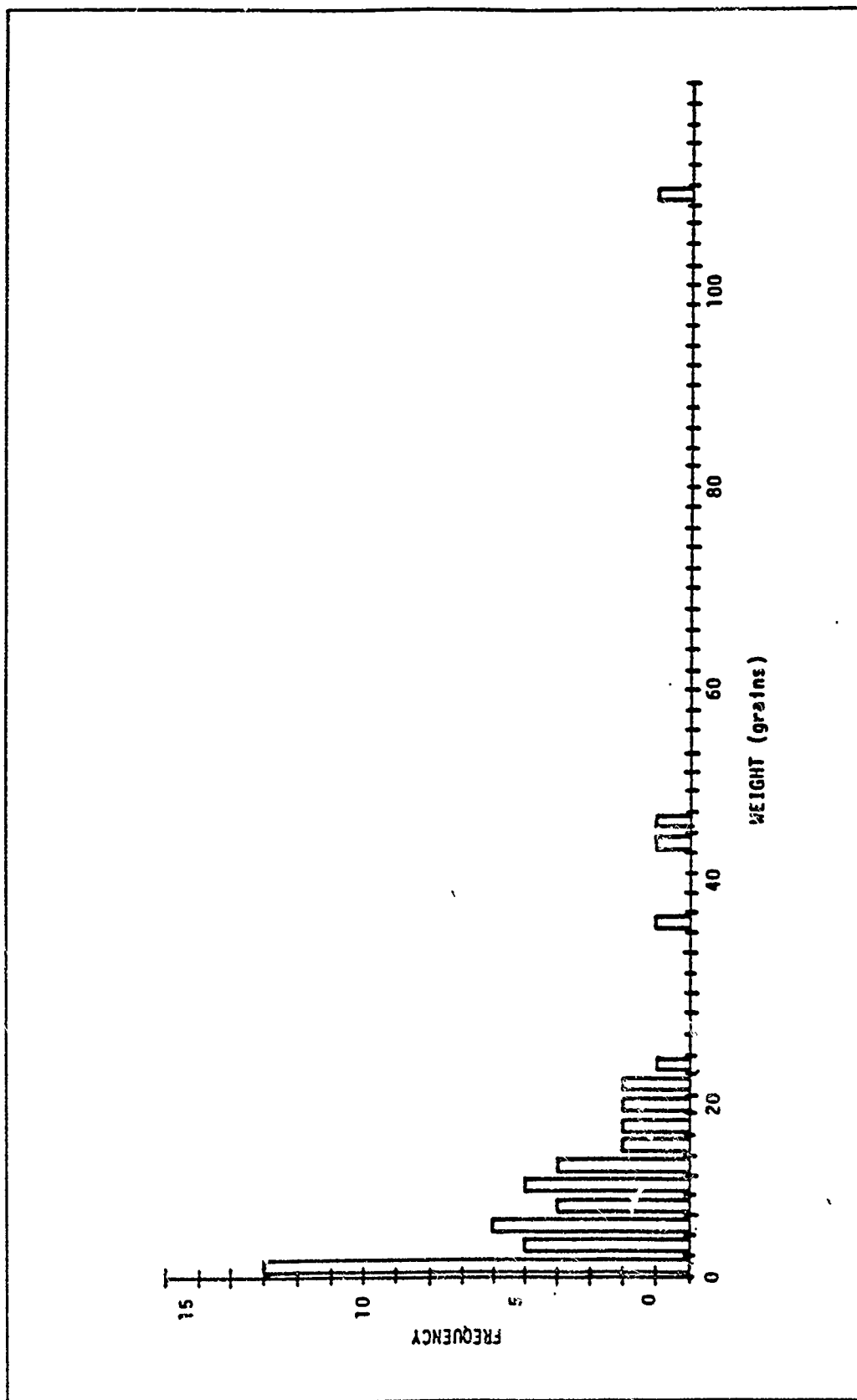


Figure 32. Fragment Weight Frequency Distribution for Test #1

shots, and their summation, are listed in each cell. Because the measure is given in steradians, density comparisons between zones can be made. However, the numbers should not be interpreted as the actual number of fragments collected in that zone. The numbers shown are density figures and not fragment counts.

Rows 2 and 3 of Table 8, representing zones 11.5°-23.2° and 23.2°-34.7° respectively, show smaller fragment densities than the other zones.

In addition, most of the larger fragments are seen in the first zone, 0°-11.5°. These larger fragments are usually part of the fuse or tracer which do not breakup into small fragments.

2.4.5.3 Velocity Degradation. As mentioned in Section 2.4.3.2 Gilbert has done considerable work in the area of projectile and/or fragment velocity decay. In this study, he presents two methods of computing the "coefficient of decay" shown in Equations 15 and 16. The first method back fits or solves for the decay coefficient by knowing the velocity at two points and the distance between those points as shown in Equation 17. The values of X_1 and X_2 usually correspond to points some relative distance from the projectile/fragment origin. The value $X_2 - X_1$ must be small compared to the values of both X_1 and X_2

$$\frac{T_1(X_2 - X_1)}{(T_2 - T_1)} = \frac{(e^{kX_1} - 1)}{k} e^{-kX_b} \quad (17)$$

where :

$X_i = i=\{1,2\}$ points relative to the origin

$X_b =$ a third point down range from X_2

$T_i =$ time at which point X_i is reached

$k =$ decay coefficient

COL:MN	FRAGMENT PER STERADIAN					
	TEST #	0 to 5.0 gns	5.1 to 10.0 gns	10.1 to 20.0 gns	20.1 to 50.0 gns	>50.1 gns
PSI Degrees						% fragment by count Per Polar Zone
5.7°	1	76	50	63	50	13
0° ψ \leq 11.5°	2	76	38	13	25	38
	3	63	38	38	0	.25
	Σ	72	42	48	25	25.3
17.3	1	13	13	0	0	0
11.51 $\leq \psi$ \leq 23.2	2	25	25	0	13	0
	3	13	25	13	0	0
	Σ	17	21	4.3	4.2	0
28.8	1	28	25	38	0	0
23.21 $\leq \psi$ \leq 34.7	2	0	0	0	0	0
	3	0	0	0	0	0
	Σ	26	7.6	12.6		
40.3	1	101	50	50	0	0
34.81 $\leq \psi$ \leq 46.0	2	88	25	0	0	0
	3	88	25	13	0	0
	Σ	92.3	33.3	21		
51.6	1	0	0	0	0	0
46.0 $\leq \psi$ \leq 57.8	2	76	13	0	0	0
	3	63	76	50	0	0
	Σ	46.3	26.3	16.6		
% by Count		46.8	24.5	18.7	5.3	4.6
						26.7
						16.9

Table 8. Summary of Fragment Spatial Dispersion by Weight Range and as a Function of Polar Zone

Gilbert's second method computes the decay coefficient (K) with the following parameters and Equation 18³. (14:6)

$$\begin{aligned}
 \rho &\equiv \text{the density of air at the location and time of test} \\
 A &\equiv \text{the projectile/fragment cross-sectional area} \\
 C &\equiv \text{the coefficient of aerodynamic drag} \\
 m &\equiv \text{the projectile/fragment mass} \\
 K &= \frac{\rho \cdot A \cdot C}{2 \cdot m}
 \end{aligned}
 \tag{18}$$

In this study, Gilbert computed the decay coefficient by first knowing the velocity of the projectile/fragment at two points and the distance between them. Figure 33 shows the reference velocity, decay coefficient (K), and zone (ψ_c) for several fragments. Although there is a weight column shown, no values are recorded because the velocities were once again not associated with a particular fragment weight. Clearly, from Equation 18, there is a definite relationship between the velocity and the fragment weight via the mass (m) and the cross-sectional area (A) parameters.

2.4.6 Avery Study This study, completed in 1979, examined "... the response of fiber composite structural materials to nonnuclear threat mechanisms including ballistic impact, blast, and laser irradiation (2)." As a part of this study, John Avery describes the general fragmentation principles of both static and dynamic detonation of HEI projectiles. The primary purpose was to study the damage to composite panels, but some 23-mm HEI fragment data is provided. Table 9 shows a summary of the three 23-mm HEI projectiles used in the damage tests.

³Gale S Weeding uses similar but not exactly the same equations to determine the projectile/fragment velocity at a given distance from the detonation point. (32:12)

FRAGMENT INITIAL VELOCITY (V_R) DATA FOR TEST #3

FRAC NO.	REF. VEL. (V_R)	K	Y
1	3775.31	0.040667	2.57
2	3715.75	0.054176	2.57
3	3750.43	0.053357	2.57
4	3671.70	0.042464	2.57
5	3735.78	0.042647	2.57
6	3651.13	0.036960	2.57
7	3825.04	0.057122	2.57
8	3864.51	0.071744	2.57
9	3853.41	0.041434	2.57
10	4110.00	0.077742	2.57
11	3790.83	0.042322	2.57
12	3576.49	0.061301	2.57
13	3813.77	0.046193	2.57
14	3753.90	0.042946	2.57
15	3751.00	0.065350	2.57
16	4148.08	0.077813	2.57
17	4400.00	0.057476	2.57
18	4102.28	0.052554	2.57
19	4202.86	0.057518	2.57
20	4432.00	0.053056	2.57
21	4320.49	0.042939	2.57
22	4247.18	0.036126	2.57
23	5300.74	0.042617	2.57
24	4545.45	0.025764	2.57
25	4764.40	0.077510	2.57
26	4557.17	0.047603	2.57
27	4638.47	0.037781	2.57
28	4320.66	0.066323	2.57
29	4649.98	0.032167	2.57
30	4710.85	0.039001	2.57
31	4267.20	0.062924	2.57
32	4230.15	0.062414	2.57
33	4066.87	0.047033	2.57
34	4240.46	0.070043	2.57
35	4475.44	0.097882	2.57
36	4149.33	0.086484	2.57
37	1927.55	0.045048	2.57
38	4079.67	0.066538	2.57
39	4132.46	0.077112	2.57
40	4152.19	0.077918	2.57
41	4704.02	0.033138	2.57
42	4738.93	0.038169	2.57
43	4544.16	0.032530	2.57
44	4199.64	0.052061	2.57
45	399.97	0.016974	2.57
46	60.89	0.002588	2.57
47	5300.74	0.097882	2.57
48	4594.31	0.012344	2.57
49	43	43	2.57
50	3757.58	0.054520	2.57
51	3741.69	0.045602	2.57

LEGEND:

Velocity - fps

k - ft⁻¹

Mean Fragment Initial Velocity for the Three Sample Population

$V_R = 4125$ fps

Figure 33. Fragment Initial Velocity Data for Test #3

PROJECTILE SECTION		STATIC VELOCITY*	MEAN STATIC DIRECTION	NUMBER OF FRAGMENTS	AVERAGE FRAG. WEIGHT	TOTAL FRAG. WEIGHT
		(FT/SEC)	(DEG)		(GRAINS)	Σ (GRAINS)
PROJECTILE A	FUSE	1300	0	5	(a)	296
	FUSE ATTACHMENT	2200	65	30	10	300
	SIDE SPRAY ▲	2610	93	604	1.99	1202
	BASE	1550	140	20	32	640
PROJECTILE B	FUSE	750	0	8	(b)	1359
	FUSE ATTACHMENT	-	-	-	-	-
	SIDE SPRAY ▲	2593	93	745	7.07	5270
	BASE	1420	135	14	82	1148
PROJECTILE C	FUSE	600	0	3	600	1800
	FUSE ATTACHMENT	1250	87	30	75	2250
	SIDE SPRAY ▲	2450	93	844	32	27,000
	BASE	630	160	3	734	2200
<p>(a) 2 fragments @ $m = 118$ gr and 3 fragments @ $m = 20$ gr.</p> <p>(b) 1 fragment @ 470 gr, 4 fragments @ 196 gr each, and 3 fragments @ 35 gr each.</p> <p>▲ Mott size distribution</p> <p>* Assumed to be constant</p>						

Ref: AFFDL-TR-136

*Effects of Internal Blast on
Combat Aircraft Structures*

Reprinted from (2:102)

Table 9. Fragmentation Data for Projectiles A, B, and C

Figure 34 shows the typical 23-mm HEI projectile used in this study and its static fragmentation. The fragment number and weight breakdown for this projectile is listed below. A broad description of each of the three individual projectiles used is shown in Table 10.

FUSE FRAGMENTS:

1 @ 470 grains

4 @ 196 grains

3 @ 35 grains

SIDE SPRAY:

745 @ 7.07 grains

BASE SPRAY:

14 @ 82 grains

2.4.6.1 Fragment Size. Although the other studies reviewed considered the fragments to be 'irregular' in shape, the Avery study did not.

In order to determine the damage size from a fragment penetration, the fragment presented length, L_p , must be known Based on an examination of typical HE fragments the following expression is recommended for L_p :

$$L_p = 0.23(w)^{\frac{1}{3}} \quad (\text{HE fragments})$$

where :

w = the weight of the fragment in grains.

This expression is based on a limited amount of data, and is most accurate for fragments in the 10 to 300 grain range. (2:106)

2.5 HEI Blast Pressure

Air pressures are difficult to study because they are generated from multiple sources within a single explosion. In addition, the magnitude of the pressure is very

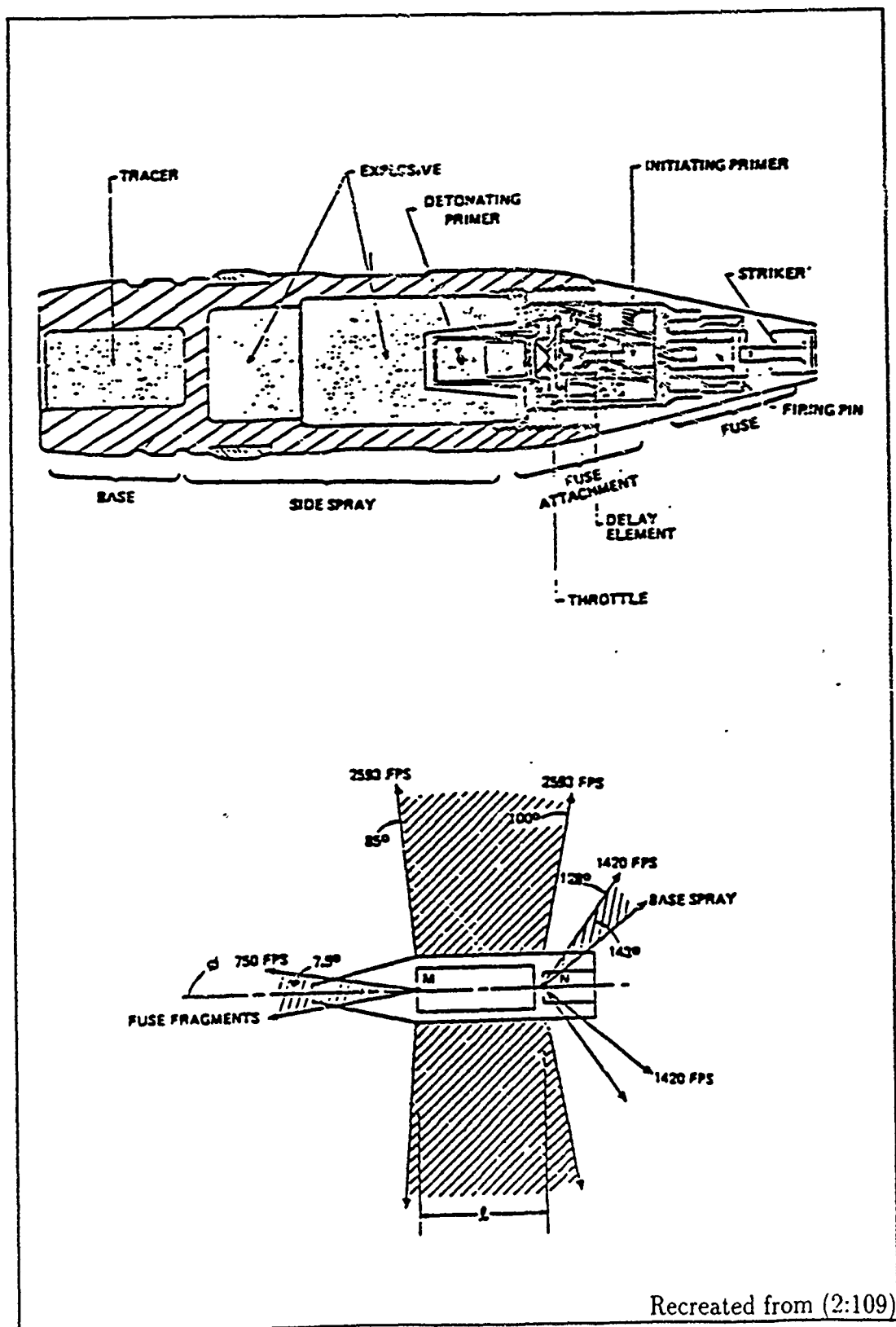


Figure 34. Typical Model of 23-mm HEI and Static Fragmentation

Projectile Segment Contributing Fragments	Static Velocity (ft/sec)	φ, Cone Angle				Num. of Fragments	Average Fragment Weight		Average Penetrated Length (Lp) (Inch)
		φ ₁ (deg)	φ ₂ (Outer) (deg)	φ ₃ (Inner) (deg)	φ ₄ (Inner) (deg)		(grains)	(Inch)	
PROJECTILE A (1.2-1.7-in)	1500	-	7.5	-	0	2/3	118/20	1.13/.62	
	2200	67.5	72.5	-	65	30	10	.50	
	2610	85.5	100.5	-	93	604	2	.28	
	1650	132.5	147.5	-	140	20	32	.73	
PROJECTILE B (1.2-1.7-in)	750	-	7.5	-	0	1/4/3	470/190/35	1.79/1.34/.75	
	2583	85.5	100.5	-	63	745	7	.44	
	1420	127.5	142.5	-	135	14	82	1.00	
PROJECTILE C (1.2-1.7-in)	810	-	7.5	-	0	3	600	1.04	
	1250	79.5	94.5	-	87	30	75	.97	
	2460	85.5	100.5	-	93	644	32	.73	
	630	152.5	107.5	-	160	3	734	2.07	

Reprinted from (2:111)

Table 10. HEI Fragment Distribution and Static Firing Data

sensitive to the surrounding environmental conditions. A few of these environmental conditions are:

- the size and intensity of the ignition source.
- the volume enclosed by any surrounding structure.
- the amount and location of venting (holes).

The detonation of a 23mm HEI in an enclosed structure such as a fuel tank ullage will result in an internal pressure due to the blast and release of gases. The HEI also has the potential of changing the chemical composition of the gases present in the tank.

The pressure encountered in the ullage of a fuel tank when a 23mm HEI projectile detonates is composed of several frequency components and can be divided into 3 areas: (1) the highly dynamic blast pressure (shock waves) which radiate from the detonation point, reflect off the fuel tank walls, and reverberate for several cycles; (2) the quasi-static overpressure resulting from the release of gas from the HEI detonation, which effectively causes a step increase in tank pressure and a slow decline as the gases are vented from the tank; (3) the quasi-static overpressures generated by the fuel and oxygen combustion. The term "quasi-static" is used in this report to differentiate between the pressure that the walls of the TWS feel due to gas pressure and that due to the blast shock waves. Figure [35] depicts the three distinct frequency components as they would exist if they could be separated. It is important to obtain a good understanding of the projectile's contribution to tank overpressure so that the combustion overpressure can be differentiated from the blast pressures. (1:7-8)

2.5.1 Jones Study This is the same study examined in Section 2.4.3. It was completed in 1976 by Steven R. Jones, (20), and examines the differences between a standard and two modified 20-mm HEI projectiles. Table 1 and Figure 20 from Section 2.4.3 show the weight of various sub-components, and the projectile casings respectively. In this section the study's blast pressure results are presented.

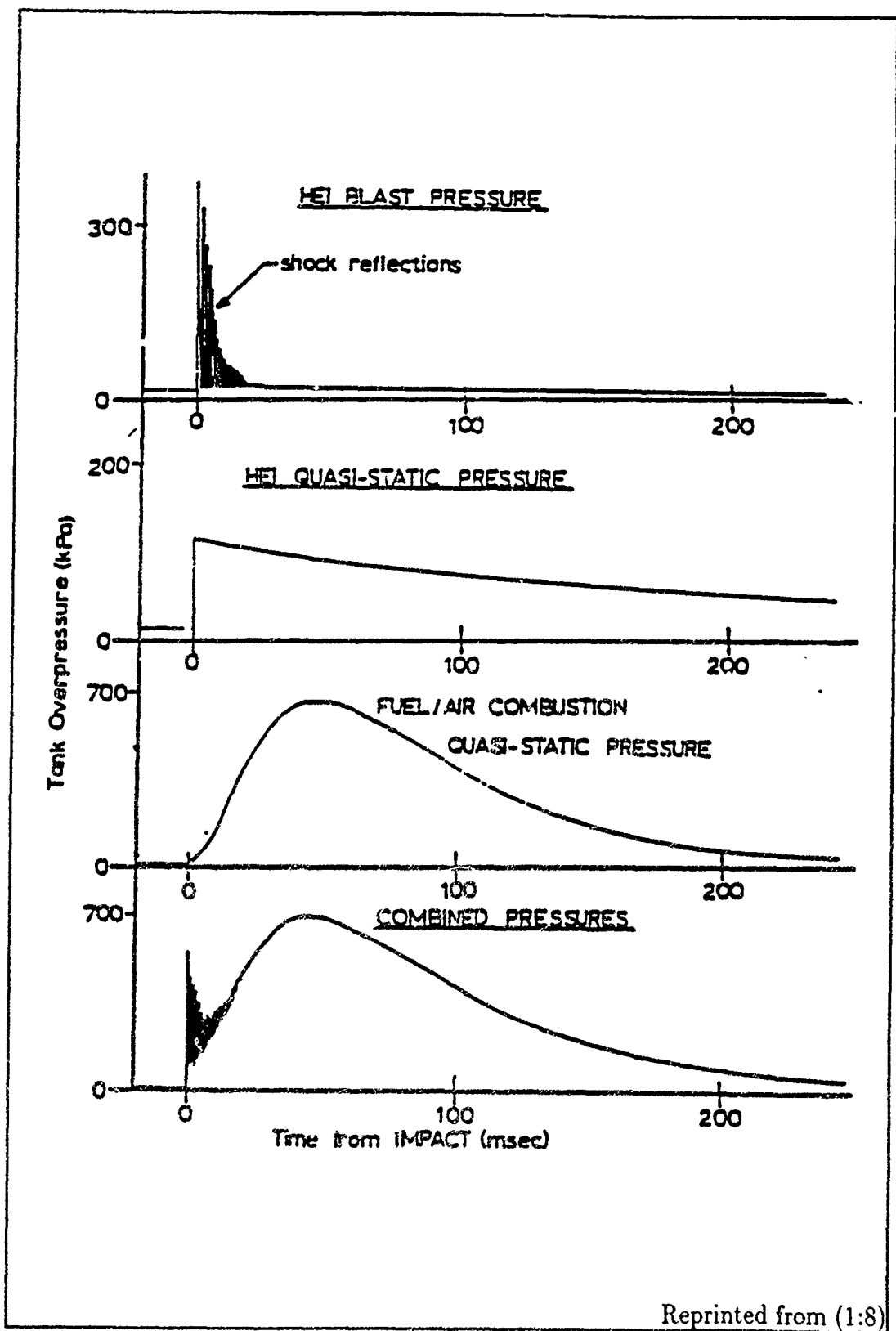


Figure 35. 23-mm HEI Pressure Breakdown

The test projectiles were statically detonated in a specially designed airblast arena. Figure [36] is a top view of the test arena, showing the location of six pressure transducers (P1 through P6) and fragment deflectors. The pressure sensors and the centroid of the test item were elevated 5 feet above ground level This was a sufficient height to allow completion of the positive phase pressure pulse prior to the arrival of the ground reflected shock wave.

The test projectile was positioned nose-up, with its longitudinal axis vertical, on top of a wooden support A break-wire circuit was attached to the projectile to record the time of detonation, t_0 . The pressure sensors were mounted transversely in aerodynamic probes behind fragment deflectors. Axhead probes containing PCB transducers were mounted with the transducer sensing surfaces opposite one another at a 1.5-foot distance from the projectile centroid. Positioned further from the projectile were modified Susquehanna Instruments Model ST-7 probes containing sensing elements at distances of 4.0 and 4.5 feet.

The PCB Piezotronics Series 102 piezoelectric transducer was used at the closest measurement position. It has a range of 0 to 5,000 psi with a moderately high output (1 or 10 MV [milli-volt] per psi) and high natural frequency (500 kHz). The ST-7 piezoelectric sensor has a range of 0 to 500 psi, and a natural frequency of 250 kHz. All signal conditioning and recording equipment (including the Bell and Howell VR 3700B FM recorder), along with the calibration procedures, is discussed in detail in ADTC-TR-74-117, *Airblast Measurement of Unconfined Spherical Experimental Explosives* (U), CONFIDENTIAL, December, 1974, ADC000740L. (20:5-7)

The summary data shown in Table 11 is an average of six observations at each distance for each projectile type. These observations result from pressure records at two opposing sensors a given distance from the projectile on three detonations of the given projectile type. Table 12 shows this same data but averaged on only the three detonations of the given projectile type. The six pressure sensors are listed individually for each projectile type.

Note that the average pressures listed in Table 12 for the same distance and projectile type are different. Because these pressure figures are averages, the actual pressure differences between paired, opposing sensors is assumed to be erratic. Possible reasons for this are briefly discussed in Section 2.5.4.

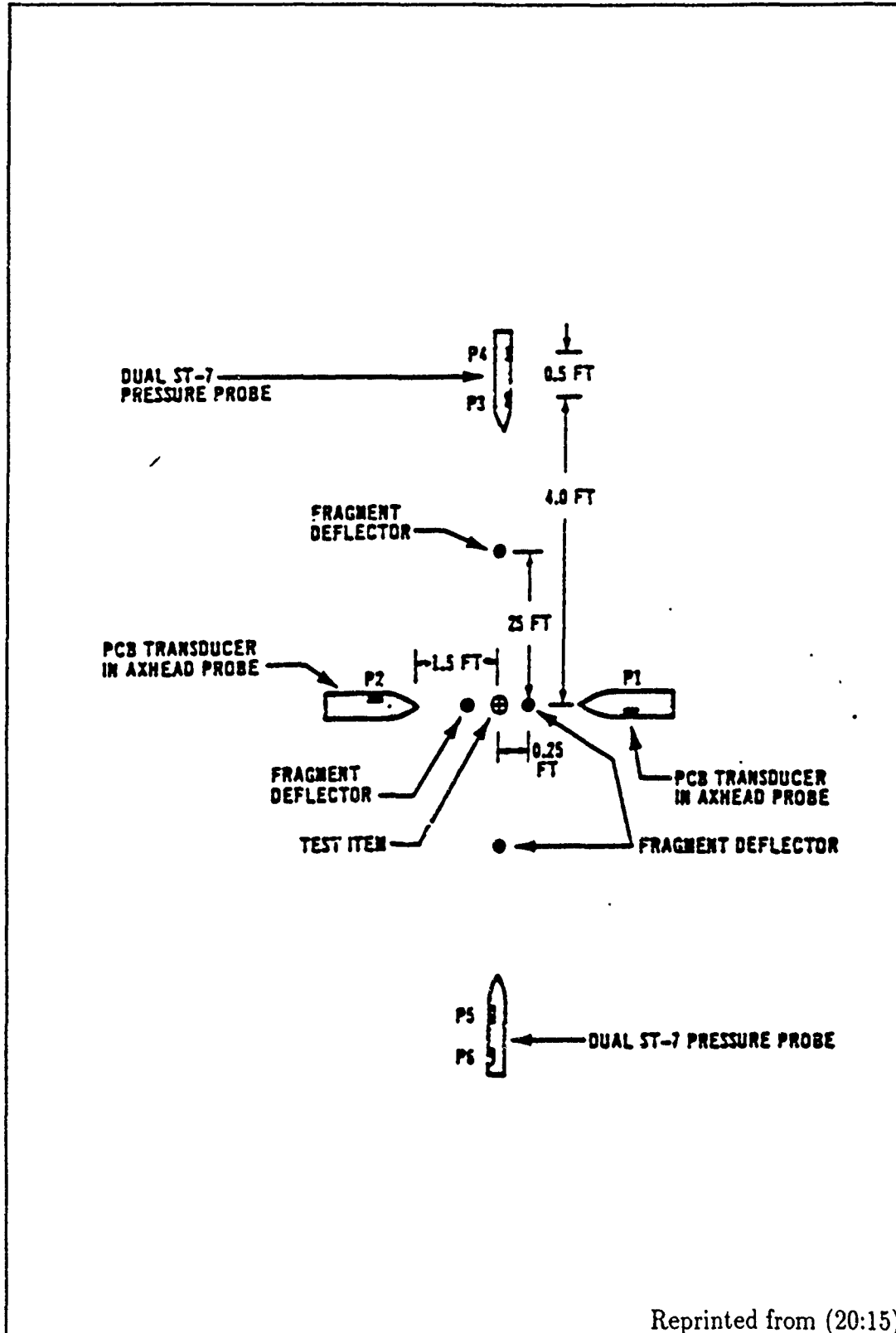


Figure 36. Schematic of 20-mm Airblast Measurement Arena

Projectile	Peak pressure, psi (P _{max})				Impulse, psi x ms (I)			
	Distance ^a (in.)			Avg ^b	Distance ^a (in.)			Avg ^b
	18	48	54		18	48	54	
Type S, standard M56A4	20.2	5.2	4.5	12.5	2.5	1.4	1.0	1.9
Type A, minimum weight	25.0	6.8	5.1	15.5	2.8	1.6	1.2	2.1
Type B, maximum HE	30.0	6.2	4.7	17.7	3.2	1.7	1.3	2.4
^a Distance from projectile centroid to sensing surface. ^b Calculated from equation of $X_{avg} = \frac{X_{18} + \frac{X_{48} + X_{54}}{2}}{2}$								

Reprinted from (20:24)

Table 11. Summary of 20-mm Projectile Airblast Data

The peak pressure measured in psi⁴ is the maximum pressure recorded by the sensor. This maximum pressure is (by virtually all accounts) at the leading edge of the wave as shown in the Pressure vs Time plot of Figure 37. The graph shown is for a sensor 18 inches from an exploding, standard 20-mm HEI projectile. All Pressure vs Time plots developed by the Jones Study are included in Appendix A. The numbers in the upper-right of these plots represent:

SWA The Shock Wave Arrival time shown in the upper-right corner is the time at which the peak pressure arrived⁵. Time, measured here in milliseconds⁶ is often measured in microseconds⁷ because of the short duration of the pressure wave.

⁴Pounds per Square Inch (psi).

⁵SWA is actually the time at which 20% of the peak pressure arrives. This 20% allows leeway for small pressure waves caused by the passage of a fragment.

⁶1 millisecond = 1/1,000 second

⁷1 microsecond = 1/1,000,000 second.

Type S, standard M56A4		Type A, minimum weight		Type B, maximum HE	
Peak pressure (psi)	Impulse (psi x ms)	Peak pressure (psi)	Impulse (psi x ms)	Peak pressure (psi)	Impulse (psi x ms)
Station P1, 1.5-ft distance ^a					
19.8	2.4	25.3	2.7	31.8	3.2
Station P2, 1.5-ft distance ^a					
20.5	2.5	25.6	2.8	28.3	^b
Station P3, 4.0-ft distance ^a					
5.5	1.4	6.5	1.6	7.1	1.9
Station P5, 4.0-ft distance ^a					
4.8	1.3	7.0	1.5	5.3	1.5
Station P4, ^c 4.5-ft distance ^a					
---	---	---	---	---	---
Station P6, 4.5-ft distance ^a					
4.5	1.0	5.1	1.2	4.7	1.3
^a Distance from projectile centroid to transducer sensing surface. ^b Impulse calculation invalid due to "ringing" on transducer (believed to be caused by fragment impact). ^c Station P4 data invalid due to improper calibration setting.					

Reprinted from (20:172)

Table 12. 20-mm Airblast Summary

Max Max is the peak pressure measured in psi.

Impulse Impulse is the integration or area under the curve over the positive pressure time period. The positive pressure time period is measured from the SWA time and the time at which the pressure returns to 0.0.

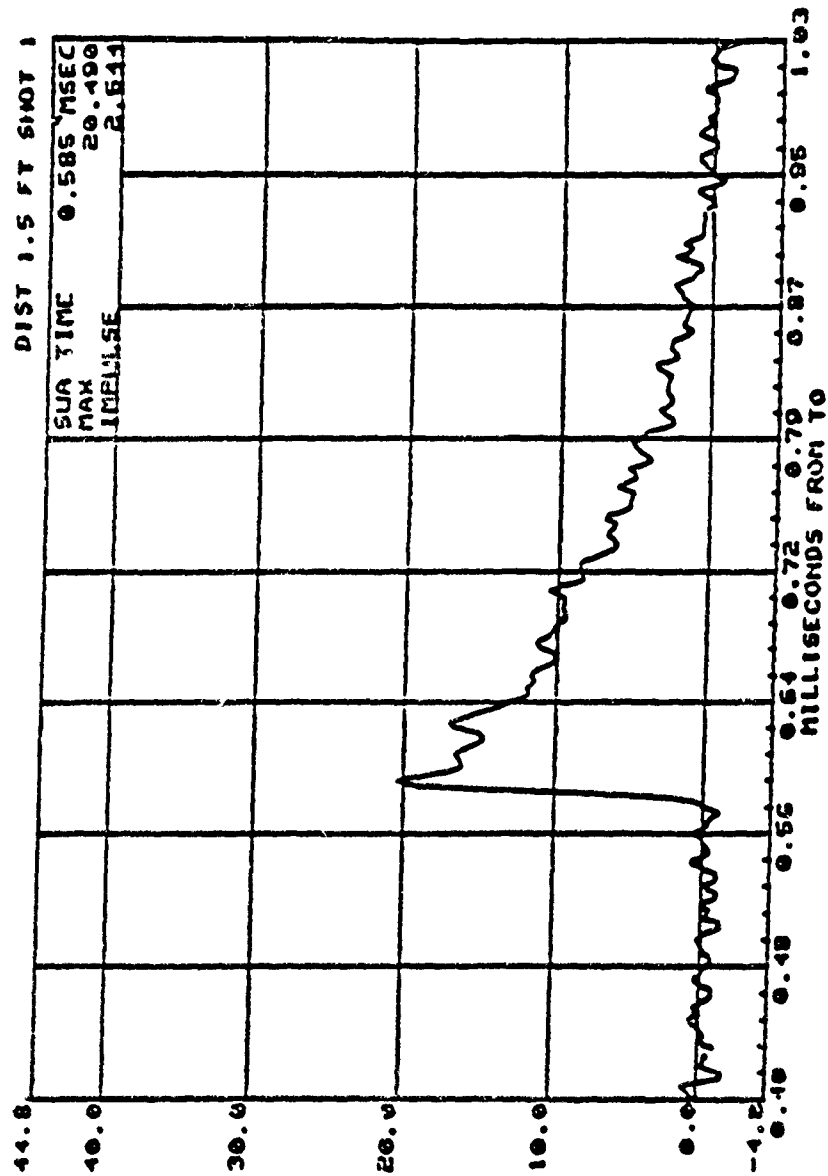
2.5.2 Weeding Study A study completed in 1986 by Cale S. Weeding examined the terminal ballistics of a 30-mm HEI projectile (32). Late in this study additional instrumentation was added to the testing chamber to measure pressures. This testing chamber was a 0.75 inch, heavy-walled steel tank. Testing conditions within the tank were very precisely controlled. Pressure data was collected for both 0° and 45° obliquity angle test shots.

Two pressure sensors were used. One was placed 48.0 inches to the side of the target (or striking) plate. The fuse was initiated on this target plate, and the detonation would occur shortly after and beyond this plate. The second sensor was placed 83 inches to the side and 20 inches in front of the target plate. This second sensor was placed to record reflected pressures within the tank.

It is unclear in the study whether the recorded overpressures represent blast pressures or the longer duration, residual pressures following after the blast wave. This authors interprets the data as a combination of both. Additionally, because the testing chamber has very little venting⁸ and a very thick, hard wall the pressures build upon one another. The blast wave radiates out from the detonating HEI leaving the residual pressure in its wake. But, the blast wave is reflected inward upon itself as it bounces off and between the chamber walls. This reflecting of the blast wave prolongs and may intensify the residual pressures.

The combustion pressures from the explosion of the gas/air mixture initiated by the exploding HEI follow shortly after the initial blast wave. Combustion pressures

⁸The testing chamber is entirely enclosed except for the projectile flight tube through which the 30-mm HEI projectile is shot into the chamber. (32)



Reprinted from (20:155)

Figure 37. Pressure vs Time Plot for a Standard 20-mm HEI

are definitely increased by the high pressures preceding them. Their pressures then build upon the already present overpressures within the chamber. The combustion pressure does not create a pressure wave as does the blast pressure but a change more like a step increase in the pressure level. All longer duration pressure levels are directly affected by the available venting.

There is a strong relationship between overpressure interactions and temperature increases. To some extent not fully understood by this author, there is a trade off of energy between the overpressures and the temperatures. Further insight into these energy exchanges is found in both fluid dynamics and thermal energy transfer textbooks. Studies of this energy exchange due to high energy explosions date back to the WW II era. Early papers on the subject were not released until the early 1950's. The earliest of these papers was authored by Sir Geoffery Taylor, F.R.S. (31)

2.5.2.1 Pressure Building. The pressure building effects of the reflecting blast wave, residual blast pressure, and combustion pressure are substantiated in Table 13. The results shown were obtained from tests conducted at a 45° obliquity which developed four peak pressure spikes as shown in the table. The higher pressure reading of the third passage (second reflection) of the blast wave is consistently higher as indicated by the Side-On Pressure P_3 .

The overall level of these pressure spikes depended greatly on the target material thickness. Figure 38 graphically shows this relationship. The increased plate thickness required an associated increase in the projectile velocity due to the ballistic limit of the material. When comparisons were made between different material with similar ballistic limits, the overpressures were essentially the same.

2.5.2.2 Pressure Variations. It is interesting to point out that the pressures recorded on the 0.5 inch aluminum plates decreased with increases in projectile velocity.

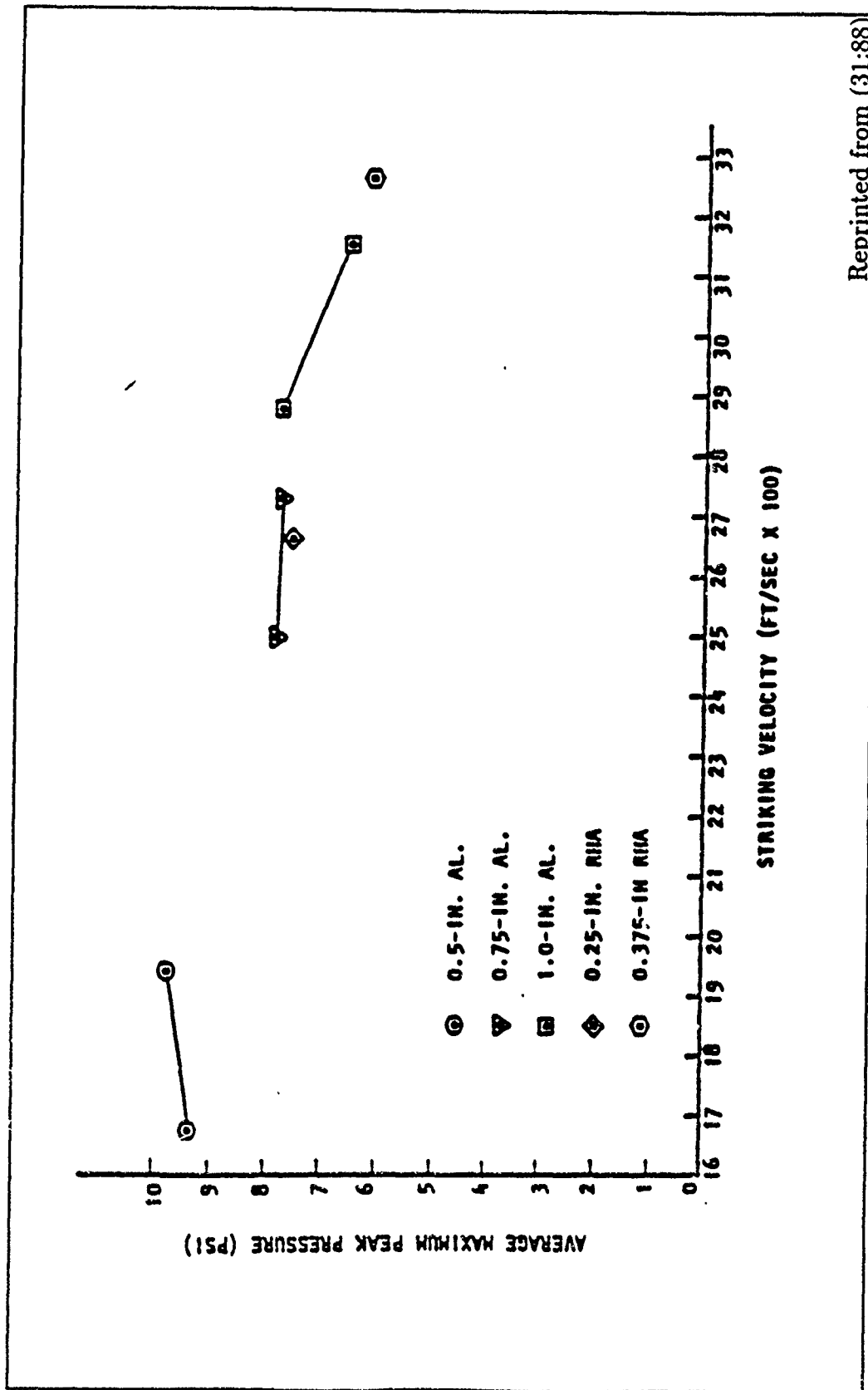


Figure 38. Average Maximum Side-On Peak Pressure Versus Striking Velocity for Several Target Plates at 45 Degrees Obliquity

Test No.	Striking Velocity (ft/sec)	Side-On					Reflected	
		Pressure (psi)				Time (msec)	Pressure (psi)	Time (msec)
		P ₁	P ₂	P ₃	P ₄	τ	P	τ
1	1588	3.46	5.13	9.42	6.21	2.08	5.24	1.72
2	1690	3.89	7.11	9.80	6.98	2.16	5.58	1.80
3	1700	4.40	6.80	8.60	6.27	2.01	5.75	1.79
4	1694	3.87	5.87	9.20	6.40	2.09	5.86	1.86
5	1706	4.27	6.53	9.47	7.73	2.13	6.26	1.83
6	1949	4.27	—	8.80	6.40	2.12	5.75	1.89
8	1914	3.73	6.13	10.40	7.60	1.98	5.65	1.83
9	1958	4.13	5.47	10.10	7.47	2.04	5.75	1.82
10	1935	5.20	6.53	9.73	7.07	2.01	5.85	1.79

Reprinted from (31:83)

Table 13. Peak Pressure for HEI Against 0.5-inch Aluminum Target Plates at 45 Degree Obliquity

... the overpressures tend to decrease with increasing striking velocity. It is believed that this is probably a geometry effect rather than an energy effect. Since the pressure gauges are located 90 degrees from the projectile flight path, it may be that the combination of kinetic and explosive energy is being propagated along the extended flight path leaving less blast energy normal [perpendicular] to the flight path, i.e., the moving charge effect. Another factor that may have influenced the test results could be that, at the higher velocities, the HEI projectile body is further into the target plate at time of detonation leaving less blast energy on the impact side and lowering the overpressures at the gauge locations. Had pressure gauges been located near the extended flight path beyond the target, they probably would have shown an increase in pressure with increasing striking velocity. (31:84)

2.5.5 Avery Study This study by John Avery also identifies the different causes of overpressure. Avery depicts the general relationship of these pressures in Figure 39. The combustion pressures shown in Figure 35 are not shown here since the ignition of a fuel source is not considered in this study.

There are two types of blast pressures generated by HE projectiles: dynamic overpressure and confined gas pressure. Regardless of whether the blast is internal ... or external ..., the structure will initially experience a dynamic overpressure, often referred to as a shock wave. This pressure loading is of very short duration, typically lasting ten micro-seconds or less. However, the peak pressure can be very high, and this overpressure can cause extensive damage

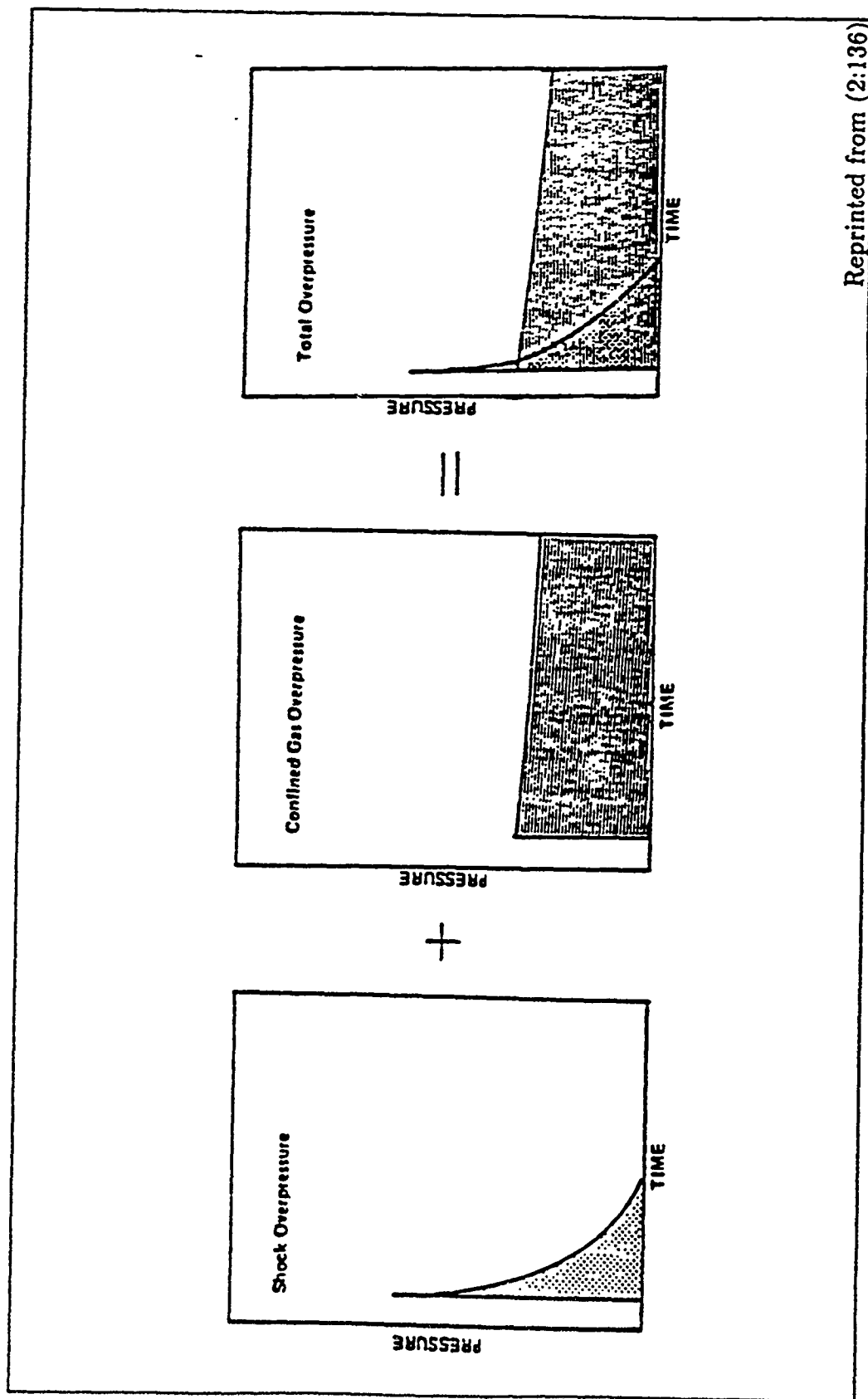
With HE projectiles, the interior structure may experience a residual pressure after the shock wave has dissipated, caused by the confinement of explosive gasses. This confined gas pressure typically has a lower peak value than the shock overpressure, but it has a much longer duration and can be a devastating failure mechanism (2:121)

2.5.3.1 Blast Loading. The Avery study outlines the relationship between the blast conditions and the extent of their damage to composite materials.

In doing this the study highlights some important characteristics of the overpressures.

Pulse duration refers to the time interval over which the overpressure is sustained. "The pulse duration is a function of explosive type and quantity, and the distance between the center of detonation and the structural element [target] (2:137)." The orientation of the target is also a factor in determining the pressure and its duration on the target. The pressure is therefore "... a function of the angle of incidence of the shock front, β , defined as the angle between a tangent to the shock front and the structural plane (2:137)." Simply stated, the shock wave may not originate from a point perpendicular (directly in front of) the target surface. The origin of the shock wave origin may be to one side of the target as shown in Figure 40.

The peak confined gas pressures or residual pressures and their duration "... varies with explosive quantity, altitude, cell size, [and] the amount of venting area relative to the cell size (2:138)." The altitude parameter determines the surrounding air pressure. All of these parameters are explained in previous sections.



Reprinted from (2:136)

Figure 39. Overpressure From Confined Detonation is the Result of Two Pressure Components

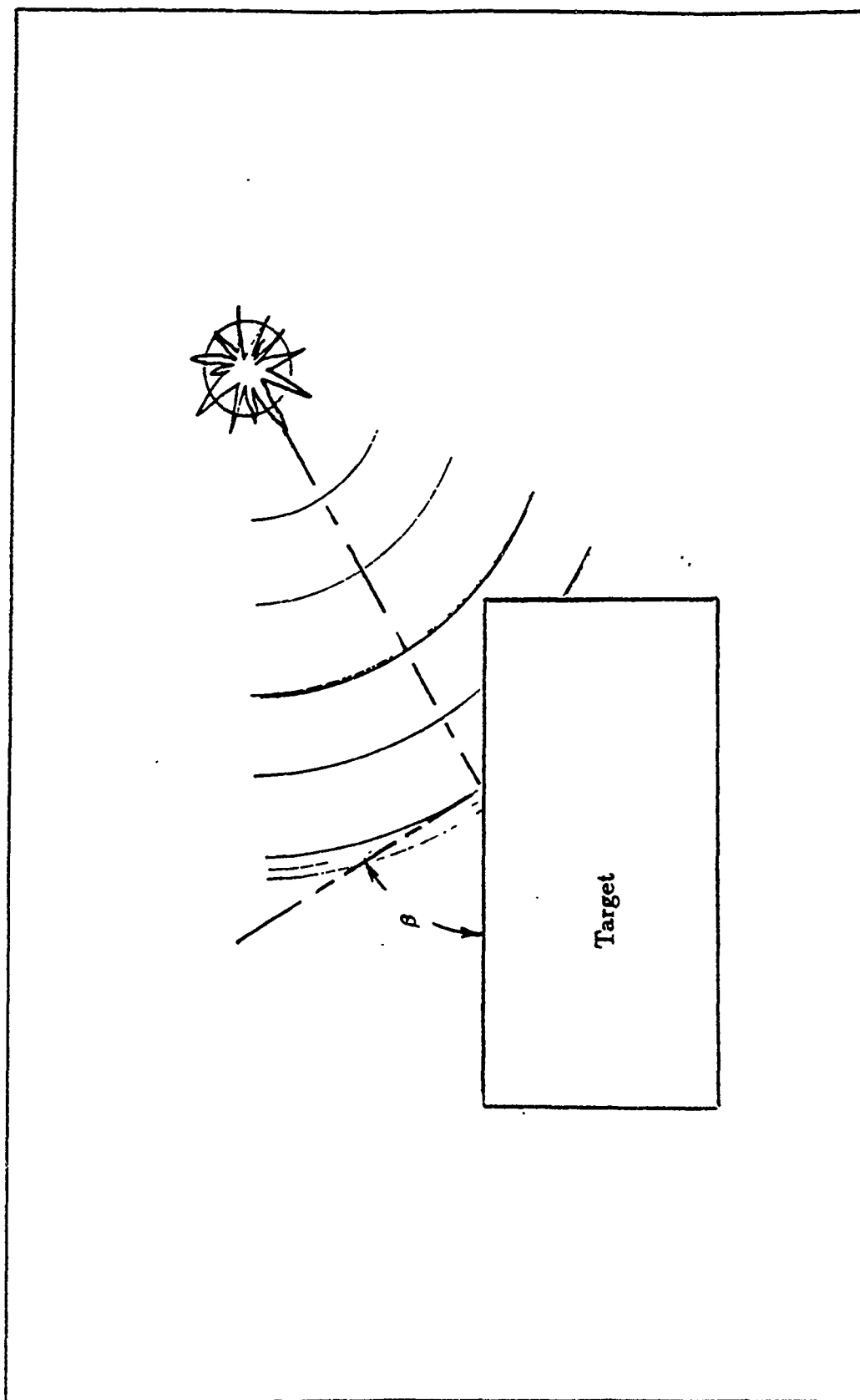


Figure 40. Blast Pressure Angle of Incidence

2.5.4 Inconsistent Pressure Measurements The pressures listed in Table 12 for the same distance and projectile type indicate an erratic pressure behavior. From one point to another around a circle centered on the explosion point, the pressures are different. Assuming the test was accurate, the cause of these differences could possibly be random or randomly based on the surrounding air environment. It is possible that the different pressures could be based on the particular fragmentation pattern caused by the explosion. The number, size, and location of the fragments may absorb more or less of the explosion energy.

2.6 Related Material

Because of the complexity of HEI threat, many studies have been conducted. These studies usually concentrate on only one aspect for a particular HEI type. Unfortunately there are many more problems and questions than there are studies to answer them. Some of these studies are used and referenced directly in this document. Others are not, but the information that they contain was very valuable to the complete understanding of the problems, concerns, and issues presented.

To round out the information already outlined, the next several sub-sections briefly present some of the related studies which may point the reader to his or her particular area of interest.

2.6.1 Target Overlay Grid Section 2.2 mentions the use of a target overlay grid several times. The definition of grid or grid size was also defined in that section.

A grid is most easily visualized as graph paper. It is usually used in conjunction with a specific 2-dimensional view or picture of the target aircraft. The grid size is usually scaled so that the length/width of one square is equal to a specified size on the scaled view of the target. This specified size is often two, four, six, or eight inches (6:Vol I, pp.12).

Kevin McArdle completed a study of the grid in 1987. In that study, differences between the results of centered and randomly chosen shot lines were quantified. A centered shot line is one which passes directly through the center as opposed to a randomly selected point within each grid square. Testing was conducted on several different component shapes. (25)

In general, the centered shot line performed better. The criterion used for assessment was the accuracy of each method in predicting the likelihood that a component would be struck, and the exposure of the component to the threat. The results varied somewhat based on component shape.

2.6.2 Ballistic Limit The ballistic limit of a projectile or fragment refers to the ability of the projectile or fragment to penetrate a plate. This ability to penetrate is dependent on the plate's thickness and material composition.

Studies of ballistic limit vary in their emphasis and scope. Some examine the ballistic limit of a particular projectile while others examine the ballistic limit of a certain type of material. In either case, the results specify the required projectile size, shape, mass, velocity, and angles at which the plate material is penetrated. This can be very important to the study of the 23-mm HEI threat.

Eventually, the ballistic limit data of the 23-mm HEI will be incorporated into the simulation of this threat against the aircraft and its fuel cell. A study conducted by Stephen J. Bless in 1981 looks at the ballistic limit of various aircraft components. (5)

William A. Schmeling conducted ballistic limit tests on the 20-mm, 25-mm, and 30-mm HEI projectiles. His tests were conducted against mild steel and aluminum plates at very high obliquity angles. The tests determined at what angles, and velocities the various projectiles either penetrated the plate or ricocheted off the plate. The tests also evaluated the effect of different fuse types. (30)

Gale S. Weeding conducted 30-mm ballistic limit tests for both API (Armor Piercing Incendiary) and HEI projectiles. These tests were conducted on 0.5 inch, 1.0 inch, and 2.0 inch aluminum plates at 0° and 45° obliquity angles. The HEI was also tested against RHA plates. As a part of these tests the "behind plate spall" was measured. Spall is the aluminum that flakes or is shattered off the back side of the plate by the impact of the projectile on the front surface. Because aluminum burns at high temperatures these particles can increase the combustion and associated pressure from any explosion or fire. (32)

2.6.3 Fire Suppression Many studies could be mentioned here. The driving force behind this paper and the resulting simulation is the need for a good, environmentally safe fire extinguishing/suppressant system. Because of the ozone depletion problem, the military use of halon as a fire extinguisher/suppressant is being banned. The issue of its use is even mentioned in political rhetoric.

2.6.3.1 Heinonen Study. Because of halon's threat to the environment, the Wright Research and Development Center is conducting tests of various other fire suppressants/extinguishers. A report on these tests was published by Everett W. Heinonen in Oct of 1990. The report outlines the purpose and testing results. (17)

2.6.3.2 Anderson Study. Charles Anderson tested the ability of both Halon 1301 and nitrogen to suppress/extinguish fires. Using a very controlled environment he was able to combine very exact ratios of fuel, air and oxygen; along with specific levels of pressure, temperature, and venting for these tests. Thus, all tests consistently subjected optimal explosive characteristics to the HEI threat. The fire ignition source was a 23-mm HEI because it is both a common and very powerful ignition source. (1)

Not only did the Anderson study look at the fire inerting ability of both halon and nitrogen, it also optimized the amounts needed to effectively inert the fire. As a part of this effort, it was determined that an exploding 23-mm HEI consumes or alters a specific level of oxygen even though the explosion itself does not need oxygen. Thus, the HEI partially inerts itself.

The size of the ignition source is a critical parameter in determining the overall reaction in the fuel tank ullage. With a point ignition source, the flame front initiates from a point and radiates spherically throughout the fuel tank. For conditions encountered in an aircraft fuel tank, a fuel/air explosion will be a deflagration (subsonic flame front speed) and not a detonation (supersonic flame front speed). The pressure rise time of the explosion is directly related to the flame front speed and the dimensions of the tank. When heat transfer and especially venting are considered, the rise time becomes extremely important. During the finite time that is required for an explosion to occur (i.e., time from beginning to end of combustion), venting and heat transfer combine to reduce the peak combustion pressure. Shorter rise times of the combustion pressure leave less time for venting and heat transfer to reduce the peak combustion pressure. (1:3)

This chapter closes with this quote because it reflects and creates a vivid image of why this and other studies are being done.

III. Analysis and Test Recommendations

Hypothesis:

The fragmentation and blast pressure peculiar to an HEI are dependent upon the quantity and type of explosive, and the projectile structure.

Premise:

The altitude and relative temperature at which detonation occurs influence the outcome but not the fundamental shape and magnitude of the explosion.

Upon first glance the hypothesis stated above may not appear profound or especially insightful. And most likely, it would meet with little opposition as a fundamental statement of the difference between HEI projectile types. But, the hypothesis, as stated, is intended to suggest that the entire explosive effect of an HEI could be predicted by knowing only the projectile characteristics listed below.

That is not to say that external forces and objects will not change the explosive effects. Rather, the local environmental characteristics also listed below, will alter the explosive effect slightly. Even the target itself will change the explosive effect depending on its (the target's) characteristics. But, regardless of what external forces are present, the projectile characteristics will not change. It is these stochastic¹ projectile characteristics that define the basic fragmentation and blast pattern.

Projectile Characteristics:

- The projectile structural shape and material
- The amount and type of explosive charge

Environmental Characteristics:

¹The effects are not exactly the same for each projectile. There are slight variations due to machining, explosive mixture, etc .

- The air pressure (altitude) and temperature

Target Characteristics:

- The angle of attack; obliquity angle
- The impact velocity
- Potential pressure confines
- Available venting
- Potential for heat transfer

The projectile structural shape and material refers to much more than the outside dimension, i.e., more than just 'a 23-mm HEI which is 4.33 inches in length'. The shape of the walls, the fuse type, the shape and size of the tracer, any bands or scoring, etc ... are also part of the structure and must be specified. It is these projectile differences, along with the amount and type of explosive that cause different fragment patterns. This has been proven through the study conducted by Steven R. Jones (reference Section 2.4.3).

3.0.4 Statistical Proof Although the hypothesis seems plausible or at least worth investigating there is insufficient data to prove or disprove it.

The data that is available describes the fragment direction, velocity, and number; and the blast pressure perpendicular to the exploding projectile. However, each individual datum is isolated unto itself. None of the fragment weight data is associated with velocity data. Similarly none of the blast data is associated with the fragment weight or velocity data. The interrelationship of these parameters is therefore not quantifiable at this time.

In order to prove the original hypothesis, the following propositions need to be investigated.

Proposition A: There is a dependence between a fragment's size/weight and its velocity when statically detonated.

Proposition B: There is a dependence between a fragment's position within the projectile casing prior to explosion and its direction of flight when statically detonated.

Proposition C: There is a dependence between a fragment's size/weight and position within the casing prior to explosion.

Proposition D: There is a dependence between the blast pressure and the fragment directions.

3.0.4.1 Proposition A. Proposition A tests the dependence between a fragment's size/weight and its velocity. The test should be performed with static detonation data from each zone individually. If the dependence is proven and the relationship determined, the simulated fragments will take on realistic parameters. These parameters determine where, at what angle, and with how much force a fragment will impact the target component. Thus, both the velocity and mass would be associated with a specific target hit. Much of a program's expected or simulated damage depends on the fragment's striking obliquity angle, mass, and velocity. Without these, the expected or simulated damage is just a guesstimate.

Although the studies reviewed do gather data on both the fragment's velocity and weight, they do not associate the two parameters. The velocity data is gathered through the use of light screens, or low voltage screens. The weight data is gathered from fragments collected after the test shot(s). The analyst gathering this data does not usually know which fragment collected from the collection bundles is associated with each velocity measurement. In fact, the number of fragments gathered for weight data does not usually equal the number of velocity measurements. How the analyst accounts for the disparity is not usually reported by the study.

New studies are not likely to associate velocity and weight data unless the requirement for this association is firmly made. To accomplish the association, test

set-ups must improved so as to isolate individual velocity measurements to collection bundles sized so as to gather only one fragment. Recommendations for such a test are made in Section 3.0.5.

3.0.4.2 Proposition B. Proposition B tests the dependence between a fragment's direction when statically detonated and its origin on the projectile. The fact that different projectile casing shapes can cause different fragment patterns as shown by Jones (reference Section 2.4.3) suggests that this dependence exists. In addition, the picture of an exploding 30-mm projectile, Figure 41², also indicates that such a dependence exists. In this figure, the fragments appear to form a smooth convex curve of outwardly moving fragments. No fragments appear to be crossing from one end of the projectile to the other. If such a dependence does exist, the fragments pictured would not be expected to form the definite curvature shown in the figure.

Proof of this proposition requires additional information on the projectile body. The projectile casing needs to be subdivided into the appropriate number of zones and weighed. Likewise the fragments from each zone need to be weighed and totaled. The total fragment weight for a zone must include all fragments in that zone or be adjusted to account for the portion of the zone that is represented (reference Section 2.4.1.3). This is necessary since the area of each zone is different. If the proposition is true, the relative weight of the zones will be correlated to the relative weight of the casing sections³.

Such a test could be easily accomplished with the fragment data already available if relative casing section weigh's were made available. This would eliminate the need for additional projectile tests. Only one projectile casing needs to be cut since

²This figure is repeated from an earlier section; Figure 31

³The correlation may be effected by Proposition C. Therefore due consideration of that proposition should be made prior to testing.

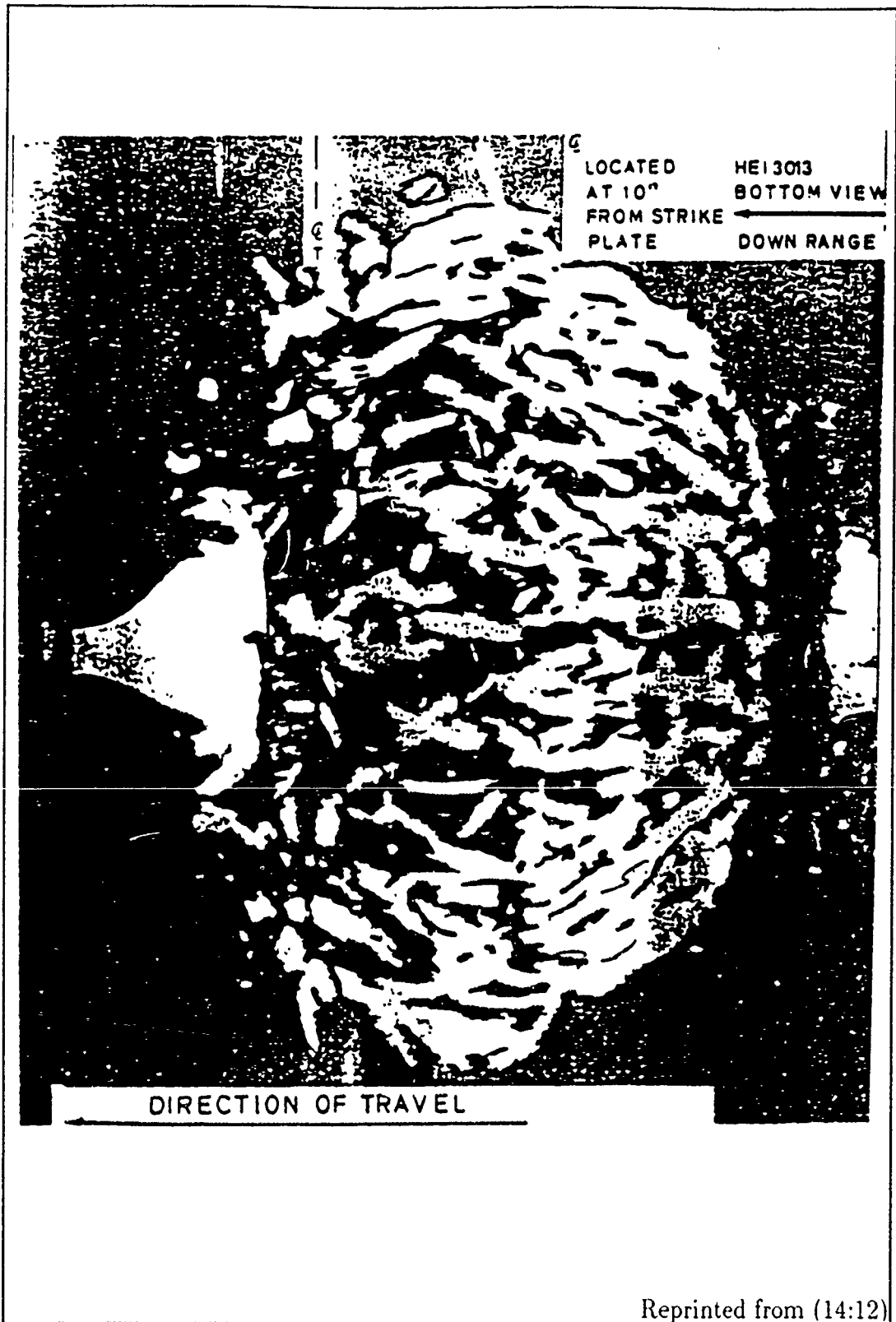


Figure 41. Flash X-Ray of the 30-mm Projectile Case Break-up

they are virtually identical. The cuts separate the projectile latitudinally into an appropriate number of zones to match the available fragment data.

3.0.4.3 Proposition C. Proposition C tests the dependence between a fragment's size/weight and position within the casing prior to explosion. It appears from Figure 41 that such a relationship may exist. Fragments close to the fuse end are smaller and there are fewer of them. Fragments toward the tracer end are larger and much more densely packed. Testing requires special care since there are two aspects to this proposition.

First, the explosive force of the projectile may affect the fragments differently based on how far they are from the fuse end. This possibility exists because the entire explosive material does not explode simultaneously. The time span is very short but the material actually explodes like a wave passing from the fuse end to the tracer end. This means that the fuse end fragments may experience somewhat different explosive forces than tracer end fragments.

Second, the projectile casing is not of a uniform thickness. The casing of many HEI have a thinner wall at the fuse end and a thicker wall at the tracer end. Therefore the fragments may again be different from end to end. To illustrate this imagine two plates of glass: one very thin, the other very thick. Hitting the first plate with a hammer will cause it to shatter into many small pieces. Hitting the larger piece may only break it into a few large pieces. Of course, depending on the type of material, the reactions may be reversed.

The end results of both the propagation of the explosion (the first aspect) and the casing shape (the second aspect) are confounded. That is, when both aspects are present, their individual effects can not be distinguished. Therefore, the propagation of the explosion must be eliminated while testing the casing shape and/or vice versa. Once one of the aspects has been tested and its effects determined the other aspect can be tested with or without being isolated.

For instance, the casing shape aspect can be eliminated by using a straight bore of the casing so that its thickness is uniform over the entire length. With this straight bore, the progressive explosion can be tested. Once the progressive explosion effect is understood the casing shape effect can be tested with or without elimination of the progressive explosion effects. If the progressive explosion effects are not eliminated, they must be backed out of the casing shape test results.

3.0.4.4 Proposition D. Proposition D tests the dependence between blast pressure and fragment directions. Section 2.5.4 and the data shown in Figure 14⁴ suggest that the blast pressures are not uniform and dependent only on the distance traveled. An explosion from a spherical, unencumbered charge is expected to be uniform in all directions. The HEI explosion is not spherical nor unencumbered. The HEI has a barrel shaped charge which, when exploded, is expected to be uniform across the longitudinal axis. The HEI explosion is encumbered by the projectile casing, fuse, and tracer.

Newton's third law⁵ also indicates that a difference in blast pressure from one side to the other can be expected since any blast wave pressure pushing the fragments outward will diminish the force of that pressure. In every explosion, some finite amount of blast pressure is exerted upon the fragments thus leaving less blast pressure force (or energy) to radiate outward in the direction of the fragment. Under this law, the mass and number of the fragments as well as their directions will influence the blast pressure.

The laws of energy also dictate a trade off between energy used to propel the fragments, energy used to generate the blast wave, and energy used to create heat. Assuming a finite uniform distribution of energy, a greater fragment mass on one side of the projectile can be expected to reduce the blast pressure on that side.

⁴Table 12 is repeated here for convenience

⁵For every action (force) there is an equal and opposite reaction (force).

Type S, standard M56A4		Type A, minimum weight		Type B, maximum HE	
Peak pressure (psi)	Impulse (psi x ms)	Peak pressure (psi)	Impulse (psi x ms)	Peak pressure (psi)	Impulse (psi x ms)
Station P1, 1.5-ft distance ^a					
19.8	2.4	25.3	2.7	31.8	3.2
Station P2, 1.5-ft distance ^a					
20.5	2.5	25.6	2.8	28.3	^b
Station P3, 4.0-ft distance ^a					
5.5	1.4	6.5	1.6	7.1	1.9
Station P5, 4.0-ft distance ^a					
4.8	1.3	7.0	1.5	5.3	1.5
Station P4, ^c 4.5-ft distance ^a					
---	---	---	---	---	---
Station P6, 4.5-ft distance ^a					
4.5	1.0	5.1	1.2	4.7	1.3
^a Distance from projectile centroid to transducer sensing surface. ^b Impulse calculation invalid due to "ringing" on transducer (believed to be caused by fragment impact). ^c Station P4 data invalid due to improper calibration setting.					

Reprinted from (20:172)

Table 14. 20-mm Airblast Summary

To illustrate this, imagine putting air into an old balloon tire. A weak or thin area on the tire is likely to protrude out from the rest of the tire. If too much air is put into the tire, the weak spot would be expected to pop first. Similarly, a balloon when over inflated will burst. Fragments of the balloon may be evenly dispersed around the explosion point, or they may lie in only one area. Although the rubber material of the balloon and the tire completely surround the force of air pressure, once either bursts, the fragments may not be uniformly distributed. Also the force of the escaping air is not likely to be uniform in all directions.

To test this proposition the distribution of fragments must be gathered not only by zone (latitudinal sections) but also by longitudinal sections. Pressure instrumentation must be included with the fragment velocity, mass and direction instrumentation so

correlations can be developed. The placement of pressure instrumentation should include several points on at least two distinct planes. One of these planes should bisect the projectile latitudinally much like the equator bisects the earth into an upper and lower hemisphere. The other plane should bisect the projectile longitudinally much like the prime meridian passing through Greenwich England.

3.0.5 Test Recommendations The data and test requirements stated in the above discussions need to be simultaneously accomplished. The reason for this is the great interdependence of each of the propositions. In fact, the propositions may have to be iteratively considered and refined.

One possible test configuration to gather all of the data described above is very similar to the test arena described in Section 2.4.2. This test arena consisted of a circular area bordered by 8 foot high Celotex bundles used to capture fragments. The projectile is placed in the center of this arena at a level that horizontally bisects the bundles. The fuse end is pointed toward the 0° zone boundary, and the tracer end is pointed toward the 180° zone boundary.

To gather velocity data in association with specific fragments, a low voltage velocity screen should be placed on the bundles at a point level with the projectile. This velocity screen or some similar velocity instrumentation, should be no more than 4 inches high. It can completely encircle the projectile as a 4 inch band bisecting the bundles all the way around the circle. Or, it can be placed much like a dashed line 4 inches high but still encircling the projectile. The velocity screen(s) must be made of many small strips not much larger than 4 inches high by 8 inches long. The small size makes it possible to gather individual fragments and associate their velocity to their size. The size of the individual velocity screens depends on the arena size and the general dispersion of fragments. They can be smaller or larger so long as they measure

only one fragment per shot. With multiple shots a fairly large data base of associated fragment weight and velocity data can be built.

In addition to the velocity screens, pressure instrumentation also need to be positioned in the arena. Each instrument should be protected from direct fragment impact by some sort of axehead deflector. The deflection should be within zone and not between zone deflection. As described above, there should be at least two planes with several pressure sensors per plane. The first plane should bisect the projectile longitudinally and need only go half way around (180°) the projectile. The second plane should bisect the projectile latitudinally and needs to fully encircle the projectile (360°). These two planes measure the relative pressure levels between zones, and from side to side (or sector to sector) respectively.

After each test shot, data should be gathered on the fragments per zone, blast pressure per zone, fragments per longitudinal sector, and blast pressure per sector. The fragment data should always include the number of fragments and a weight distribution. In addition, fragments that had their velocity measured need to have their individual weight recorded in association with the velocity. At this point, there should be no multiple shot averaging of the data.

Sufficient test shots need to be performed so that a good sampling of all data is available. This data can then be analyzed using Response Surface Methodology (RSM) to determine the interrelationship of the parameters.

3.1 Simulating the Dependence

Because the data is not available to statistically prove or disprove the dependencies proposed in the last section, the dependency was simulated. The simulation developed as part of this thesis and described in Chapter 4 was used to accomplish this. In this simulation an enhancement module was integrated into the basic simulation.

The basic simulation models the fragments and blast pressure resulting from an HEI detonation. The fragment and blast characterization found in the literature is recorded in a data file which is used by the simulation. The simulation reads this file to randomly select the number of fragments per zone; and each fragment's weight, velocity, and direction.

3.1.1 Standard Fragmentation The standard characterization found in the literature assumes that the fragment's weight and velocity are independent and normally distributed. And, although not directly discussed or examined, the literature studies show, at least to some degree, the dependence between a fragment's origin on the projectile and its velocity. This can be seen in the previous graphs of fragment velocity by zone. Early zones have a lower average velocity which increases toward the mid zones and then decreases again in the later zones. This pseudo dependency is modeled in the standard fragmentation module of the TS simulation. The reference to a pseudo dependency reflects the fact that within a zone, the literature assumes (or implies) that the velocity is normally distributed. This assumption and dilemma is consistently applied for zones sizes of 5° through 15° alike.

In a similar manner the fragment weight characterization found in the literature shows a dependence upon its position along the projectile. The zone weight data usually shows a trend which depends on the shape and type of projectile. But, this trend is not directly discussed or investigated in the literature. And, just as with the velocity, the fragment weight is assumed (or implied) to be normally distributed within a zone.

This standard fragmentation with independent selections of fragment weight and velocity is performed by the REGFRAG routine within the TS simulation. This standard fragmentation is selected by the user by setting the fragmentation type indicator to '1' in the SCENARIO.DAT file. This file is the user's primary means of controlling the simulation. Reference Chapter 4.

3.1.2 Dependent Fragmentation An additional module was incorporated into the TS simulation code to model the dependence between a fragment's weight and its velocity. The module called TSTFRAGS accomplishes this and it is selected by setting the fragmentation type indicator to '2' in the SCENARIO.DAT file. The only difference between this module and the standard fragmentation module, REGFRAGS, is the selection process for a fragment's velocity.

Common random numbers are used for all other random fragment characteristics, i.e., the number of fragments per zone; and each fragment's obliquity angle, rotation, and weight. The only difference is therefore the velocity selection for each fragment.

A fragment's velocity is based upon its randomly selected weight. If the randomly selected weight is 1.4 standard deviations above the mean weight for that zone, then the velocity is set 1.4 standard deviations below the mean velocity for that zone. Thus a direct and inverse dependency is achieved between the mass and the velocity of the fragment.

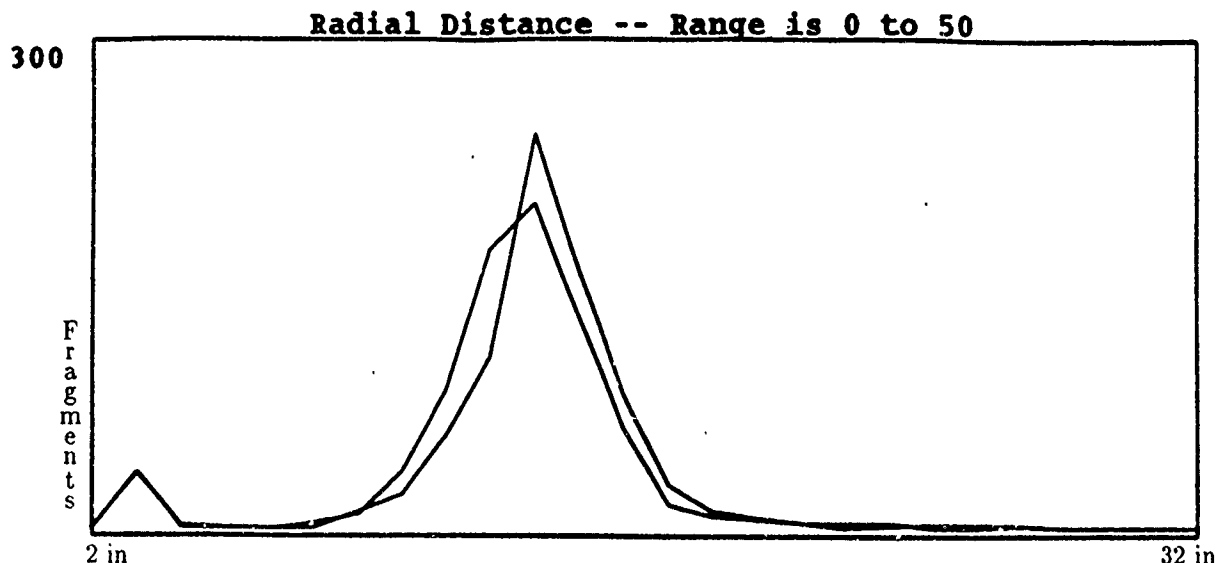


Figure 42. Test Results of the Radial Position

3.1.3 Comparison of Results Both of these fragmentation modules were simulated using the 23MMHEI fragment characterization file. Their results are overlaid one on top of the other in the following two graphs. This graph clearly shows the difference / similarity of results.

The first graph, shown in Figure 42, shows the radial dispersion of fragments impacting the target component. The X axis measures the radial distance from a low of zero inches on the left to a high of 50 inches on the right. The Y axis records the number of fragments impacting the target at specific radial distances. The very sharply pointed line shows the results from the module assuming complete independence of the mass and velocity parameters. The not so sharply pointed line shows the results from the module assuming a negative dependence between the mass and the velocity.

The lines are very close but not exactly the same. Some difference is expected since different velocities were selected by the two modules. But, the difference is very small. Further, it is believed that the observed difference would be statistically diminished as the number of observations is increased. Only one observation was used in this study.

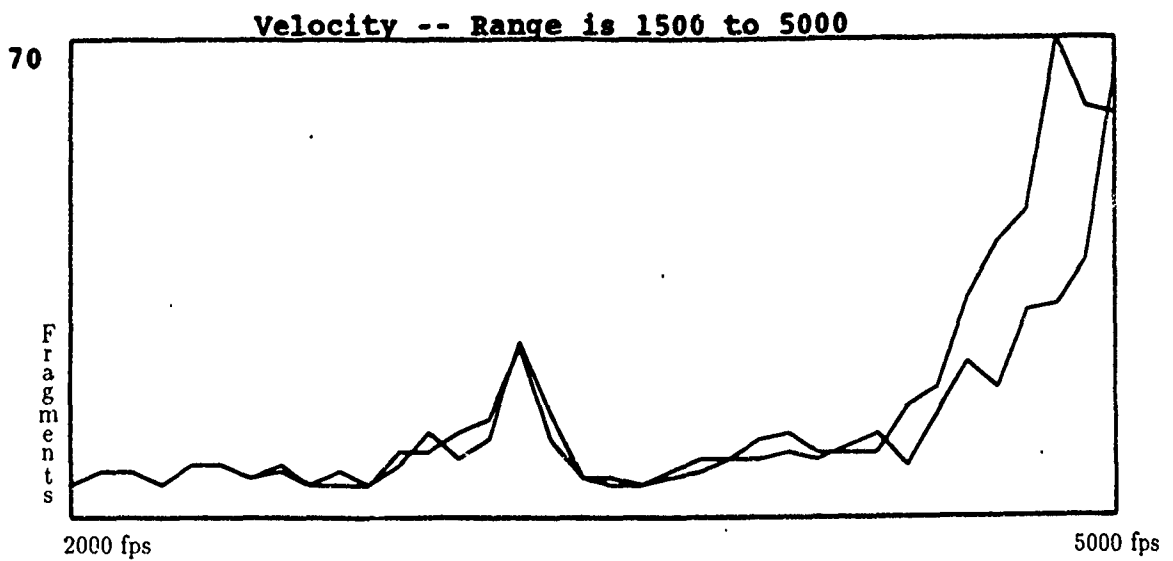


Figure 43. Test Results of the Velocity

The second graph, shown in Figure 43, shows the distribution of velocities. The X axis shows the velocity and ranges from a low of 1500 feet per second (fps) on the left, to a high of 5000 fps on the right. The Y axis shows the number of fragments having a particular velocity. Both lines on this graph are also very close. And again, the difference that is observed is expected to decrease with additional observations.

IV. Methodology

To aid the testing and development of alternative dry bay fire suppressant systems a versatile simulation was developed. The simulation was developed using SLAM II and FORTRAN coded modules. These modules describe the processes and movements of fragments and blast pressure throughout the simulated dry bay. The timing and order of fragment impacts and blast pressures is controlled via the SLAM II time incrementing routines. The simulation time is measured in microseconds since both the fragments and the blast pressure wave travel at very high speeds.

This simulation provides the user with a simple interface with which to adjust the attack scenario, the dry bay configuration, and the type of projectile to be simulated. Each of these is specified by the user via simple data files. In this way the changes can be made quickly, and there is no need to recompile the simulation program.

More extensive modifications can be added via user programmed modules that are recompiled with the existing simulation code. Changes of this type might include a module with fire retardant specifications, or a module specifying the interaction between HEI fragments and the fuel cell.

The following sections walk the reader through the simulation's design starting with a brief overview of the major program routines. The actual code and full documentation can be found in Appendix C.

4.1 Simulation Overview

The simulation models the actions of the HEI immediately following its entry into the dry bay. The actions modeled include both the fragments and the blast pressure wave. The simulation starts with user input specifying the attack scenario and the dry bay configuration. The user must also specify a projectile type and an output file name.

4.1.1 Simulation Modules There are 7 major modules to the simulation. These modules are listed below and discussed in the subsequent sections. The modular architecture of the simulation was developed to provide the user with exceptional control over the projectile and dry bay configuration to be simulated.

- Static fragmentation.
- Dynamic shift.
- Attack scenario.
 - Burst point.
 - Direction / orientation.
- Component construction.
 - Placement and orientation within the dry bay.
 - Shape / bounding edges of the object surface.
- Target / component impact.
- Blast pressure through distance.
- Blast pressure through time.

Additional modules can be added without the normally associated maintenance to every existing module. Thus, the user can easily add or remove modules. For example, the user may add several modules describing several fire suppressant systems. Each of these fire suppressant systems can be simulated with a user specified dry bay configuration and attack scenario.

4.1.2 Simulation Output The system outputs histograms of the fragment velocity, the fragment weight, and the radial distribution of fragments. The outputs also include the coordinates of each fragment impacting the target component along

with the impact velocity, weight and angle of impact. These outputs are not particularly significant in and of themselves. The real information from these outputs is their ability to show how different projectile types and different attack scenarios affect the dispersion and distributions describing the fragmentation.

The simulation also outputs a file containing blast wave pressure data. This data file reports the pressure at specific distances from the detonation point. The distances for which a pressure is reported range from 1 to 36 inches on one inch intervals. Thus, there are 36 pressure measurements through distance. In addition, the output file contains pressure data through time. Every 10 microseconds from the time of detonation, the pressure, through the distances just described, is recorded in the output file.

The pressure data reported on the output file can be thought of as a matrix with 36 columns of data. Each successive column represents an additional distance of one inch from the detonation point. The number of rows depends on the velocity of the blast wave. Each row represents an additional 10 microseconds from the time of detonation. The pressures through time are recorded every 10 microseconds until they return to normal atmospheric pressure over the entire 36 inch range.

4.1.3 Provisions for Future Enhancements The simulation design allows for the integration of enhancements. These enhancements are incorporated through the use of user written FORTRAN modules. A module might describe component interactions or various modifications to the underlying principles of projectile fragmentation. One such modification to the underlying fragmentation principle was made and tested as a part of this thesis. The modification and its results are discussed in Chapter 3.

4.2 User Inputs

The user's primary control of the simulation is through a data file called SCENARIO.DAT. This file must exist before the simulation can be run. Entries in this file control the attack scenario and the placement of component surfaces within the dry bay. The first component surface is regarded as the target by the simulation. Therefore, at least one component surface must be entered in this file. An example of this file is shown in Figure 44. The entries are listed and described below.

- Output file name.
- Projectile name.
- Projectile attack angle.
- Projectile rotation angle.
- Projectile velocity.
- Fuse / detonation delay.
- Component shape indicator.
- Number of component surface corners.
- Component corner coordinates.

Line 1; Entry 1 An output file name with a maximum of 8 characters. Upper case letters should be used but the simulation will automatically convert any lower case letters to upper case.

Line 1; Entry 2 The type of projectile to be simulated. This entry is limited to 8 characters which should be upper case.

If lower case letters are entered, they are automatically converted to upper case by the simulation. A '.DAT' extension is automatically added to this name.

```

TEST 23MMHEI ; Output file name, Projectile type
0.0 0.0 2500 75 ; Obliquity angle, Rotation, Velocity, Fuse delay
1 ; Component shape indicator
4 ; Number of corner points
48 48 18 ; (X,Y,Z) point coordinates
48 -48 18 ;
-48 -48 18 ;
-48 48 18 ;

```

Figure 44. Example of the SCENARIO.DAT Data File

Line 2; Entry 1 The obliquity angle of the projectile to the dry bay (aircraft) surface. This is a real valued entry measured in positive or negative degrees. The range of this entry is between -90° and $+90^{\circ}$ and should be entered without the ($^{\circ}$) unit designator.

Line 2; Entry 2 The rotation of the obliquity angle around the normal to the dry bay surface. This is a real valued entry also measured in positive or negative degrees. The effective range of this entry is between -360° and $+360^{\circ}$ but any value can be entered. Again, the value should be entered without the ($^{\circ}$) unit designator.

Line 2; Entry 3 The velocity of the projectile measured in feet per second. This is a real valued entry.

Line 2; Entry 4 The fuse delay specified in microseconds. The entry is real valued.

Line 3; Entry 1 This integer valued entry designates the type of fragmentation to be simulated. Valid entries for this field are currently limited to "1" or "2" only. The "1" indicates that a regular fragmentation of the projectile, as found

in the literature, is to be accomplished. The "2" indicates that a hypothesized fragmentation of the projectile is to be accomplished. This hypothesized fragmentation was tested in Chapter 3.

Line 4; Entry 1 The number of corner points which are used to define the component surface placement within the dry bay. This is an integer valued entry which must match the number of corner points input on the following lines.

Line 5-n; Entries 1, 2, 3 The 'n' designates that multiple lines are entered here as designated by Line 4; Entry 1. Entries 1, 2, and 3 are the **X**, **Y**, and **Z**, coordinates respectively. They are real valued and measured in inches from the projectile's entry point into the dry bay. Each line designates the coordinates of one corner point of the component surface being defined.

The last two lines of entries listed above can be repeated any number of times. Thus, any number of surfaces can be defined within the dry bay. Only the first surface defined acts as the target plate. Other surfaces act as simple fragment barriers, although future enhancements may define specific interaction routines for these other surfaces.

4.2.1 Output File Name This file name is used to generate two files for simulation output. A '.FRG' extension is added to the supplied name to open a file for fragment information output. A '.BLP' extension is added to the supplied name to open a file for blast pressure output.

An additional file name of 'DBAY.OUT' is automatically created and opened by the SLAM II simulation package. This output file contains histograms on the fragment velocity, fragment weight, and radial impact point of the fragments impacting the target component.

4.2.2 Projectile Type A '.DAT' extension is added to this file name and causes the simulation to open the appropriate input file describing the projectile. A frag-

ment characterization file with this name must already exist. The simulation then generates the appropriate fragmentation and blast characteristics for the projectile. These characteristics include the following information.

- Amount of RDX explosive material measured in grams.
- The number of zones used to define the fragment dispersion.
- The number of fragments per zone.
- The upper boundary for each successive zone.
- The mean fragment weight per zone.
- The standard deviation of fragment weight per zone.
- The mean fragment velocity per zone.
- The standard deviation of fragment velocity per zone.

The upper boundary of each zone is measured in degrees. The lower boundary for each zone is the same as the upper limit of the previous zone. The lower limit of the first zone is of course 0°. The upper limit of the last zone cannot exceed 180°; it can be less than 180°. The number of fragments per zone is assumed to be from a poisson distribution. The fragment weight and velocity are assumed to be normally distributed as suggested by the literature.

Additional projectile types can be developed by the user. Each data file created must have a unique name with a '.DAT' extension. The files are simple ASCII files which can be created with almost any word processing package. Figure 45 shows an example of this file.

4.2.3 Obliquity Angle The obliquity angle is measured in degrees off a line normal¹ to the dry bay (aircraft) surface. This obliquity angle is swung to the left

¹A line which is *normal* to a surface is perpendicular to that surface

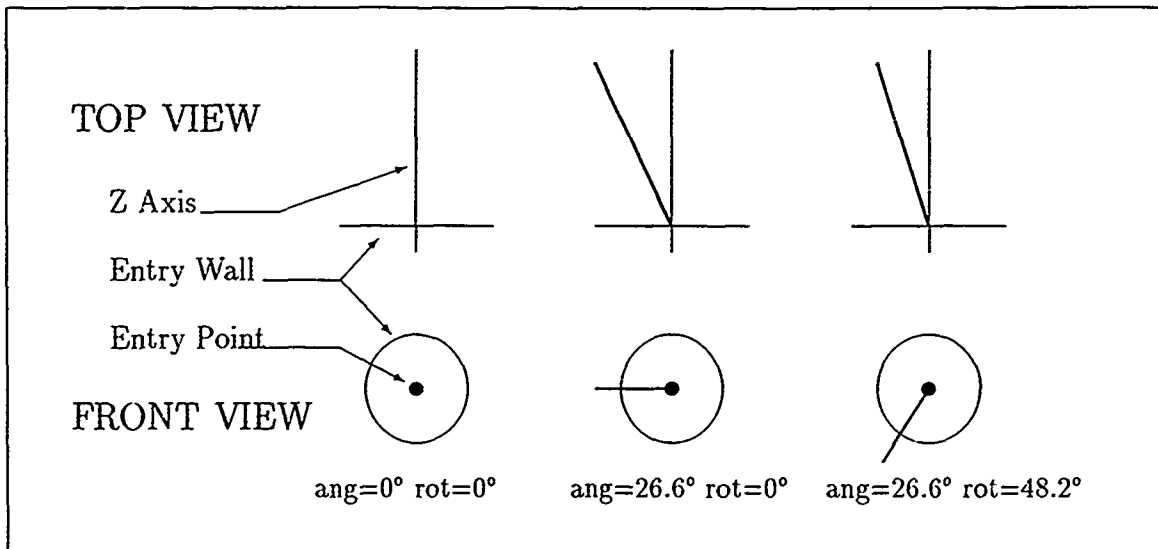


Figure 46. Obliquity Angle and Rotation Angle

This yaw changes the ballistic limit of penetration, the type of detonation², and the fragment dispersion. Reference Section 2.3.1.2 for further insight on the yaw.

4.2.6 Fuse Delay The fuse delay depends on the type of fuse, the impact velocity, and the impact angle. These differences between fuses have not been studied as part of this effort and are completely ignored by the simulation. For this reason, the fuse delay time must be input by the user. The delay time specified by the user is used directly by the simulation with no variability.

4.2.7 Object Surface The user also controls the placement of component surfaces in the dry bay. The only object recognized by the simulation without being input is the entry wall, or point of projectile entry. It is this entry point that marks the origin of a three dimensional cartesian coordinate system. All other components are positioned in the dry bay relative to the entry point.

The units of this coordinate system are measured in inches. Since this is a three dimensional system the dimension directions are specified as **X**, **Y**, and **Z**.

²Detonation magnitude changes as the angle and velocity of the impacting projectile changes.

The positive **X** direction follows a horizontal line on the entry wall toward the right of a viewer outside that wall. The positive **Y** direction goes vertically straight up from the entry point. The positive **Z** direction starts at the entry point and goes further inside the aircraft dry bay along a normal to the entry wall.

Figure 47 shows a graphic representation of a target plate within the dry bay. The plate is 36 inches wide by 48 inches high and is centered in the dry bay 18 inches into the dry bay³. The four corner coordinates given in terms of (**X**, **Y**, **Z**) are (18,24,18), (18,-24,18), (-18,-24,18), and (-18,24,18).

Any number of component surfaces can be input by the user but at least one has to be placed. The type of surface to be placed is designated by a single letter. However, the simulation only handles one type of surface at this time. This one type of surface is a polygon. Section 4.5 discusses the placement of component surfaces and the limitation on its shape.

4.3 Static Fragmentation

This routine generates the fragments that will occur when the projectile detonates. The fragment's obliquity angle off the projectile flight line is determined along with the fragment rotation, velocity, and weight. Each of these parameters is determined based on the distributions specific to the zone from which the fragment will originate.

The zone data is specified in a data file supplied by the user. One such data file already exists for the 23-mm HEI-T and has a file name of 23MMHEI.DAT on the computer disk. The information contained in this file and an example are discussed in Section 4.2.2.

The data used to create the data file can usually be found in the literature. The file must exist before the simulation is run. The projectile type and thus this

³The plate is located 18 inches behind the entry point; the Z-axis = 18 inches.

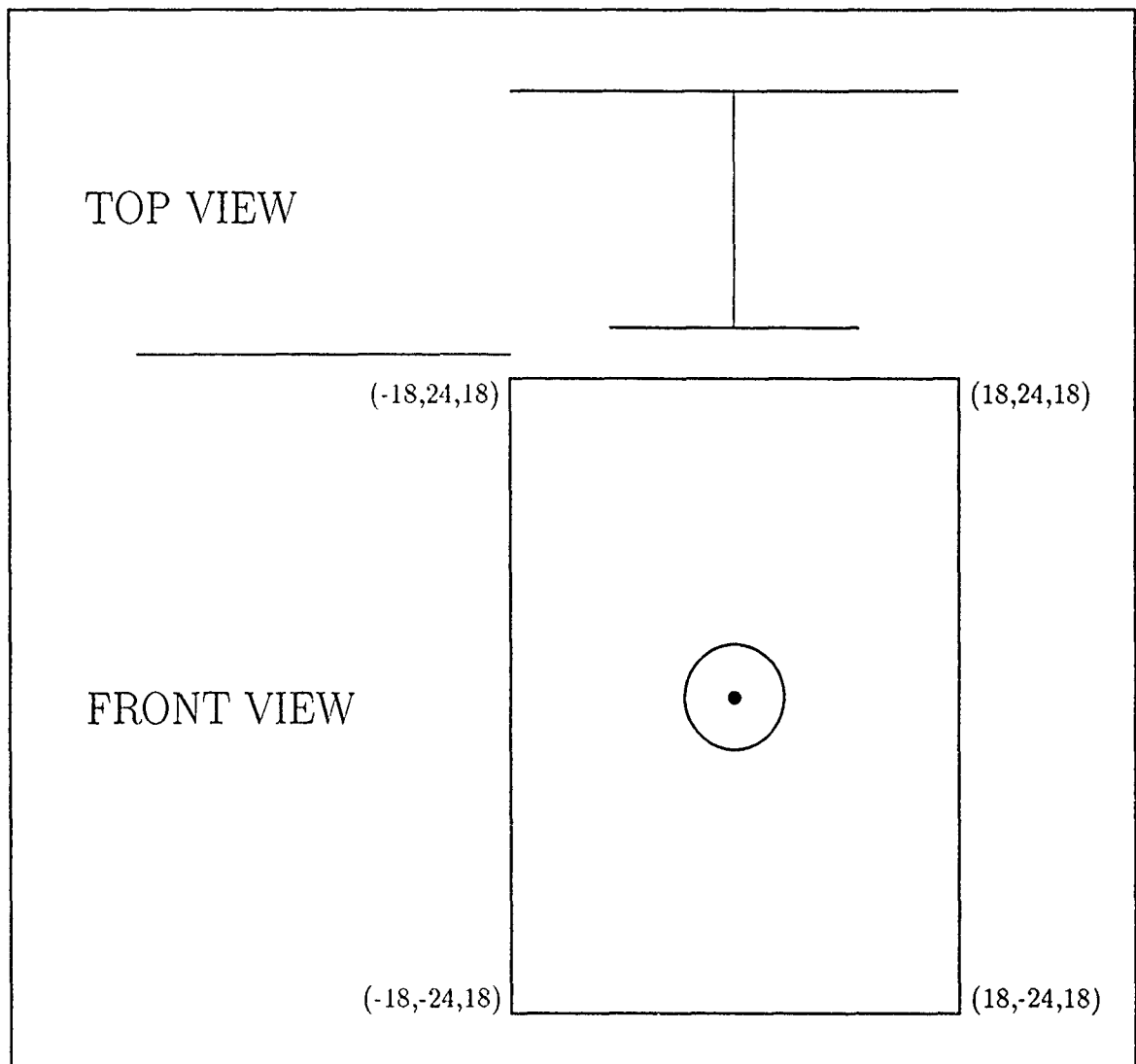


Figure 47. Component Placement

data file, are specified by the user via the SCENARIO.DAT file. This file is used by the simulation to generate a random fragmentation of the projectile simulated.

For each zone specified in the data file, a random, poisson distributed number of fragments are generated. Each fragment has a weight and velocity randomly selected from a normal distribution based on the parameters specified in the data file. The weight and velocity are independently selected in the REGFRAG subroutine specified by a '1' in the SCENARIO.DAT file described earlier. In the TSTFRAG subroutine, the velocity is dependent upon the randomly selected weight. If the randomly selected fragment weight is 1.4 standard deviations above the mean weight, then the velocity will be set 1.4 standard deviations below its mean.

The dependence between velocity and weight is thought to be based primarily upon the weight. The fragment velocity that is generated by a detonating HEI is thought by the author, to be based on the zone or projectile position from which the fragment originates, and the fragment's weight or mass. The heavier the fragment the lower the generated velocity. There are many other dependencies which the author believes will effect the velocity but only the weight dependency has been modeled.

The static fragmentation routine also determines the direction the fragment will take upon detonation. The fragment is not actually moved from the surface of the projectile at this time. Only the direction of flight upon detonation is determined. The angular direction or obliquity angle is determined first. This direction is randomly selected from a uniform distribution between the lower and upper boundaries of the zone from which the fragment generates. The upper and lower boundaries of the zone are specified in the projectile characterization file. The only such file currently available on the computer disk is for a 23-mm HEI-T projectile.

The longitudinal direction of this fragment around the projectile is randomly selected from a uniform distribution between 0° and 360°. The FORTRAN routines actually use radians rather than degrees. Therefore, the degrees specified in

the characterization file are converted to radians, and the longitudinal direction is selected from a uniform distribution between 0 and $2 \cdot \pi$.

At the end of this routine, a computer matrix representation is established. Each row of the matrix describes one fragment. The columns of the matrix describe the following information. The matrix as a whole is called the 'fragment matrix' throughout this chapter.

- The X coordinate of fragment impact.
- The Y coordinate of fragment impact.
- The Z coordinate of fragment impact.
- The fragment's obliquity angle.
- The fragment's rotational or longitudinal angle.
- The fragment's weight in grains.
- The fragment's velocity in feet per second.
- The object struck by this fragment.

The coordinates of fragment impact are set to zero and are meaningless at this point since the fragment has not impacted any object as of yet. The fragment has not even left the surface of the projectile since the detonation has not yet taken place in the simulation. Likewise, the object struck by the fragment is also meaningless and is set at -1 to indicate this.

4.4 Attack Scenario

The required inputs of obliquity angle, rotation, projectile velocity, fuse delay, and projectile type define the attack scenario. These inputs are specified in the SCENARIO.DAT file described in Section 4.2. There are two routines which adjust the fragment direction and velocity; and the origin of both the fragments and the blast pressure for the defined attack scenario.

4.4.1 *Dynamic Shift* The first routine performs a dynamic shift of the static fragmentation. The fragments themselves remain on the surface of the projectile but their direction and velocity are changed from their previously established levels randomly selected in the static fragmentation routine. This routine shifts the vector of fragment velocity and direction forward to account for the forward velocity of the projectile just before detonation. The calculations that accomplish this are shown below. Only the velocity and direction data is used to perform the dynamic shift; the fragment's weight does not effect the shift.

$$V_d = \left[V_p^2 + V_s^2 + 2 \cdot V_p \cdot V_s \cdot \cos(\alpha) \right]^{1/2} \quad (19)$$

$$\beta = \arcsin \left[\frac{V_s \cdot \sin(\alpha)}{V_d} \right] \quad (20)$$

where: V_s is the static fragment velocity.

V_p is the projectile velocity.

V_d is the dynamic fragment velocity.

α is the static fragment's obliquity angle.

β is the dynamic fragment's obliquity angle.

This routine performs a simple trigonometric shift of the fragment direction and calculates a new velocity. The *dynamic shift* of direction and velocity depend on the original fragment direction and velocity obtained from the fragment matrix previously defined; and the projectile velocity. The results of this shift are re-stored in the fragment matrix.

4.4.2 *Burst Point and Projectile Direction* This routine first calculates the burst point of the projectile using the attack obliquity angle, the rotation, the projectile velocity, and the fuse delay. The burst point is measured in inches from the entry point on a three dimensional cartesian coordinate system. The calculation is

shown below. The coordinates of the burst point are stored in the simulations 'burst point array.'

$$D = \frac{t}{1000000} \cdot V_p \cdot 12 \quad (21)$$

$$Z = \cos(\rho) \cdot D \quad (22)$$

$$X = \cos(\theta) \cdot Z \quad (23)$$

$$Y = \sin(\theta) \cdot Z \quad (24)$$

where: t is the fuse delay time in microseconds.

V_p is the projectile velocity in feet per sec.

ρ is the projectile obliquity angle.

θ is the projectile rotation angle.

D is the distance the projectile will fly before detonating
and after impacting the aircraft surface.

X is the X coordinate of the burst point.

Y is the Y coordinate of the burst point.

Z is the Z coordinate of the burst point.

The fragments generated from the projectile detonation must be adjusted for the direction of the projectile. The original fragment direction was measured in a euclidean space with the Z direction aligned with the flight line of the projectile. But, the direction should be measured relative to the coordinate system of the dry bay. To accomplish this the original euclidean space oriented with the projectile flight path is rotated to account for the direction of the projectile within the dry bay. The rotation of this space requires two matrices and the original vector representation of the fragment direction. This fragment direction is obtained from the obliquity and rotational angles stored in the fragment matrix.

The first matrix multiplication of the original direction vector rotates the space for the projectile's obliquity angle. Thus the euclidean space is rotated around the Y axis. The second matrix multiplication adjusts the space for the projectile rotation. Thus, this matrix rotates the euclidean space around the Z axis. The resulting vector specifies the direction of the fragment in the coordinate system oriented on the dry bay.

$$\begin{bmatrix} x \\ y \\ z \end{bmatrix} = \begin{bmatrix} \cos(\psi) \cdot \sin(\alpha) \\ \sin(\psi) \cdot \sin(\alpha) \\ \cos(\alpha) \end{bmatrix} \quad (25)$$

$$\begin{bmatrix} X \\ Y \\ Z \end{bmatrix} = \begin{bmatrix} \cos(\theta) & -\sin(\theta) & 0 \\ \sin(\theta) & \cos(\theta) & 0 \\ 0 & 0 & 1 \end{bmatrix} \begin{bmatrix} \cos(\rho) & 0 & -\sin(\rho) \\ 0 & 1 & 0 \\ \sin(\rho) & 0 & \cos(\rho) \end{bmatrix} \begin{bmatrix} x \\ y \\ z \end{bmatrix} \quad (26)$$

where: α is the fragment's obliquity angle.

ψ is the fragment's rotation angle.

ρ is the projectile obliquity angle.

θ is the projectile rotation angle.

$\begin{bmatrix} x & y & z \end{bmatrix}^T$ is the fragment direction in the projectile space.

$\begin{bmatrix} X & Y & Z \end{bmatrix}^T$ is the fragment direction in the dry bay space.

It should be emphasized that the *fragment direction* vectors are not coordinate points of the fragment within either the projectile's or the dry bay's euclidean space. Rather, they are direction vectors within the dry bay oriented space. The actual coordinates of the fragments within this space still need to be adjusted to the burst point of the projectile.

Coordinate points are not yet desired. Only the fragment direction is desired but it must be specified as an angle and rotation rather than a vector. The vector result shown above is therefore now transformed into an angle and rotation. This new angle and rotation calculated with the equations below, is aligned with the Z axis of the dry bay's euclidean space.

$$\Theta = \arccos(Z) \quad (27)$$

$$\Phi = \arccos \left[\frac{X}{\Theta} \right] \quad (28)$$

where: Z is the magnitude of the fragment's Z direction in the dry bay space.

X is the magnitude of the fragment's X direction in the dry bay space.

Θ is the new angle of fragment direction.

Φ is the new rotation of fragment direction.

Each of these calculations is performed on every fragment in order to determine its direction of flight within the dry bay. Up to this point the fragments have not been moved out of their position on the projectile. Only the direction they will take has been determined.

The results of this rotation of space are used to establish an obliquity angle and rotation for each individual fragment, relative to the dry bay coordinate system. This new obliquity angle and rotation for the fragment is re-stored in the fragment matrix.

4.5 Object Construction

Objects are defined by the surface corner points input by the user as described in Section 4.2. These points are located in three dimensional space. Since they do not necessarily define a convex area, some amount of analysis must be performed on

the points. This analysis in essence, describes the object surface to the computer. Without this analysis, the computer would not be able to distinguish area within the surface boundaries from area outside the boundaries. After all, the computer does not actually have eyes to view the object, and the only descriptive information it has are the corner point locations within the dry bay.

The only object surface currently definable within the dry bay is a polygon. The corner points of the polygon can be entered in either the clockwise or counter clockwise direction, but they must be entered in order. Any number of corner points can be input.

Because the object surface could be positioned at a complex angle within the dry bay, the exact corner points may be difficult to specify. Remember that a polygon lies completely on a single two dimensional plane. Even if the object is a perfect square of 6.4356 inches per side, specifying the coordinate locations of the square's corners within the dry bay can be difficult. For instance suppose the square is oriented at an angle of 45° to the X , Y , and Z axis. With this somewhat complex orientation of the square within the dry bay, determining the exact location of the corners would be difficult, particularly when the length of each side is 6.4356 inches.

For this reason, the coordinates of the corner points specifying

the object's location are not required to lie on one single plane. This laxity in defining the corner points makes it much easier for the user to specify the object's position. Now, only approximate point coordinates need to be specified. If one or more of those coordinates is slightly off the actual plane of that surface, the simulation will recognize the general shape and proceed without difficulty.

4.5.1 Limitation on Object Definition There is one limitation on the shape of the object surface. If this limitation is violated, the simulation will still proceed but the shape of the object will not be correctly recognized by the computer. Some

amount of additional surface area will be include that should not have been included, and/or some amount of the surface area may be accounted for twice.

The limitation requires that the first half of the surface must be convex to the rest of the surface. This first half is defined by a vector drawn from the first corner point defined, through the third point; and a similar vector drawn from the first corner point through the last point. If the lines describing the first two edges of the surface, i.e., by a line drawn from point one to point two, and a line drawn from point two to point three, are not convex to the rest of the surface, this limitation is violated. This limitation is also violated when either of the two vectors drawn, i.e., the vector from point one through point three and the vector from point one through the last point, crosses a defining edge of the surface past the third or last points respectively. If either of these vectors crosses an edge beyond the third or last point, the object surface is said to *hook* back upon itself.

This limitation is shown graphically in Figures 48 and 49. Examples of both properly and improperly defined surfaces are shown.

4.5.2 Object Analysis If there are N corner points, the analysis creates $N - 1$ vectors which originate at the first point and go through each of the other $N - 1$ corner points. The angle between the first vector and each of the other vectors is then determined. A rank order of the magnitude of these angles is used to determine how the object's surface shape should be broken up.

The rank order of angle magnitude is then converted back to the corner points of the object. The computer then steps around the object surface from corner to corner in the order specified by the ranking just computed. This stepping around the surface will generate a triangle with one corner at the first point input by the user and the second two corner points taken from the ordered list of points until that order causes the computer to back track to a lower numbered point, i.e., the rank order is higher but the number associated with the order of input is lower.

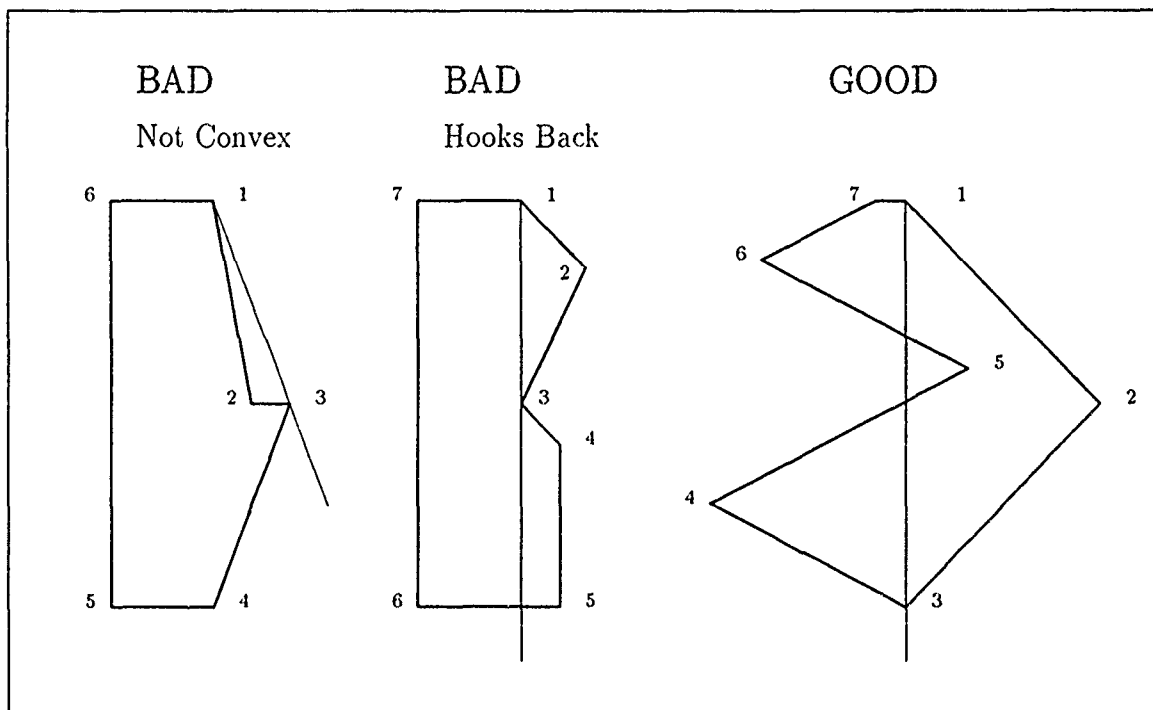


Figure 48. Object Limitation - Part A

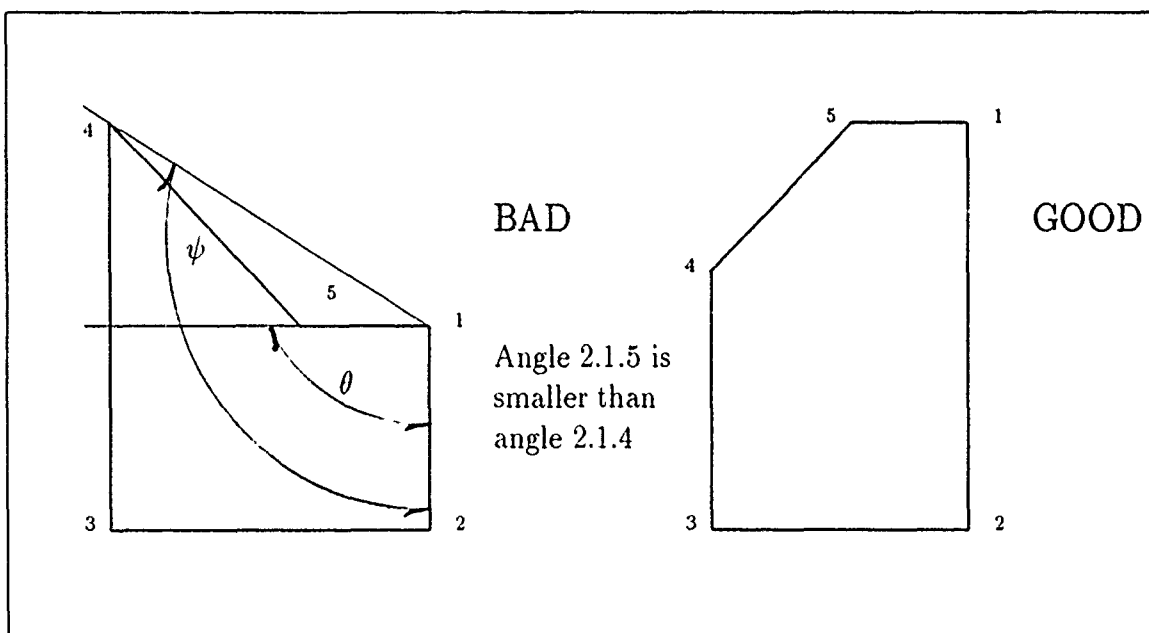


Figure 49. Object Limitation - Part B

For example, suppose the ranked order of corner points based upon the vector angles described above, is in the order listed below.

1 2 3 4 7 5 6 8

The simulation will create triangles specified by the corner points:

- 1, 2, 3
- 1, 3, 4
- 1, 4, 7
- 1, 7, 8

The corner points 5 and 6 were skipped because their input order number was less than the rank order of the previously used corner point of 7. The simulation now processes the corner points of:

4 5 6 7

A rank order of the surface defined by these points is accomplished in a similar manner to form two additional triangles. There are distance checks which accompany the above described routine to assure the proper definition of triangles within the object surface.

The shape is broken into a total of $N - 2$ triangles. The triangles forming the shape are then stored and will later be used to determine whether or not the object is hit by a fragment. The triangular shape is used because of its special properties. The first of these properties is that the three corner points uniquely define a plane. With this property a fragment's line of flight can be easily tested for an intersection with the triangle's plane. This property makes it possible for the user to only put

approximate corner locations. Without this property, the user or the computer would have to precisely calculate every corner point location on a strict plane.

The second property of the triangle allows the computer to test whether or not a fragment's line of flight intersects the plane within the region of the triangle. Vectors are created from the intersecting point to the three corner points of the triangle. The angle between each of the three pairs of vectors is then calculated. For any point within the triangle the sum of these three angles is always equal to 360° . A point intersecting the plane outside the triangle has a sum of the angles less than 360° .

4.6 Target Impact

The fragments, their velocities, and directions; and the objects are all processed before the simulation actually detonates the projectile. Once all this pre-processing is accomplished, the simulation allows time to advance. The first advance of time starts at the projectile's entry into the dry bay: t_0 . Time is immediately advanced an amount equal to the fuse delay time measured in microseconds. At this time the burst point is used as the origin of all fragments.

Time momentarily is halted while the flight of each fragment for the burst point is determined. Each fragment's flight line is tested with each triangle defining the objects to determine if it intersects one or more of the objects. A record of each object hit by a fragment is made. After all objects hit by a single fragment's flight line are recorded, the closest object intersection (to the burst point) is determined. The time at which this closest object will be hit by this fragment is then determined using the fragment's velocity and the distance between the burst point and the object intersection. All other object intersections are disregarded for this fragment. The fragment is then scheduled to impact the object after the appropriate amount of time has lapsed using SLAM II discrete event simulation. This is accomplished for every fragment individually before the simulation's time clock is allowed to advance.

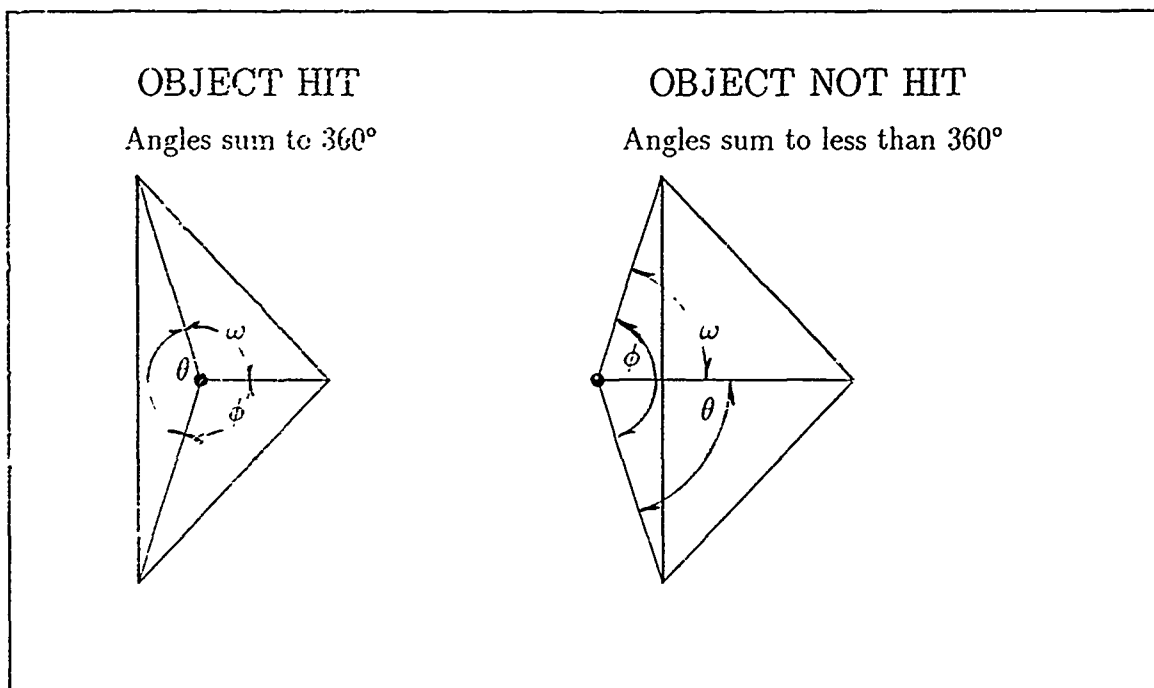


Figure 50. Determining if an Object is Hit

Each fragment is evaluated separately for its intersection with each individual object. An object impact is scheduled for the closest object impacted by a fragment. Figure 50 graphically shows how object impact is determined.

4.7 Peak Blast Pressure on the Target

The peak blast pressure wave at 36 locations is computed by scaling the peak pressure of a one ton explosion TNT. Table 15 shows the peak overpressure at specific distances from the burst point for a one ton explosion of TNT. This table is scaled back by the simulation for the size of projectiles RDX charge. The 36 distances range from 1 to 36 inches in 1 inch increments.

For example, the 23-mm HEI-T has approximately 11.5 grams of RDX. RDX achieves an explosion characteristic of 1.62 times its weight in TNT. And, the ambient air pressure is 14.7 pounds. With this information the following scaling is performed.

(24)

Distance	Peak Pressure	Arrival Time	Duration	Decay Parameter
5.0,	192.0,	0.28,	2.5,	10.0,
10.0,	76.0,	0.60,	1.5,	7.5,
15.0,	35.0,	1.29,	0.6,	6.0,
20.0,	21.0,	2.22,	1.9,	5.0,
25.0,	14.0,	3.34,	5.6,	4.5,
30.0,	9.3,	4.70,	6.0,	3.5,
35.0,	6.8,	6.20,	6.5,	2.8,
40.0,	4.9,	8.10,	7.4,	2.3,
45.0,	3.6,	10.1,	8.3,	1.7,
50.0,	2.7,	12.3,	9.3,	1.5,
55.0,	2.1,	14.7,	10.2,	1.2,
60.0,	1.65,	17.3,	11.1,	1.1,
65.0,	1.32,	20.1,	12.0,	1.0,
70.0,	1.10,	23.2,	12.9,	0.9,
75.0,	0.95,	26.6,	13.8,	0.9,
80.0,	0.85,	29.9,	14.6,	0.9,
85.0,	0.73,	33.3,	15.3,	0.9,
90.0,	0.68,	36.8,	16.0,	0.9,
95.0,	0.62,	40.3,	16.7,	0.9,
100.0,	0.57,	43.9,	17.3,	0.9,
105.0,	0.52,	47.6,	17.9,	0.9,
110.0,	0.48,	51.3,	18.4,	0.9,
115.0,	0.44,	55.1,	18.7,	0.9,
120.0,	0.41,	58.9,	19.0,	0.9,
125.0,	0.38,	62.8,	19.3,	1.0,
130.0,	0.35,	66.7,	19.6,	1.0,
135.0,	0.33,	70.6,	19.8,	1.0,
140.0,	0.31,	74.5,	20.1,	1.0,
145.0,	0.292,	78.4,	20.4,	1.0,
150.0,	0.276,	82.3,	20.6,	1.0,
155.0,	0.262,	86.3,	20.9,	1.0,
160.0,	0.250,	90.3,	21.2,	1.0,
165.0,	0.238,	94.3,	21.5,	1.1,
170.0,	0.227,	98.3,	21.8,	1.1,
175.0,	0.217,	102.4,	22.0,	1.1,
180.0,	0.208,	107.0,	22.3,	1.1,
185.0,	0.200,	111.0,	22.6,	1.1,
190.0,	0.193,	115.0,	22.9,	1.1,
195.0,	0.186,	119.0,	23.2,	1.1,
200.0,	0.181,	123.0,	23.4,	1.1,
205.0,	0.174,	127.0,	23.6,	1.1,
210.0,	0.168,	131.0,	23.8,	1.2,
215.0,	0.162,	135.0,	23.9,	1.2,
220.0,	0.156,	138.0,	24.1,	1.2,
225.0,	0.151,	144.0,	24.2,	1.2,
230.0,	0.146,	148.0,	24.3,	1.2,
235.0,	0.141,	152.0,	24.4,	1.2

Table 15. One Ton Detonation of TNT

$$W_o = 2000 \text{ lbs. of TNT}$$

$$W = \frac{11.5 \text{ gm. of RDX}}{453.59 \text{ gms./lbs}} \cdot 1.62$$

$$\left[\frac{W_o}{W} \right]^{1/3} = \text{Scaling} \quad (29)$$

$$\left[\frac{2000 \text{ lbs.}}{.04107 \text{ lbs.}} \right]^{1/3} = 36.51687 \quad (30)$$

This value is then multiplied by the distance of interest; the distance is measured in feet. Suppose the target plate is 18 inches or 1.5 feet from the burst point. The result (from multiplying the scaling factor times the distance in feet) evaluates to a distance in feet which is to be looked up in the table. At 55 feet the peak pressure is 2.1 times the ambient air pressure. At sea level the ambient air pressure is roughly 14.7 psi. Therefore the peak pressure 18 inches from the burst point is roughly 30.9 psi.

$$1.5 \text{ ft.} \cdot 36.51687 = 54.77530 \text{ ft.} \quad (31)$$

$$2.1 \cdot 14.7 \text{ psi} = 30.9 \text{ psi} \quad (32)$$

The arrival time of this peak pressure is calculated by scaling the arrival time shown in the table with the scaling factor computed above. The calculation for the current example is shown below.

$$\frac{14.7 \text{ milliseconds}}{36.51687} = .40255 \text{ milliseconds} \quad (33)$$

All of these calculations assume that the relative air pressure is equal to 14.7 psi, and that the temperature is 70°F. If the actual air pressure or temperature is different the calculation would need to be adjusted slightly. The simulation also assumes the air pressure and temperature are 14.7 psi and 70°F respectively.

4.8 *Blast Pressure Decay on the Target*

As the peak blast pressure moves past each of the 36 distances, the remaining pressure dissipates through time. The pressure is automatically updated at each of these 36 distances every 10 microseconds. Because of the simulation's module architecture the pressure can be updated at any time as required by other fragment or pressure interactions. But, the maximum time between pressure updates is 10 microseconds. The following equation is used to calculate the pressure on the target through time. (24)

$$\begin{aligned}
 p^o &= \text{the peak pressure} \\
 p &= \text{the pressure at time } t \\
 t_d &= \text{scaled pressure duration from the table} \\
 \alpha &= \text{the decay parameter from the table} \\
 p &= p^o(1 - t/t_d) \exp(-\alpha \cdot t/t_d)
 \end{aligned}
 \tag{34}$$

4.9 *Outputs*

The outputs from the simulation include:

- A matrix describing the pressure at 36, one inch increments of distance from the detonation point, through time.
- A matrix of fragment information including:

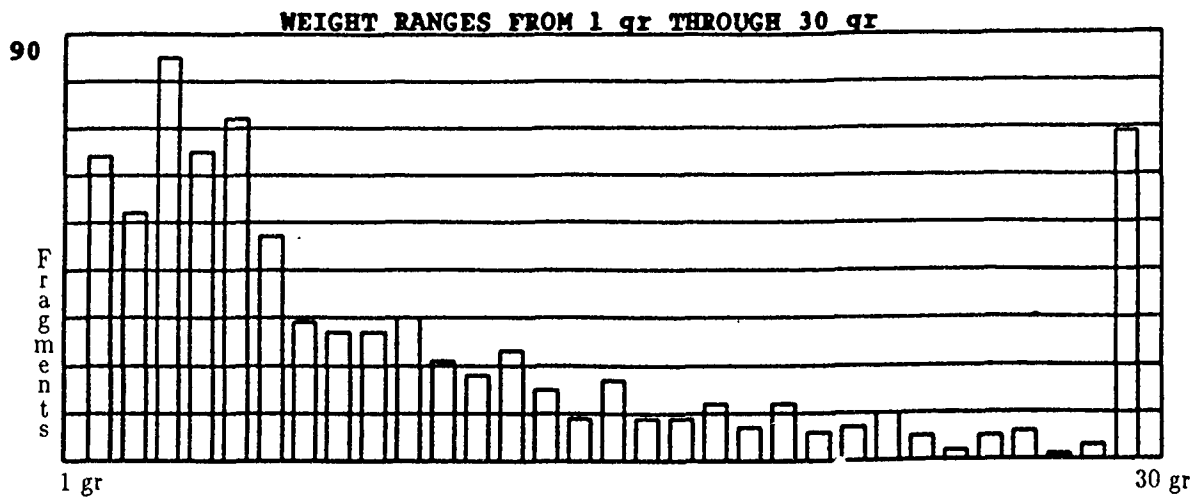


Figure 51. Weight Histogram

- The X coordinate of fragment impact.
- The Y coordinate of fragment impact.
- The Z coordinate of fragment impact.
- The fragment's weight in grains.
- The fragment's velocity in feet per second.

• Histograms of:

- Fragment weight
- Fragment velocity
- Radial location of fragments impacting a centered target

Figure 51 shows an example histogram of fragment weights. The weight increases by one grain starting on the left at one grain and ending on the right at 30 grains. The height of each bar represents the number of fragments of that weight.

Figure 52 shows an example of the fragment velocity histogram for three different projectile velocities. The velocity ranges from 2000 feet per second on the far left to 5000 feet per second on the far right. The height of the line represents the

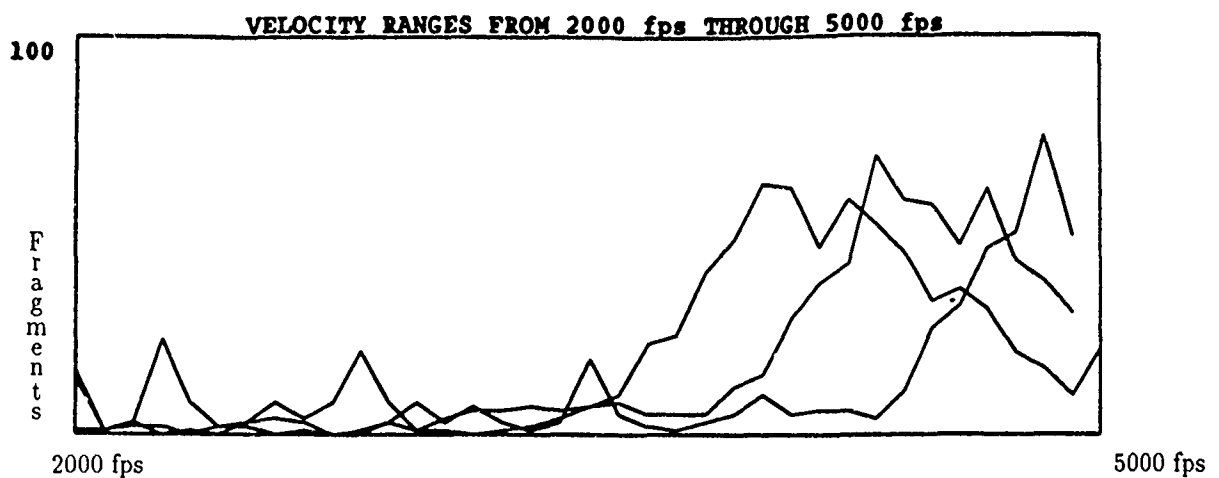


Figure 52. Velocity Histogram

number of fragments having that particular velocity. There are three lines shown. The first line (showing the lowest velocity) was developed from a projectile with a velocity of 2500 feet per second (fps). The second and third lines were from projectiles with respective velocities of 3200 fps and 4000 fps. As the velocity of the projectile increases, the velocities of the fragments also increase.

Figure 53 shows a histogram of the radial position (or distance from the center of the target) at which fragments impact the target. Three lines are also shown on this chart. Each of the lines again represents a different projectile velocity. The first line, closest to the left (0 inches) edge represents a projectile velocity of 400 fps. The second and third lines respectively represent projectile velocities of 3200 fps and 2500 fps. As the velocity of the projectile increases, the fragments are shifted (via the dynamic shift) closer to the projectile's flight line and therefore closer to the zero radial position.

Figure 54 shows a graphic image of the dispersion of fragment impact points on the target surface.

Figure 55 is a surface plot showing the blast pressure through distance and time. The axis coming out and toward the left of the picture represents the distance

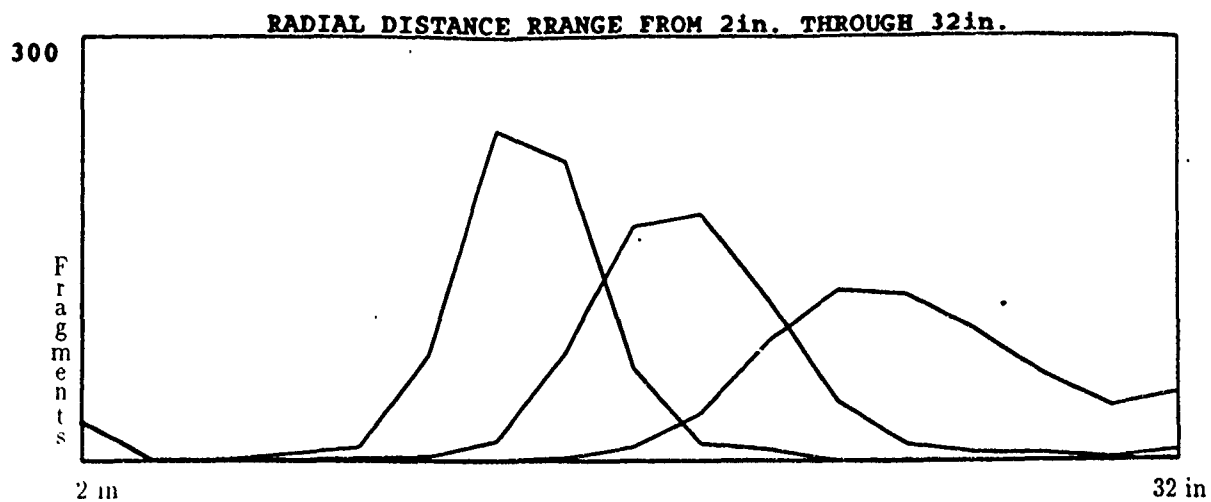


Figure 53. Radial Position Histogram

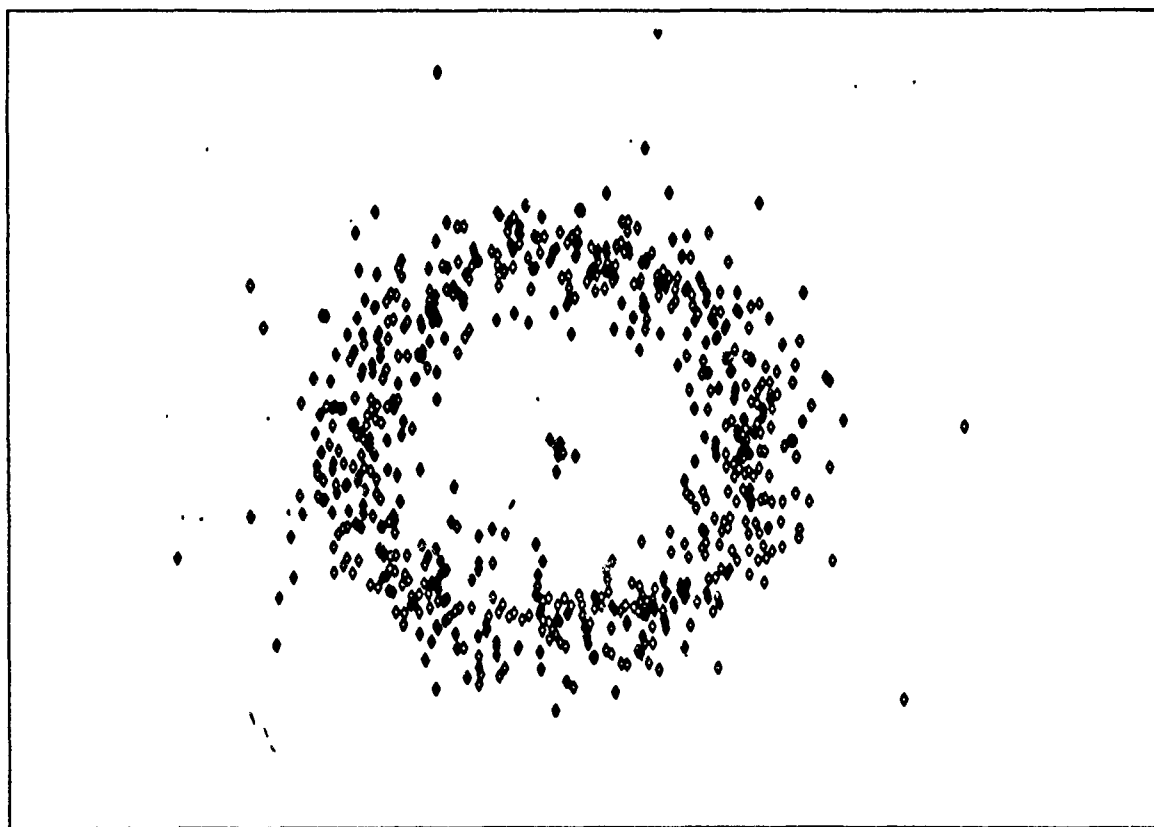


Figure 54. Simulated Target Impacted by Fragments

measure. The distances shown start at 6 inches and increase to 36 inches. The axis that comes out and toward the right, the longer axis, represents time. This time axis starts at HEI detonation time, t_o and increases by 10 microsecond intervals.

The pressures located very close to the detonating HEI are very high and decrease as the distance from detonation increases. Also, the blast wave arrives at later and later times as the distance from the detonation increases. Finally, at any particular distance, the pressure dissipates at a slower and slower rate as the distance increases.

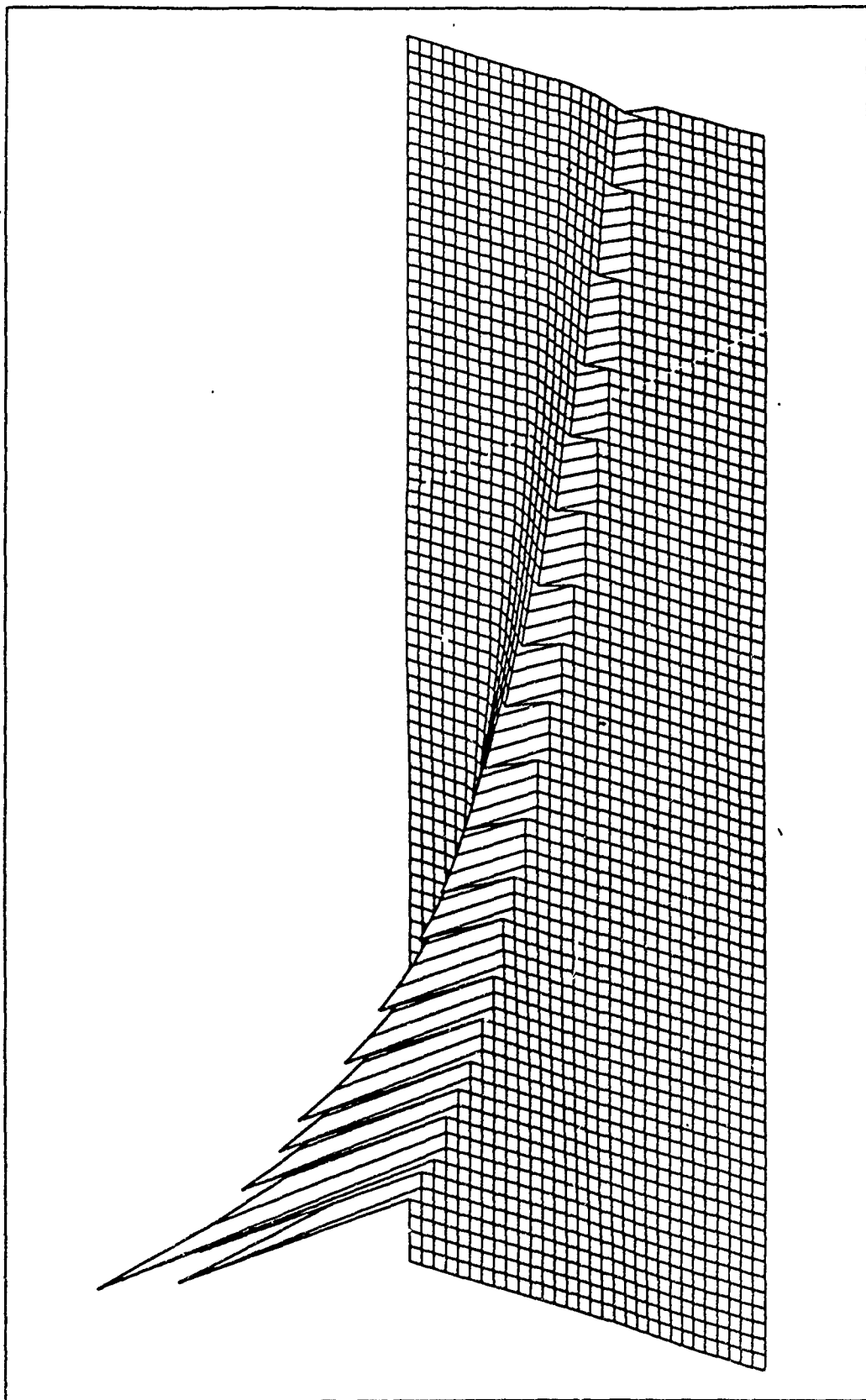


Figure 55. Surface Plot of the Blast Pressure Through Distance and Time

V. Recommendations & Conclusions

The prevalent fire suppressant system in use, Halon 1301, is being banned from DOD use because of its impact on the ozone layer surrounding the earth. Other fire suppressant systems are either clumsy to use, very heavy, or inadequate. Because of this, the office of WL/FIVS located at Wright Patterson AFB, Ohio is investigating and testing alternative fire suppressant systems. Understanding the explosion processes may lead to alternative fire suppressant systems which attack the precursors of the fire rather than the fire itself.

5.1 HEI Process Descriptions

This thesis has brought together a vast array of information from various sources in order to describe the fragments and blast pressure from an exploding HEI projectile. The sources of this information varied from the study of ballistic limits to the description of a one ton detonation of TNT. This thesis is the first known paper to bring together all of this information. As such, this thesis paper describes the individual and combined processes of fragmentation and blast pressure. Several dependencies between these processes are also suggested and supported.

At several points throughout this thesis paper the need for associated data has been pointed out. In the past, there was not an overriding reason or need to associate fragment weight with fragment velocity or blast pressure. In fact, many of the information sources reviewed had no way of associating the data. Either the information source gathered limited data or they gathered so much that it became impossible to associate particular fragment and blast pressure data.

The reasons and need for associated data is made clear in this thesis. The data that needs to be associated or linked includes fragment weight, fragment velocity, projectile shape and type, projectile blast pressure, and pressure wave shape. Only

with associated data can the processes of an exploding HEI be fully understood and described.

When the HEI explosion processes of fragmentation and blast pressure are fully understood, better, more efficient fire suppressant systems will be designed. The goal of this thesis was to further the understanding of these explosion processes. The thesis paper therefore describes the HEI processes that can lead to a fire, i.e., the combination of pressure, heat, flammable material, and an ignition source. Eliminating any one of the contributing factors may completely or partially eliminate the fire.

5.2 HEI Simulation

With the development and testing of fire suppressants in mind, this thesis has both outlined the major HEI explosion processes and developed a computer simulation of these processes. It is hoped that the computer simulation will be used to test and develop alternative fire suppressant systems before high cost empirical testing is accomplished. The simulation program was specifically designed for the addition and testing of alternative fire suppressant systems.

The simulation program is a modular architecture allowing the addition of program modules which describe the interaction between the fire suppressant system and the HEI explosion processes. The modular architecture also makes the maintenance of the system very easy. For instance, when the dependence between a fragment's weight and velocity is understood, the simulation can be updated by a simple exchange of one program module. For a fragment's weight and velocity dependence, the current static fragmentation module would be replaced by a new module describing the weight / velocity dependence.

Virtually any attack scenario can be defined via a data file. The simulation user can easily modify the attack scenario by changing a few simple parameters in the data file. In addition, the user can specify any configuration of the dry bay

within this same data file. Only the corner point locations of a component surface need to be specified.

The simulation automatically creates a mathematical representation of the dry bay. The corner points are converted into a representation that the computer recognizes as a solid surface. These surfaces are not required to be convex nor do they have to be defined on a single, two dimensional plane within the dry bay. This provides the user with a simple means of defining the dry bay configuration.

5.3 Data and Testing Recommendations

A data base of associated data is needed. This data should include fragment velocity, fragment weight, projectile blast pressure, and projectile schematic. Each data item needs to be linked with its associated data. A fragment's velocity should also be associated with its weight and a particular detonation of the particular projectile type. The blast data should be associated with a particular projectile detonation, a radial position (zone) around the projectile, and a rotational (longitudinal) position around the projectile.

Specific information of the data to be collected and the means to collect this data is outlined in Chapter 3. Basically, the test setup requires only slight modification to the static test arena already in use. The changes include the addition of pressure sensors surrounding a statically detonated HEI. These pressure sensors encircle the HEI on a single plane which longitudinally bisects the projectile.

In addition, the already existent velocity screens included in the test setup need to reduce in size. The reduced screen size allows only one fragment's velocity to be measured. This fragment's velocity is then associated to its weight when recovered from the fragment collection bundles. The fragment collection bundles already exist but the area represented by these bundles should be increased wherever possible.

5.4 *Future Study*

Future studies should further describe the dependence between the fragment data and the blast data. In addition, the simulation should be enhanced with modules describing specific interaction between components and the HEI fragment and blast processes. One such module should describe the interaction of the HEI and the fuel cell. This interaction has already been specified in Crawford's study and therefore needs only to be integrated into the HEI simulation developed as part of this thesis.

Other component interactions should include electronics, fuel and hydraulic lines, etc Additional HEI projectile types should be specified in the static fragmentation data files. These data files describe the fragment dispersion patterns, zone velocity distributions, zone weight distributions, and the amount of RDX explosive carried by the HEI.

Appendix A. *Data from Jones Study*

FOI AR ZONE	DEGREES	AVERAGE VELOCITY (FT/SEC)		VBAR	VMAX	VMIN	# OF HITS	SD
1	0-5	0					0	
2	5-10	0					0	
3	10-15	0					0	
4	15-20	0					0	
5	20-25	0					0	
6	25-30	0					0	
7	30-35	0					0	
8	35-40	599	593	596	599	593	5	4.0
9	40-45	2467	1575	1487	2467	951	4	716.4
10	45-50	2023	955	2028	2028	2028	1	0.0
11	50-55	2953	2118	2298	2953	1824	3	586.0
12	55	1910	1787	1813	1910	1742	3	86.9
13	60-65	1645		1645	1645	1645	1	0.0
14	65-70	0					0	
15	70-75	1782	870	1326	1782	870	2	645.2
16	75-80	0					0	
17	75-80	0					0	
18	85-90	1384		1384	1384	1384	1	0.0

Re-created from (20:35-36)

Table 16. Minimum Weight 20-mm HEI Data and Statistics - Shot #1

POLAR ZONE	DEGREES	AVERAGE VELOCITY (FT/SEC)					VBAR	VMAX	VMIN	# OF HITS	SD
19	90-95	3896					3896	3896	3896	1	0.0
20	95-100	4598	4546	4385	4332	4196	3797	4598	3053	19	460.2
		4082	3974	3922	3875	3685					
		3636	3604	3561	3516	3364					
		3303	3282	3264	3053						
21	100-105	3640	3564	3255	3206	3080	3349	3640	3080	5	241.6
22	105-110	3448	2985	2490	2437	2175	2707	3448	2175	5	507.3
23	110-115	2839	2649	2505	2474		2617	2839	2474	4	116.6
24	115-120	2451					2451	2451	2451	1	0.0
25	120-125	0								0	
26	125-130	0								0	
27	130-135	0								0	
28	135-140	0								0	
29	140-145	0								0	
30	145-150	0								0	
31	150-155	1694					1694	1694	1694	1	0.0
32	155-160	0								0	
33	160-165	0								0	
34	165-170	0								0	
35	170-175	2673	2609	2601	2108		2498	2673	2108	4	261.8
36	175-180	2530					2530	2530	2530	1	0.0

Re-created from (20:35-36)

Table 16. Minimum Weight 20-mm HEI Data and Statistics - Shot #1 (con't)

POLAR ZONE	DEGREES	AVERAGE VELOCITY (FT/SEC)			VBAR	VMAX	VMIN	# OF HITS	SD
1	0-5	0						0	
2	5-10	0						0	
3	10-15	0						0	
4	15-20	0						0	
5	20-25	0						0	
6	25-30	0						0	
7	30-35	0						0	
8	35-40	0						0	
9	40-45	1349			1349	1349	1349	1	0.0
10	45-50	0						0	
11	50-55	3155	1920	1630	1470	3155	1470	4	764.0
12	55-60	3318	3243	1787	1780	3318	1017	9	852.2
		1651	1170	1162	1017			0	
13	60-65	1508				1508	1508	1	0.0
14	65-70	0						0	
15	70-75	0						0	
16	75-80	1591				1591	1591	1	0.0
17	80-85	0						0	
18	85-90	0						0	

Re-created from (20:37-38)

Table 17. Minimum Weight 20-mm HEI Data and Statistics - Shot #2

POLAR ZONE	DEGREES	AVERAGE VELOCITY (FT/SEC)				VBAR	VMAX	VMIN	# OF HITS	SD
19	90-95	2873				2873	2873	2873	1	0.0
20	95-100	4230	4086	4027	3822	3628	4230	3139	12	355.6
		3644	3564	3406	3377					
		3249	3139							
21	100-105	4091	3974	3960	3896	3672	4091	3000	13	332.9
		3838	3666	3482	3432					
		3358	3279	3000						
22	105-110	2988	2885	2087		2653	2988	2087	3	492.9
23	110-115	2980				2980	2980	2980	1	0.0
24	115-120	1987	1951			1969	1987	1951	2	25.1
25	120-125	0							0	
26	125-130	0							0	
27	130-135	0							0	
28	135-140	0							0	
29	140-145	1654	1621			1637	1654	1621	2	23.2
30	145-150	0							0	
31	150-155	0							0	
32	155-160	0							0	
33	160-165	0							0	
34	165-170	0							0	
35	170-175	2264	2236	1896		2132	2264	1896	3	205.1
36	175-180	3020	2866	2618		2835	3020	2618	3	202.8

Re-created from (20:37-38)

Table 17. Minimum Weight 20-mm HEI Data and Statistics - Shot #2 (con't)

POLAR ZONE	DEGREES	AVERAGE VELOCITY (FT/SEC)			VBAR	VMAX	VMIN	# OF HITS	SD
1	0-5	0						0	
2	5-10	0						0	
3	10-15	0						0	
4	15-20	0						0	
5	20-25	0						0	
6	25-30	0						0	
7	30-35	0						0	
8	35-40	3013			3013	3013	3013	1	0.0
9	40-45	2442	1610	791	1409	2442	791	4	789.6
10	45-50	2444			2444	2444	2444	1	0.0
11	50-55	2939	1897	1728	1513	2939	778	6	848.5
		778							
12	55-60	2179	1640		1910	2179	1640	2	381.2
13	60-65	0						0	
14	65-70	1759			1759	1759	1759	1	0.0
15	70-75	0							
16	75-80	0							
17	80-85	0							
18	85-90	0							
19	90-95	5286	5210	4918	4743	4706			
		4598	4523	3991	3939	3734			
		3704	3681	3644	3618	3579			
		3432	3380						
								17	644.2

Re-created from (20:39-40)

Table 18. Minimum Weight 20-mm HEI Data and Statistics - Shot #3

POLAR ZONE	DEGREES	AVERAGE VELOCITY (FT/SEC)						VBAR	VMAX	VMIN	# OF HITS	SD
20	95-100	5286	5210	4918	4743	4706	4146	5286	3380	610.6	19	
		4598	5623	4206	3978	3952						
		3888	3734	3704	3681	3644						
		3618	3579	3432	3380							
21	100-105	4756	4737	4467	4439	4281	4132	4756	3352	461.9	11	
		4176	3987	3952	3770	3536						
		3352										
22	105-110	0									0	
23	110-115	2978	2771	2376			2708	2978	2376	305.6	3	
24	115-120	3387	2754	2532			2891	3387	2532	443.5	3	
25	120-125	0									0	
26	125-130	0									0	
27	130-135	0									0	
28	135-140	0									0	
29	140-145	0									0	
30	145-150	0									0	
31	150-155	0									0	
32	155-160	2147	1881				2014	2147	1881	188.0	2	
33	160-165	2009	2004				2007	2009	2004	3.2	2	
34	165-170	0									0	
35	170-175	2944	2738	2691			2791	2944	2691	134.6	3	
36	175-180	3586	3371	3144	2951	2934	3137	3586	2839	290.0	6	
		2839										

Re-created from (20:39-40)

Table 18. Minimum Weight 20-mm HEI Data and Statistics - Shot #3 (con't)

POLAR ZONE	DEGREES	AVERAGE VELOCITY (FT/SEC)	VBAR	VMAX	VMIN	# OF HITS	SD
1	0-5	0				0	
2	5-10	0				0	
3	10-15	0				0	
4	15-20	0				0	
5	20-25	0				0	
6	25-30	0				0	
7	30-35	0				0	
8	35-40	0				0	
9	40-45	2432 1603	2013	2432	1603	2	586.6
10	45-50	757	757	757	757	1	0.0
11	50-55	2001 1285	1643	2001	1285	2	506.2
12	55-60	3172 1472	2322	3172	1472	2	1201.7
13	60-65	3211 1621	2416	3211	1621	2	1124.7
14	65-70	1413	1413	1413	1413	1	0.0
15	70-75	0				0	
16	75-80	0				0	
17	80-85	3488	3488	3488	3488	1	0.0
18	85-90	0				0	

Re-created from (20:44-45)

Table 19. Maximum Explosive 20-mm HEI Data and Statistics - Shot #1

POLAR ZONE	DEGREES	AVERAGE VELOCITY (FT/SEC)						VBAR	VMAX	VMIN	# OF HITS	SD
19	90-95	3715	3604	3396	3312	2839	2839	3272	3715	2767	6	391.3
		2767										
20	95-100	3727	3543	3020	2932	2882	2882	2795	3727	2206	15	409.0
		2839	2793	2750	2671	2641	2641					
		2616	2551	2424	2329	2206	2206					
21	100-105	3952	3934	3888	3742	3625	3625	3183	3952	2289	14	597.1
		3557	3285	3114	2773	2634	2634					
		2618	2584	2573	2289							
22	105-110	2277						2277	2277	2277	1	0.0
23	110-115	0									0	
24	115-120	0									0	
25	120-125	0									0	
26	125-130	0									0	
27	130-135	0									0	
28	135-140	0									0	
29	140-145	0									0	
30	145-150	0									0	
31	150-155	0									0	
32	155-160	0									0	
33	160-165	1980						1980	1980	1980	1	0.0
34	165-170	0									0	
35	170-175	2551	2437					2494	2551	2437	2	80.6
36	175-180	2875	2651	2597				2708	2875	2597	3	147.5

Re-created from (20:44-45)

Table 19. Maximum Explosive 20-mm HEI Data and Statistics - Shot #1 (con't)

POLAR ZONE	DEGREES	AVERAGE VELOCITY (FT/SEC)		VBAR	VMAX	VMIN	# OF HITS	SD
1	0-5	0					0	
2	5-10	0					0	
3	10-15	638		638	638	638	1	0.0
4	15-20	640		640	640	640	1	0.0
5	20-25	640		640	640	640	1	0.0
6	25-30	0					0	
7	30-35	0					0	
8	35-40	864	863	864	864	863	2	0.9
9	40-45	2273		2273	2273	2273	1	0.0
10	45-50	2055	1577	1816	2055	1577	2	337.9
11	50-55	0					0	
12	55-60	1611	1501 1480 1463	1514	1611	1463	4	66.9
13	60-65	2267	1654 1646	1856	2267	1646	3	356.3
14	65-70	3349		3349	3349	3349	1	0.0
15	70-75	1605		1605	1605	1605	1	0.0
16	75-80	0					0	
17	80-85	4301		4301	4301	4301	1	0.0
18	85-90	0					0	
19	90-95	3754	3742 3655 3640	3161	3754	2596	13	437.7
		3059	2965 2934 2880					
		2759	2736 2596					

Re-created from (20:46-47)

Table 20. Maximum Explosive 20-mm HEI Data and Statistics - Shot #2

POLAR ZONE	DEGREES	AVERAGE VELOCITY (FT/SEC)					VBAR	VMAX	VMIN	# OF HITS	SD
20	95-100	3412	3130	2924	2763	2731	2934	3412	2645	6	290.3
		2645									
21	100-105	4096	4049	3834	3673	3582	3403	4096	2512	10	532.1
		3368	3033	2970	2913	2512					
22	105-110	2287					2287	2287	2287	1	0.0
23	110-115	0								0	
24	115-120	0								0	
25	120-125	0								0	
26	125-130	0								0	
27	130-135	0								0	
28	135-140	0								0	
29	140-145	0								0	
30	145-150	1857					1857	1857	1857	1	0.0
31	150-155	1938					1938	1938	1938	1	0.0
32	155-160	2299					2299	2299	2299	1	0.0
33	160-165	2049					2049	2049	2049	1	0.0
34	165-170	0								0	
35	170-175	2771					2771	2771	2771	0	0.0
36	175-180	2961	2817	2715			2831	2961	2715	3	123.4

Re-created from (20:46-47)

Table 20. Maximum Explosive 20-mm HEI Data and Statistics - Shot #2 (con't)

POLAR ZONE	DEGREES	AVERAGE VELOCITY (FT/SEC)							VBAR	VMAX	VMIN	# OF HITS	SD
20	95-100	3465	3306	2968	2824	2462	2398	3465	952	12	695.1		
		2426	2326	2320	1975	1965							
		1787	952										
21	100-105	4096	3711	3681	3035	2837	3227	4095	2528	7	598.2		
		2703	2528										
22	105-110	2042	2018	1989	1735		1946	2042	1735	4	142.3		
23	110-115	0								0			
24	115-120	0								0			
25	120-125	0								0			
26	125-130	0								0			
27	130-135	0								0			
28	135-140	0								0			
29	140-145	0								0			
30	145-150	0								0			
31	150-155	1734					1734	1734	1734	1	0.0		
32	155-160	1835					1835	1835	1835	1	0.0		
33	160-165	0								0			
34	165-170	2271					2271	2271	2271	1	0.0		
35	170-175	0								0			
36	175-180	2671	2611				2641	2671	2611	2	42.5		

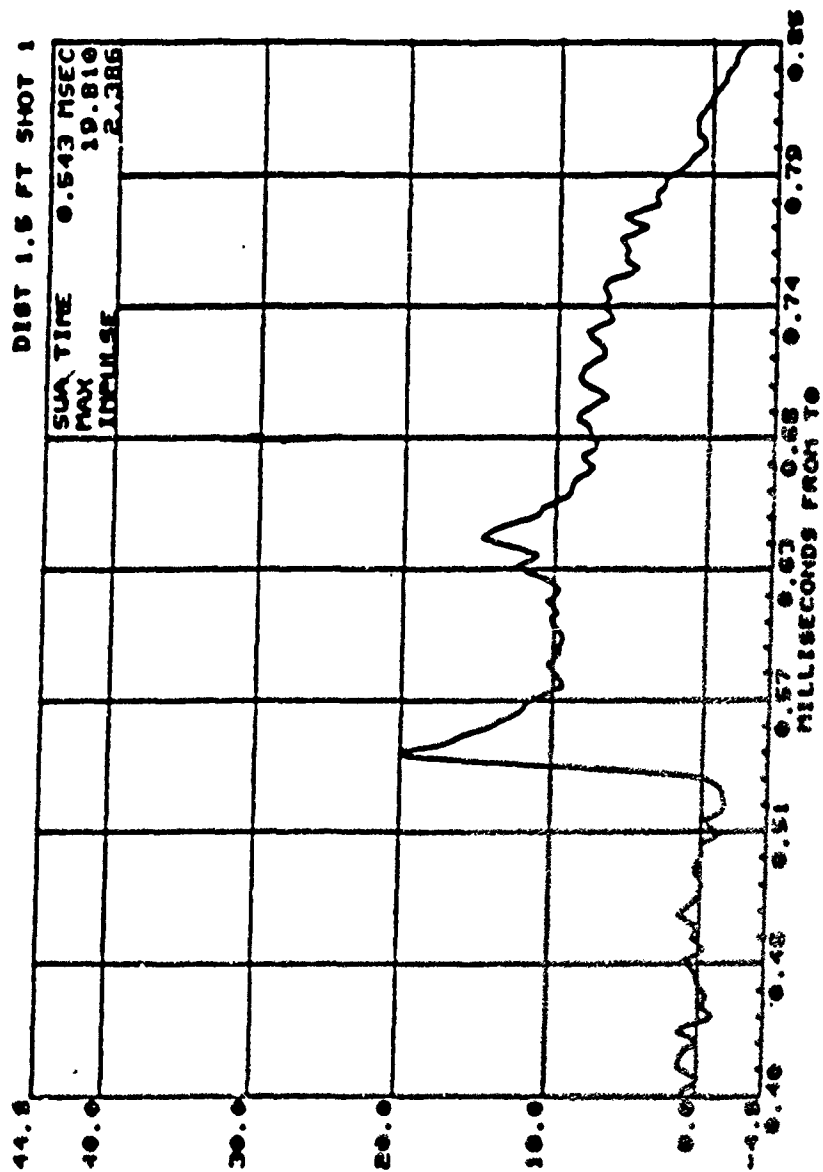
Re-created from (20:48-49)

Table 21. Maximum Explosive 20-mm HEI Data and Statistics - Shot #3

POLAR ZONE	DEGREES	AVERAGE VELOCITY (FT/SEC)						VBAR	VMAX	VMIN	# OF HITS	SD
20	95-100	3465	3306	2968	2824	2462	2398	3465	952	12	695.1	
		2426	2326	2320	1975	1965						
		1787	952									
21	100-105	4096	3711	3681	3035	2837	3227	4095	2528	7	598.2	
		2703	2528									
22	105-110	2042	2018	1989	1735		1946	2042	1735	4	142.3	
23	110-115	0								0		
24	115-120	0								0		
25	120-125	0								0		
26	125-130	0								0		
27	130-135	0								0		
28	135-140	0								0		
29	140-145	0								0		
30	145-150	0								0		
31	150-155	1734					1734	1734	1734	1	0.0	
32	155-160	1835					1835	1835	1835	1	0.0	
33	160-165	0								0		
34	165-170	2271					2271	2271	2271	1	0.0	
35	170-175	0								0		
36	175-180	2671	2611				2641	2671	2611	2	42.5	

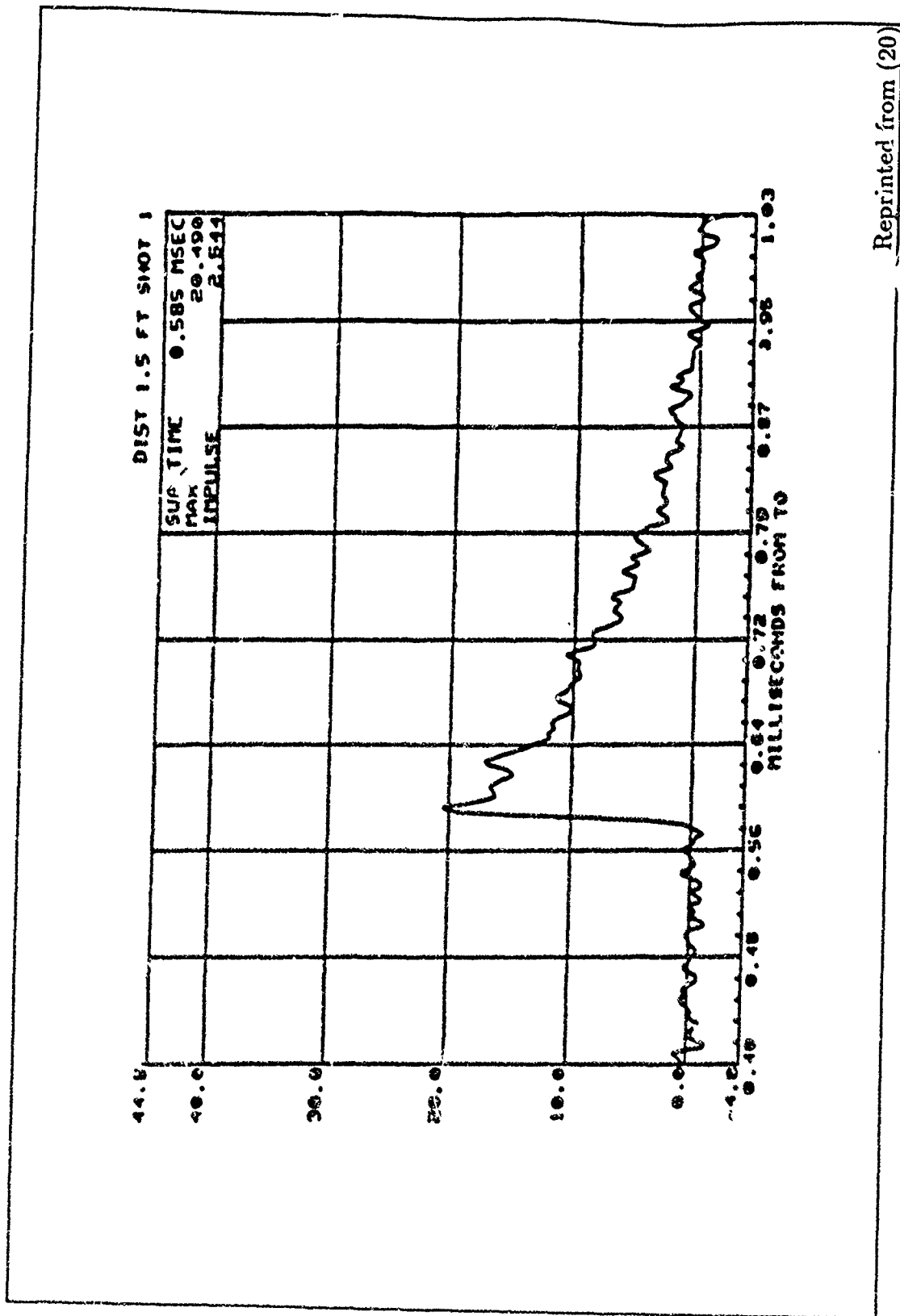
Re-created from (20:48-49)

Table 21. Maximum Explosive 20-mm HEI Data and Statistics - Shot #3 (con't)



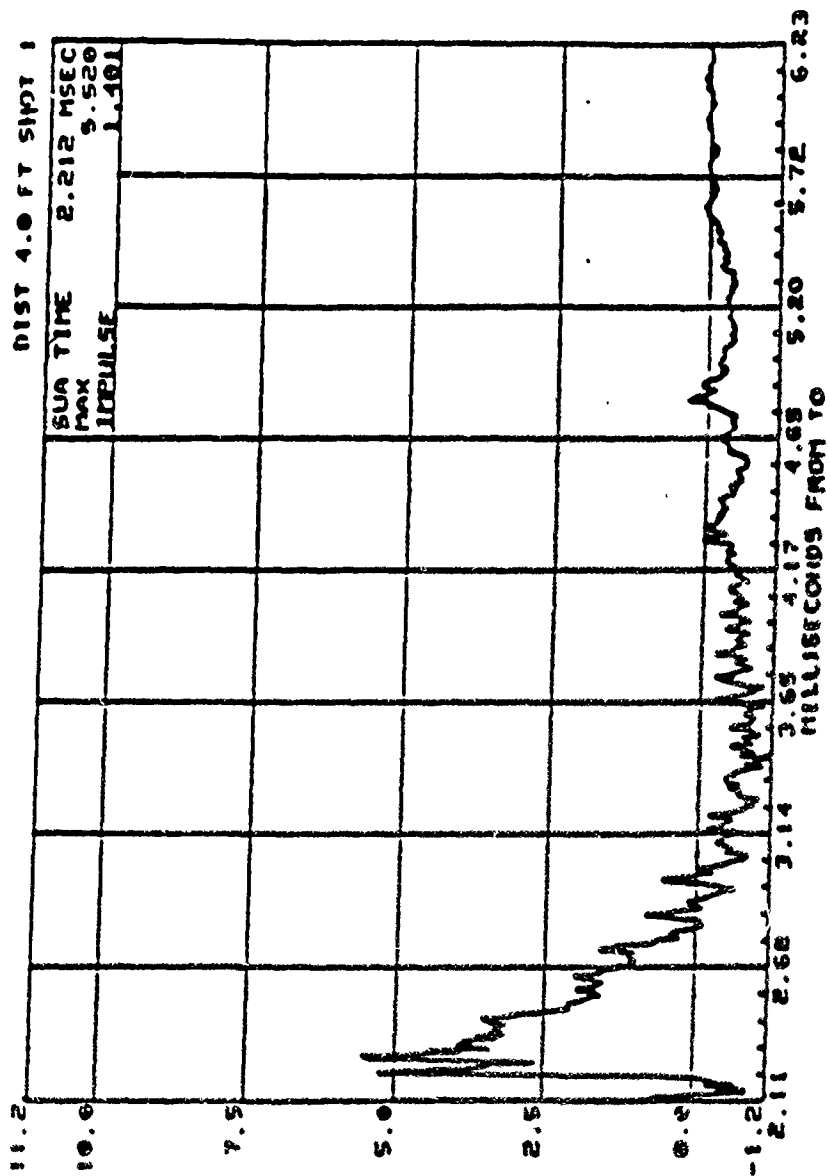
Reprinted from (20)

Figure 56. Pressure vs Time Plot for a Standard 20-mm HEI at P1=1.5 Feet



Reprinted from (20)

Figure 57. Pressure vs Time Plot for a Standard 20-mm HEI at P2=1.5 Feet



Reprinted from (20)

Figure 58. Pressure vs Time Plot for a Standard 20-mm HEI at P3=4.0 Feet

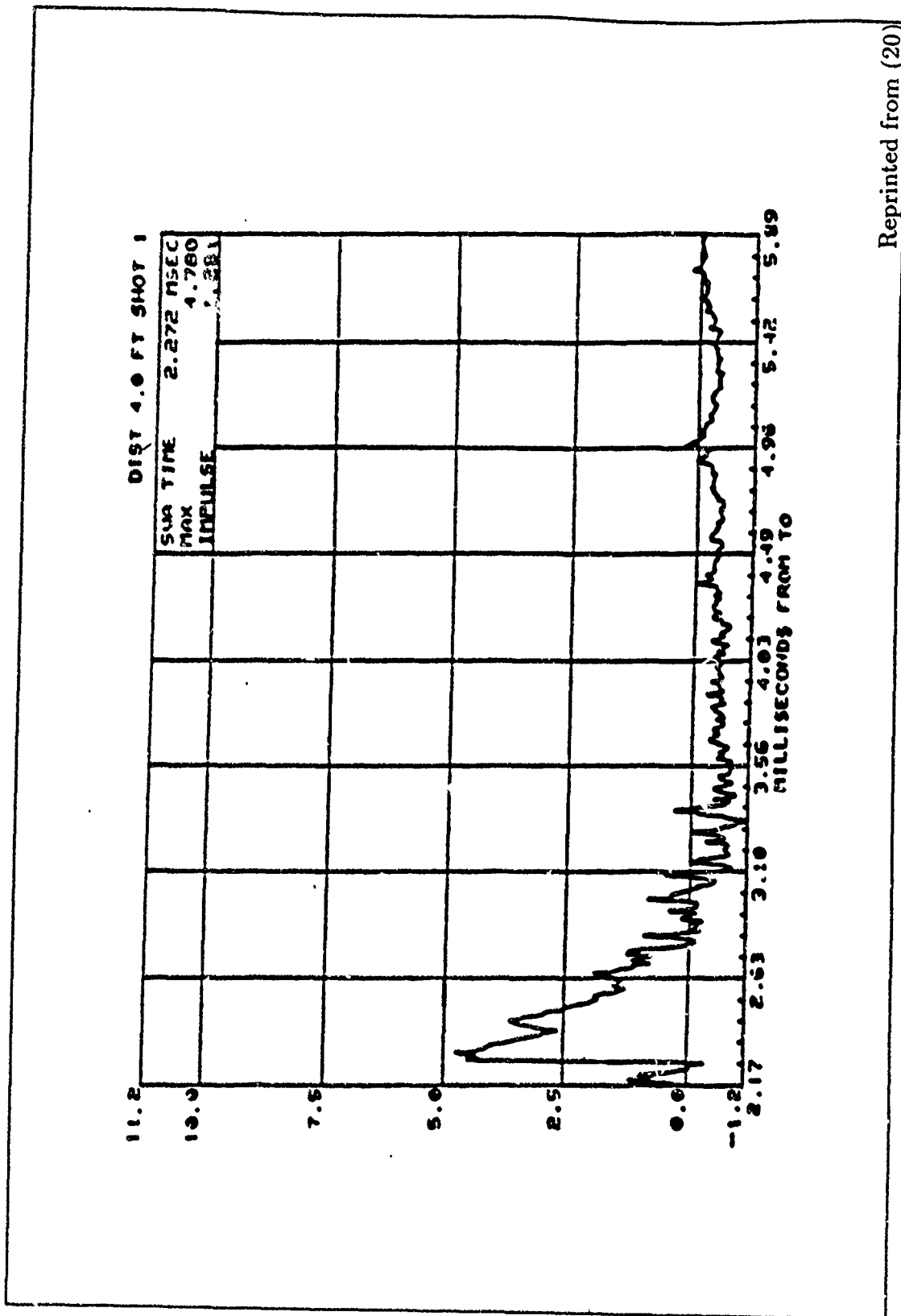
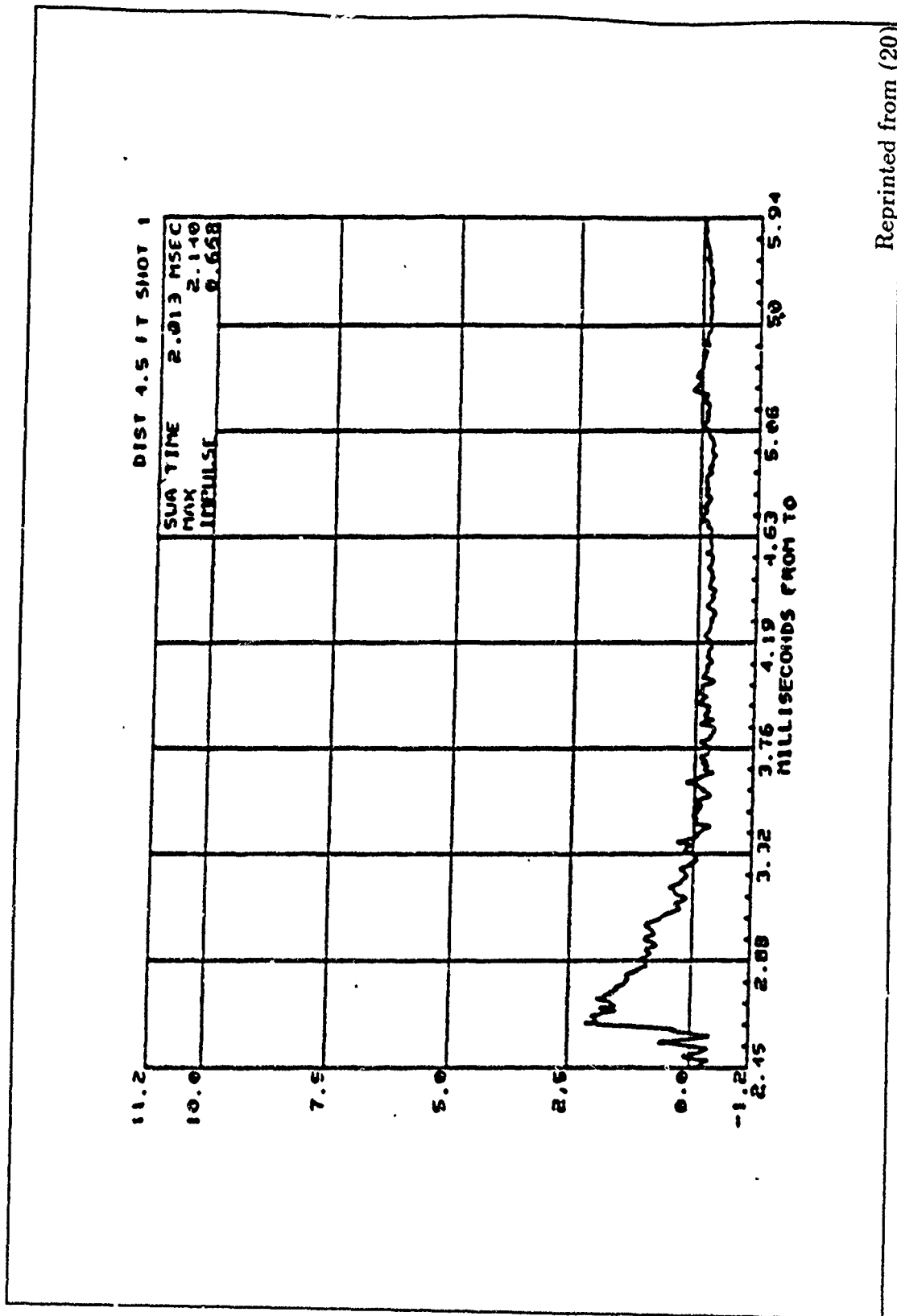
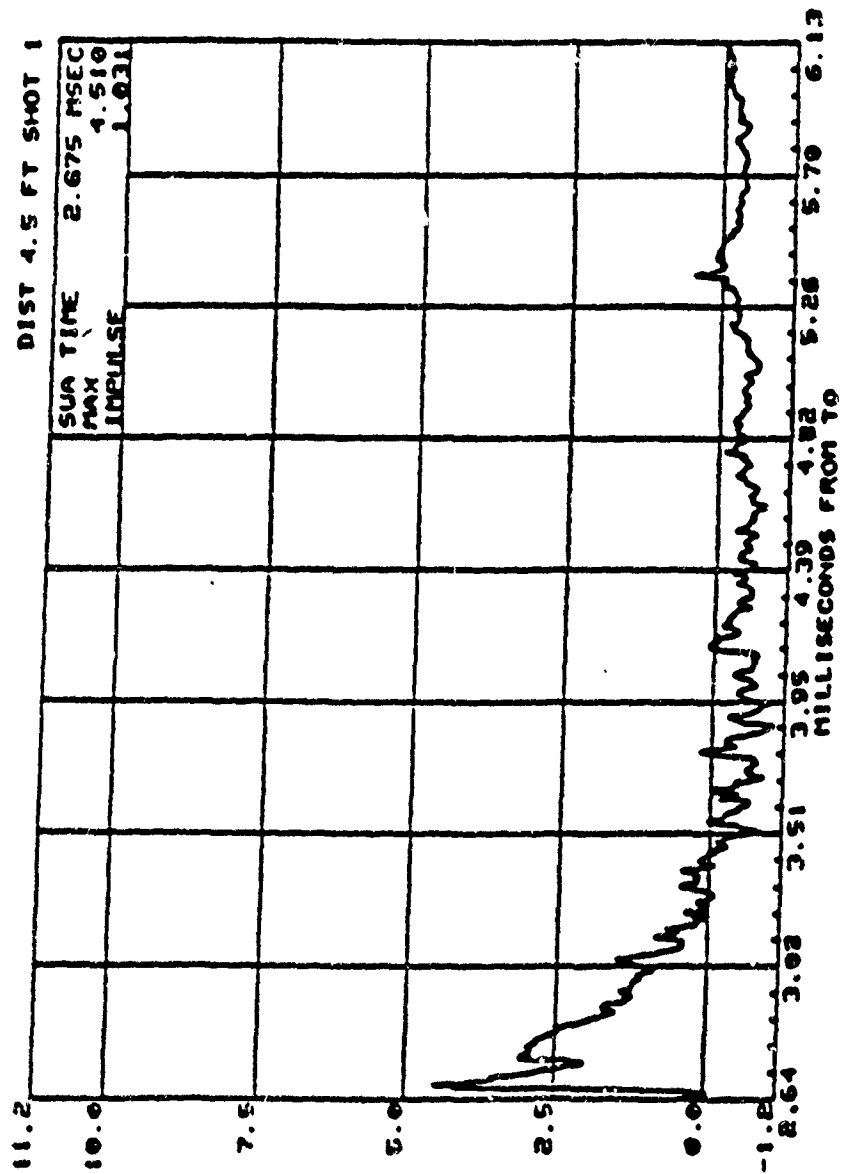


Figure 59. Pressure vs Time Plot for a Standard 20-mm HE1 at P5=4.0 Feet



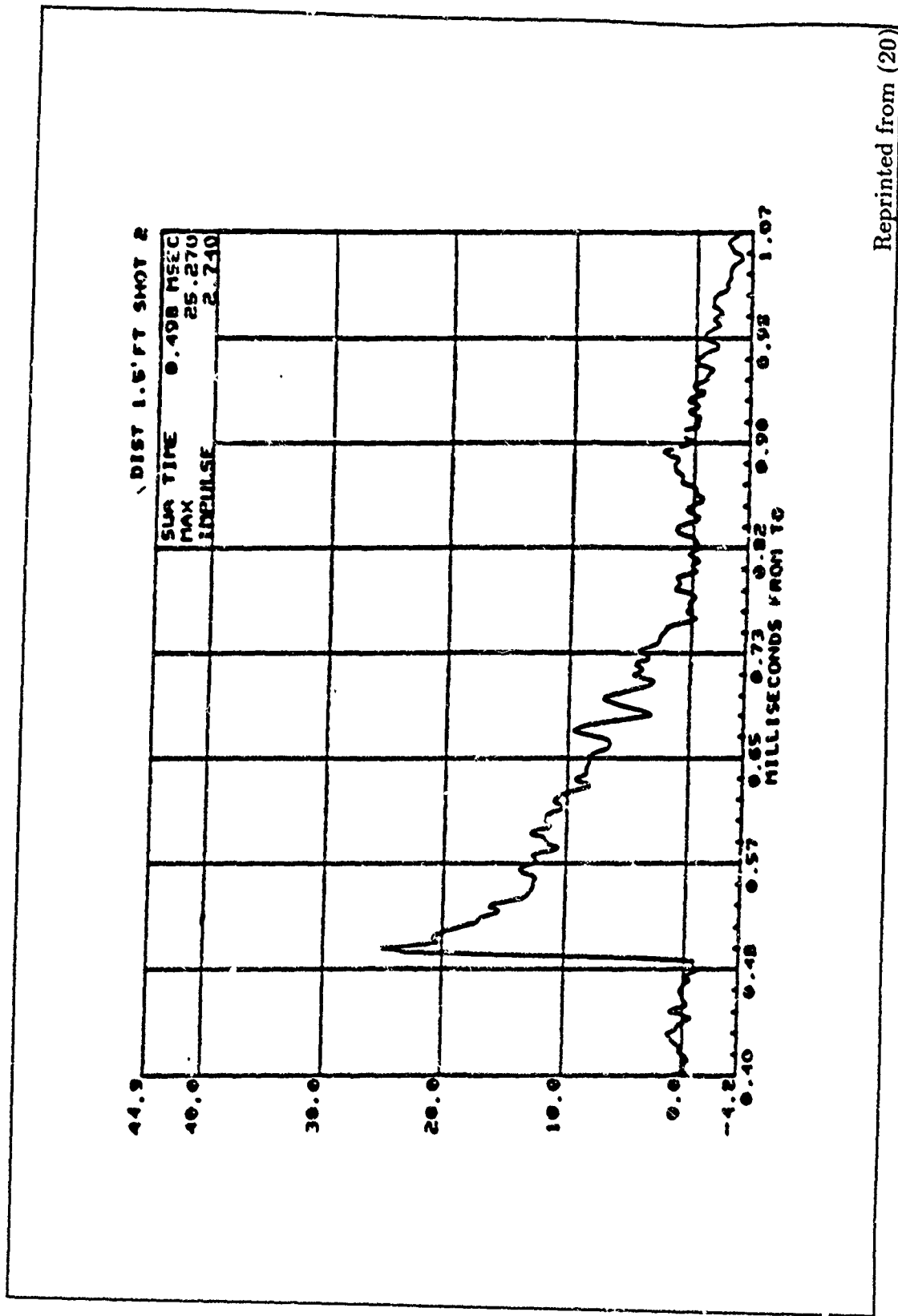
Reprinted from (20)

Figure 60. Pressure vs Time Plot for a Standard 20-mm HEI at P4=4.5 Feet



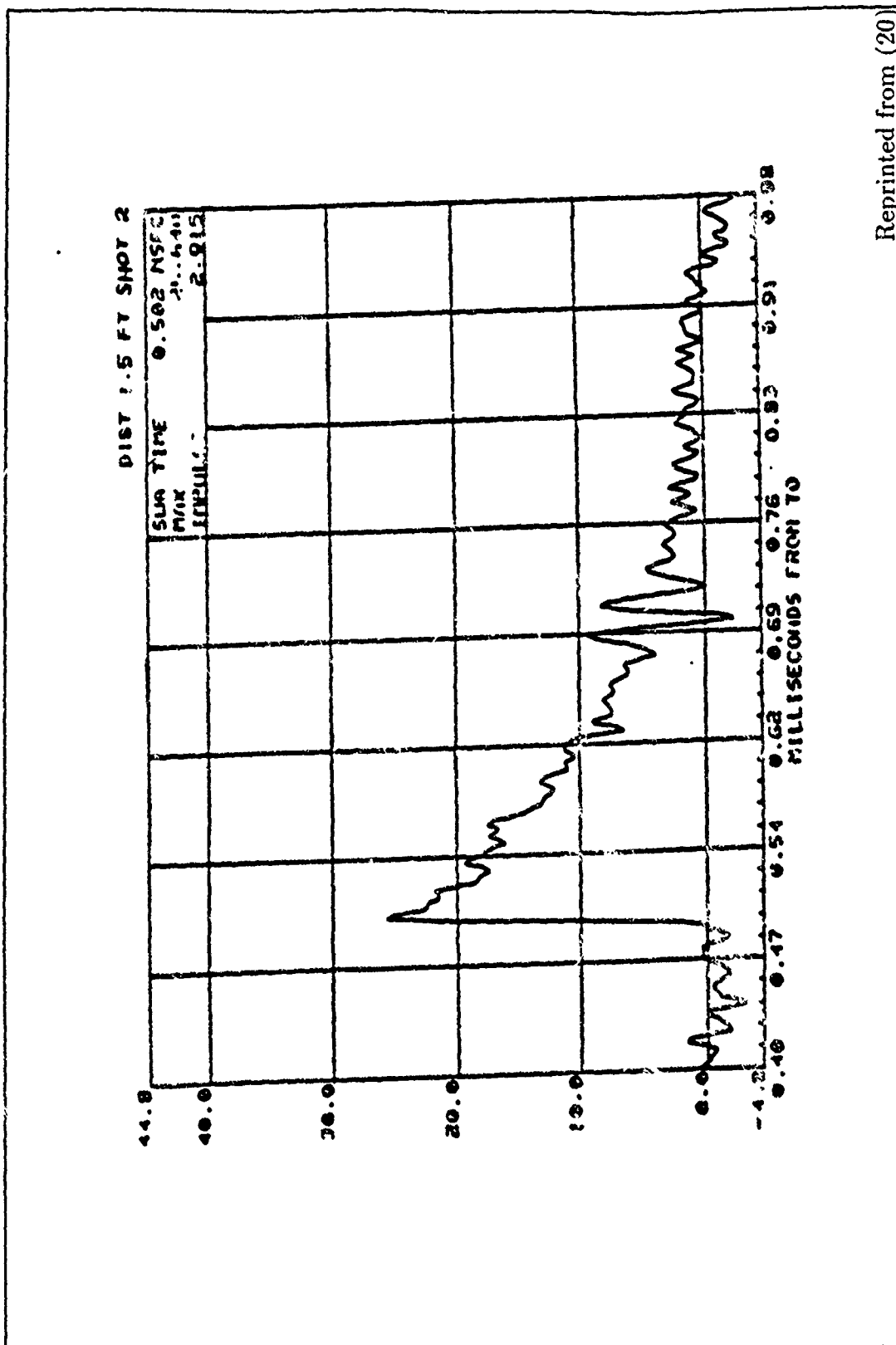
Reprinted from (20)

Figure 61. Pressure vs Time Plot for a Standard 20-mm HEJ at P6=4.5 Feet



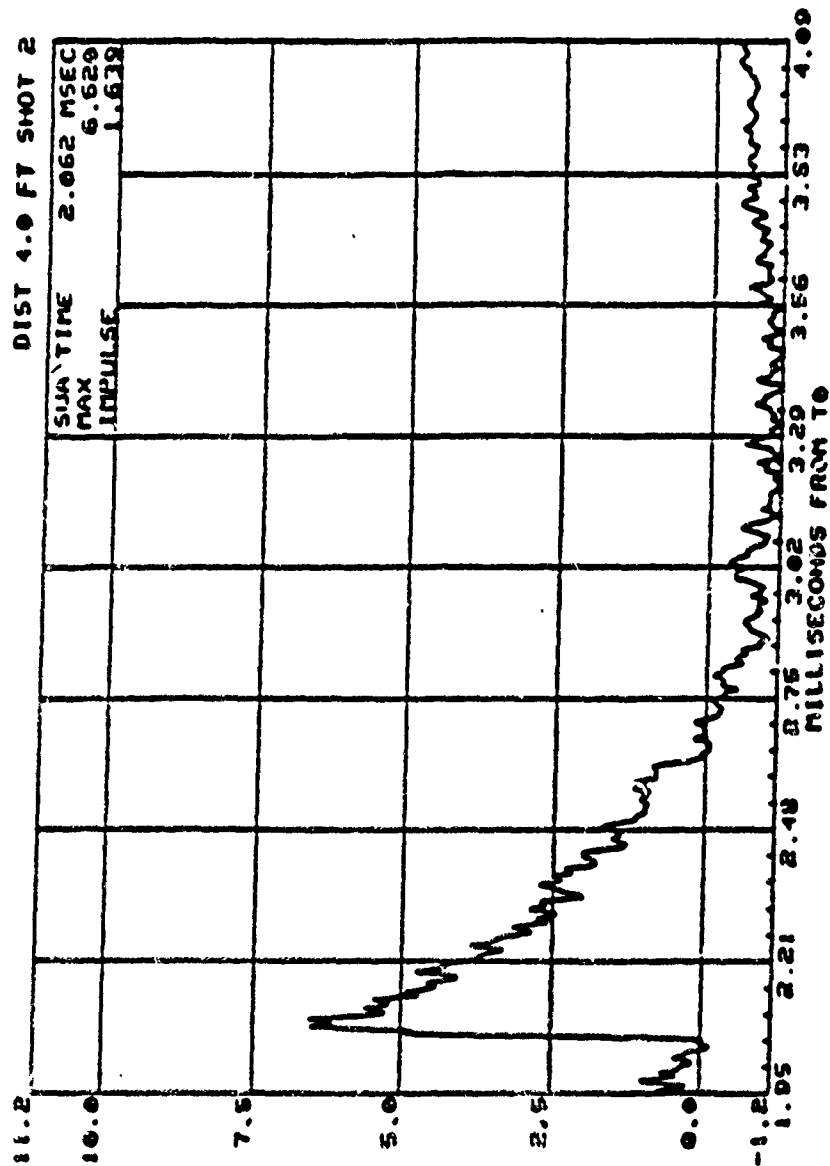
Reprinted from (20)

Figure 62. Pressure vs Time Plot for a Minimum Weight 20-mm HEI at P1=1.5 Feet



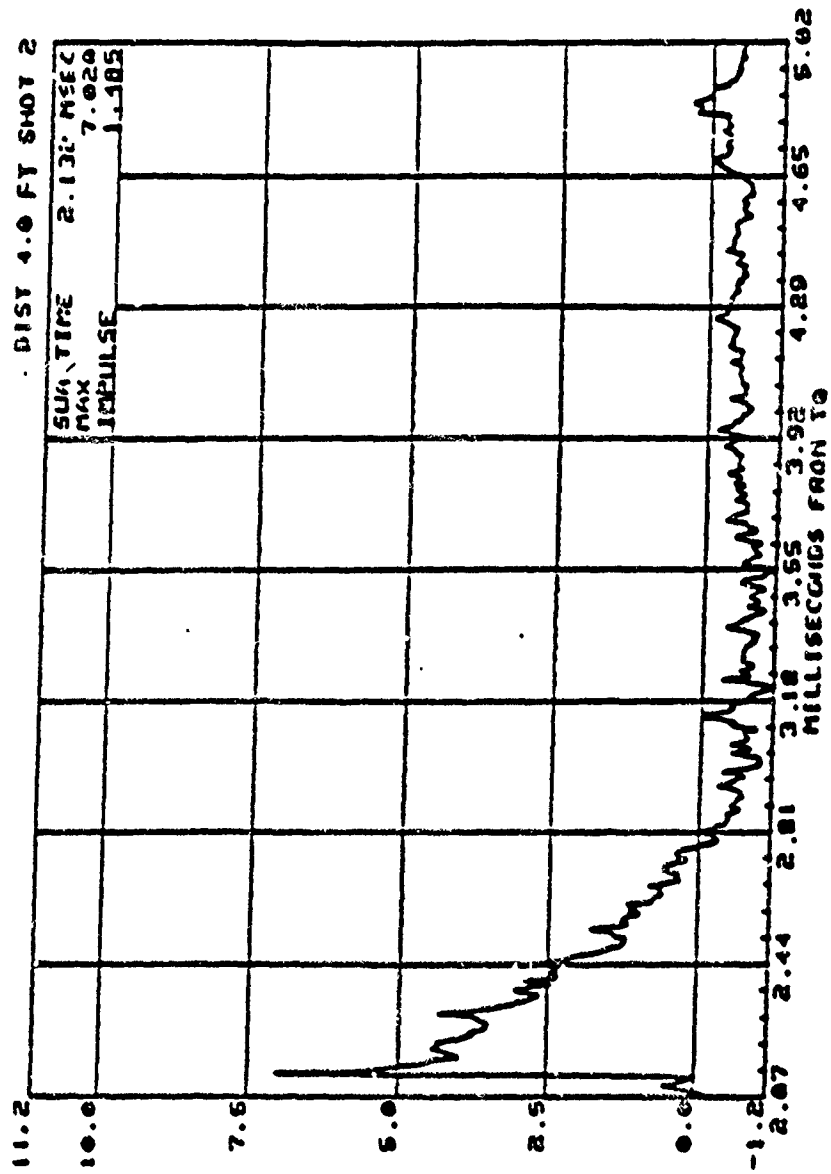
Reprinted from (20)

Figure 63. Pressure vs Time Plot for a Minimum Weight 20-mm HEI at P2=1.5 Feet



Reprinted from (20)

Figure 64. Pressure vs Time Plot for a Minimum Weight 20-mm HEI at P3=4.0 Feet



Reprinted from (20)

Figure 65. Pressure vs Time Plot for a Minimum Weight 20-mm HEI at P5=4.0 Feet

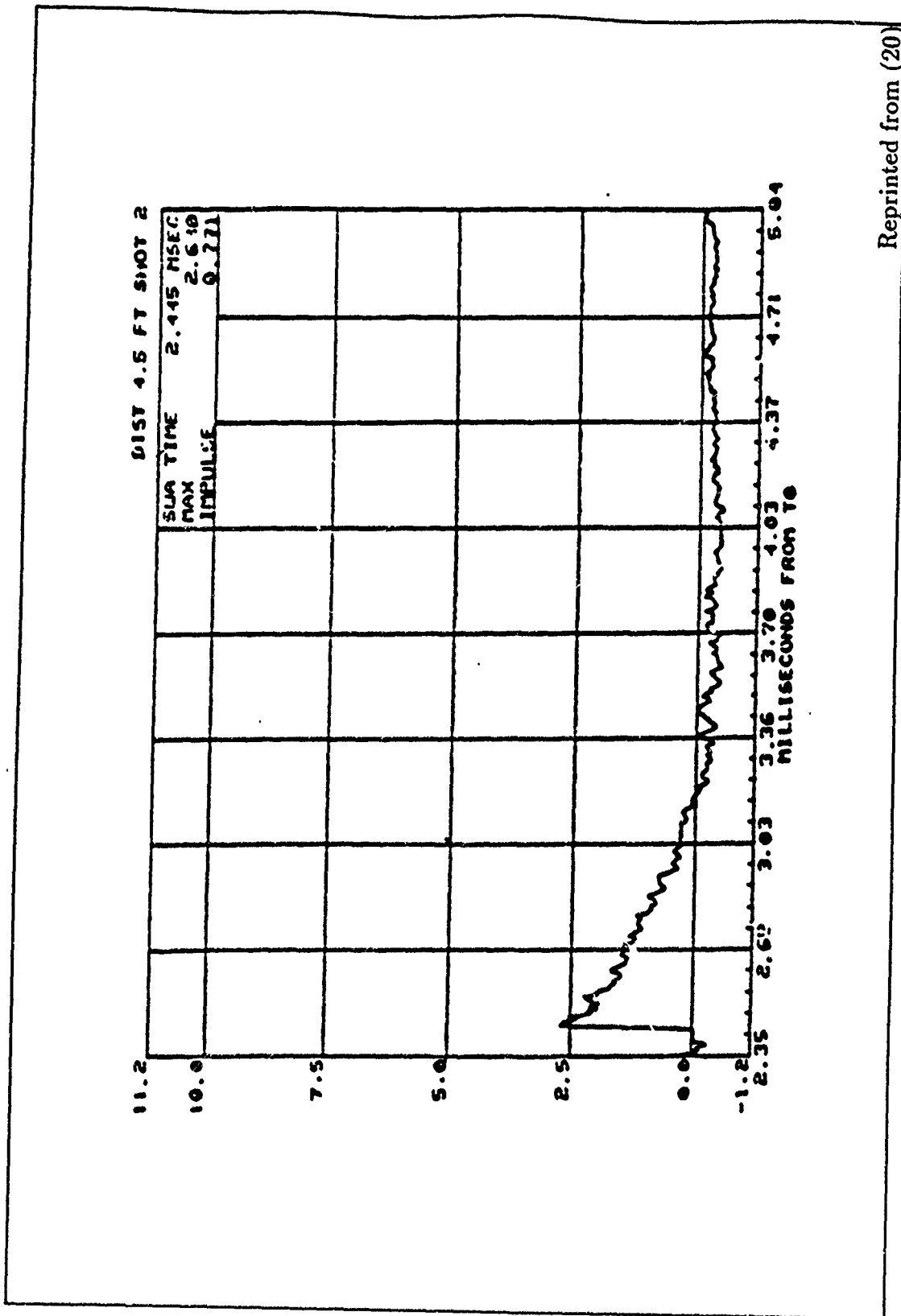
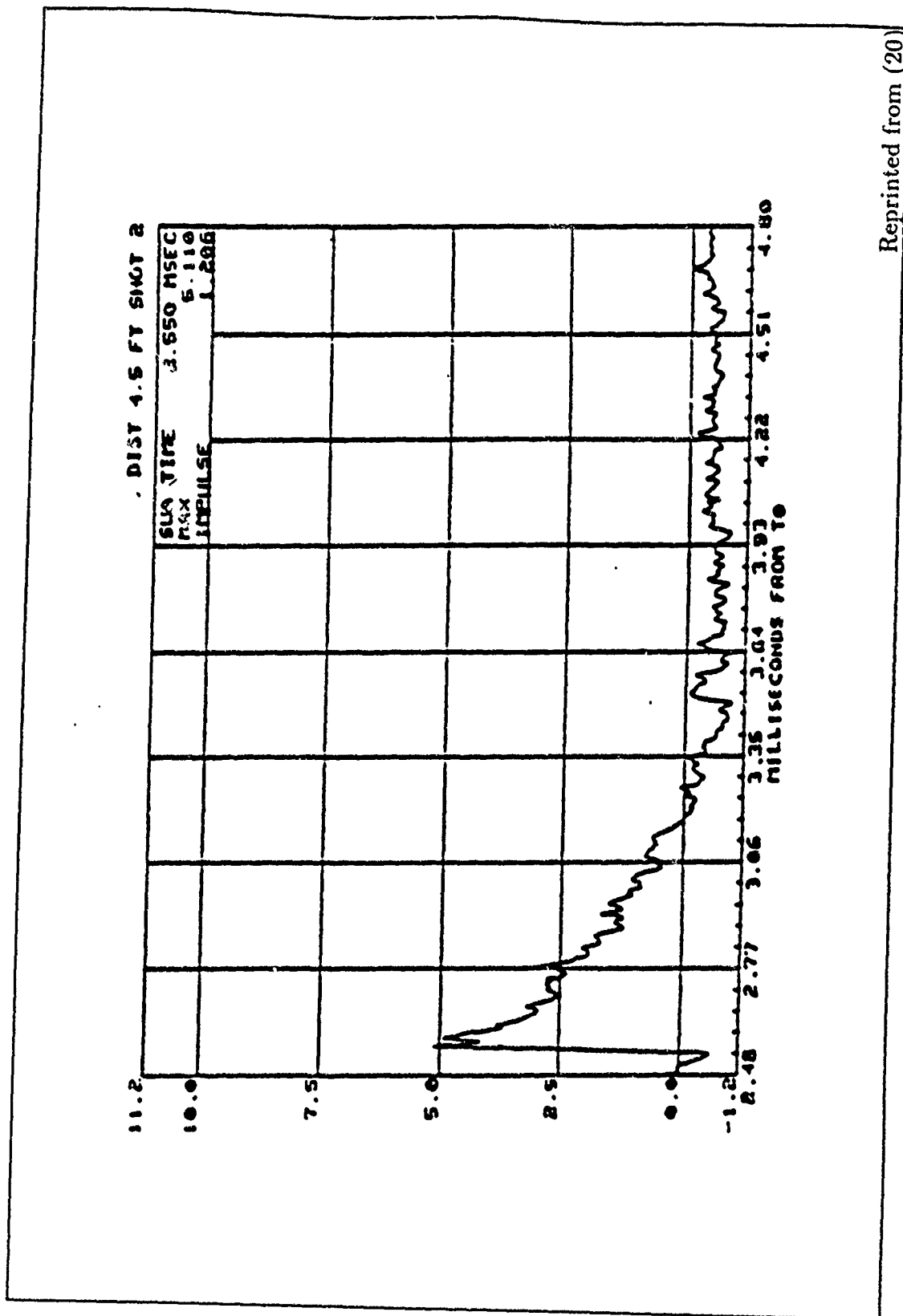
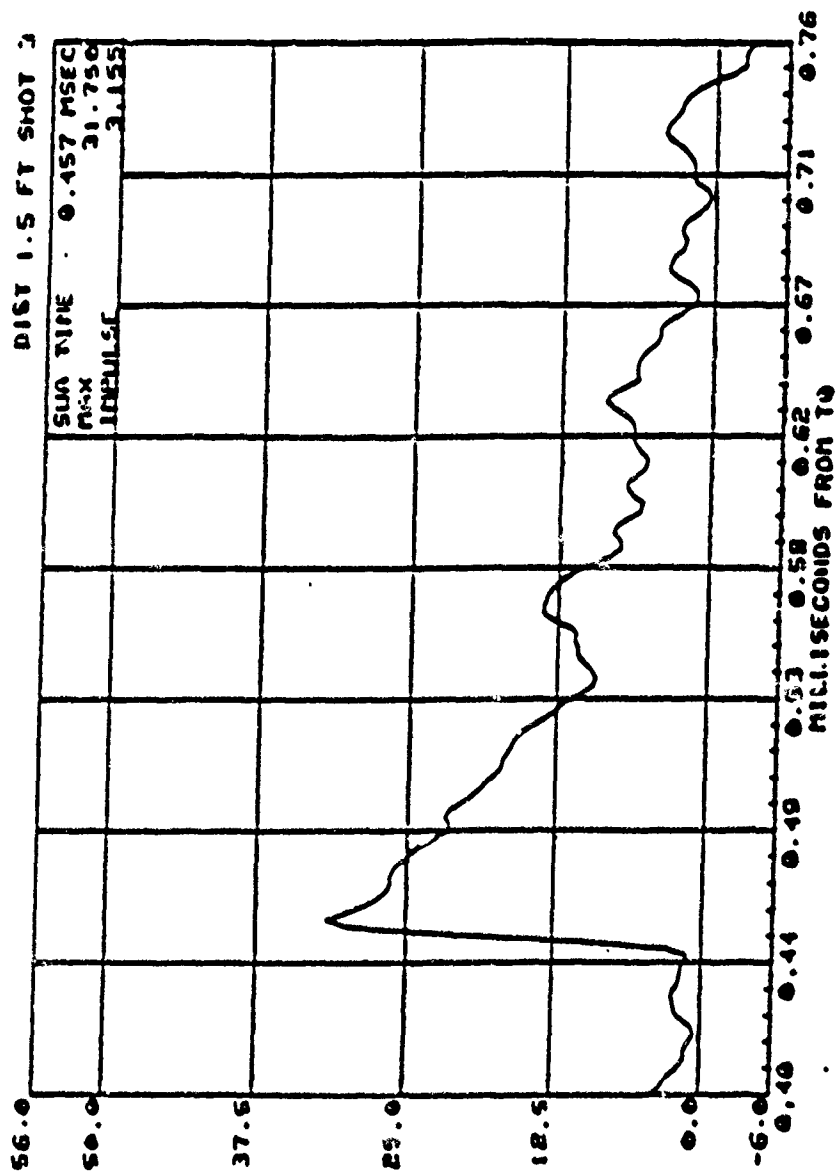


Figure 66. Pressure vs Time Plot for a Minimum Weight 20-mm HEI at P4=4.5 Feet



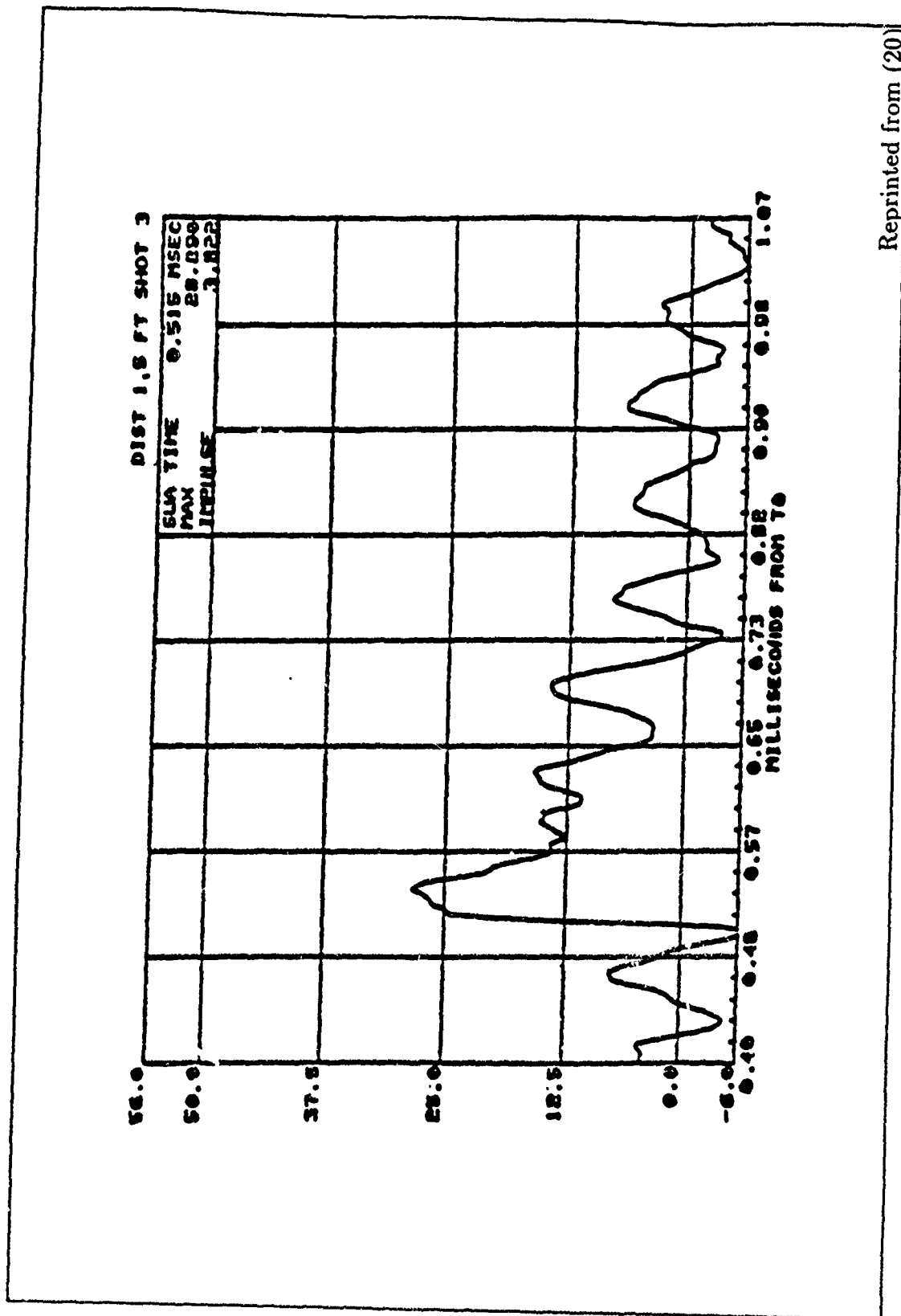
Reprinted from (20)

Figure 67. Pressure vs Time Plot for a Minimum Weight 20-mm HEI at P6=4.5 Feet



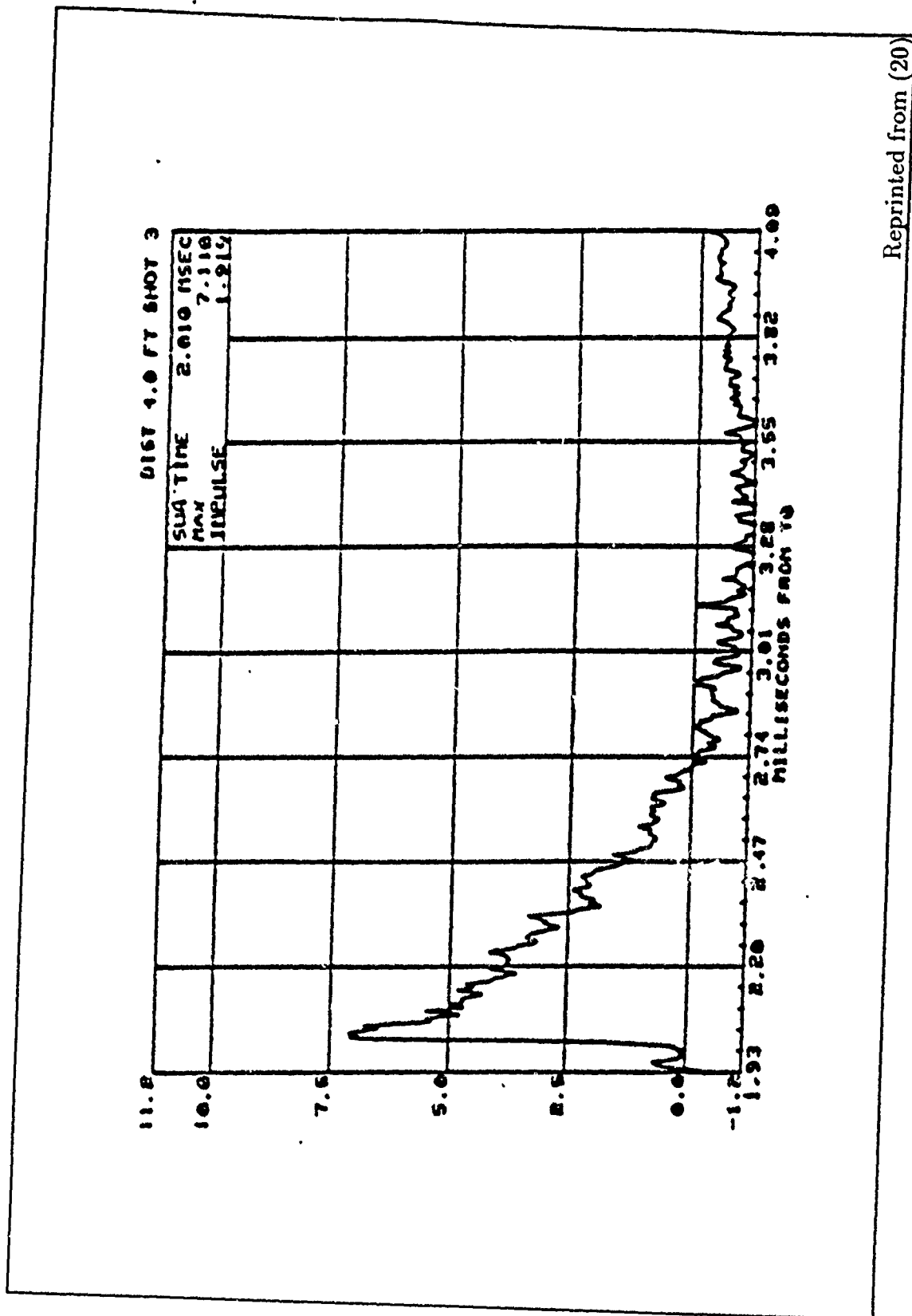
Reprinted from (20)

Figure 68. Pressure vs Time Plot for a Maximum Explosive 20-mm HEI at P1=1.5 Feet



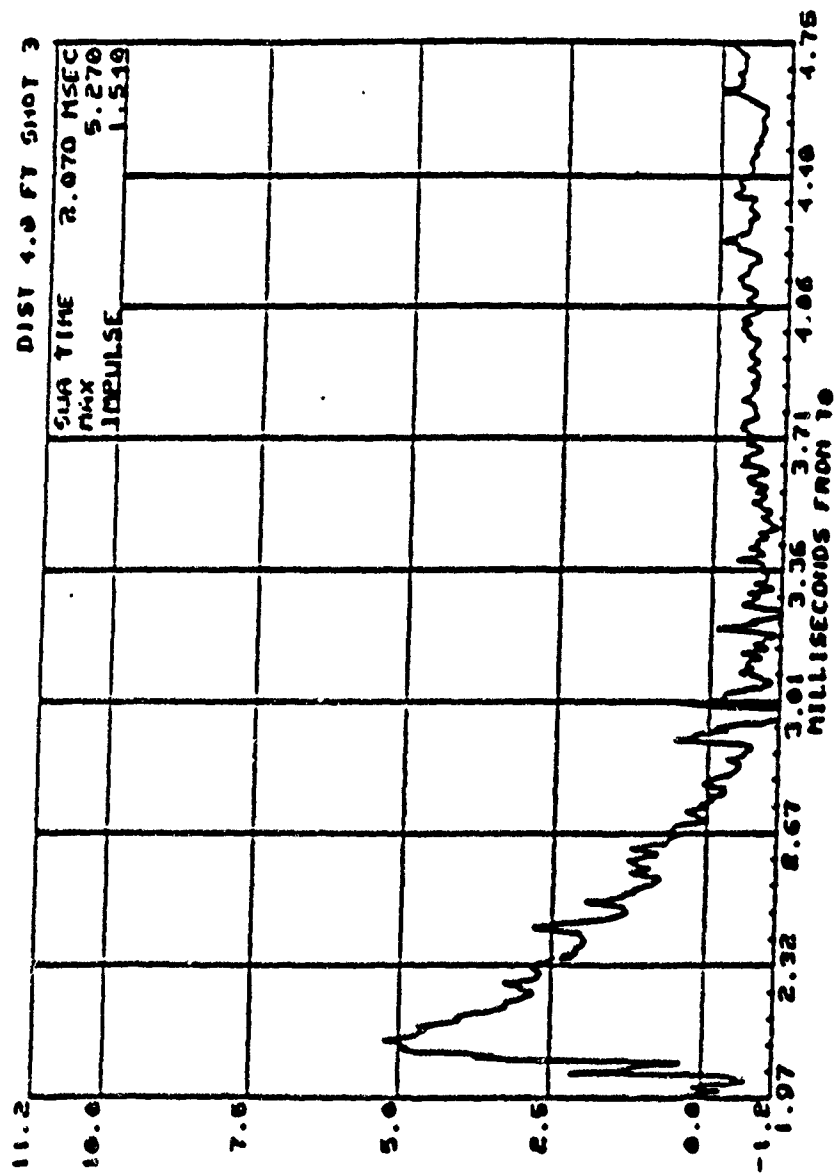
Reprinted from (20)

Figure 69. Pressure vs Time Plot for a Maximum Explosive 20-mm HEI at P2=1.5 Feet



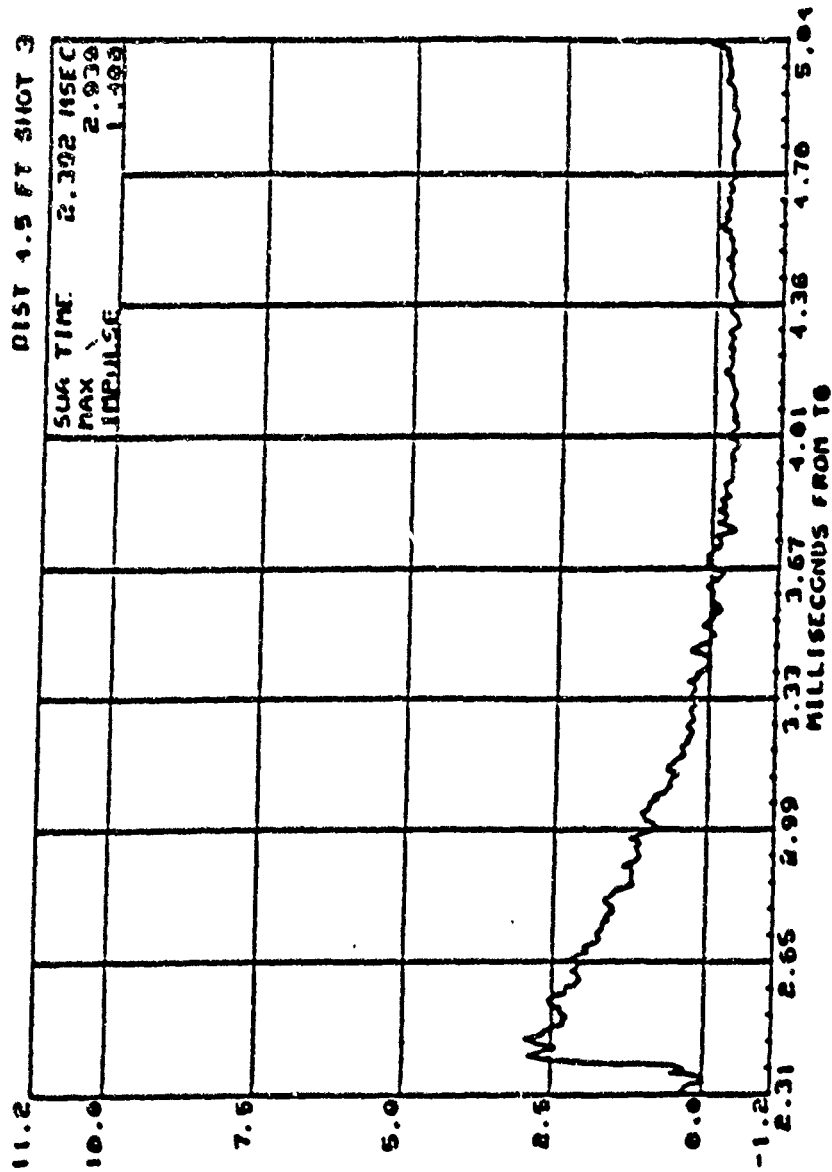
Reprinted from (20)

Figure 70. Pressure vs Time Plot for a Maximum Explosive 20-mm HEI at P3=4.0 Feet



Reprinted from (20)

Figure 71. Pressure vs Time Plot for a Maximum Explosive 20-mm HEI at P5=4.0 Feet



Reprinted from (20)

Figure 72. Pressure vs Time Plot for a Maximum Explosive 20-mm HEI at P4=4.5 Feet

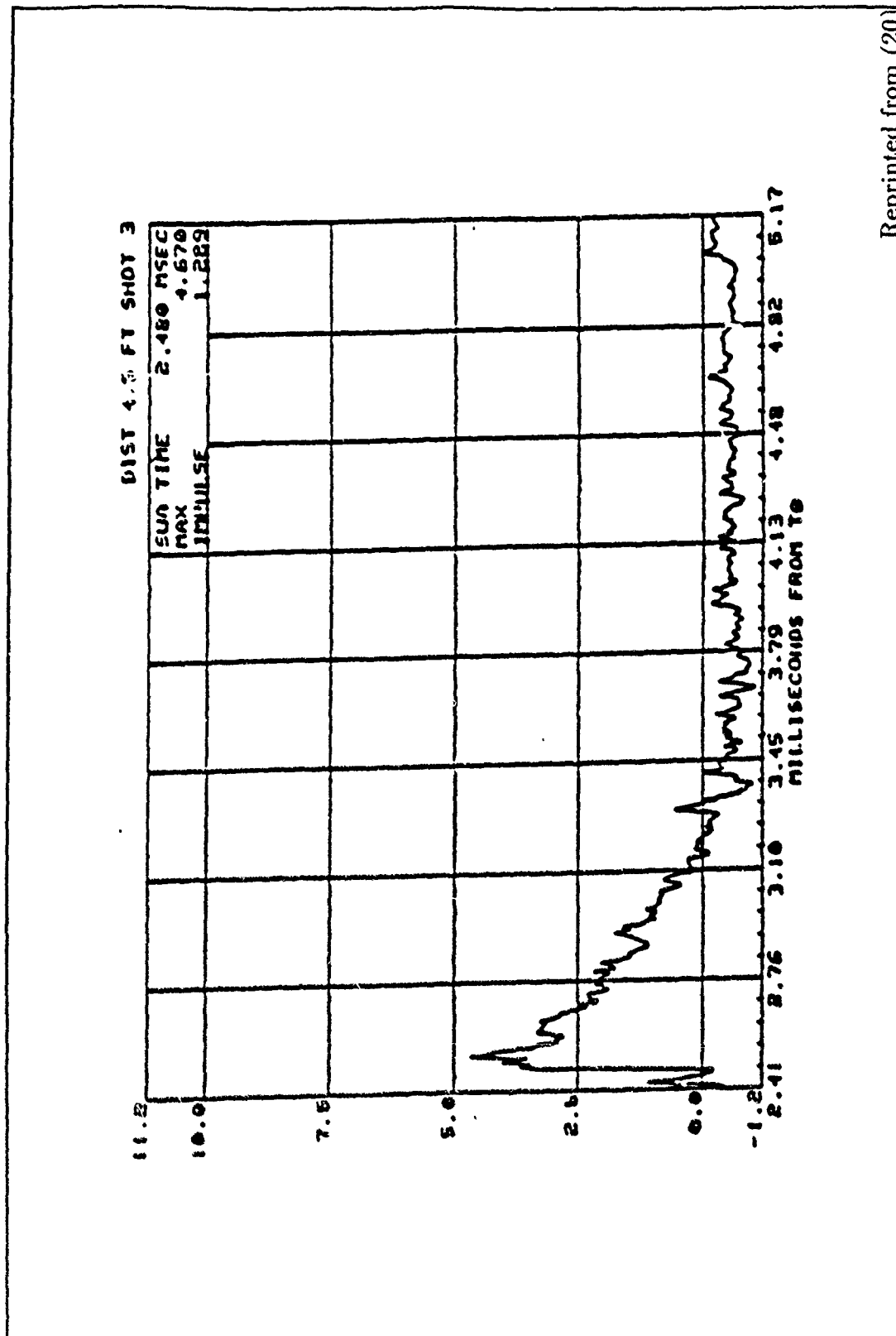


Figure 73. Pressure vs Time Plot for a Maximum Explosive 20-mm HEI at P6=4.5 Feet

Appendix B. *Data from Reeves Study*

POLAR ZONE (DEG)	AVERAGE OF HEAVIEST FRAGMENTS (GRAMS)	AVERAGE FRAGMENT WEIGHT (GRAMS)	TOTAL FRAGMENT WEIGHT (GRAMS)	NUMBER OF FRAGMENTS	FRAGMENTS PER STERADIAN	INITIAL VELOCITY (M/SEC)
0.0- 2.5	0.000	0.0	0.0	0.0	6.6	0
2.5- 7.5	0.000	0.0	0.0	0.0	0.0	0
7.5- 12.5	0.184	0.013	0.013	1.00	10.0	816
12.5- 17.5	0.137	0.009	0.009	1.00	7.0	815
17.5- 22.5	0.000	0.0	0.0	0.0	0.0	0
22.5- 27.5	0.000	0.0	0.0	0.0	0.0	0
27.5- 32.5	0.000	0.0	0.0	0.0	0.0	0
32.5- 37.5	0.000	0.0	0.0	0.0	0.0	0
37.5- 42.5	0.000	0.0	0.0	0.0	0.0	0
42.5- 47.5	0.000	0.0	0.0	0.0	0.0	0
47.5- 52.5	0.000	0.0	0.0	0.0	0.0	0
52.5- 57.5	0.000	0.0	0.0	0.0	0.0	0
57.5- 62.5	0.000	0.0	0.0	0.0	0.0	0
62.5- 67.5	0.000	0.0	0.0	0.0	0.0	0
67.5- 72.5	0.058	0.007	0.014	0.94	13.5	1223
72.5- 77.5	0.067	0.004	0.028	6.98	13.2	1223
77.5- 82.5	0.248	0.010	0.070	7.00	13.0	1223
82.5- 87.5	1.172	0.025	1.053	42.12	77.1	1223
87.5- 92.5	4.931	0.036	2.262	62.29	150.1	1178
92.5- 97.5	0.527	0.012	0.674	56.15	102.6	1178
97.5-102.5	0.475	0.020	0.280	14.01	26.0	1178
102.5-107.5	0.431	0.019	0.199	10.46	19.8	1133
107.5-112.5	0.000	0.0	0.0	0.0	0.0	0
112.5-117.5	0.000	0.0	0.0	0.0	0.0	0
117.5-122.5	0.000	0.0	0.0	0.0	0.0	0
122.5-127.5	0.110	0.009	0.027	3.39	7.5	905
127.5-132.5	1.106	0.043	0.289	6.73	16.9	905

Reprinted from (28)

Table 22. Fragmentation Data Summary for the Soviet 23-mm HEI-T Projectile Used in the NR/NS-23 Aircraft Guns

POLAR ZONE (DEG)	AVERAGE OF HEAVIEST FRAGMENTS (GRAMS)	AVERAGE FRAGMENT WEIGHT (GRAMS)	TOTAL FRAGMENT WEIGHT (GRAMS)	TOTAL NUMBER OF FRAGMENTS	FRAGMENTS PER STERADIAN	INITIAL ^a VELOCITY (M/SEC)
132.5-137.5	0.000	0.0	0.0	0.0	0.0	0.
137.5-142.5	0.729	0.266	1.115	1.87	5.6	726.
142.5-147.5	4.004	0.115	0.544	4.73	15.0	726.
147.5-152.5	4.698	0.504	0.359	1.18	4.3	680.
152.5-157.5	0.691	0.035	0.057	1.64	7.1	680.
157.5-162.5	0.000	0.0	0.0	0.0	0.0	0.
162.5-167.5	0.000	0.0	0.0	0.0	0.0	0.
167.5-172.5	0.036	0.003	0.002	1.00	10.5	69.
172.5-177.5	2.601	0.042	0.231	5.50	115.1	69.
177.5-180.0	2.789	0.046	0.110	2.50	416.0	69.

AVERAGE OF 2 BOUNDS TESTED AT 441°
SCALE FACTOR EQUALS 1.003
K EQUALS 648 GRAMS PER CUBIC INCH

The flash X-Ray for this projectile, initial velocity results obtained from Table IV. When fragments were observed from the flash X-Ray to have an initial velocity of 69 m/sec, other fragments in the 137.5° - 142.5° polar zone had the initial velocity presented in the above table. The scale factor indicates a 99.5% as fired total weight recovery. However, the actual percent recovery (79.5%) was increased by 20% to account for fragments purposely not recovered. This increase was based on the results of 20-mm projectile fragmentation tests conducted at APC, reference APG-MT-4509.

Reprinted from (27)

Table 22. Fragmentation Data Summary for the Soviet 23-n.m HEI-T Projectile Used in the NR/NS-23 Aircraft Guns (con't)

POLAR ZONE (DEG)	AVERAGE OF HEAVIEST FRAGMENTS (GRAMS)	AVERAGE FRAGMENT WEIGHT (GRAMS)	TOTAL FRAGMENT WEIGHT (GRAMS)	TOTAL NUMBER OF FRAGMENTS	FRAGMENTS PER STERADIAN	INITIAL VELOCITY (M/SEC)
0.0- 2.5	0.000	0.0	0.0	0.0	0.0	0.
2.5- 7.5	0.000	0.0	0.0	0.0	0.0	0.
7.5- 12.5	0.000	0.0	0.0	0.0	0.0	0.
12.5- 17.5	0.000	0.0	0.0	0.0	0.0	0.
17.5- 22.5	0.000	0.0	0.0	0.0	0.0	0.
22.5- 27.5	0.023	0.002	0.002	1.02	4.4	1037.
27.5- 32.5	0.000	0.0	0.0	0.0	0.0	0.
32.5- 37.5	0.000	0.0	0.0	0.0	0.0	0.
37.5- 42.5	0.012	0.001	0.002	2.46	7.0	1134.
42.5- 47.5	0.000	0.0	0.0	0.0	0.0	0.
47.5- 52.5	0.000	0.0	0.0	0.0	0.0	0.
52.5- 57.5	0.000	0.0	0.0	0.0	0.0	0.
57.5- 62.5	0.034	0.002	0.007	3.42	7.2	1204.
62.5- 67.5	0.000	0.0	0.0	0.0	0.0	0.
67.5- 72.5	0.000	0.0	0.0	0.0	0.0	0.
72.5- 77.5	0.000	0.0	0.0	0.0	0.0	0.
77.5- 82.5	0.275	0.008	0.224	28.02	51.9	1250.
82.5- 87.5	1.023	3.019	1.067	56.15	102.6	1250.
87.5- 92.5	1.217	6.016	1.012	63.22	115.3	1250.
92.5- 97.5	1.607	9.012	2.022	168.46	308.5	1250.
97.5-102.5	0.636	0.012	1.009	84.05	155.7	1250.
102.5-107.5	0.195	0.010	0.070	6.98	13.2	1235.
107.5-112.5	0.016	0.001	0.003	3.47	6.7	1235.
112.5-117.5	0.000	0.0	0.0	0.0	0.0	0.
117.5-122.5	0.000	0.0	0.0	0.0	0.0	0.
122.5-127.5	0.090	0.0	0.0	0.0	0.0	0.
127.5-132.5	0.000	0.0	0.0	0.0	0.0	0.
132.5-137.5	0.000	0.0	0.0	0.0	0.0	0.
137.5-142.5	0.000	0.0	0.0	0.0	0.0	0.
142.5-147.5	0.000	0.0	0.0	0.0	0.0	0.

Reprinted from (27)

Table 23. Fragmentation Data Summary for the Soviet 23-mm HEI Projectile Used in the AM-23 and GSh Aircraft Guns

POLAR ZONE (DEG)	AVERAGE OF HEAVIEST FRAGMENTS (GRAMS)	AVERAGE FRAGMENT WEIGHT (GRAMS)	TOTAL FRAGMENT WEIGHT (GRAMS)	TOTAL NUMBER OF FRAGMENTS	FRAGMENTS PER STERADIAN	INITIAL VELOCITY (M/SEC)
0.0- 2.5	0.000	0.0	0.0	0.0	0.0	0.
2.5- 7.5	0.000	0.0	0.0	0.0	0.0	0.
7.5- 12.5	0.000	0.0	0.0	0.0	0.0	0.
12.5- 17.5	0.000	0.0	0.0	0.0	0.0	0.
17.5- 22.5	0.000	0.0	0.0	0.0	0.0	0.
22.5- 27.5	0.023	0.002	0.002	1.02	4.4	1037.
27.5- 32.5	0.000	0.0	0.0	0.0	0.0	0.
32.5- 37.5	0.000	0.0	0.0	0.0	0.0	0.
37.5- 42.5	0.012	0.001	0.002	2.46	7.0	1134.
42.5- 47.5	0.000	0.0	0.0	0.0	0.0	0.
47.5- 52.5	0.000	0.0	0.0	0.0	0.0	0.
52.5- 57.5	0.000	0.0	0.0	0.0	0.0	0.
57.5- 62.5	0.034	0.002	0.007	3.42	7.2	1204.
62.5- 67.5	0.000	0.0	0.0	0.0	0.0	0.
67.5- 72.5	0.000	0.0	0.0	0.0	0.0	0.
72.5- 77.5	0.000	0.0	0.0	0.0	0.0	0.
77.5- 82.5	0.275	0.008	0.224	28.02	51.9	1250.
82.5- 87.5	1.023	0.019	1.067	56.15	102.6	1250.
87.5- 92.5	1.217	0.016	1.012	61.22	115.3	1250.
92.5- 97.5	1.607	0.012	2.022	168.46	308.5	1250.
97.5-102.5	0.636	0.012	1.009	64.05	155.7	1250.
102.5-107.5	0.195	0.010	0.070	6.98	13.2	1235.
107.5-112.5	0.016	0.001	0.003	3.47	6.7	1235.
112.5-117.5	0.000	0.0	0.0	0.0	0.0	0.
117.5-122.5	0.000	0.0	0.0	0.0	0.0	0.
122.5-127.5	0.090	0.0	0.0	0.0	0.0	0.
127.5-132.5	0.000	0.0	0.0	0.0	0.0	0.
132.5-137.5	0.000	0.0	0.0	0.0	0.0	0.
137.5-142.5	0.000	0.0	0.0	0.0	0.0	0.
142.5-147.5	0.000	0.0	0.0	0.0	0.0	0.

Reprinted from (27)

Table 23. Fragmentation Data Summary for the Soviet 23-mm HEI Projectile Used in the AM-23 and GSh Aircraft Guns

POLAR ZONE (DEG)	AVERAGE LP HEAVIEST FRAGMENTS (GRAMS)	AVERAGE FRAGMENT WEIGHT (GRAMS)	TOTAL FRAGMENT WEIGHT (GRAMS)	TOTAL NUMBER OF FRAGMENTS	FRAGMENTS PER STERADIAN	INITIAL VELOCITY (M/SEC)
147.5-152.5	0.000	0.0	0.0	0.0	0.0	0.
152.5-157.5	0.000	0.0	0.0	0.0	0.0	0.
157.5-162.5	0.000	0.0	0.0	0.0	0.0	0.
162.5-167.5	0.000	0.0	0.0	0.0	0.0	0.
167.5-172.5	0.787	0.044	0.088	2.00	21.0	808.
172.5-177.5	2.245	0.116	0.348	3.00	62.8	802.
177.5-180.0	0.000	0.0	0.0	0.0	0.0	0.

AVERAGE OF 2 ROUNDS TESTED AT AA1

SCALE FACTOR EQUALS 1.043

X EQUALS 723 GRAMS PER CUBIC INCH

The scale factor indicates a 95.9% as fired metal weight recovery. However, the actual percent recovery (75.9%) was increased by 20% to account for fragments purposely not recovered. This increase was based on the results of 30-mm projectile fragmentation tests conducted at AFQ, reference, AFQ-WT-4609.

Reprinted from (28)

Table 25. Fragmentation Data Summary for the Soviet 23-mm HEI Projectile Used in the AM-23 and GSh Aircraft Guns (con't)

POLAR ZONE (DEG)	AVERAGE OF HEAVIEST FRAGMENTS (GRAMS)	AVERAGE FRAGMENT WEIGHT (GRAMS)	TOTAL FRAGMENT WEIGHT (GRAMS)	TOTAL NUMBER OF FRAGMENTS	FRAGMENTS PER STERADIAN	INITIAL VELOCITY (M/SEC)
0.0- 2.5	0.000	0.0	0.0	0.0	0.0	0.
2.5- 7.5	0.237	0.015	0.015	1.00	20.9	816.
7.5- 12.5	0.033	0.002	0.002	1.00	10.5	816.
12.5- 17.5	0.030	0.002	0.002	0.0	7.0	816.
17.5- 22.5	0.000	0.0	0.0	0.0	0.0	0.
22.5- 27.5	0.176	0.011	0.011	1.02	4.4	1020.
27.5- 32.5	0.000	0.0	0.0	0.0	0.0	0.
32.5- 37.5	0.620	0.040	0.079	1.97	6.3	1133.
37.5- 42.5	0.000	0.0	0.0	0.0	0.0	0.
42.5- 47.5	0.724	0.038	0.285	7.51	19.3	1133.
47.5- 52.5	0.473	0.031	0.104	3.36	8.0	1201.
52.5- 57.5	0.000	0.0	0.0	0.0	0.0	0.
57.5- 62.5	0.000	0.0	0.0	0.0	0.0	0.
62.5- 67.5	0.000	0.0	0.0	0.0	0.0	0.
67.5- 72.5	0.000	0.0	0.0	0.0	0.0	0.
72.5- 77.5	0.034	0.002	0.014	6.98	13.2	1223.
77.5- 82.5	0.585	0.017	0.357	21.01	38.9	1223.
82.5- 87.5	0.213	0.010	0.211	21.06	38.7	1223.
87.5- 92.5	0.762	0.013	0.165	28.10	51.3	1178.
92.5- 97.5	0.551	0.013	1.049	80.72	147.8	1178.
94.5-102.5	0.643	0.011	0.655	59.53	110.3	1178.
102.5-107.5	0.470	0.010	0.140	13.95	26.3	1133.
107.5-112.5	0.000	0.0	0.0	0.0	0.0	0.
112.5-117.5	0.014	0.001	0.007	6.90	13.9	1133.
117.5-122.5	0.013	0.001	0.007	6.85	14.4	905.
122.5-127.5	0.000	0.0	0.0	0.0	0.0	0.
127.5-132.5	0.949 ^a	0.510	0.696	1.20	2.0	905.

Reprinted from (28)

Table 26. Fragmentation Data Summary for the Soviet 23-mm HEI-T Projectile Used in the ZU-23 and ZSU-23-4 Weapon Systems

POLAR ZONE (DEG)	AVERAGE OF HEAVIEST FRAGMENTS (GRAMS)	AVERAGE FRAGMENT WEIGHT (GRAMS)	TOTAL FRAGMENT WEIGHT (GRAMS)	TOTAL NUMBER OF FRAGMENTS	FRAGMENTS PER STERADIAN	INITIAL VELOCITY (M/SEC)
132.5-137.5	0.490 ^a	0.125	0.776	6.21	16.0	726.
137.5-142.5	0.191	0.012	0.030	2.46	7.0	726.
142.5-147.5	0.150	0.010	0.070	7.00	25.1	726.
147.5-152.5	0.434	0.017	0.101	5.94	21.7	480.
152.5-157.5	0.000	0.0	0.0	0.0	0.0	0.
157.5-162.5	0.201	0.013	0.013	1.00	5.3	480.
162.5-167.5	0.000	0.0	0.0	0.0	0.0	0.
167.5-172.5	0.000	0.0	0.0	0.0	0.0	0.
172.5-177.5	0.355	0.341	1.304	2.41	59.4	69.
177.5-180.0	2.791	0.181	0.181	1.00	167.2	69.

AVERAGE OF 2 RECORDS TESTED AT AA1

SCALE FACTOR EQUALS 1.077

K EQUALS 670 GRAINS PER CUBIC INCH

^aThese fragments were observed from the flash X-Ray to have an initial velocity of 69 m/sec. Other fragments in the 127.5 - 137.5° polar zones had the initial velocities presented in the above table. The scale factor (indicates a 92.9% as fired metal) weight recovery. However, the actual percent recovery (72.9) was increased by 20% to account for fragments purposely not recovered. This increase was based on the results of 20-mm projectile fragmentation tests conducted at APG, reference AG-MT-4609.

Reprinted from (28)

Table 27. Fragmentation Data Summary for the Soviet 23-mm HEI-T Projectile Used in the ZU-23 and ZSU-23-4 Weapon Systems (con't)

Appendix C. *Simulation Code*

C.1 MAIN

```
PROGRAM MAIN
DIMENSION NSET(100000)
INCLUDE '$DIR:PARAM.INC'
COMMON/SCOM1/ATRB(MATRB),DD(MEQT),DDL(MEQT),DTNOW,II,MFA,
1 MSTOP,NCLNR,NCRDR,NPRNT,NNRUN,NNSET,NTAPE,SS(MEQT),
2 SSL(MEQT),TNEXT,TNOW,XX(MMXXV)
COMMON QSET(100000)
EQUIVALENCE (NSET(1),QSET(1))
NNSET=100000
NCRDR=5
NPRNT=6
NTAPE=7
NPLOT=2
CALL SLAM
STOP
END
```

C.2 INTLC

```
SUBROUTINE INTLC
  INCLUDE '$DIR:PARAM.INC'
  COMMON/SCOM1/ATRB(MATRB),DD(MEQT),DDL(MEQT),DTNOW,II,MFA,
1  MSTOP,NCLNR,NCRDR,NPRNT,NNRUN,NNSET,NTAPE,SS(MEQT),
2  SSL(MEQT),TNEXT,TNOW,XX(MMXXV)
  COMMON/FRAGMENT/FRAGS(1000,8),NFRAGS,BURSTPT(3),DELAY
  REAL ANG, ROT, VEL, DELAY, FRAGS, BURSTPT
  CHARACTER*8 FILENAME, PROJTYPE, UPPER
  CHARACTER*12 FILE1, FILE2
  INTEGER IOERR, NFRAGS, FRAGMODL, N

  OPEN (10,FILE='SENARIO.DAT',STATUS='OLD',ERR=500,IOSTAT=IOERR)
  READ(10,'(A8)') FILENAME
  N=LEN(FILENAME)
  FILE1=FILENAME(1:N) // '.FRG'
  FILE2=FILENAME(1:N) // '.BLP'
  OPEN (4,FILE=FILE1,STATUS='NEW',ERR=500,IOSTAT=IOERR)
  OPEN (12,FILE=FILE2,STATUS='NEW',ERR=500,IOSTAT=IOERR)

  II=0
  READ(10,*) ANG, ROT, VEL, DELAY
  READ(10,23) FRAGMODL, PROJTYPE
23  FORMAT(I1,1X,A8)

  IF (FRAGMODL .EQ. 1) THEN
    CALL REGFRAGS(UPPER(PROJTYPE))
```

```

ELSE IF (FRAGMODL.EQ. 2) THEN
    CALL TSTFRAGS(UPPER(PROJTYPE))
ENDIF

CALL DYNCSHFT(VEL)
CALL ATTCK(ANG,ROT,VEL)
CALL OBJECT
CALL BLASTUP
CALL SCHDL(1,DELAY,ATRI)
C    CALL SCHDL(4,100,ATRI)
    CALL SCHDL(5,100000.0,ATRI)
RETURN
500 IF (IOERR.NE. 0) THEN
    STOP=-1
    PRINT *, 'FILES NOT OPENING PROPERLY'
ENDIF
END

```

C.3 STATE

```
SUBROUTINE STATE
INCLUDE '$DIR:PARAM.INC'
COMMON/SCOM1/ATRB(MATRB),DD(MEQT),DDL(MEQT),DTNOW,II,MFA,
1 MSTOP,NCLNR,NCRDR,NPRNT,NNRUN,NNSET,NTAPE,SS(MEQT),
2 SSL(MEQT),TNEXT,TNOW,XX(MMXXV)
COMMON/BLASTPRS/RDX,BLASTPD(36,4)
REAL RDX, BLASTPD

IF (II .EQ. 0) GO TO 400
DO 100 I=1,36
  IF (SS(I) .LE. 0.0) THEN
    DD(I)=0
  ELSE
    P=BLASTPD(I,1)
    TO=BLASTPD(I,2)
    D=BLASTPD(I,3)
    A=BLASTPD(I,4)
    T=(TNOW/1000)-TO
    DD(I)=(-P/D)*(EXP(-A*T/D))*(1+A-(T*A/D))
  ENDIF
100  CONTINUE

400  RETURN
END
```

C.4 EVENT

```
SUBROUTINE EVENT(I)
  INCLUDE '$DIR:PARAM.INC'
  COMMON/SCOM1/ATRB(MATRB),DD(MEQT),DDL(MEQT),DTNOW,II,MFA,
1  MSTOP,NCLNR,NCRDR,NPRNT,NNRUN,NNSET,NTAPE,SS(MEQT),
2  SSL(MEQT),TNEXT,TNOW,XX(MMXXV)
  COMMON/FRAGMENT/FRAGS(1000,8),NFRAGS,BURSTPT(3),DELAY
  COMMON/BLASTPRS/RDX,BLASTPD(36,4)
  REAL RADDIS, FRAGS, BURSTPT, DELAY, X, Y, V, W, RDX, BLASTPD
  INTEGER NFRAGS, N
  GO TO (1,2,3,4,5),I

1  CALL FRAGHIT
  II=1
  RETURN

2  N=ATRB(1)
  X=FRAGS(N,1)
  Y=FRAGS(N,2)
  W=FRAGS(N,6)
  V=FRAGS(N,7)
  CALL COLCT(W,2)
  CALL COLCT(V,3)
  RADDIS=SQRT(X**2 + Y**2)
  CALL COLCT(RADDIS,1)
  WRITE(4,100) X, Y, Z, W, V, RADDIS, TNOW
  RETURN
```

```

3      N=ATRI(1)
      SS(N)=BLASTPD(N,1)
      RETURN

4      CALL SCHDL(4,100.0,ATRI)
      CALL BLASTIME
      RETURN

5      STOP=-1
      RETURN

100    FORMAT(1X,F6.2,1X,F6.2,1X,F6.2,1X,F7.3,1X,F9.1,1X,F6.2,1X,F9.1)
      END

```

C.5 RECOBJ

```
SUBROUTINE RECOBJ
  INCLUDE '$DIR:PARAM.INC'
  COMMON/SCOM1/ATRB(MATRB),DD(MEQT),DDL(MEQT),DTNOW,II,MFA,
1  MSTOP,NCLNR,NCRDR,NPRNT,NNRUN,NNSET,NTAPE,SS(MEQT),
2  SSL(MEQT),TNEXT,TNOW,XX(MMXXV)
  COMMON/OBJECTS/PLN(1000,4,3),NPLN,NOBJECTS
  REAL PLN, V1(3), V2(3), X,Y,Z, X2,Y2,Z2, X1,Y1,Z1,
+   TP(100,3), P(3), TV(100,4), LEN, VECTMULT, VECTLGTH,
+   SX, SY, SZ
  INTEGER NPLN, NPTS, I, J, K, L, N, ORDR(100), NOBJECTS, IOERR
  READ(10,*,END=500,ERR=500) NPTS
  IF (NPTS .GT. 100) THEN
    WRITE(4,*) ' TO MANY POINTS'
    GO TO 500
  ENDIF
  DO 20 I=1, NPTS
    READ(10,*,END=499,ERR=500,IOSTAT=IOERR)
    TP(I,1),TP(I,2),TP(I,3)
20  CONTINUE

  I=1
  Z=NPTS
  NOBJECTS=NOBJECTS+1
30  DO 50 N=1, Z-I
    DO 40 J=1, 3
      TV(N,J)=TP(N+I,J)-TP(I,J)
```

```

40.    CONTINUE
50    CONTINUE
      DO 55 J=1,3
        V1(J)=TV(1,J)
55    CONTINUE
      LEN=VECTLGTH(V1)
      TV(1,4)=0.0
      ORDR(1)=1
      DO 60 N=2, Z-I
        DO 57 J=1, 3
          V2(J)=TV(N,J)
57    CONTINUE
          TV(N,4)=ACOS(VECTMULT(V1,V2) / (VECTLGTH(V2)*LEN)).
          ORDR(N)=N
60    CONTINUE

      N=1
70    IF (N .GE. Z-I) GO TO 75
        J=ORDR(N)
        K=ORDR(N+1)
        IF (TV(K,4) .LT. TV(J,4)) THEN
          ORDR(N)=K
          ORDR(N+1)=J
          IF (N.GT.1) N=N-1
        ELSE
          N=N+1
        ENDIF
      GO TO 70

```

```

75      CONTINUE

      DO 80 N=1, Z-I
          ORDR(N)=ORDR(N)+I
80      CONTINUE

      Z=Z-I
      J=1
100     N=J
110     J=J+1
          IF ((ORDR(J) .LT. ORDR(N)) .AND. (J .LT. Z)) GO TO 110
          IF (J-N .GT. 1) THEN
              ATRIB(1)=N
              ATRIB(2)=J
              CALL FILEM(1,ATRIB)
          ENDIF
          NPLN=NPLN+1
          DO 200 L=1, 3
              PLN(NPLN,1,L)=TP(I,L)
200     CONTINUE
              DO 210 L=1, 3
                  PLN(NPLN,2,L)=TP(ORDR(N),L)
210     CONTINUE
              DO 220 L=1, 3
                  PLN(NPLN,3,L)=TP(ORDR(J),L)
220     CONTINUE
              PLN(NPLN,4,1)=NOBJECTS
              IF (J .LT. Z) GO TO 100

```

```

      IF (NNQ(1).EQ. 0) GO TO 400
      CALL RMOVE(1,1,ATLIB)
      I=ATLIB(1)
      Z=ATLIB(2)
      GO TO 30
400   RETURN
499   WRITE(4,*) 'ENCOUNTERED END OF FILE BEFORE EXPECTED'
500   IF (IOERR .NE. 0) THEN
         STOP=-1
         WRITE(4,*) 'ERROR IN THE OBJECT COORDINATE DATA'
      ENDIF
      END

```

C.6 DYNCSHFT

```
SUBROUTINE DYNCSHFT(PVEL)
COMMON/FRAGMENT/FRAGS(1000,8),NFRAGS,BURSTPT(3),DELAY
REAL FRAGS, PVEL, SVEL, DVEL, SA, DA, BURSTPT, DELAY
INTEGER NFRAGS, I
DO 10 I=1, NFRAGS
    SA=FRAGS(I,4)
    SVEL=FRAGS(I,7)
    DVEL=SQRT((PVEL**2)+(SVEL**2)+2*SVEL*PVEL*COS(SA))
    DA=ASIN( (SVEL*SIN(SA))/DVEL )
    FRAGS(I,4)=DA
    FRAGS(I,7)=DVEL
10  CONTINUE
END
```

C.7 OBJECT

```
      SUBROUTINE OBJECT
      COMMON/OBJECTS/PLN(1000,4,3),NPLN,NOBJECTS
      REAL PLN
      INTEGER NPLN, NOBJECTS
      CHARACTER*1 TYPE, UPPER
      NPLN=0
      NOBJECTS=0
10     READ(10,'(A1)',END=500,ERR=999) TYPE
      IF (UPPER(TYPE) .EQ. 'R') THEN
          CALL RECOBJ
          GO TO 10
      ENDIF

500    RETURN
999    PRINT *, 'ERROR IN INPUT OBJECTS'
      STOP=-1
      END
```

C.8 OBJHIT

```
INTEGER FUNCTION OBJHIT(HIT,XC,YC,ZC)
  REAL HIT(3), XC(3), YC(3), ZC(3), VECTMULT, VECTLGTH,
+ V1(3), V2(3), V3(3), A1, A2, A3

  V1(1)=XC(1)-HIT(1)
  V1(2)=YC(1)-HIT(2)
  V1(3)=ZC(1)-HIT(3)
  V2(1)=XC(2)-HIT(1)
  V2(2)=YC(2)-HIT(2)
  V2(3)=ZC(2)-HIT(3)
  V3(1)=XC(3)-HIT(1)
  V3(2)=YC(3)-HIT(2)
  V3(3)=ZC(3)-HIT(3)

  A1=ACOS( VECTMULT(V1,V2) / (VECTLGTH(V1)*VECTLGTH(V2)))
  A2=ACOS( VECTMULT(V2,V3) / (VECTLGTH(V2)*VECTLGTH(V3)))
  A3=ACOS( VECTMULT(V1,V3) / (VECTLGTH(V1)*VECTLGTH(V3)))

  IF ((A1+A2+A3) .GT. 6.274) THEN
    OBJHIT=1
  ELSE
    OBJHIT=0
  ENDIF
END
```

C.9 ELINE

```
SUBROUTINE ELINE(PT1,PT2,L1,L2,L3)
REAL PT1(3), PT2(3), L1(4), L2(4), L3(4), DX, DY, DZ
DX= PT2(1) - PT1(1)
DY= PT2(2) - PT1(2)
DZ= PT2(3) - PT1(3)
L1(1)=DY
L1(2)=-DX
L1(3)=0.0
L1(4)=PT1(1)*DY - PT1(2)*DX
L2(1)=0.0
L2(2)=DZ
L2(3)=-DY
L2(4)=PT1(2)*DZ - PT1(3)*DY
L3(1)=DZ
L3(2)=0.0
L3(3)=-DX
L3(4)=PT1(1)*DZ - PT1(3)*DX
RETURN
END
```

C.10 ROWSWAP

```
      SUBROUTINE ROWSWAP(L1,L2)
      REAL L1(4), L2(4), T(4)
      INTEGER I

      DO 10 I=1,4
          T(I)=L1(I)
          L1(I)=L2(I)
          L2(I)=T(I)
10      CONTINUE
      END
```

C.11 INTERSCT

```
SUBROUTINE INTERSCT(PC,L1,L2,HIT)
REAL PC(4), L1(4), L2(4), HIT(3), C

IF (PC(1) .EQ. 0.0) THEN
  IF (L1(1) .NE. 0.0) THEN
    CALL ROWSWAP(PC,L1)
  ELSE
    CALL ROWSWAP(PC,L2)
  ENDIF
ENDIF

C=1/PC(1)
DO 50 I=1,4
  PC(I)=C*PC(I)
50  CONTINUE
C=L1(1)
DO 80 I=1,4
  L1(I)=L1(I)-C*PC(I)
80  CONTINUE
C=L2(1)
DO 100 I=1,4
  L2(I)=L2(I)-C*PC(I)
100 CONTINUE

IF (L1(2) .EQ. 0.0) CALL ROWSWAP(L1,L2)
C=1/L1(2)
```

```

DO 150 I=1,4
    L1(I)=C*L1(I)
150  CONTINUE
    C=L2(2)
    DO 180 I=1,4
        L2(I)=L2(I)-C*L1(I)
180  CONTINUE
    C=PC(2)
    DO 200 I=1,4
        PC(I)=PC(I)-C*L1(I)
200  CONTINUE

```

```

    C=1/L2(3)
    DO 250 I=1,4
        L2(I)=C*L2(I)
250  CONTINUE
    C=PC(3)
    DO 280 I=1,4
        PC(I)=PC(I)-C*L2(I)
280  CONTINUE
    C=L1(3)
    DO 300 I=1,4
        L1(I)=L1(I)-C*L2(I)
300  CONTINUE

```

```

HIT(1)=PC(4)
HIT(2)=L1(4)
HIT(3)=L2(4)

```

1000 END

C.12 ATTCK

```
SUBROUTINE ATTCK(ANG,ROT,VEL)
COMMON/FRAGMENT/FRAGS(1000,8),NFRAGS,BURSTPT(3),DELAY
REAL FRAGS, ANG, ROT, VEL, SSA, CSA, SSR, CSR, SAA, CAA, SAR,
+   CAR, NZ, NX, NA, NR, RADIUS, BURSTPT, DELAY, DIST
INTEGER NFRAGS, I
SAA=SIN(ANG)
CAA=COS(ANG)
SAR=SIN(ROT)
CAR=COS(ROT)

DIST=VEL*(DELAY/1000000)*12.0
BURSTPT(3)=DIST*CAA
RADIUS=DIST*SAA
BURSTPT(1)=RADIUS*CAR
BURSTPT(2)=RADIUS*SAR
DO 100 I=1, NFRAGS
    SSA=SIN(FRAGS(I,4))
    CSA=COS(FRAGS(I,4))
    SSR=SIN(FRAGS(I,5))
    CSR=COS(FRAGS(I,5))
    NZ=-SAA*SSA*CSR+CAA*CSA
    NX=CSR*SSA*CAR*CAA-SSR*SSA*SAR-CSA*CAR*SAA
    NA=ACOS(NZ)
    NR=ACOS( NX / SIN(NA) )
    FRAGS(I,4)=NA
    FRAGS(I,5)=NR
```

IF (NZ .LE. 0.0) FRAGS(I,8)=0.0
100 CONTINUE
END

C.13 EPLANE

```
SUBROUTINE EPLANE(X,Y,Z,PC)
REAL X(3), Y(3), Z(3), PC(4), E1, E2, E3

DO 10 I=1,3
    PC(I)=0.0
10 CONTINUE
IF ((X(1).EQ.X(2)).AND.(X(2).EQ.X(3))) THEN
    PC(1)=0.0
    PC(4)=X(1)
    GO TO 500
ENDIF
IF ((Y(1) .EQ. Y(2)) .AND. (Y(2) .EQ. Y(3))) THEN
    PC(2)=1.0
    PC(4)=Y(1)
    GO TO 500
ENDIF
IF ((Z(1) .EQ. Z(2)) .AND. (Z(2) .EQ. Z(3))) THEN
    PC(3)=1.0
    PC(4)=Z(1)
    GO TO 500
ENDIF
PC(1)= (Y(1)*(Z(2)-Z(3)) + Y(2)*(Z(3)-Z(1)) + Y(3)*(Z(1)-Z(2)))
PC(2)= (X(1)*(Z(3)-Z(2)) + X(2)*(Z(1)-Z(3)) + X(3)*(Z(2)-Z(1)))
PC(3)= (X(1)*(Y(2)-Y(3)) + X(2)*(Y(3)-Y(1)) + X(3)*(Y(1)-Y(2)))
E1= X(1)*(Y(3)*Z(2)-Y(2)*Z(3))
E2= X(2)*(Y(1)*Z(3)-Y(3)*Z(1))
```

E3= X(3)*(Y(2)*Z(1)-Y(1)*Z(2))

PC(4)=E1+E2+E3

500

RETURN

END

C.14 VECTLGTH

```
REAL FUNCTION VECTLGTH(VC)
REAL VC(3)
VECTLGTH=SQRT(VC(1)**2+VC(2)**2+VC(3)**2)
END
```

```
REAL FUNCTION VECTMULT(V1,V2)
REAL V1(3), V2(3)
VECTMULT=(V1(1)*V2(1) + V1(2)*V2(2) + V1(3)*V2(3))
END
```

C.15 UPPER

CHARACTER*(*) FUNCTION UPPER(INSTRG)

CHARACTER*(*) INSTRG

CHARACTER*1 CH

CHARACTER*255 OUTSTR

INTEGER POS, ICH, SHIFT

INTRINSIC CHAR, ICHAR, LEN, LGE, LLE

SHIFT = ICHAR('A') - ICHAR('a')

DO 10 POS = 1, LEN(INSTRG)

CH = INSTRG(POS:POS)

ICH = ICHAR(CH)

IF (LGE(CH, 'a') .AND. LLE(CH, 'z'))

+ CH = CHAR(ICH + SHIFT)

IF (POS .EQ. 1) THEN

UPPER = CH

ELSE

OUTSTR = UPPER

UPPER = OUTSTR(1:POS-1) // CH

ENDIF

10 CONTINUE

RETURN

END

C.16 DET

```
REAL FUNCTION DET(L1,L2,L3)
REAL L1(4), L2(4), L3(4), P1, P2
P1=L1(1)*L2(2)*L3(3)+L1(2)*L2(3)*L3(1)+L1(3)*L2(1)*L3(2)
P2=L1(3)*L2(2)*L3(1)+L1(1)*L2(3)*L3(2)+L1(2)*L2(1)*L3(3)
DET=P1-P2
RETURN
END
```

C.17 FRAGHIT

```
SUBROUTINE FRAGHIT
  INCLUDE '$DIR:PARAM.INC'
  COMMON/SCOM1/ATRB(MATRB),DD(MEQT),DDL(MEQT),DTNOW,II,MFA,
1  MSTOP,NCLNR,NCRDR,NPRNT,NNRUN,NNSET,NTAPE,SS(MEQT),
2  SSL(MEQT),TNEXT,TNOW,XX(MMXXV)
  COMMON/FRAGMENT/FRAGS(1000,8),NFRAGS,BURSTPT(3),DELAY
  COMMON/OBJECTS/PLN(1000,4,3),NPLN,NOBJECTS
  REAL FRAGS, BURSTPT, PLN, XC(3), YC(3), ZC(3), PC(4), V(3), DEF,
+   L1(4), L2(4), L3(4), X, Y, Z, MINLEN, HIT(3), TIME,
DELAY
+   VECTLGTH
  INTEGER NFRAGS, NPLN, NOBJECTS, I, N, J, IND, OBJHIT, GG

  DO 1000 I=1, NFRAGS
    IF ( FRAGS(I,8) .EQ. 0.0 ) GO TO 1000
    V(3)=10*COS(FRAGS(I,4))
    V(1)=10*COS(FRAGS(I,5))*SIN(FRAGS(I,4))
    V(2)=10*SIN(FRAGS(I,5))*SIN(FRAGS(I,4))
    DO 50 N=1, 3
      V(N)=V(N)+BURSTPT(N)
50  CONTINUE
    CALL ELINE(BURSTPT,V,L1,L2,L3)
    DO 500 N=1, NPLN
      DO 100 J=1,3
        XC(J)=PLN(N,J,1)
        YC(J)=PLN(N,J,2)
```

```

        ZC(J)=PLN(N,J,3)
100    CONTINUE
        CALL EPLANE(XC,YC,ZC,PC)
        IF (DET(PC,L1,L2) .NE. 0.0) THEN
            CALL INTERSCT(PC,L1,L2,HIT)
        ELSE IF (DET(PC,L1,L3) .NE. 0.0) THEN
            CALL INTERSCT(PC,L1,L3,HIT)
        ELSE IF (DET(PC,L2,L3) .NE. 0.0) THEN
            CALL INTERSCT(PC,L2,L3,HIT)
        ELSE
            FRAGS(I,8)=0.0
            GO TO 500
        ENDIF
        IND=OBJHIT(HIT,XC,YC,ZC)
        IF (IND .EQ. 0) GO TO 500
        DO 200 K=1, 3
            V(K)= HIT(K) - BURSTPT(K)
            ATRIB(K+2)=HIT(K)
200    CONTINUE
            ATRIB(1)=VECTLGTH(V)
            ATRIB(2)=PLN(NPLN,4,1)
            CALL FILEM(1,ATRIB)
500    CONTINUE

        IF (NNQ(1) .GT. 0) THEN
            CALL RMOVE(1,1,ATRIB)
            MINLEN=ATRIB(1)
            FRAGS(I,8)=ATRIB(2)

```

```

DO 550 K=1,3
    FRAGS(I,K)=ATRI(K+2)
550  CONTINUE
600  IF (NNQ(1) .GT. 0) THEN
    CALL RMOVE(1,1,ATRI)
    IF (MINLEN .GT. ATRI(1)) THEN
    MINLEN=ATRI(1)
    FRAGS(I,8)=ATRI(2)
    DO 650 K=1,3
        FRAGS(I,K)=ATRI(K+2)
650  CONTINUE
    ENDIF
    GO TO 600
    ENDIF
    ATRI(1)=I
    TIME= (MINLEN*1000000.0) / (12.0*FRAGS(I,7))
    CALL SCHDL(2,TIME,ATRI)
    ENDIF
1000 CONTINUE
    END

```

C.18 BLASTUP

```
SUBROUTINE BLASTUP
INCLUDE '$DIR:PARAM.INC'
COMMON/SCOM1/ATRIB(MATRB),DD(MEQT),DDL(MEQT),DTNOW,II,MFA,
1 MSTOP,NCLNR,NCRDR,NPRNT,NNRUN,NNSET,NTAPE,SS(MEQT),
2 SSL(MEQT),TNEXT,TNOW,XX(MMXXV)
COMMON/BLASTPRS/RDX,BLASTPD(36,4)
INTEGER I,J,K
REAL RDX, TABLEXI(47,5), SCALING, BLASTPD
+   D, W, V1(3), V2(3), V(3), SI
INTRINSIC MOD
DATA ( (TABLEXI(I,J),J=1,5),I=1,47)
```

/ 5.0,	192.0,	0.28,	2.5,	10.0,
+ 10.0,	76.0,	0.60,	1.5,	7.5,
+ 15.0,	35.0,	1.29,	0.6,	6.0,
+ 20.0,	21.0,	2.22,	1.9,	5.0,
+ 25.0,	14.0,	3.34,	5.6,	4.5,
+ 30.0,	9.3,	4.70,	6.0,	3.5,
+ 35.0,	6.8,	6.20,	6.5,	2.8,
+ 40.0,	4.9,	8.10,	7.4,	2.3,
+ 45.0,	3.6,	10.1,	8.3,	1.7,
+ 50.0,	2.7,	12.3,	9.3,	1.5,
+ 55.0,	2.1,	14.7,	10.2,	1.2,
+ 60.0,	1.65,	17.3,	11.1,	1.1,
+ 65.0,	1.32,	20.1,	12.0,	1.0,
+ 70.0,	1.10,	23.2,	12.9,	0.9,
+ 75.0,	0.95,	26.6,	13.8,	0.9,
+ 80.0,	0.85,	29.9,	14.6,	0.9,
+ 85.0,	0.73,	33.3,	15.3,	0.9,
+ 90.0,	0.68,	36.8,	16.0,	0.9,
+ 95.0,	0.62,	40.3,	16.7,	0.9,
+ 100.0,	0.57,	43.9,	17.3,	0.9,
+ 105.0,	0.52,	47.6,	17.9,	0.9,
+ 110.0,	0.48,	51.3,	18.4,	0.9,
+ 115.0,	0.44,	55.1,	18.7,	0.9,
+ 120.0,	0.41,	58.9,	19.0,	0.9,

+ 125.0,	0.38,	62.8,	19.3,	1.0,
+ 130.0,	0.35,	66.7,	19.6,	1.0,
+ 135.0,	0.33,	70.6,	19.8,	1.0,
+ 140.0,	0.31,	74.5,	20.1,	1.0,
+ 145.0,	0.292,	78.4,	20.4,	1.0,
+ 150.0,	0.276,	82.3,	20.6,	1.0,
+ 155.0,	0.262,	86.3,	20.9,	1.0,
+ 160.0,	0.250,	90.3,	21.2,	1.0,
+ 165.0,	0.238,	94.3,	21.5,	1.1,
+ 170.0,	0.227,	98.3,	21.8,	1.1,
+ 175.0,	0.217,	102.4,	22.0,	1.1,
+ 180.0,	0.208,	107.0,	22.3,	1.1,
+ 185.0,	0.200,	111.0,	22.6,	1.1,
+ 190.0,	0.193,	115.0,	22.9,	1.1,
+ 195.0,	0.186,	119.0,	23.2,	1.1,
+ 200.0,	0.181,	123.0,	23.4,	1.1,
+ 205.0,	0.174,	127.0,	23.6,	1.1,
+ 210.0,	0.168,	131.0,	23.8,	1.2,
+ 215.0,	0.162,	135.0,	23.9,	1.2,
+ 220.0,	0.156,	138.0,	24.1,	1.2,
+ 225.0,	0.151,	144.0,	24.2,	1.2,
+ 230.0,	0.146,	148.0,	24.3,	1.2,
+ 235.0,	1.141,	152.0,	24.4,	1.2 /

W=RD_X*1.62/453.59

SCALING=(2000.0/W)**(1.0/3.0)

DO 100 I=1,36

```

SS(I)=0.0
D=SCALING*I/12
J=INT(D/5)
SI=MOD(D,5.0)/5.0
IF (J .EQ. 0) THEN
    DO 10 K=1,5
        V1(K)=TABLEXI(1,K)
        V2(K)=TABLEXI(1,K)
10    CONTINUE
    ELSE IF (J .GE. 47) THEN
        DO 20 K=1,5
            V1(K)=TABLEXI(47,K)
            V2(K)=TABLEXI(47,K)
20    CONTINUE
    ELSE
        DO 30 K=1,5
            V1(K)=TABLEXI(J,K)
            V2(K)=TABLEXI(J+1,K)
30    CONTINUE
    ENDIF
    DO 40 K=1,5
        V(K)= (V1(K)*(1-SI)+V2(K)*SI)
40    CONTINUE
    BLASTPD(I,1)= V(2)*14.7
    BLASTPD(I,2)= V(3)/SCALING
    BLASTPD(I,3)= V(4)/SCALING
    BLASTPD(I,4)= V(5)
    ATRIB(1)=I

```

```
TIME=BLASTPD(I,2)*1000  
CALL SCHDL(3,TIME,ATRIE)  
100 CONTINUE  
RETURN  
END
```

C.19 BLASTIME

```
SUBROUTINE BLASTIME
  INCLUDE '$DIR:PARAM.INC'
  COMMON/SCOM1/ATRB(MATRB),DD(MEQT),DDL(MEQT),DTNOW,II,MFA,
1  MSTOP,NCLNR,NCRDR,NPRNT,NNRUN,NNSET,NTAPE,SS(MEQT),
2  SSL(MEQT),TNEXT,TNOW,XX(MMXXV)
  INTEGER I
  REAL V(36)

  DO 100 I=1,36
    V(I)=SS(I)
100  CONTINUE

  WRITE(12,*) V
  RETURN
END
```

C.20 TSTFRAGS

```
SUBROUTINE TSTFRAGS(FILE)
COMMON/FRAGMENT/FRAGS(1000,8),NFRAGS,BURSTPT(3),DELAY
COMMON/BLASTPRS/RDX,BLASTPD(36,4)
INTEGER NZONES, ZONE, NFRAG, NFRAGS, I, IOERR
REAL FRGMTTN(50,6), FRAGS, ZONEL, ZONEH, MWEIGHT, RDX,
+ SDWEIGHT, MVEL, SDVEL, BURSTPT, DELAY, BLASTPD, SD
CHARACTER*8 FILE

OPEN(11,FILE='FILE',STATUS='OLD',ERR=500,IOSTAT=IOERR)
READ(11,*) NZONES, RDX

ZONEH=0.0
R=3.141592654/180
I=0
DO 100 ZONE=1,NZONES
  ZONEL=ZONEH
  READ(11,*) ZONEH, NFRAGS, MWEIGHT, SDWEIGHT, MVEL, SDVEL
  IF ((FRGMTTN(ZONE,2) .EQ. 0.0) .OR. (FRGMTTN(ZONE,3) .EQ. 0.0))
+   GO TO 100
  ZONEL=FRGMTTN(ZONE,1)*R
  ZONEH=ZONEL+(5.0*R)
  IF ((ZONE .EQ. 1) .OR. (ZONE .EQ. 37))
+   ZONEH=ZONEH-(2.5*R)
  MWEIGHT=FRGMTTN(ZONE,3)
  SDWEIGHT=FRGMTTN(ZONE,4)
  MVEL=FRGMTTN(ZONE,5)
```

```

SDVEL=FRGMTTN(ZONE,6)
NFRAG= NPSSN(FRGMTTN(ZONE,2),1)
IF (NFRAG .EQ. 0) GO TO 100
DO 80 N=1,NFRAG
    I=I+1
    IF (I .GT. 1000) GO TO 200
    FRAGS(I,4)=UNFRM(ZONEL,ZONEH,2)
    FRAGS(I,5)=UNFRM(0.0,6.2831853,3)
50    FRAGS(I,6)=RNORM(MWEIGHT,SDWEIGHT,4)
        IF (FRAGS(I,6) .LE. 0.0) GO TO 50
        SD= (FRAGS(I,6)-MWEIGHT)/SDWEIGHT
        FRAGS(I,7)=MVEL-SD*SDVEL
        FRAGS(I,8)=-1.0
80    CONTINUE
100   CONTINUE
        NFRAGS=I
        CLOSE(11)
        RETURN

200   WRITE(4,*) 'INCREASE ALLOWABLE FRAGS ; EXCEEDED 1000'
500   IF (IOERR .EQ. 0) THEN
        WRITE(4,*) 'ERROR READING THE FRAGMENTATION FILE'
    ENDIF
    STOP=-1
    END

```

C.21 REGFRAGS

```
SUBROUTINE REGFRAGS(FILE)
COMMON/FRAGMENT/FRAGS(1000,8),NFRAGS,BURSTPT(3),DELAY
COMMON/BLASTPRS/RDX,BLASTPD(36,4)
INTEGER NZONES, ZONE, NFRAG, NFRAGS, I, IOERR
REAL FRGMTTN(50,6), FRAGS, ZONEL, ZONEH, MWEIGHT, RDX,
+ SDWEIGHT, MVEL, SDVEL, BURSTPT, DELAY, BLASTPD, SD
CHARACTER*8 FILE
CHARACTER*12 FILENAME

FILENAME= FILE // '.DAT'
OPEN(11,FILE='FILENAME',STATUS='OLD',ERR=500,IOSTAT=IOERR)
READ(11,*) NZONES, RDX
ZONEH=0.0
R=3.141592654/180
I=0
DO 100 ZONE=1,NZONES
  ZONEL=ZONEH
  READ(11,*) ZONEH, NFRAGS, MWEIGHT, SDWEIGHT, MVEL, SDVEL
  IF ((FRGMTTN(ZONE,2) .EQ. 0.0) .OR. (FRGMTTN(ZONE,3) .EQ. 0.0))
+   GO TO 100
  ZONEL=FRGMTTN(ZONE,1)*R
  ZONEH=ZONEL+(5.0*R)
  IF ((ZONE .EQ. 1) .OR. (ZONE .EQ. 37))
+   ZONEH=ZONEH-(2.5*R)
  MWEIGHT=FRGMTTN(ZONE,3)
  SDWEIGHT=FRGMTTN(ZONE,4)
```

```

MVEL=FRGMTTN(ZONE,5)
SDVEL=FRGMTTN(ZONE,6)
NFRAG= NPSSN(FRGMTTN(ZONE,2),1)
IF (NFRAG .EQ. 0) GO TO 100
DO 80 N=1,NFRAG
I=I+1
IF (I .GT. 1000) GO TO 200
FRAGS(I,4)=UNFRM(ZONEL,ZONEH,2)
FRAGS(I,5)=UNFRM(0.0,6.2831853,3)
50  FRAGS(I,6)=RNORM(MWEIGHT,SDWEIGHT,4)
      IF (FRAGS(I,6) .LE. 0.0) GO TO 50
60  FRAGS(I,7)=RNORM(MVEL,SDVEL,5)
      IF (FRAGS(I,7) .LE. 0.0) GO TO 60
FRAGS(I,8)=-1.0
80  CONTINUE
100 CONTINUE
NFRAGS=I
CLOSE(11)
RETURN

200  WRITE(4,*) 'INCREASE ALLOWABLE FRAGS ; EXCEEDED 1000'
500  IF (IOERR .NE. 0) THEN
      WRITE(4,*) 'ERROR READING THE FRAGMENTATION FILE'
ENDIF
STOP=-1
END

```

Bibliography

1. Anderson, Charles L. *Test and Evaluation of Halon 1301 and Nitrogen Inerting Against 23mm HEI Projectiles*. Technical Report AFFDL-TR-78-66, Air Force Flight Dynamics Laboratory, 1978.
2. Avery, John G. and others. *Survivable Composite Structure for Combat Aircraft*. Technical Report AFFDL-TR-79-3132, Air Force Flight Dynamics Laboratory, 1979.
3. Ballistic Research Laboratory. *The GIFT Code User Manual, Volume I, Introduction and Input Requirements* (Brl report no. 1802 Edition), July 1975. DTIC:AD B006 037L.
4. Bennet, Mike, "Staff Analyst, WL/FIVS," 1991. Personal Interviews.
5. Bless, Stephen J. and Antonios Challita. *Ballistic Analysis of Generic Aircraft Components*. Technical Report ASD-TR-80-5052, Aeronautical Systems Division, 1981.
6. Bruenning, Leonard E. Jr. and Alyndia S. Womble. *High - Explosive Incendiary Vulnerability Assessment Model (HEIVAM)*. Technical Report AFATL-TR-86-38, AF Armament Laboratory, 1985.
7. Coulter, George A. and others. *Blast Loading on Above Ground Barricaded Munition Storage Magazines - II*. Technical Report BRL-TR-2694, US Army Materiel Command, 1985.
8. Crawford, Angela. "Simulation of an Aircraft Dry Bay Fuel Fire Caused by a 23-mm High Energy Incendiary Explosive." This thesis effort is currently underway.
9. Cudney, Donald E. *CONVERT (Program 7054) Users' Manual*. Technical Report AFATL-TR-79-46, Air Force Armament Laboratory, 1979.
10. Cudney, Donald E. *CONVERT (Program 7058) User Manual*. Technical Report AFATL-TR-79-45, Air Force Armament Laboratory, 1979.
11. Gilbert, Lillard E. *Surface-to-Air Missile Warhead Fragment Velocity Data Collection Systems Design and Analysis Techniques*. Technical Report AFFDL-TR-79-3056, Air Force Flight Dynamics Laboratory, 1979.
12. Gilbert, Lillard E. *Warhead Fragment Velocity Prediction Model Evaluation*. Technical Report AFWAL-TR-81-3172, Air Force Wright Aeronautical Laboratories, 1982.
13. Gilbert, Lillard E. *Dynamic Warhead Fragment Threat Model Validation*. Technical Report AFWAL-TR-83-3047, Air Force Wright Aeronautical Laboratories, 1983.

14. Gilbert, Lillard E. *Soviet 30mm 155 High Explosive Incendiary Projectile Fragment Threat Performance Model*. Technical Report AFWAL-TR-85-3028, Air Force Flight Dynamics Laboratory, 1985.
15. Gilbert, Lillard E. and Timothy Seymour. "30mm HEI Test Notes." This information was gathered during the 30mm HEI characterization.
16. Gilbert, Lillard E. and Timothy Seymour. *Soviet 30mm 155 High Explosive Incendiary Projectile Fragment Threat Performance Model*. Technical Report AFWAL-TR-85-3028, AFWAL/FIES, 1985.
17. Heinonen, Everett W. and others. *Fire/Explosion Protection Characterization and Optimization Phase II: Alternative Dry Bay Fire Suppression Agent Screening*. Report JTCG/AS-90-T-003, Wright Research and Development Center, 1990.
18. Joint Technical Coordinating Group for Munitions Effectiveness. *Shot Generator Computer Program, Volume I. User Manual and Volume II. Analyst Manual* (61jtcg/me-71-5-1 and -2 Edition), July 1970.
19. Joint Technical Coordinating Group for Munitions Effectiveness (Anti-Air). *Penetration Equations Handbook for Kinetic-Energy Penetrators* (61jtcg/me-77-16 Edition), November 1977. Change 1, dated August 1984.
20. Jones, Steven R., Capt. *Fragmentation and Air Blast Tests of Experimental 20-mm and 25-mm High Explosive Incendiary (HEI) Projectiles*. Technical Report ADTC-TR-76-46-Vol-1, Air Force Armament Laboratory, 1976.
21. JTCG/ME. *COVART II - A Simulation Program for Computation of Vulnerability Areas and Repair Times*. User Manual 61 JTCG/ME-84-3, Joint Technical Coordinating Group for Munitions Effectiveness, 1984.
22. Kingery, Charles N. and Gerald Bulmash. *Effect of Shock Tube Blockage on Target Loading*. Technical Report BRL-TR-2689, US Army Materiel Command, 1985.
23. Kingery, Charles N. and others. *Blast Parameters From Explosions in Model Earth Covered Magazines*. Memorandum Report BRL-MR-2680, USA Ballistic Research Laboratories, 1976.
24. Kinney, Gilbert Ford. *Explosive Shock in Air* (1st ed. Edition). The MacMillan Company, 1962.
25. McArdle, Kevin T. *The Accuracy of Presented Area Measurements Implicit in Computerized Vulnerability Analyses*. Technical Report AFATL-TR-86-101, Air Force Armament Laboratory, 1987.
26. Page, Henry E. and others. *Point Burst Ray Generator (PGEN) Computer Program, Volume I Users Manual and Volume II Analyst Manual*. Technical Report AFATL-TR-82-64, Air Force Armament Laboratory, 1982.

27. Program, Joint Live Fire Test, "Joint Live Fire Test Program Aircraft Systems Fiscal 1986." Video Presentation of HEI Fuel Fire Test Results.
28. Reeves, Harry J. *Terminal Ballistic Characteristics of Soviet 23mm HEI Projectiles*. Technical Report BRL-MR-2681, USA Ballistic Research Laboratories, 1976. DTIC:AD-C008-171.
29. Rieder, William, "IG Safety Inspector," 1989-1991. Personal Interviews.
30. Schmeling, William A. *HEI Projectile Penetration and Ricochet Model*. Technical Report AFATL-TR-83-82, Air Force Armament Laboratory, 1983.
31. Taylor, Sir Geoffrey F.R.S. "The Formulation of a Blast Wave by a Very Intense Explosion," *unknown*, 201:159-186 (22 March 1950).
32. Weeding, Gale S. *Ballistic Limit Velocities for GAU-8 Against RHA and Aluminum Targets*. Technical Report AFATL-TR-85-71, Air Force Armament Laboratory, 1986.

REPORT DOCUMENTATION PAGE

Form Approved
OMB No. 0704-0188

Public reporting burden for this collection of information is estimated to average 1 hour per response, including the time for reviewing instructions, searching existing data sources, gathering and maintaining the data needed, and completing and reviewing the collection of information. Send comments regarding this burden estimate or any other aspect of this collection of information, including suggestions for reducing this burden, to Washington Headquarters Services, Directorate for Information Operations and Reports, 1215 Jefferson Davis Highway, Suite 1204, Arlington, VA 22202-4302, and to the Office of Management and Budget, Paperwork Reduction Project (0704-0188), Washington, DC 20503.

1. AGENCY USE ONLY (Leave blank)	2. REPORT DATE March 1992	3. REPORT TYPE AND DATES COVERED Master's Thesis	
4. TITLE AND SUBTITLE MODULAR SIMULATION OF HEI FRAGMENTATION AND BLAST PRESSURE		5. FUNDING NUMBERS	
6. AUTHOR(S) Gordon L. Galloway, Captain, USAF			
7. PERFORMING ORGANIZATION NAME(S) AND ADDRESS(ES) Air Force Instituted of Technology, WPAFB OH 45433-6583		8. PERFORMING ORGANIZATION REPORT NUMBER AFIT/GOR/ENS/92M-11	
9. SPONSORING/MONITORING AGENCY NAME(S) AND ADDRESS(ES)		10. SPONSORING/MONITORING AGENCY REPORT NUMBER	
11. SUPPLEMENTARY NOTES			
12a. DISTRIBUTION/AVAILABILITY STATEMENT Approved for public release; distribution unlimited.		12b. DISTRIBUTION CODE	
13. ABSTRACT (Maximum 200 words) The fragmentation and blast pressure of High Explosive Incendiary projectiles are major causes of aircraft fuel fires. Because Halon 1301 is being banned from DoD use as a fire suppressant, alternative fire suppressants must be developed and tested. These new suppressants must counteract the fire directly or eliminate one or more of the factors which cause the fire. To this end, this thesis takes a detailed look at the HEI processes that lead to a fire. A comprehensive review of the current knowledge and understanding of these processes is presented. In addition, hypothesized dependencies between the various processes are stated. These hypothesized dependencies can not be proved or disproved with data at this time. Therefore, tests and test set-ups are outlined to collect the necessary data. The evidence in support of these dependencies is also presented. To aid the testing of various fire suppressant systems and the hypothesized HEI explosion dependencies a simulation of the HEI explosion was developed. This simulation allows the user to simulate any configuration of the aircraft dry bay, and any attack scenario for the projectile. Using this simulation, one of the hypothesized dependencies was tested and shown to be possible.			
14. SUBJECT TERMS High Explosive Projectiles, Pressure Signature, Projectile Fragments, Simulation, Surface Analysis, Pressure Pressure Gradient, Projectile Cases, Pressure Distribution		15. NUMBER OF PAGES 255	
		16. PRICE CODE	
17. SECURITY CLASSIFICATION OF REPORT Unclassified	18. SECURITY CLASSIFICATION OF THIS PAGE Unclassified	19. SECURITY CLASSIFICATION OF ABSTRACT Unclassified	20. LIMITATION OF ABSTRACT UL

GENERAL INSTRUCTIONS FOR COMPLETING SF 298

The Report Documentation Page (RDP) is used in announcing and cataloging reports. It is important that this information be consistent with the rest of the report, particularly the cover and title page. Instructions for filling in each block of the form follow. It is important to *stay within the lines* to meet *optical scanning requirements*.

Block 1. Agency Use Only (Leave blank)

Block 2. Report Date Full publication date including day, month, and year, if available (e.g. 1 Jan 88). Must cite at least the year.

Block 3. Type of Report and Dates Covered State whether report is interim, final, etc. If applicable, enter inclusive report dates (e.g. 10 Jun 87 - 30 Jun 88).

Block 4. Title and Subtitle A title is taken from the part of the report that provides the most meaningful and complete information. When a report is prepared in more than one volume, repeat the primary title, add volume number, and include subtitle for the specific volume. On classified documents enter the title classification in parentheses.

Block 5. Funding Numbers To include contract and grant numbers; may include program element number(s), project number(s), task number(s), and work unit number(s). Use the following labels:

C - Contract	PR - Project
G - Grant	TA - Task
PE - Program Element	WU - Work Unit Accession No.

Block 6. Author(s) Name(s) of person(s) responsible for writing the report, performing the research, or credited with the content of the report. If editor or compiler, this should follow the name(s).

Block 7. Performing Organization Name(s) and Address(es) Self-explanatory

Block 8. Performing Organization Report Number Enter the unique alphanumeric report number(s) assigned by the organization performing the report.

Block 9. Sponsoring/Monitoring Agency Name(s) and Address(es) Self-explanatory

Block 10. Sponsoring/Monitoring Agency Report Number. (If known)

Block 11. Supplementary Notes Enter information not included elsewhere such as: Prepared in cooperation with...; Trans. of...; To be published in... When a report is revised, include a statement whether the new report supersedes or supplements the older report.

Block 12a. Distribution/Availability Statement Denotes public availability or limitations. Cite any availability to the public. Enter additional limitations or special markings in all capitals (e.g. NOFORN, REL, ITAR).

DOD - See DoDD 5230.24, "Distribution Statements on Technical Documents."

DOE - See authorities.

NASA - See Handbook NHB 2200.2.

NTIS - Leave blank.

Block 12b. Distribution Code

DOD - Leave blank.

DOE - Enter DOE distribution categories from the Standard Distribution for Unclassified Scientific and Technical Reports.

NASA - Leave blank.

NTIS - Leave blank.

Block 13. Abstract Include a brief (*Maximum 200 words*) factual summary of the most significant information contained in the report.

Block 14. Subject Terms Keywords or phrases identifying major subjects in the report.

Block 15. Number of Pages Enter the total number of pages.

Block 16. Price Code Enter appropriate price code (*NTIS only*).

Blocks 17 - 19. Security Classifications Self-explanatory. Enter U.S. Security Classification in accordance with U.S. Security Regulations (i.e., UNCLASSIFIED). If form contains classified information, stamp classification on the top and bottom of the page.

Block 20. Limitation of Abstract This block must be completed to assign a limitation to the abstract. Enter either UL (unlimited) or SAR (same as report). An entry in this block is necessary if the abstract is to be limited. If blank, the abstract is assumed to be unlimited.